



Kent Academic Repository

Oyeka, Dumtoochukwu Obiora (2015) *Digitally Fabricated Epidermal Transfer Tattoo UHF Radio Frequency Identification Tags*. Doctor of Philosophy (PhD) thesis, University of Kent,.

Downloaded from

<https://kar.kent.ac.uk/56651/> The University of Kent's Academic Repository KAR

The version of record is available from

This document version

UNSPECIFIED

DOI for this version

Licence for this version

UNSPECIFIED

Additional information

Versions of research works

Versions of Record

If this version is the version of record, it is the same as the published version available on the publisher's web site. Cite as the published version.

Author Accepted Manuscripts

If this document is identified as the Author Accepted Manuscript it is the version after peer review but before type setting, copy editing or publisher branding. Cite as Surname, Initial. (Year) 'Title of article'. To be published in *Title of Journal*, Volume and issue numbers [peer-reviewed accepted version]. Available at: DOI or URL (Accessed: date).

Enquiries

If you have questions about this document contact ResearchSupport@kent.ac.uk. Please include the URL of the record in KAR. If you believe that your, or a third party's rights have been compromised through this document please see our [Take Down policy](https://www.kent.ac.uk/guides/kar-the-kent-academic-repository#policies) (available from <https://www.kent.ac.uk/guides/kar-the-kent-academic-repository#policies>).

Digitally Fabricated Epidermal Transfer Tattoo UHF Radio Frequency Identification Tags

A Thesis Submitted to The University of Kent
for the Degree of Doctor of Philosophy
in Electronic Engineering

By
Dumtoochukwu Obiora Oyeka

Abstract

This thesis focuses on the inkjet printing of UHF RFID tags in the form of transfer tattoos for use on the skin. Inkjet printing of these tags is proposed as a cheaper and more appropriate alternative to conventional etching.

The work seeks to assesses the performance of inkjet printed epidermal RFID tags using parameters such as read range, transmitted power and backscattered power. The effect of different printing parameters such as the number of conductive ink layers, sintering time and temperature on the performance of the tags are assessed by simulation and measurement. Additionally, techniques to reduce the volume of conductive ink used for the fabrication of the tag are also examined and compared with an aim to determine which has the best achieved read range and ink utilization balance. This would help to reduce the cost of fabrication of the tags.

Also, due to some defects being introduced to the tags during the printing process because of printing conditions and characteristics inherent to the printing technology, the effects of these defects on the performance of the printed tag is also examined by simulation and measurement. The robustness of the epidermal transfer tattoo tag was further experimentally determined by exposure to everyday use conditions and situations involving sweat and mechanical friction.

Finally, a diversity study on an inkjet printed tag integrated with a medical sticking plaster was performed. This involved the use of two to four tags placed horizontally and vertically in order to determine which orientation offers better read coverage in each of the diversity setups while a volunteer carried out a set of motions.

Dumtoochukwu Oyeka

December 2015

Acknowledgements

I would like to express my immense gratitude to my supervisor Prof. John Batchelor for his support, invaluable advice and suggestions and for pushing me to achieve my best throughout my study at Kent. His desire for high quality research work is indeed inspiring.

My Gratitude also goes to Dr. Ali Ziai for his support and advice both technical and informal throughout the course of this work. His ever ready assistance with operation of laboratory equipment is also highly appreciated.

I would like to thank Simon Jakes for all his help with the fabrication of some of the samples used in this work, assistance with operation of workshop equipment and good technical advice which he was always available to offer. My gratitude also goes to other staff in the mechanical workshop, IT and technical support department for their help throughout my research. My thanks also goes to the rest of the staff in the School of Engineering and Digital Arts for all their support.

Additionally I would like to thank my friends Badredin Turki and Dr Kehinde Adefila for their encouragement and support throughout my research. I would also like to thank my colleagues who have helped me in ways such as measurements and professional advice especially Osman Rakibet, Srijittra Swaisaenyakorn, Anthony Aighobahi and Liang Bin.

Finally, I would like to thank my parents Profs. Cyprian and Amechi Oyeka and also my sisters Adaora, Añulika and Chilota for their support, understanding, encouragement and steadfast prayers throughout my study. Without your belief in me all this would not have been attained.

Table of Contents

Abstract	i
Acknowledgements	ii
List of Figures	vi
List of Tables.....	xi
CHAPTER 1	1
1.1 Introduction	2
1.2 History of RFID	2
1.3 Advantages and Challenges of RFID Technology.....	4
1.4 RFID Use on the Human Body	6
1.5 Inkjet Printing of RFID Tags	6
1.6 Research Objectives and Contributions	8
1.6.1 Objectives.....	8
1.6.2 Contributions.....	9
1.7 Thesis Outline	9
1.8 Publications Arising From This Work	10
References	12
CHAPTER 2	14
2.1 Introduction	15
2.2 Overview of RFID Technology	16
2.2.1 Classification of RFID Tags	16
2.2.2 Operation of RFID Tags	18
2.2.3 RFID Operating Parameters	21
i) Tag Read Range	21
ii) Backscattered Power.....	21
iii) Transmitted Power.....	21
iv) Tag Sensitivity.....	22
v) EIRP	22
vi) Input Impedance and Radiation Resistance.....	23
2.3 RFID Tag Impedance Matching.....	24
2.3.1 Inductively Coupled Loop Matching	24
2.3.2 T-Match.....	25
2.3.3 Nested Slot Matching	27
2.3.5 Capacitive Tip Loading	28

2.3.6	<i>Meandering</i>	28
2.4	Body Mounted RFID Tags.....	29
2.4.1	<i>Effect of the Human Body on RFID Tags</i>	29
2.4.2	<i>Tag Designs for Use on Human Body</i>	30
2.5	Printing Processes for RFID Tag Fabrication	31
2.5.1	<i>Overview of Inkjet Printing</i>	32
2.5.2	<i>Advantages of Inkjet printing</i>	32
2.6	Inkjet Printed On-Body RFID Tags	33
2.7	Summary	33
	References	35
	CHAPTER 3	40
3.1	Introduction	41
3.2	Tag Simulation	41
3.3	Tag Fabrication	46
3.3.1	<i>Selection of RFID Chip</i>	46
3.3.2	<i>Copper Prototype</i>	47
3.3.3	<i>Inkjet Printing of Tags</i>	49
3.4	Tag Measurement.....	55
3.5	Conclusion	59
	References	60
	CHAPTER 4	63
4.1	Introduction	64
4.2	Inkjet Printing of Tattoo RFID Tags.....	65
4.3	Effect of Number of Conductive Ink Layers (Total Thickness) on Tag Performance	69
4.3.1	<i>Simulated Effects</i>	69
4.3.2	<i>Measured Effects</i>	72
i.	<i>DC Resistance Measurement</i>	73
ii.	<i>Read Range</i>	74
ii.	<i>Transmitted Power</i>	78
4.4	Tag Performance on Different Individuals Due to Variations in Body Electrical Properties	79
4.5	Effect of Tag Location on Measured Read Range	87
4.6	Ink Usage Minimization Techniques	88
4.6.1	<i>Selective Deposition on Conductive Ink on High Current Areas of the Tag</i>	89

4.6.2	<i>Trimming of Low Current Density Areas of the Tag</i>	90
4.6.3	<i>Use of Gridded Designs</i>	95
4.7	Conclusions	99
	References	101
	CHAPTER 5	104
5.1	Introduction	105
5.2	Sources of Printing Defects	107
5.3	Defects Study	109
5.3.1	<i>Simulated Defects Study</i>	111
5.3.2	<i>Measured Defects Study</i>	121
5.4	Tag Robustness Test	126
5.4.1	<i>Transfer Tattoo Performance When Mounted On Skin.</i>	126
5.4.2	<i>Effect of Sweat on Tag Performance</i>	131
5.4.3	<i>Effect of Showering on Tag Performance</i>	135
5.5	Conclusion	137
	References	139
	CHAPTER 6	141
6.1	Introduction	142
6.2	Sticking Plaster RFID Tag Design	143
6.2.1	<i>Tag Modelling and Simulation</i>	143
6.2.2	<i>Parametric Analysis of the On-body Sticking Plaster Tag</i>	146
6.3	Fabrication of the On-Body RFID Tag with Inkjet printing	148
6.4	Tag Measurements	148
6.4.1	<i>Read Range On and Off Body</i>	149
6.4.2	<i>Two Tag Diversity</i>	150
6.4.3	<i>Three Tag Diversity</i>	163
6.4.4	<i>Four Tag Diversity</i>	167
6.5	Tag Diversity Performance with Regular Body Movements	173
6.6	Conclusion	178
	References	181
	CHAPTER 7	183
7.1	Conclusions	184
7.2	Further work	189
	References	190

List of Figures

Fig. 2.1 Block diagram of a UHF RFID system	19
Fig. 2.2 A typical Passive RFID tag Architecture [18].....	20
Fig. 2.3 Equivalent Circuit of an RFID Tag	23
Fig. 2.4 A depiction of an inductively coupled loop and its equivalent circuit [22]..	25
Fig. 2.5 T-match antenna with an equivalent circuit [22]	26
Fig. 2.6 A typical H-slot antenna [22]	27
Fig. 2.7 A Capacitively Loaded RFID Tag Antenna [19].....	28
Fig. 2.8 A meandered dipole tag antenna with shunt capacitance [19].....	29
Fig. 3.1 Simulated Human Phantom	43
Fig. 3.2 Schematic for Transfer Tattoo Tag (Dimensions in mm).....	43
Fig. 3.3 Simulated Surface Current on Transfer Tattoo Tag.....	44
Fig. 3.4 Simulated Return Loss for Transfer Tattoo Tag on Human Phantom.....	44
Fig. 3.5 3D Plot of Farfield Gain for Transfer Tattoo Tag on Phantom	45
Fig. 3.6 Simulated Transfer Tattoo Tag $E\theta$ component elevation (y-z) plane	45
Fig. 3.7 Simulated Transfer Tattoo Tag $E\phi$ component azimuth (x-z) plane.....	46
Fig. 3.8 Schematic of showing tag dimensions of (a) NXP G2X chip and (b) Higgs-4 chip	47
Fig. 3.9 Read Range Measurement of Etched Copper Tag on Arm	48
Fig. 3.10 Dimatix DMP-2831 Materials Printing System	49
Fig. 3.11 Dimatix Printer Cartridge	50
Fig. 3.12 Transfer Tattoo Paper [15].....	51
Fig. 3.13 Sintering of Deposited Conductive Ink	52
Fig. 3.14 Profile Measurement of Inkjet-Printed Tags	54
Fig. 3.15 (a) Tagformance lite unit (b) wideband antenna.....	56
Fig. 3.16 Transfer Tattoo Tag performance measurement setup	57
Fig. 3.17 Measurement of Skin Dielectric Parameters with the DAK.....	58
Fig. 4.1 Drop Spacing of 15 μ m and 20 μ m	66
Fig. 4.2 Electrical Performance of Tags with Different Drop Spacing and Thickness [18]	66
Fig. 4.3 Effect of Excess Sintering Time and Temperature on Transfer Tattoo Paper	67

Fig. 4.4 Ink Sintered on (a) Tattoo paper (b) PEL paper [19].....	68
Fig. 4.5 Poorly Defined Pattern due to a Low Viscosity Ink	69
Fig. 4.6 Effect of Ink Layer Thickness on Tag Efficiency.....	70
Fig. 4.7 Effect of Ink Layer Thickness on Resonance Frequency	71
Fig. 4.8 Effect of Ink Layer Thickness on Resonance Frequency	73
Fig. 4.9 Measured DC Resistance of Inkjet Printed Tag of Transfer Tattoo Paper ...	74
Fig. 4.10 Application of Transfer Tattoo Tag.....	76
Fig. 4.11 Measured Read Range of Transfer Tattoo Tags	77
Fig. 4.12 Measured Transmitted Power of Transfer Tattoo Tags	78
Fig. 4.13 Measured Body Permittivity of 10 Individuals.....	80
Fig. 4.14 Measured Body Conductivity of 10 Individuals.....	81
Fig. 4.15 Effect of Arm Circumference on Relative Permittivity	82
Fig. 4.16 Effect of Arm Circumference on Relative Permittivity.....	82
Fig. 4.17 Relationship Between Measured Relative Permittivity and Conductivity .	83
Fig. 4.18 Effect of Relative Permittivity on Read Range	84
Fig. 4.19 Effect of Conductivity on Read Range	84
Fig. 4.20 Effect of Conductivity on Transmitted Power	85
Fig. 4.21 Effect of Permittivity on Transmitted Power.....	85
Fig. 4.22 Effect of Conductivity on Transfer Tattoo Tag	86
Fig. 4.23 Effect of Permittivity on Transfer Tattoo Tag	87
Fig. 4.24 Tag Read Range in Different Parts of the Body	88
Fig. 4.25 Selective Deposition of Conductive Ink	89
Fig. 4.26 Percentage Read Range of Selectively Deposited Conductive Ink Tags....	89
Fig. 4.27 Relationship between Utilized Ink and Achieved Read Range of Selectively Deposited Conductive Ink Tags with Reference to a Full 3 Layer Tag..	90
Fig. 4.28 Trimmed Tags.....	91
Fig. 4.29 Efficiencies of the Trimmed Transfer Tattoo Tags	91
Fig. 4.30 Measured Read Range of Trimmed Tags	92
Fig. 4.31 Measured Reader Transmission Power for Trimmed Tags	93
Fig. 4.32 Measured Backscattered Power of Trimmed Tags	93
Fig. 4.33 Mass of Silver Nanoparticles and Ink Utilized Per Tag	94
Fig. 4.34 Gridded Designs	95
Fig. 4.35 Percentage Read Range of Gridded Tags	96
Fig. 4.36 Percentage Increase in Transmitted Power	96

Fig. 4.37 Percentage Backscattered Power	97
Fig. 4.38 Mass of Silver Nanoparticles and Ink Utilized Per Gridded Tag	97
Fig. 4.39 Comparison of Ink Reduction Techniques	100
Fig. 5.1 Illustration of coffee stain [3]	106
Fig. 5.2 Influence of surface energy on ink interaction [13].....	106
Fig. 5.3 Effect of drop spacing on printed track quality [7].....	107
Fig. 5.4 The effect of substrate temperature on print quality.....	108
Fig. 5.5 Defects on the RFID tag port due to non-bonding of adjacent print lines..	109
Fig. 5.6 Pinhole defects on the RFID tag port.....	110
Fig. 5.7 Pinhole on feedline	110
Fig. 5.8 Notched defect on edges	110
Fig. 5.9 Variation in feedline width	111
Fig. 5.10 Simulated Tag Feed Area Without defects	112
Fig. 5.11 Pinhole defects.....	113
Fig. 5.12 Notched defects.....	114
Fig. 5.13 Cut on Feedline.....	114
Fig. 5.14 Simulated Tag Efficiency	115
Fig. 5.15 Effect of defect on tag impedance	117
Fig. 5.16 Pinhole Defects on Feedline	120
Fig. 5.17 Fabricated Defects	123
Fig. 5.18 Measured Tag Read Range as Percentage of Perfect Tag	124
Fig. 5.19 Percentage Read Range Comparison.....	125
Fig. 5.20 Measured Transmitted Power	125
Fig. 5.21 Inkjet Printed Transfer Tattoo Tag initially mounted on arm.....	127
Fig. 5.22 Crease on the Inkjet Printed Transfer Tattoo Tag During Use.....	128
Fig. 5.23 Measured Tag Read Range Over 8 hours	128
Fig. 5.24 Inkjet Printed Transfer Tattoo Tag Robustness Test	130
Fig. 5.25 Tag on Torso (a) Before Sleep (b) After Sleep.....	130
Fig. 5.26 Read Range of Transfer Tattoo Tag Before and After Sleep	131
Fig. 5.27 Tattoo Tag mounted on Torso for Gym Test.....	132
Fig. 5.28 Read Range of Transfer Tattoo Tag Before and Immediately After Gym Activities	132
Fig. 5.29 Experiment Setup.....	133
Fig. 5.30 Resistance Measurement Points	134

Fig. 5.31 Resistance measurements of sample tags	134
Fig. 5.32 Transfer Tattoo Tag During Shower.....	135
Fig. 5.33 Measured Read Range of Transfer Tattoo Tag Before and After Shower	136
Fig. 5.34 Transfer Tattoo Tag After Shower.....	136
Fig. 6.1 Principal dimensions for the on-body tag with 867 MHz centre match	143
Fig. 6.2 On-body Tag surface current distribution (A/m) at 867MHz.....	144
Fig. 6.3 3D Torso Model.....	144
Fig. 6.4 Simulated On-body Tag $E\theta$ component elevation (y-z) plane.....	145
Fig. 6.5 Simulated On-body Tag $E\phi$ component azimuthal (x-z) plane	145
Fig. 6.6 Loop length, LL vs. matched frequency and reflection coefficient.....	146
Fig. 6.7 Loop length, LL vs. input impedance at 867MHz.....	147
Fig. 6.8 Feed width, FW vs. matched frequency and reflection coefficient	147
Fig. 6.9 Feed width, FW vs. input impedance at 867MHz	147
Fig. 6.10 Inkjet printed Tag using conductive ink	148
Fig. 6.11 Read range measurements for tag mounted on different parts of the body	149
Fig. 6.12 Tag mounting setup showing three optical markers	150
Fig. 6.13 Horizontal tags mounted on opposing sides of a 70mm thick expanded polystyrene block	151
Fig. 6.14 Read sectors of horizontal tags, white and grey sectors correspond to single tag and no tag read angles respectively	151
Fig. 6.15 Tag read sector measurement setup	152
Fig. 6.16 Tag read boundary calculation.....	153
Fig. 6.17 Individual read boundaries for horizontal tags on the chest-back setup...	155
Fig. 6.18 Individual read boundaries for vertical tags on the chest and back setup.	155
Fig. 6.19 Individual read boundaries for horizontal tags on the arms setup	156
Fig. 6.20 Individual read boundaries for vertical symmetric tags on the arms setup.....	156
Fig. 6.21 Individual Read boundaries for vertical asymmetric tags on the arms setup.....	157
Fig. 6.22 Average read boundaries for 2 tag diversity setups	157
Fig. 6.23 Read sector plot for horizontally oriented tags placed on the chest and back	158

Fig. 6.24 Read sector plot for vertically oriented tags placed on the chest and back	159
Fig. 6.25 Azimuth plots for	160
Fig. 6.26 Read sector plot for vertical tags mounted symmetrically on upper arms.....	161
Fig. 6.27 Read sector plot for Horizontal tags mounted symmetrically on upper arms	161
Fig. 6.28 Read sector plot for Vertical tags mounted asymmetrically on upper arms	162
Fig. 6.29 Individual read boundaries for 3 horizontally oriented tags	164
Fig. 6.30 Individual read boundaries for 3 vertically oriented tags	164
Fig. 6.31 Read sector plot for 3 Horizontal tags. White, black and grey sectors are single tag read, 2 tag read and no-read sectors respectively.	166
Fig. 6.32 Read sector plot for 3 vertical tags. White and black sectors are single tag read and 2 tag read respectively.....	166
Fig. 6.33 Individual read boundaries for 4 horizontally oriented tags	168
Fig. 6.34 Individual read boundaries for 4 horizontally oriented tags	168
Fig. 6.35 Read sector plot for 4 Horizontal tags. White and black are single tag and 2 tag read sectors respectively	169
Fig. 6.36 Read sector plot for 4 Vertical tags. White, black and hashed are single tag, 2 tag and 3 tag read sectors respectively.....	170
Fig. 6.37 Picking Motion	173
Fig. 6.38 Bending Motion	173
Fig. 6.39 Twisting Motion	174
Fig. 6.40 Picking motion with 2 tags on chest and back.....	174
Fig. 6.41 Bending motion with 2 tags on chest and back	175
Fig. 6.42 Twisting motion with 2 tags on chest and back.....	175
Fig. 6.43 Picking motion with 3 tags on body	175
Fig. 6.44 Bending motion with 3 tags on body	176
Fig. 6.45 Twisting motion with 3 tags on body	176
Fig. 6.46 Picking motion with 4 tags on body	176
Fig. 6.47 Bending motion with 4 tags on body	177
Fig. 6.48 Twisting motion with 4 tags on body	177

List of Tables

Table 1.1 Advancements in RFID Technology [8]	3
Table 1.2 UHF RFID Operating Regulations [11]	4
Table 2.1 Classification of RFID Tags Based on Memory Type	17
Table 2.2 Classification of RFID Tags Based on Operating Frequency	17
Table 2.3 Classification of RFID Tags Based on Generation	18
Table 3.1 Voyantic Tagformance Lite Specifications	55
Table 4.1 Conductivity of Printed Tags By Drop Spacing (dp) and Thickness [18].	67
Table 4.2 Simulated Return Loss of Printed Tags by Drop Spacing and Thickness .	72
Table 4.3 Measured Dielectric Values	80
Table 4.4 Comparison of Ink Usage Minimization Techniques	98
Table 5.1 Simulated Tag Gain and Return Loss (S_{11})	116
Table 5.2 Calculated Percentage Change in Tag Read Range	118
Table 5.3 Pinhole Defects	120
Table 5.4 Tag Resistance Measurements	134
Table 6.1 Standard Deviation of Tag Read Sector Boundaries	158
Table 6.2 Read Sector Widths for 2 Tag Diversity On and Off Body	163
Table 6.3 Standard Deviation of Tag Read Sector Boundaries	165
Table 6.4 Read Sector Widths for 3 Tag Diversity	167
Table 6.5 Standard Deviation of Tag Read Sector Boundaries	169
Table 6.6 Read Sector Widths for 4 Tag Diversity	170
Table 6.7 Tag Read Sector Widths for 2, 3 and 4 Tag Diversity	171
Table 6.8 Percentage Tag Read Sector Widths for 2, 3 and 4 Tag Diversity	172
Table 6.9 Read Percentage for 2, 3 and 4 Tag Diversity	178
Table 6.10 Tag Diversity Performance Assessment	180
Table 7.1 Fabrication and Performance Parameters for Cost Effective Inkjet Printed Epidermal Transfer Tattoo Tag	188

CHAPTER 1

INTRODUCTION

1.1 Introduction

Radio Frequency Identification (RFID) can be used for a variety of applications such as health care for patient monitoring, pharmaceuticals for protection against counterfeiting, airports for passenger safety, retail for inventory tracking, entertainment, manufacturing for tracking of items on the manufacturing line, transportation for payment and passenger tracking and in office environments for personnel tracking and access restriction.

There has been a steady increase in the deployment of RFID systems in the past decade. In 2013 there was an estimated 3-4 billion RFID-tagged items and this estimate was for UHF only [1]. There is also a 35% to 40% year on year growth rate on the use of RFID. It further cements the assertion that RFID technology has achieved a solid penetration throughout commerce worldwide. This is boosted by dynamic growth from retail apparel implementations.

Further expansion in the use of RFID technology is expected with the growing research in the use of RFID as sensors. These tags have been used as sensors without the need for additional on-tag electronics by studying the changes in their parameters such as backscattered power or read range and relating this to variations in the physical property being sensed such as temperature or moisture [2].

1.2 History of RFID

The earliest history of the concept of Radio Frequency Identification can be traced back to the Second World War when German aeroplanes identified themselves when they received indication that they were being illuminated by friendly Radar. The pilots rolled their planes in order to change the signal being reflected (backscattered signal).

RFID benefitted greatly from the advances made in the field of Radar technology during the war and by 1948 the landmark paper on “Communications by Means of Reflected Power” by Harry Stockman was published [3].

The 1960s saw more work in the field of RFID technology by R. F. Harrington with his publications such as “Field Measurements Using Active Scatterers” and “Theory of Loaded Scatterers” [4],[5]. Robert Richardson and J. H. Vogelman also contributed immensely [6]. By this time, commercialization of RFID technology had also started with the development by Knogo and other companies of Electronic Article Surveillance (EAS) for use as anti-theft protection. This was the first commercial use of RFID [7].

The advancement of RFID technology is summarized in Table 1.1[8] .

TABLE 1.1 ADVANCEMENTS IN RFID TECHNOLOGY [8]

Decade	Advancement
1940 – 1950	Radar refined and used, major World War II development effort. RFID invented in 1948.
1950 – 1960	Early explorations of RFID technology, laboratory experiments.
1960 – 1970	Development of the theory of RFID. Start of applications field trials.
1970 – 1980	Explosion of RFID development. Tests of RFID accelerate. Very early adopter implementations of RFID.
1980 – 1990	Commercial applications of RFID enter mainstream.
1990 – 2000	Emergence of standards. RFID widely deployed. RFID becomes a part of everyday life.
2000 – Present	RFID explosion continues

A further boost was given to the growth of RFID technology in the early 2000s due to the increased interest from organizations such as the United States Department of Defence and major retailers including Wal-Mart and Tesco. Each of these organizations aimed to offer competitive pricing by lowering of operating cost with the use of RFID stock inventory [9].

In the 21st Century, the driving force behind the expansion of RFID is and will be the growing area of Internet of Things (IOT) where RFID is expected to play a key role as a means of low power interconnection between devices [10]. In April 2015, major companies such as Google, Impinj, Intel and SMARTRAC formed the Radio Frequency Identification (RAIN) alliance which symbolizes the synergy between UHF RFID and cloud computing with the anticipated surge in data storage and processing requirements with the increasing popularity of IOT. The vision of this alliance is to connect 28 billion devices by 2020 with RFID [1].

The UHF RFID frequency spectrum is divided into geographical sub-spectra each with its own equivalent isotropically radiated power (EIRP). The frequency regulations for RFID technology in North America are set by the Federal Communications Communication (FCC) and in Europe by the European Telecommunications Standards Institute (ETSI). Other countries adapt either of these standards as deemed fit. The UHF operating frequency and allowable power for some of the countries are presented in Table 1.2

TABLE 1.2 UHF RFID OPERATING REGULATIONS [11]

Region	Frequency Band (MHz)	EIRP (W)
Europe	865.6 – 867.6	3.28
United states	902 – 928	4
China	840.5 – 844.5, 920.5 – 924.5	3.28
Australia	920 – 926	4
	918 – 926	1
Japan	952 – 956.4	4

1.3 Advantages and Challenges of RFID Technology

RFID has the benefit of speed because identification of items by RFID is not as demanding in the presentation of the tag as barcode scanning. Therefore there is greater effectiveness in the processing of goods which involves item receiving,

packaging and shipping. Furthermore, unlike identifications systems such as barcodes, RFID is not a serial system which means that tagged items can be read simultaneously. This implies that goods can be moved through the supply chain more efficiently and by doing so the demands of updating large inventories can be minimized.

The automation provided by RFID makes it straight forwards to tell when an item is out of stock. This can lead to increase in revenue. In order words, RFID permits better asset control and auditing.

Use of RFID as a means of personnel tracking and access control helps to account for the location of personnel in a building in case of emergency. It also helps to restrict access to secure locations of a building by ensuring that only authorized personnel with the right privileges can access the said location and that access can be denied dynamically by reprogramming the authentication database.

Even with all these advantages, RFID technologies has some challenges. One of such is standardization as global RFID standards are still being set, manufacturers implement RFID in different ways and some of these are proprietary. The implication of this is that a service provider has to pay the parent company to use its RFID device. Alternatively, if every provider should have their own proprietary system, the consumer would not benefit from unified technologies, resulting in the need for many devices serving various individual systems.

RFID systems can also be subjected to intentional jamming. As they use wireless transmission, they can be jammed by a signal with the right amount of power at the right frequency. This could slow transmission or cause an outage. Similarly collision between multiple readers or multiple tags in a vicinity could occur although this can be prevented by careful system set up as well as by use of robust anti-collision protocols.

There could also be security concerns over the widespread adoption of RFID technology. The contactless nature of RFID tags is a security vulnerability since they can be read without the knowledge of the user. This implies that details of a contactless card can be read along with other personal details. [12].

1.4 RFID Use on the Human Body

RFID has been used on the human body for different purposes including personnel tracking and identification and access control in office environments. More complex use on humans involves the embedding of RFID tags under the skin for medical purposes [13] as well as use as sensors [14].

In the near future, RFIDs are expected to play a significant role in the field of body area networks (BAN) which can be used for ensuring workplace safety [15]. In the growing concept of the Internet of Things (IoT), on body RFID can be a major player through applications such as environmental passive sensors and data processing and human behaviour analysis such as gesture recognition and remote controlling of living environments [16]. A prototype of such system has already been presented in [17].

With all of these present and potential uses of RFID, there has been research on how best to make tags more efficient in the face of large losses when close to the human body and in other harsh environments. While this research continues to solve some of the problems, maintaining a low tag cost is also an objective. This is key to realising the full potential of RFID technology because it will make the technology more accessible to consumers.

In an aim to drive down the cost of RFID tags/technology, research has given rise to some ingenious tag designs and fabrication methods. One of such fabrication method is inkjet fabrication of the RFID tags which will be explored in this work.

1.5 Inkjet Printing of RFID Tags

The origin of inkjet printing can be traced back to the 18th century with the publication in 1749 by Jean-Antoine Nollet of his work on the effect of electricity on a stream of droplets. This was followed in 1833 by the discovery by Felix Savart of the basics of the principle used in modern inkjet printers which is the ability of an acoustic energy to break up a laminar flow-jet into a train of droplets. The first inkjet device known as the Siphon recorder was invented by William Thomson in 1858 and was used for the automatic recording of telegraph messages [18]. With the use of acoustic energy in a

print head, the frequency of mechanical vibrations can be approximately equal to the spontaneous drop-formation rate. Following other research, the first patent for a continuous inkjet printer was filed in 1951 by Rune Elmqvist. By the 1960s inkjet printers driven by electrical signals were produced.

Apart from the continuous deposition of inks (jetting), the use of drop-on-demand (DOD) which enabled the release of ink only when required was introduced in 1971 by the Casio Company when their 500 Typuter with an electrostatic pull DoD device was released. Since then, inkjet printers have continued to evolve until the present day.

Inkjet printing is widely used for graphical applications, however, it was only within the past 10 years that it has grown to a mature patterning technique. It has gained specific attention in scientific research owing to its high precision and its additive nature which means that only the necessary amount of functional material is deposited. This makes Inkjet printing of conductive materials a relatively cheap alternative for the fabrication of electronic devices when compared to other techniques such as photolithography, laser patterning and multi stage conventional wet etching which causes material wastage as well as exposure to hazardous chemicals. The potential low cost that Inkjet printing affords due to its mask free nature and efficient resource use is particularly attractive for RFID technology due to the desire for low cost and disposable tags.

Although metals such as copper and gold have been used for inkjet ink formulation, direct inkjet printing of conductive silver tracks onto flexible substrates has gained interest due to silver having the lowest resistivity value and the relatively simple synthesis of silver nanoparticles [19]. This has enabled the use of silver nanoparticles ink in applications such as organic thin-film transistors, interconnections for circuitry on a printed circuit board, disposable displays and radio frequency identification (RFID) tags.

For body mounted RFID tags such as the epidermal transfer tattoo tag presented in this work, inkjet printing provides some important unique features. First is the flexibility of the deposited ink which is an essential physical property for a tag that is

mounted on the skin. This is because of the need for the comfort of the user which is of prime importance. Also there should be no risk of the tag causing irritation and abrasion to the skin as a result of the skin being folded in an unnatural way by the transfer. Finally, flexibility gives the tag some degree of tolerance to elastic distortion.

Another positive feature of inkjet printing for the fabrication of transfer tattoo tags is the delicate nature of the transfer tattoo paper on which the tag is printed. The non-contact of inkjet printing as well as the lack of corrosive liquid chemicals involved in the printing process makes the use of this substrate possible. This, in addition to the aforementioned, means that other fabrication methods are not appropriate.

1.6 Research Objectives and Contributions

1.6.1 Objectives

The main objective of this research is to develop a very low profile skin mounted tag which is in the form of a tattoo by inkjet printing using conductive ink. This is to be done while maintaining low fabrication cost by exploring some unique features of inkjet printing. Other objectives of this work are:

- (1) To evaluate the effect of inkjet printing fabrication parameters on the performance of epidermal transfer tattoo tags.
- (2) To evaluate the effect of fabrication cost minimization by ink volume minimization on the performance of epidermal transfer tattoo tags.
- (3) To evaluate the impact of the limitations of inkjet printing which lead to defects in the printed tags on the performance of epidermal transfer tattoo tags.
- (4) To assess the robustness of transfer tattoo tags upon exposure to routine everyday activities.
- (5) To assess the diversity of performance of multiple printed tags when used on body.

1.6.2 Contributions

The contributions to knowledge from this thesis are:

- (1) The development of an inkjet printed epidermal RFID tag with optimized conductive ink usage.
- (2) Evaluation and quantification of the impact of variations in dielectric properties of the body on the performance of inkjet printed epidermal transfer tattoo RFID tags.
- (3) Establishment of the effect of conductive ink conservation techniques on the performance of inkjet printed epidermal transfer tattoo RFID tags.
- (4) Evaluation of the impact of fabrication defects on the performance of inkjet printed epidermal transfer tattoo RFID tags.
- (5) Determination of the robustness of inkjet printed epidermal RFID tag for suitability for everyday use.
- (6) Diversity performance evaluation of multiple body mounted RFID tags.

1.7 Thesis Outline

The organization of this thesis is as follows:

Chapter 2 presents an overview of RFID tag technology. Aspects such as classification, operating principles and some basic RFID operating parameters are covered. Also discussed are the various design methods by which a match can be achieved between an RFID antenna and an RFID chip. The antenna designs that have been used for RFID tags mounted on a human Body are presented. Inkjet printing technology as a means of RFID tag fabrication is also discussed.

Chapter 3 discusses the simulation and fabrication of the transfer tattoo tag. The simulation procedure and the prototyping of the tags with conventional wet etching of a copper clad Mylar sheet is explained. The chapter also introduces the inkjet printing of the epidermal transfer tattoo tags as well as their limitations. Also discussed is the various measurement equipment in terms of modes of operation, calibration, measurement procedure and steps taken to ensure accurate measurement results.

Chapter 4 considers the printing of epidermal transfer tattoo tags with a focus on the printing parameters and considerations including the effect of the number of deposited conductive ink layers on the performance. Tag performance on different individuals and placement on different parts of the body is also examined. Techniques for ink usage reduction are also presented in this chapter.

Chapter 5 describes the effects of defects arising from inkjet printing and printing tolerances on inkjet printed epidermal RFID tags are examined. The sources of these defects in the printed tags are also discussed. The effects of typical geometric defects are studied by simulation and measurement using an etched copper sample. A robustness test of the tattoo tag by testing tag read range over a period of time intervals and over different conditions is included.

Chapter 6 presents an Inkjet printed tag integrated with medical sticking plaster. This tag was fabricated for use in a medical environment where it could easily be a substitute for the currently used wristbands as well as the potential for including a sensor. A diversity study of the tag reads was conducted to establish how many tags would be needed to achieve an omni-directional read around a subject. Both horizontal and vertical polarizations were examined for cases involving two tags up to a maximum of four tags.

Chapter 7 concludes the thesis and includes relevant future work that can develop the research further.

1.8 Publications Arising From This Work

Published:

- (1) D.O. Oyeka, M.A. Ziai and J.C. Batchelor, “RFID Sticking Plasters”, Antennas and Propagation Conference (LAPC), 2012 Loughborough. Pp 1 – 4, 2012.
- (2) D.O. Oyeka, M. A. Ziai, J. C. Batchelor, E. A. Parker, V. Sanchez-Romaguera, and S. G. Yeates, “Developing inkjet printing to enable low cost UHF RFID transfer tattoo tags”, [Antennas and Propagation Society International Symposium \(APS-URSI\), 2013 IEEE, Orlando, Florida, pp 1726 – 1727, 2013.](#)

- (3) V. Sanchez-Romaguera, M. A. Ziai, D. Oyeka, S. Barbosa, J. S. R. Wheeler, J. C. Batchelor, E. A. Parker, and S. G. Yeates, "Towards inkjet-printed low cost passive UHF RFID skin mounted tattoo paper tags based on silver nanoparticle inks," *J. Mater. Chem. C*, vol. 1, no. 39, pp. 6395–6402, 2013.
- (4) D. O. Oyeka, M. A. Ziai, J. C. Batchelor, V. Sanchez-Romaguera, S. G. Yeates, S. Wunscher, and U. S. Schubert, "Inkjet printed epidermal RFID tags", *Antennas and Propagation (EuCAP), 2014 8th European Conference on*. Pp 1403 – 1406, 2014.
- (5) D. O. Oyeka and J. C. Batchelor, "Conductive Ink Usage Optimization Using Grid Designs for Inkjet Printed Epidermal RFID" *Antennas and Propagation Conference (LAPC), 2012 Loughborough*. 10 – 11 Nov. 2014
- (6) D. O. Oyeka, J. C. Batchelor, V. Sanchez-Romaguera, S. . Yeates, and R. . Saunders, "Effect of Conductive Area Trimming on the Read Range of Inkjet Printed Epidermal RFID Tags", in *The 9th European Conference on Antennas and Propagation (EuCAP 2015)*, 2015 Lisbon.
- (7) D. O. Oyeka, J. C. Batchelor, and B. M. Turki, "Enhanced read range Tattoo RFID tags," *Antennas and Propagation & USNC/URSI National Radio Science Meeting, 2015 IEEE International Symposium on*. Vancouver BC, Canada. pp. 197–198, 2015.
- (8) V. Sanchez-Romaguera, S. Wunscher, B. M. Turki, R. Abbel, S. Barbosa, D. J. Tate, D. Oyeka, J. C. Batchelor, E. A. Parker, U. S. Schubert, and S. G. Yeates, "Inkjet printed paper based frequency selective surfaces and skin mounted RFID tags: the interrelation between silver nanoparticle ink, paper substrate and low temperature sintering technique," *J. Mater. Chem. C*, 2015.
- (9) J. Tribe, D. Oyeka, J. Batchelor, N. Kaur, D. Segura-Velandia, A. West, R. Kay, K. Vega, and W. Whittow, "Tattoo Antenna Temporary Transfers Operating On-Skin (TATTOOS)," in *Design, User Experience, and Usability: Users and Interactions SE - 65*, vol. 9187, A. Marcus, Ed. Springer International Publishing, 2015, pp. 685–695.

Submitted:

- (10) Tag Diversity of Inkjet Printed Body-Worn Integrated Medical Sticking Plasters – *IEEE Transactions on Antennas and Propagation*.

In Preparation:

- (11) Effect of Gridded Antenna Design on the Performance of Inkjet Printed Epidermal RFID Tags - *IEEE Transactions on Antennas and Propagation*

References

- [1] “Internet of Things Promises Huge RFID Growth - SMARTRAC N.V.” [Online]. Available: <https://www.smartrac-group.com/internet-of-things-promises-huge-rfid-growth.html>. [Accessed: 10-Nov-2015].
- [2] M. A. Ziai and J. C. Batchelor, “Multi-State Logging Freeze Detection Passive RFID Tags,” *Antennas and Propagation, IEEE Transactions on*, vol. 62, no. 12. pp. 6406–6411, 2014.
- [3] H. Stockman, “Communication by Means of Reflected Power,” *Proceedings of the IRE*, vol. 36, no. 10. pp. 1196–1204, 1948.
- [4] R. F. Harrington, “Field Measurements Using Active Scatterers (Correspondence),” *Microwave Theory and Techniques, IEEE Transactions on*, vol. 11, no. 5. pp. 454–455, 1963.
- [5] R. F. Harrington, “Theory of loaded scatterers,” *Electrical Engineers, Proceedings of the Institution of*, vol. 111, no. 4. pp. 617–623, 1964.
- [6] V. D. Hunt, A. Puglia, and M. Puglia, *RFID - A Guide to Radio Frequency Identification*. Hoboken, NJ, USA: John Wiley & Sons, Inc., 2007.
- [7] J. Landt, “Shrouds of Time - The History of RFID - History of RFID White Paper.pdf,” 2001. [Online]. Available: https://www.transcore.com/sites/default/files/History_of_RFID_White_Paper.pdf. [Accessed: 10-Dec-2015].
- [8] J. Landt, “The history of RFID,” *Potentials, IEEE*, vol. 24, no. 4. pp. 8–11, 2005.
- [9] R. Want, “An introduction to RFID technology,” *Pervasive Computing, IEEE*, vol. 5, no. 1. pp. 25–33, 2006.
- [10] “RFID Stakeholders Need to Prepare for the Internet of Things - RFID Journal.” [Online]. Available: <http://www.rfidjournal.com/articles/view?11806>. [Accessed: 10-Nov-2015].
- [11] “UHF for RFID Regulations - UHF_Regulations.pdf.” [Online]. Available: http://www.gs1.org/docs/epc/UHF_Regulations.pdf. [Accessed: 10-Nov-2015].
- [12] “Problems With RFID.” [Online]. Available: <http://www.technovelgy.com/ct/Technology-Article.asp?ArtNum=20>. [Accessed: 11-Nov-2015].
- [13] N. Jebali, S. Beldi, and A. Gharsallah, “An RFID antenna implanted in the human arm for medical applications,” in *2015 2nd World Symposium on Web Applications and Networking (WSWAN)*, 2015, no. 1, pp. 1–4.
- [14] S. Milici, S. Amendola, A. Bianco, and G. Marrocco, “Epidermal RFID passive sensor for body temperature measurements,” *RFID Technol. Appl. Conf. (RFID-TA), 2014 IEEE*, pp. 140–144, 2014.
- [15] M. Sole, C. Musu, F. Boi, D. Giusto, and V. Popescu, “RFID Sensor Network for Workplace Safety Management,” *Emerg. Technol. Fact. Autom. (ETFa)*,

2013 *IEEE 18th Conf.*, pp. 1–4, 2013.

- [16] S. Amendola, R. Lodato, S. Manzari, C. Occhiuzzi, and G. Marrocco, “RFID Technology for IoT-based Personal Healthcare in Smart Spaces,” *IEEE Internet Things J.*, vol. PP, no. 99, pp. 1–1, 2014.
- [17] “NightCare System - RADIO6ENSE - Radio Frequency Identification (RFID) Systems.” [Online]. Available: <http://www.radio6ense.com/Products--Services/night-care-system>. [Accessed: 11-Nov-2015].
- [18] Jolke Perelaer and Ulrich S. Schubert (2010). Inkjet Printing and Alternative Sintering of Narrow Conductive Tracks on Flexible Substrates for Plastic Electronic Applications, Radio Frequency Identification Fundamentals and Applications Design Methods and Solutions, Cristina Turcu (Ed.), ISBN: 978-953-7619-72-5, InTech, DOI: 10.5772/7983. Available from: <http://www.intechopen.com/books/radio-frequency-identification-fundamentals-and-applications-design-methods-and-solutions/inkjet-printing-and-alternative-sintering-of-narrow-conductive-tracks-on-flexible-substrates-for-pla>
- [19] G. Schmid, *Nanoparticles*. Weinheim, FRG: Wiley-VCH Verlag GmbH & Co. KGaA, 2003.

CHAPTER 2

RFID BACKGROUND AND LITERATURE REVIEW

This chapter presents an overview of RFID tag technology. Aspects such as classification, operating principles and some basic RFID operating parameters are covered. Also discussed are the various design methods by which a match can be achieved between an RFID antenna and an RFID chip. The antenna designs that have been used for RFID tags mounted on a human Body are presented in this chapter. Inkjet printing technology as a means of RFID tag fabrication is also discussed.

2.1 Introduction

Radio Frequency Identification is a wireless communication technology used to uniquely identify tagged objects and people [1]. Although Radio identification has existed since the 1940s, recent years have seen a steady increase in the use of this technology [2]. Applications have diversified from the ordinary item level tracking in retail systems, to use in access restriction in locations and secure payment in transactions [3]. It has also been used in transportation networks to build customer profiles and for analytics [4].

This increase in the use of RFID has given rise to technical problems associated with its reliability and efficiency and a body of work addresses these issues using new antenna designs and fabrication methods. These problems include how the tags function in challenging environments such as on the human body and near metals, both of which tend to reduce the tag efficiency [5]. Also limited energy availability presents challenges in operation [6].

With the increasing progress made in the Internet of Things (IOT), the use of tags on the human body is a growing use of RFID technology. Applications such as patient tracking in hospital environments [7], [8], [9], assistive technologies[10], deployment to ensure the safety of workers in the workplace [11] and entertainment have all been reported [12].

The total cost of an RFID tag which is between 7 – 15 cents for a passive tag, is from the antenna, the chip and the assembly [13]. In order for the huge potential of RFID technology to be achieved, there is need to make the cost lower than it presently is. This has driven research into methods to reduce the cost of production. Avenues such as tag chip manufacturing and tag fabrication materials are all being explored. One new fabrication method for the tag conductor and even the tag substrate is Inkjet printing.

This chapter will present some of the advances made in the field of RFID technology with particular emphasis on the design and fabrication of on-body RFID tattoo tags. The layout of this chapter is as follows: Section 2.2 provides an overview of RFID technology. Section 2.3 presents an overview of RFID tag impedance matching techniques. In Section 2.4 Body mounted RFID tags are discussed. Section 2.5

presents printing processes with a focus on inkjet printing and Section 2.6 discusses on-body tags that have been fabricated with the inkjet printing process. Section 2.7 is a summary of the chapter.

2.2 Overview of RFID Technology

2.2.1 Classification of RFID Tags

There are different criteria used to classify RFID tags. One division is based on their method of sourcing power and gives rise to Active, Passive and Semi-passive RFID tags.

When a tag has an on-board power supply (in the form of a battery) it is said to be an active tag. Active RFID tags are the most sophisticated type, usually having a sensor embedded in them which performs specific roles. The battery powers the sensors as well as the transmissions between the tag and the reader. In addition to having larger memory than other types of tag, active RFIDs also have a longer read range of about 300 feet (91 metres). These active tags are known as Electronic Product Code (EPC) Class 4 and Class 5.

Passive tags have no on-board power source but instead rely solely on the received electromagnetic energy from the reader antenna. They are not as complex as the active RFIDs hence they are cheaper to produce. Owing to the lack of an independent power source they do not have long read ranges (about 40 feet or 12 metres) and cannot ordinarily support sensors. Passive RFIDs have small memory size in the order of a few kilobytes, and usually powerful readers are required [1]. Passive tags belong to EPC Class 0, Class 1 and Class 2.

Some tags have the features of both active and passive tags and are known as semi-passive. With these tags the battery is only for the operation of the embedded sensor, while the power for transmission of information between the tag and the reader is obtained entirely from the RF energy received from the reader antenna. Semi-passive tags have the read reliability of active tags but shorter read ranges in the reverse link [14].

RFID tags are also classified based on memory type, frequency of operation and by generation. These classifications are summarized in Tables 2.1 – 2.3 [14].

TABLE 2.1 CLASSIFICATION OF RFID TAGS BASED ON MEMORY TYPE

EPC Device Class	Definition	Programming
Class 0	“Read only” passive tags	Programmed by the Manufacturer
Class 1	“Write-once, read-many” passive tags	Programmed by the user; cannot be reprogrammed
Class 2	Rewritable passive tags	Reprogrammable
Class 3	Semi-passive tags	
Class 4	Active tags	
Class 5	Readers	

TABLE 2.2 CLASSIFICATION OF RFID TAGS BASED ON OPERATING FREQUENCY

Band	Unlicensed Frequency	Wavelength	Classical Use
LF	125–134.2KHz	2,400 meters	Animal tagging and keyless entry
HF	13.56MHz	22 meters	
UHF	865.5–867.6MHz (Europe) 915MHz (U.S.) 950–956MHz (Japan)	32.8 centimetres	Smart cards, logistics, and item Management
ISM	2.4GHz	12.5 centimetres	Item management

TABLE 2.3 CLASSIFICATION OF RFID TAGS BASED ON GENERATION

Feature	Generation 1	Generation 2
Frequency	860–930MHz	860–960MHz
Memory capacity	64 or 96 bits	96–256 bits
Field-programmability (data entry after manufacturing)	Yes	Yes
Reprogrammability	Class 0—read only Class 1—write once/ready	NA
Other features	NA	Faster and more reliable reads than Generation 1 Better compliance with other global standards

2.2.2 Operation of Passive RFID Tags

Communication between a passive RFID tag and the reader depends on the two being coupled. Coupling methods are generally classified as: Inductive or Backscattered coupling. The coupling method used is determined by the distance between the tag and the reader and the electrical size of the antenna [15]. If the tag operates in the near field (mainly LF and HF tags) inductive coupling occurs while Backscattered coupling is used for UHF RFID. Backscattering is the reflection of a radio frequency signal back towards the reader antenna where the amount of energy reflected by the surface on which the electromagnetic wave impacts depends on the strength of resonance which determines the tag radar cross section (RCS). Figure 1 illustrates the interaction between the RFID reader and the tag.

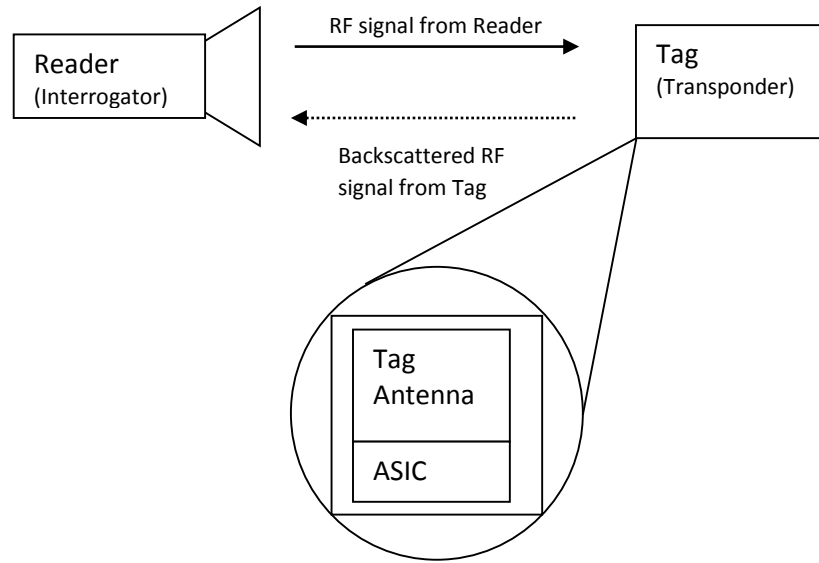


Fig. 2.1 Block diagram of a UHF RFID system

In backscatter RFID systems, the tag transponder modulates the reflected signal through a process known as backscatter modulation which is a form of amplitude shift keying (ASK) [16]. In this process the RFID chip switches its impedance between a state where it is well matched to the impedance of the antenna (low reflection), and a state in which it is completely unmatched (high reflection). This switching is done in accordance with the bit stream being sent.

As the chip depends on the tag antenna for power, the two are usually attached through a feed line and their impedances are conjugately matched. This is to ensure that maximum power is transferred from the antenna to the chip and that the chip threshold power (P_{th}) is attained. This chip threshold power has a direct effect on the read range which can be illustrated using the Friis free space formula [17] as:

$$r = \frac{\lambda}{4\pi} \sqrt{\frac{P_{reader} G_{reader} G_{tag} \tau}{P_{th}}} \quad (1)$$

where λ is the wavelength, P_{reader} is the power transmitted by the reader, G_{reader} is the gain of the reader antenna, G_{tag} is the gain of the receiving tag antenna and τ is the power transmission coefficient given by:

$$\tau = 1 - |\Gamma|^2 = \frac{4R_c R_a}{|Z_c + Z_a|^2} \quad 0 \leq \tau \leq 1 \quad (2)$$

where Γ = tag antenna voltage reflection coefficient, $Z_c = R_c - jX_c$ is chip impedance and $Z_a = R_a + jX_a$ is antenna impedance.

The chip has a capacitive impedance as a result of capacitance due to fabrication processes and the presence of a solid state switch in the chip. Therefore to achieve conjugate matching, the antenna impedance must have an equal inductive reactance.

Figure 2.2 from [18] illustrates the schematic layout of a passive RFID microchip connected to an antenna. The tag consists of a power control/rectifier to convert AC power from the reader antenna signal to DC power. It also serves as a power source for other components of the microchip. The clock extractor separates the clock signal from the reader signal while the demodulator processes the ASK received reader signal. The generated modulated signal contains the tag response which is then backscattered to the reader. The communication protocol between the tag and the reader is implemented by the logic unit while data storage is in the microchip memory. In general, this memory is segmented and consists of several blocks or fields [19]. The passive tag antenna is used to draw energy from the reader signal for the energization of the microchip which is attached directly to it and thus for exchange of information between the tags and the reader.

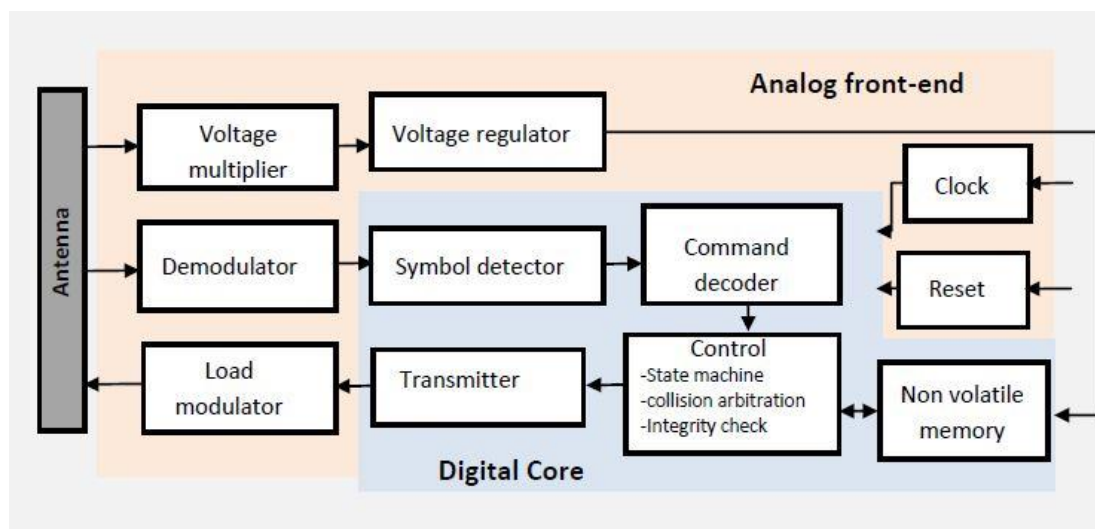


Fig. 2.2 A typical Passive RFID tag Architecture [18]

2.2.3 RFID Operating Parameters

i) Tag Read Range

The tag read range is the primary RFID parameter and it is commonly used to gauge the performance of an RFID tag. This parameter is simply the maximum distance at which the tag can be detected by the reader. The read range attained is a factor of the sensitivities of the RFID chip and reader, the power transmitted by the reader, the environment the tag is being used in such as the presence of obstacles as well as the material the tag is placed on, the reader and tag antenna gains and the co-polarization of the antennas.

ii) Backscattered Power

This is the power level of the signal received by the reader from the tag. It is defined as [20]:

$$P_{re-radiated} = K P_a G_{tag} \quad (3)$$

where P_a is the power collected by the tag antenna and G_{tag} is the gain of the tag antenna. K is a factor defined as:

$$K = \frac{4R_a^2}{|Z_a + Z_c|^2} \quad (4)$$

The above equations assume matched polarizations for reader and tag antennas.

iii) Transmitted Power

This is the power transmitted from an RFID reader to an RFID tag and should be distinguished from the transmitter power of the reader. The power received by the tag has to be at least equal to the chip threshold power (P_{th}) in order for the tag to be activated. The received transmitted power can be used to assess the tag performance as it is usually minimum at the resonant frequency. The transmitted power is given as:

$$P_{reader} = \left(\frac{\lambda_0}{4\pi r}\right)^2 \cdot G_{reader}(\theta, \phi) \cdot G_{tag}(\theta, \phi) \cdot \tau \cdot \rho(\theta, \phi) \cdot P_{tag} \quad (5)$$

Equation (5) assumes a non-perfect polarization match between the reader antenna and the tag antenna. When a perfect polarization and conjugate matching is assumed, equation (5) is simplified:

$$P_{reader} = \left(\frac{\lambda_0}{4\pi r}\right)^2 \cdot P_{tag} \cdot G_{reader} \cdot G_{tag} \quad (6)$$

iv) *Tag Sensitivity*

The minimum voltage required to activate the tag is its sensitivity. It corresponds to the minimum electric field strength at the location of the tag obtained by:

$$E_{min} = \sqrt{\frac{4\pi \eta_0 P_{th}}{\lambda_0^2 G_{tag}}} \quad (7)$$

Where η_0 is the free space impedance.

v) *EIRP*

Equivalent Isotropically Radiated Power (EIRP) is the amount of power required by an isotropic antenna to produce the maximum power density in the direction of a directional antenna's beam. It is the product of the transmitted power and antenna gain.

In an RFID system:

$$EIRP = P_{reader} G_{reader} \quad (8)$$

The RFID EIRP for various countries are specified by the Federal Communications Commission (FCC) and the European Telecommunications Standards Institute (ETSI). An EIRP of 4W is allowed for by the FCC while 2W is specified by ETSI in Europe.

vi) *Input Impedance and Radiation Resistance*

The impedance presented by an antenna at its terminals is defined as its input impedance. It is the ratio of the voltage to the current the terminals. The equation for the input impedance is:

$$Z_A = \frac{V_{in}}{I_{in}} = R_A + jX_A \quad (9)$$

where V_{in} and I_{in} = Input voltage and current respectively.

The real part of the impedance consists of two parts:

$$R_A = R_{rad} + R_L \quad (10)$$

where R_{rad} and R_L are respectively the radiation resistance and the loss resistance of the antenna.

If the antenna is connected to a device with an internal impedance, (in RFID systems, the chip), the chip impedance can be written as:

$$Z_{chip} = R_{chip} + jX_{chip} \quad (11)$$

The equivalent circuit of an RFID Tag is shown in Fig. 2.3

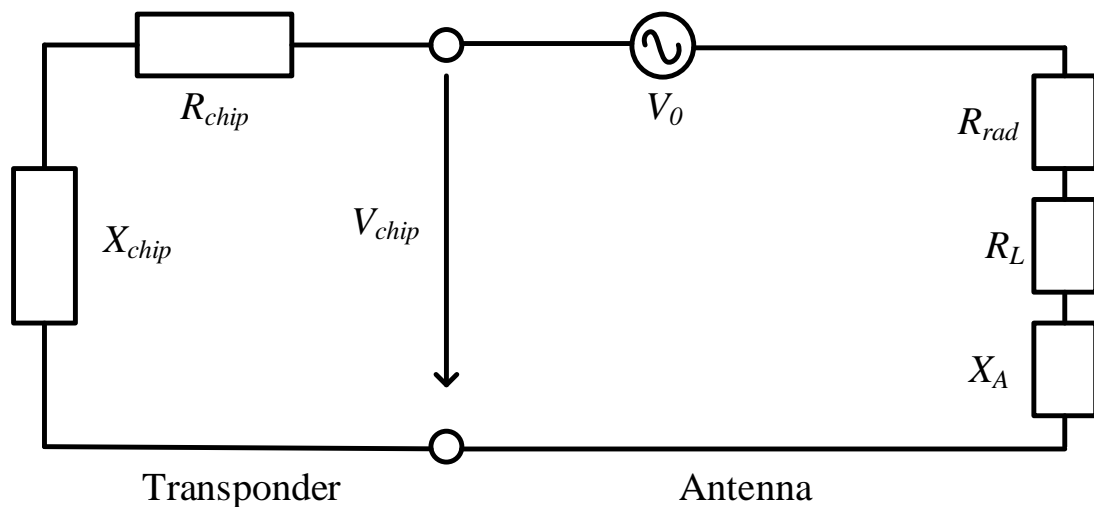


Fig. 2.3 Equivalent Circuit of an RFID Tag

The maximum power transfer between the chip and the antenna is achieved when there is a conjugate match, i.e. when:

$$R_{chip} = R_{rad} + R_L \quad (12)$$

and

$$X_A = -X_{chip} \quad (13)$$

2.3 RFID Tag Impedance Matching

Efforts are made in tag antenna design to ensure the matching of the antenna and the chip while keeping the antenna and hence the tag small. In order to achieve this matching many techniques are used. The antennas are made in such a way that changes to their dimensions would, as much as possible, independently vary their resistance and reactance. Some of these impedance matching techniques are now outlined.

2.3.1 Inductively Coupled Loop Matching

As described in [21], an inductively coupled small loop is placed close to a radiating dipole and the terminals of the loop are in turn connected to the chip. With this arrangement there is an equivalent inductance in the antenna which aids the conjugate matching with the chip. The shape (size) and the distance of the loop from the radiating body control the strength of the antenna reactance.

The inductive coupling can be modelled as a transformer and hence the input impedance from the side of the loop terminals is given as [22]:

$$Z_{in} = Z_{loop} + \frac{(2\pi fM)^2}{Z_A} \quad (14)$$

where Z_A = antenna impedance, $Z_{loop} = j2\pi fL_{loop}$ is the loop impedance and the total input reactance depends only on the loop inductance L_{loop} whether or not the dipole is

resonant. The resistance is related to the mutual inductance, M , between the radiating dipole and the small loop. The shape of the loop and the dipole-loop distance have an influence on this mutual coupling and therefore on the total input resistance, while the reactance L_{loop} is affected mainly by the loop aspect ratio.

Fig. 2.4 [22], shows the schematic of an inductively coupled loop and its equivalent circuit.

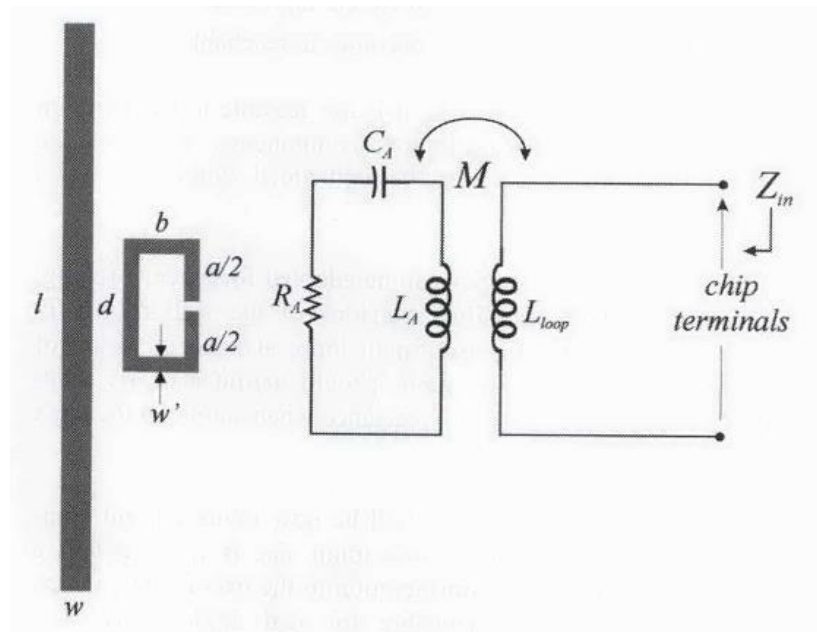


Fig. 2.4 A depiction of an inductively coupled loop and its equivalent circuit. l = length of the radiating body, b = width of the loop, d = distance of the loop from the radiating body, w = thickness of loop element, R_A = antenna resistance, L_A = inductance of the radiating body, L_{loop} = loop inductance, M = mutual coupling between the radiating body and the loop, Z_{in} = input impedance capacitance [22].

2.3.2 T-Match

This is an arrangement whereby a dipole of length l is connected to a transmission line (antenna source) by a dipole of a shorter length and smaller radius. Fig. 2.5 [22], shows the schematic of a T-match antenna design and its equivalent circuit.

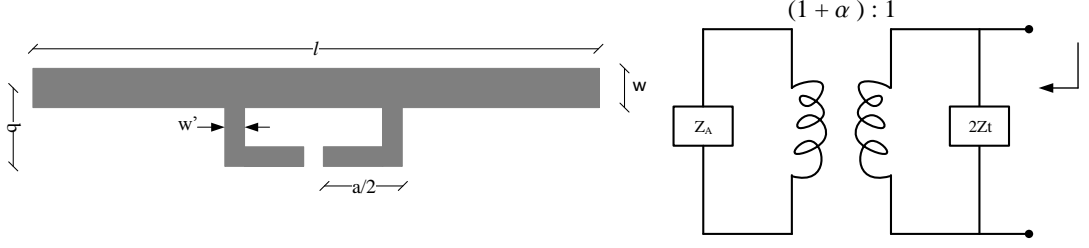


Fig. 2.5 T-match antenna with an equivalent circuit [22]

The two dipoles are separated by a small distance b . The current along these dipoles is proportional to their radii. The total input impedance can be obtained as [22]:

$$Z_{in} = R_{in} + jX_{in} = \frac{2Z_t (1 + \alpha)^2 Z_A}{2Z_t + (1 + \alpha)^2 Z_A} \quad (15)$$

where α is the current division factor between the two conductors, Z_A is the input impedance taken at the centre point free-space input impedance of the antenna in the absence of the T-match connection, and Z_t is the input impedance of the short-circuit at the ends of the T-match conductors [22]:

$$Z_t = jZ_0 \tan\left(\frac{ka}{2}\right) \quad (16)$$

Given that $Z_0 \cong 276 \log_{10}\left(\frac{b}{\sqrt{r_e r'_e}}\right)$ is the characteristic impedance of the two-conductor transmission line with spacing b , $r_e = 0.25w$ and $r'_e = 8.25w'$ are the radii of the dipole and the matching stub respectively. α represents the current division factor between the two conductors and is given as:

$$\alpha = \frac{\ln\left(\frac{b}{r'_e}\right)}{\ln\left(\frac{b}{r_e}\right)} \quad (17)$$

Matching to the chip complex impedance, Z_{chip} , is achieved by adjusting the dimensions of a , b and w' .

The T-match acts as an impedance transformer and in the case of half-wavelength dipoles, the resulting input at its terminals is inductive. When applied to smaller dipoles, the resulting impedance can be both inductive and capacitive. Additionally, depending on the configuration of a , b and w' , high input impedances could also be

generated by the T-match making it difficult to match the impedance to real microchip transmitters. The implication of these is that a single T-match would therefore not be suitable for all kinds of matching conditions and this necessitates further degrees of freedom in the structure leading to the use of multiple T-match stages as well as some shape modification of the main radiator [22].

2.3.3 Nested Slot Matching

Marrocco in [22], described the use of a nested slot antenna with the advantage of the inductive reactance property of a non-resonant slot. He noted that antennas of this form have the capability of providing the needed complex impedance matching even if the tag to be used is placed onto a high-permittivity substrate. As in other antenna types, the properties can be changed by adjusting its geometric properties. For instance in Fig. 2.6, the maximum antenna gain is a direct function of the patch side l . The impedance of the antenna can also be changed until it matches the chip by adjusting a and b . It was also observed that when the width of the slot, b , is much smaller than the external side, l , the setup has strong reactance peaks which reduce as b increases. On the other hand, when b is nearly similar to l ($2b \approx l$), the input reactance becomes slowly variable with frequency making the tag well tuned within a wide band.

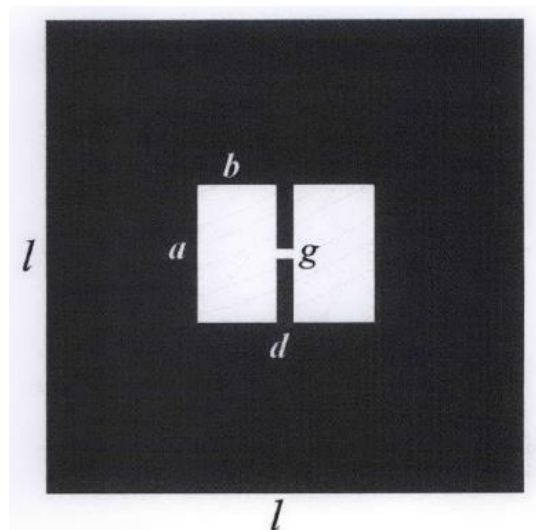


Fig. 2.6 A typical H-slot antenna [22]

2.3.5 Capacitive Tip Loading

In capacitively loaded dipole antennas, the ends of the dipole are broadened. The result of this action is an increase in the capacitance of the antenna achieving a decrease in the capacitive reactance of the antenna. By doing this, a capacitively loaded dipole becomes more inductive than an ordinary dipole of the same length [19]. A commercial tag which employs capacitive tip loading and inductive matching is shown in Fig. 2.7. With this antenna design, the capacitance is proportional to the perimeter of the broadened tip. Therefore, when used with RFID chip, the antenna reactance can be matched to that of the chip by adjusting the perimeter of the tips. These kinds of designs also provide better radiation resistance when compared to equivalent designs without the capacitive loading.

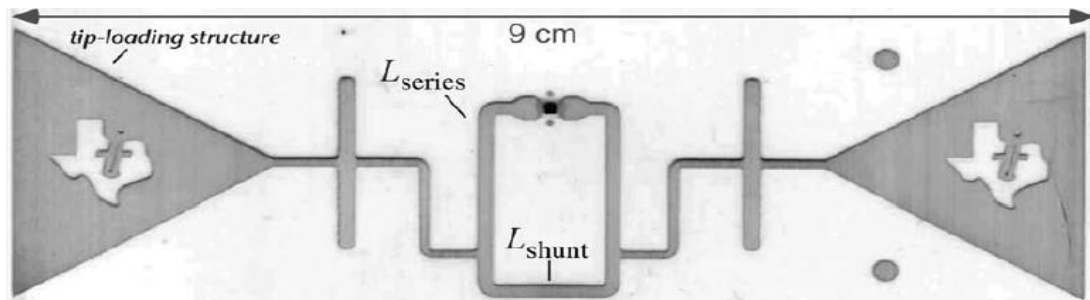


Fig. 2.7 A Capacitively Loaded RFID Tag Antenna [19]

2.3.6 Meandering

Meandering is a technique used for both matching and size reduction in antennas. When the antenna is folded, the structure has distributed capacitive and inductive reactances that affect the overall impedance. The shape of the meandered antenna can be periodic or individually optimized to match the impedance of the chip. Meandering techniques have been used in [23] where the technique was used for a gain-optimized antenna using genetic algorithm for use in RFID tag and in a very creative way in the form of letters or logos to make antennas for RFID [24].

To improve the match with the chip, the meandering of the antenna wire can be increased therefore making them longer than their resonant length. These antennas are usually inductive which will tend to cancel out the capacitance of the chip. To help trim the radiation resistance to the input resistance of the chip, an additional bar can

be added adjacent to the meander to act as a shunt capacitance. This is illustrated in Fig. 2.8, [19]

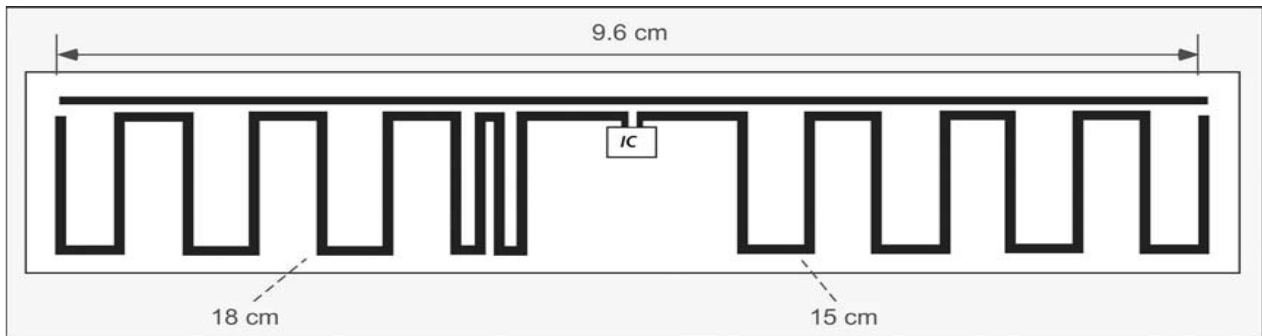


Fig. 2.8 A meandered dipole tag antenna with shunt capacitance [19]

2.4 Body Mounted RFID Tags

2.4.1 Effect of the Human Body on RFID Tags

When RFID tags are attached directly to an object with high conductivity, water content or dielectric values, the parameters of the tag such as its input impedance, operating frequency and radiation pattern will change. This influence is clearly seen when tags are placed on the human body or metals.

Kellomäki in [25] identified two ways the human body affects RFID tags: i) the dielectric loading provided by the body increases the electrical length of the antenna and hence detunes the tag and lowers its impedance. ii) absorption, which lowers the radiation efficiency of the tag and hence its gain. This effect is because of the high saline water content of the body. The water molecules absorb RF energy making limited power available to the tag [18]. Both detuning and absorption lead to a reduction in tag read range.

In order to mitigate the effects of the human body on the performance of the tag, different approaches are adopted. Some of the approaches as explained by Marrocco in [26], focus directly on the antenna design as a means of tuning mechanism for matching ASIC chip. A different approach may be taken to reduce these effects by

decoupling the antenna from the human body. Some of these methods will be presented in the following section.

2.4.2 Tag Designs for Use on Human Body

When RFID tags are required for use on the human body, it is desirable that they have the following characteristics: small dimensions, light weight and high immunity to the effects of the body [27]. In addition to these, it is also required that they do not interfere with the movement of the body and cause discomfort. Several works describe body mounted RFID tags which employ the matching techniques identified in Section 2.4, together with methods of separating the tag from the body while trying to reduce the bulkiness of the tag.

One design used for body tags is the planar inverted-F antenna (PIFA). Although an ordinary PIFA would afford a reduction in size compared to a standard patch antenna, this comes at a cost of reduced tolerance to the mounting environment. Therefore, Hirovonen et al [28] presented a platform-tolerant PIFA. This was achieved by decoupling the antenna from the body with a ground plane as well as the use of a 3mm Teflon substrate between the patch and the ground plane. Another modified PIFA antenna is demonstrated in [29] which enabled the RFID tag to be implanted under the skin of a lab rat with good performance results. This antenna had a dimension of about $13.5 \text{ mm} \times 11 \text{ mm} \times 4.25 \text{ mm}$ and operates in the 915 – 928 MHz UHF RFID band.

Dipole and monopole RFID tag antennas have been used on humans. In [30], a meandered dipole was fabricated from conductive cloth. However, in order to ensure functionality, this antenna was separated from the body by 20 mm. A meandered dipole with a T-match has been used by Kellomäki [25] with a minimum separation distance of 5 mm from the body with an assumption of use on loose clothing. In [31] a conformal magnetic substrate was used as a substrate to decouple a capacitively loaded meandered dipole from the body. Chen et al in [32] presented the use of a folded dipole antenna for RFID tags. Other works where dipoles have been used are presented in [26] where folded dipole antennas were used for RFID tags for monitoring of humans, in [33] where a folded dipole structure formed the RFID antenna which was integrated in the collar of a shirt with up to 5 – 6 metres read range when there is

a small gap between the tag and the body. The use of dipole antennas for RFID tags was also presented in [34] where a tag in the form of a wristband was demonstrated.

Loop antennas have also been created as on-body RFID tags. Švanda and Polívka in [35] presented a looped antenna for use on high dielectric materials and on metallic substrates. The separation of the tag from the body was achieved with the aid of a high permittivity substrate. The work detailed in [36] presented an inductively coupled loop antenna on a 0.76 mm thick PVC substrate for use on the human body. A dual square loop antenna on a 600 μ m silicone substrate was presented by Amendola et al [37] while in [38] a dual loop antenna with tuning slots was designed on a 1.8mm thick substrate.

The work presented in [39] and [30] respectively show the fabrication of RFID tag antennas using patches with a 1.4 mm and 4.3 mm thick foam substrate for use on human body. Manzari et al have presented in [40] a tag antenna that utilized a folded patch design with tuning capability while mounted on the body. Other tag designs using patch antennas employ the decoupling of the tag from the body using ground planes or by mounting on a dielectric substrate [41], [27], [42]–[45].

There are also works that have employed slotted antennas for RFID tags such as [46] where a slotted antenna is proposed for use on perishable foods and on the human body. This tag was fabricated on a 1.5 mm FR4 substrate with a copper ground plane and was able to attain a 2.5 m read range at 868MHz when attached to a container filled with water. Occhiuzzi et al have presented three slot based tag antenna designs [47]. These designs are a nested slot suspended patch antenna (NSSP), a meandered slot antenna (MSA) and a slot inverted-L antenna (SILA). The antennas have been fabricated on a 4 mm thick substrate.

A common trend in the presented tag designs is the presence of a ground plane, a dielectric substrate or an actual separation of the tag from the body in order to ensure good performance results.

2.5 Printing Processes for RFID Tag Fabrication

The potential for the use of printing processes for the fabrication of RFID tags have

been examined by Blayo and Pineaux in [48]. In that work the authors compared processes such as offset lithography, flexography, gravure, screen printing, inkjet printing and electrophotography. Each of these printing processes have their unique features which give them an advantage over others in different aspects such as printing speed and printing flexibility. However it was noted that the versatility of inkjet printing dominates due to its digital, non-impact and low-substrate selective nature. These features make it a good method for printed electronics.

2.5.1 Overview of Inkjet Printing

The first inkjet printers were introduced in the 1970s. The main contributors to this technology are Canon, Epson, Hewlett-Packard and Lexmark [49]. Inkjet printing has set a foundation for several other printing technologies such as 3-D printing. In addition to its ease of operation, in the general sense inkjet printing is faster and cheaper than other additive manufacturing technologies such as gravure, screen printing and flexography.

Apart from using conventional decorative ink, with inkjet printing, deposition of conductive polymers and functional materials on cellulose-based substrates has also been achieved. Conductive traces for passive or active circuitry including filters, antennas, frequency selective surfaces as well as nanoparticle microelectromechanical devices (MEMs) have been printed [50]–[52]. Structures created by inkjet printing include: thin-film transistors, light-emitting diodes, solar cells, memory and magnetic applications, contacts and conductive structures, sensors and detectors, biological and pharmaceutical applications [53][54].

2.5.2 Advantages of Inkjet printing

One advantage provided by inkjet printed technology is its drop-on-demand (DOD) feature which enables the targeted and selective deposition of inks (conductive ink or any other material being printed). This prevents waste of materials as well as optimum fabrication of printed samples, [55]–[58]. When compared to wet-etching (a subtractive process) where the unwanted metal parts are removed from the material

being etched, inkjet printing jets a single ink droplet from the nozzle to the desired position. This ensures that no waste is created leading to an economical fabrication method. The simplicity of the inkjet process is also an attractive factor with only a few fabrication steps being required.

With improving high resolution, inkjet can also be used to print narrow conductive tracks which can be seen in circuit boards (e.g. track widths of 0.2mm or less). There are only a few printing processes offering better or similar resolution to inkjet printing [49][59].

Inkjet printed conducting inks samples have also shown relatively good conductivity values when compared to bulk silver as seen in [60], [61] and [62] with up to 56% of bulk silver conductivity reported.

For the transfer tattoo tags that will be the subject of this thesis, inkjet printing is particularly attractive because it provides flexibility which is desired in a body-mounted tag. This flexibility means seamless integration on the skin which prevents the user experiencing discomfort.

2.6 Inkjet Printed On-Body RFID Tags

There has been work reported on inkjet printed RFID tags used on the human body as well as for the fabrication of biosensing tags reported in [63] which were in the form of a wrist band. A flexible magnetic composite has been used as the substrate in order to enable this close-to-body functioning. The inkjet printed RFID tag by Lee et al [64] utilized a 3mm thick Electromagnetic Band Gap (EBG) to decouple the RFID tag from the body. Finally, Inkjet printed RFID energy scavenging tags have also been developed [65] and [66].

2.7 Summary

In this chapter, an overview of RFID technology which includes classification and operating principles has been presented. The basic RFID operating parameters of read

range, backscattered power, transmitted power and tag sensitivity have also been discussed.

Various RFID tag impedance matching techniques were presented as a means to ensure good conjugate matching between an RFID tag and chip in order to enable good tag performance. These techniques include the use of inductively coupled loop, T-matching network, nested slot, meandering and capacitive loading of dipole ends. A section was also dedicated to body mounted RFID tags where a review of various tag designs specifically for body mounted RFID tags was presented.

Some other possible means for fabrication of printed RFID tags were mentioned and the advantage of inkjet printed technology was reviewed. A brief discussion of inkjet printed RFID tags used on human body was given.

References

- [1] V. D. Hunt, A. Puglia, and M. Puglia, *RFID - A Guide to Radio Frequency Identification*. Hoboken, NJ, USA: John Wiley & Sons, Inc., 2007.
- [2] G. R. Heim, W. R. Wentworth Jr., and X. (David) Peng, "The Value to the Customer of RFID in Service Applications," *Decis. Sci.*, vol. 40, no. 3, pp. 477–512, Aug. 2009.
- [3] J. Banks, M. Pachano, L. Thompson, and D. Hanny, "RFID in Payment Transactions," in *RFID Applied*, John Wiley & Sons, Inc., 2007, pp. 341–346.
- [4] "Transport for London builds customer profiles using RFID data analytics." [Online]. Available: <http://www.computerweekly.com/feature/Transport-for-London-builds-customer-profiles-using-RFID-data-analytics>. [Accessed: 18-Oct-2015].
- [5] D. M. Dobkin and S. M. Weigand, "Environmental effects on RFID tag antennas," *Microwave Symposium Digest, 2005 IEEE MTT-S International*. p. 4 pp., 2005.
- [6] P. V. Nikitin and K. V. S. Rao, "Performance limitations of passive UHF RFID systems," *2006 IEEE Antennas Propag. Soc. Int. Symp.*, pp. 1011–1014, 2006.
- [7] C. Chao, W. Jen, Y. Chi, and B. Lin, "Improving patient safety with RFID and mobile technology," *Int. J. Electron. Healthc.*, vol. 3, no. 2, p. 175, 2007.
- [8] R. S. Sangwan, R. G. Qiu, and D. Jessen, "Using RFID tags for tracking patients, charts and medical equipment within an integrated health delivery network," *Proceedings. 2005 IEEE Networking, Sens. Control. 2005.*, pp. 1070–1074.
- [9] S. Amendola, R. Lodato, S. Manzari, C. Occhiuzzi, and G. Marrocco, "RFID Technology for IoT-based Personal Healthcare in Smart Spaces," *IEEE Internet Things J.*, vol. PP, no. 99, pp. 1–1, 2014.
- [10] O. O. Rakibet, D. O. Oyeka, and J. C. Batchelor, "Passive RFID switches for assistive technologies," *Antennas and Propagation (EuCAP), 2013 7th European Conference on*. pp. 1917–1920, 2013.
- [11] M. Sole, C. Musu, F. Boi, D. Giusto, and V. Popescu, "RFID Sensor Network for Workplace Safety Management," *Emerg. Technol. Fact. Autom. (ETF A), 2013 IEEE 18th Conf.*, pp. 1–4, 2013.
- [12] O. Rashid, P. Coulton, R. Edwards, and W. Bamford, "Utilising RFID for mixed reality mobile games," *Consumer Electronics, 2006. ICCE '06. 2006 Digest of Technical Papers. International Conference on*. pp. 459–460, 2006.
- [13] C.-F. Huang, "Low-Cost Solution for RFID Tags in Terms of Design and Manufacture," in *Current Trends and Challenges in RFID*, P. C. Turcu, Ed. 2011.
- [14] C. Dighero, "RFID: The Real and Integrated Story," *Intel Technol. J.*, vol. 09, no. 03, pp. 15–16, Aug. 2005.
- [15] K. Finkensteller, *RFID Handbook*, 3rd ed. West Sussex, United Kingdom: John

Wiley & Sons Ltd, 2010.

- [16] J. Uddin, M. Reaz, and M. Hasan, "UHF RFID antenna architectures and applications," *Sci. Res. Essays*, vol. 5, no. May, pp. 1033–1051, 2010.
- [17] K. V. S. Rao, P. V. Nikitin, and S. F. Lam, "Antenna design for UHF RFID tags: A review and a practical application," *Antennas Propagation, IEEE Trans.*, vol. 53, no. 12, pp. 3870–3876, Dec. 2005.
- [18] M. Bolic, D. Simplot-Ryl, and I. Stojmenović, *RFID Systems: Research Trends and Challenges*, vol. 54. West Sussex, United Kingdom: John Wiley & Sons Ltd, 2010.
- [19] D. Dobkin, *The RF in RFID: passive UHF RFID in practice*. Oxford: Elsevier, 2008.
- [20] P. V. Nikitin and K. V. S. Rao, "Theory and measurement of backscattering from RFID tags," *IEEE Antennas Propag. Mag.*, vol. 48, no. 6, pp. 212–218, 2006.
- [21] H. . Son, C.S; Tyo, "Design of RFID tag antennas using an inductively coupled feed," *Electron. Lett.*, vol. 41, no. 18, pp. 994–996, 2005.
- [22] G. Marrocco, "The art of UHF RFID antenna design: impedance-matching and size-reduction techniques," *IEEE Antennas Propag. Mag.*, vol. 50, no. 1, pp. 66–79, Feb. 2008.
- [23] G. Marrocco, "Gain-optimized self-resonant meander line antennas for RFID applications," *IEEE Antennas Wirel. Propag. Lett.*, vol. 2, pp. 302–305, 2003.
- [24] M. Keskilammi and M. Kivikoski, "Using text as a meander line for RFID transponder antennas," *Antennas and Wireless Propagation Letters, IEEE*, vol. 3, no. 1. pp. 372–374, 2004.
- [25] T. Kellomäki, "On-body performance of a wearable single-layer RFID tag," *IEEE Antennas Wirel. Propag. Lett.*, vol. 11, pp. 73–76, 2012.
- [26] G. Marrocco, "RFID Antennas for the UHF Remote Monitoring of Human Subjects," *IEEE Trans. Antennas Propag.*, vol. 55, no. 6, pp. 1862–1870, Jun. 2007.
- [27] C. Occhiuzzi, S. Cippitelli, and G. Marrocco, "Modeling, Design and Experimentation of Wearable RFID Sensor Tag," *IEEE Trans. Antennas Propag.*, vol. 58, no. 8, pp. 2490–2498, Aug. 2010.
- [28] M. Hirvonen, P. Pursula, K. Jaakkola, and K. Laukkanen, "Planar inverted-F antenna for radio frequency identification," *Electron. Lett.*, vol. 40, no. 14, p. 848, 2004.
- [29] S. Islam, K. P. Esselle, L. Matekovits, D. Bull, and P. M. Pilowsky, "An implantable PIFA antenna with a J-shaped proximity feed for RFID telemetry," *ICECom 2013 - Conf. Proc. 21st Int. Conf. Appl. Electromagn. Commun.*, pp. 9–12, 2013.
- [30] M. Svanda and M. Polivka, "Dualband Wearable UHF RFID Antenna," *Antennas and Propagation, 2007. EuCAP 2007. The Second European Conference on*. pp. 1–5, 2007.

- [31] L. Yang, L. J. Martin, D. Staiculescu, C. P. Wong, and M. M. Tentzeris, "Conformal magnetic composite RFID for wearable RF and bio-monitoring applications," *IEEE Trans. Microw. Theory Tech.*, vol. 56, no. 12, pp. 3223–3230, 2008.
- [32] S.-L. Chen and K.-H. Lin, "A folded dipole with a closed loop antenna for RFID applications," *Antennas and Propagation Society International Symposium, 2007 IEEE*. pp. 2281–2284, 2007.
- [33] M. Takahashi, T. Nakajima, K. Saito, and K. Ito, "Characteristics of wristband type RFID antenna," *Antennas and Propagation (EuCAP), 2010 Proceedings of the Fourth European Conference on*. pp. 1–4, 2010.
- [34] T. Kellomaki, T. Bjorninen, L. Ukkonen, and L. Sydanheimo, "Shirt collar tag for wearable UHF RFID systems," *Antennas and Propagation (EuCAP), 2010 Proceedings of the Fourth European Conference on*. pp. 1–5, 2010.
- [35] S. Milan and P. Milan, "Novel dual-loop antenna placed over patch array surface for UHF RFID of dielectric and metallic objects," *Microw. Opt. Technol. Lett.*, vol. 51, no. 3, pp. 709–713, Mar. 2009.
- [36] C.-W. Chiu and M.-C. Tsai, "An inductively-feed loop tag antenna close to a human body for UHF RFID applications," *Antennas and Propagation Society International Symposium (APSURSI), 2013 IEEE*. pp. 1504–1505, 2013.
- [37] S. Amendola, S. Milici, and G. Marrocco, "Performance of Epidermal RFID Dual-loop Tag and On-Skin Retuning," *IEEE Trans. Antennas Propag.*, vol. 63, no. 8, pp. 3672–3680, Aug. 2015.
- [38] M. Svanda and M. Polivka, "Extremely low profile UHF RFID TAG antennas for identification of people," *Antennas Propag. (EuCAP), 2010 Proc. Fourth Eur. Conf.*, pp. 2–5, 2010.
- [39] H. Rajagopalan and Y. Rahmat-Samii, "On-body RFID tag design for human monitoring applications," *2010 IEEE Antennas Propag. Soc. Int. Symp.*, vol. 1, pp. 1–4, 2010.
- [40] S. Manzari, S. Pettinari, and G. Marrocco, "Miniaturized and tunable wearable RFID tag for body-centric applications," *2012 IEEE Int. Conf. RFID-Technologies Appl. RFID-TA 2012*, vol. 2, no. 1, pp. 239–243, 2012.
- [41] J. Grosinger and M. Fischer, "Evaluating On-Body RFID Systems at 900 MHz and 2.45 GHz," *2012 Fourth Int. EURASIP Work. RFID Technol.*, pp. 52–58, 2012.
- [42] S. Manzari, C. Occhiuzzi, and G. Marrocco, "Feasibility of body-centric systems using passive textile RFID tags," *IEEE Antennas Propag. Mag.*, vol. 54, no. 4, pp. 49–62, 2012.
- [43] M. Svanda and M. Polivka, "Matching Technique for an On-Body Low-Profile Coupled-Patches UHF RFID Tag and for Sensor Antennas," *Antennas and Propagation, IEEE Transactions on*, vol. 63, no. 5. pp. 2295–2301, 2015.
- [44] A. G. Santiago, J. R. Costa, and C. A. Fernandes, "Broadband UHF RFID passive tag antenna for near-body applications," *IEEE Antennas Wirel. Propag. Lett.*, vol. 12, pp. 136–139, 2013.

- [45] M. Wu and K. Ito, "Basic study on see-through microstrip antennas constructed on a window glass," in , *IEEE Antennas and Propagation Society International Symposium, 1992. AP-S. 1992 Digest. Held in Conjunction with: URSI Radio Science Meeting and Nuclear EMP Meeting, 1992*, pp. 499–502 vol.1.
- [46] A. Dubok and A. B. Smolders, "Miniaturization of Robust UHF RFID Antennas for Use on Perishable Goods and Human Bodies," *Antennas and Wireless Propagation Letters, IEEE*, vol. 13. pp. 1321–1324, 2014.
- [47] C. Occhiuzzi and C. Calabrese, "Body-matched Slot Antennas for RadioFrequency Identification," *URSI_Union Radio Sci.*, pp. 1–4, 2008.
- [48] A. Blayo and B. Pineaux, "Printing processes and their potential for RFID printing," in *Proceedings of the 2005 joint conference on Smart objects and ambient intelligence: innovative context-aware services: usages and technologies, 2005*, pp. 27–30.
- [49] B. V. Lakafosis, A. Rida, R. Vyas, L. Yang, S. Nikolaou, and M. M. Tentzeris, "Progress Towards the First Wireless Sensor Networks Consisting of Inkjet-Printed , Sensor Tags," *Proc. IEEE*, vol. 98, no. 9, pp. 1601–1609, 2010.
- [50] W. Ahmad, D. Budimir, A. Maric, and N. Ivanisevic, "Inkjet printed bandpass filters and filtennas using silver nanoparticle ink on flexible substrate," *Antennas and Propagation & USNC/URSI National Radio Science Meeting, 2015 IEEE International Symposium on*. pp. 145–146, 2015.
- [51] B. M. Turki, E. A. Parker, M. A. Ziai, J. C. Batchelor, V. Sanchez-Romaguera, and S. G. Yeates, "Study of clusters of defects in low-cost digitally fabricated frequency selective surfaces," *Antennas and Propagation (EuCAP), 2014 8th European Conference on*. pp. 779–801, 2014.
- [52] M.-M. Laurila, A. Soltani, and M. Mantysalo, "Inkjet printed single layer high-density circuitry for a MEMS device," *Electronic Components and Technology Conference (ECTC) , 2015 IEEE 65th*. pp. 968–972, 2015.
- [53] M. Singh, H. M. Haverinen, P. Dhagat, and G. E. Jabbour, "Inkjet printing-process and its applications," *Adv. Mater.*, vol. 22, no. 6, pp. 673–685, 2010.
- [54] R. Vyas, V. Lakafosis, and H. Lee, "Inkjet printed, self powered, wireless sensors for environmental, gas, and authentication-based sensing," *IEEE Sens. J.*, vol. 11, no. 12, pp. 3139–3152, 2011.
- [55] J. Siden, M. K. Fein, A. Koptuyug, and H. E. Nilsson, "Printed antennas with variable conductive ink layer thickness," *Microwaves, Antennas & Propagation, IET*, vol. 1, no. 2. pp. 401–407, 2007.
- [56] S. L. Merilampi, T. Bjorninen, A. Vuorimaki, L. Ukkonen, P. Ruuskanen, and L. Sydanheimo, "The Effect of Conductive Ink Layer Thickness on the Functioning of Printed UHF RFID Antennas," *Proc. IEEE*, vol. 98, no. 9, pp. 1610–1619, Sep. 2010.
- [57] J. Virtanen, T. Björninen, L. Ukkonen, K. Kaija, T. Joutsenoja, L. Sydänheimo, and A. Z. Elsherbeni, "The effect of conductor thickness in passive inkjet printed RFID tags," *2010 IEEE Int. Symp. Antennas Propag. CNC-USNC/URSI Radio Sci. Meet. - Lead. Wave, AP-S/URSI 2010*, no. 1, pp. 1–4, 2010.

- [58] V. Pynttari, E. Halonen, H. Sillanpaa, M. Mantysalo, and R. Makinen, "RF Design for Inkjet Technology: Antenna Geometries and Layer Thickness Optimization," *Antennas and Wireless Propagation Letters, IEEE*, vol. 11. pp. 188–191, 2012.
- [59] J. Siden and H.-E. Nilsson, "Line width limitations of flexographic-screen- and inkjet printed RFID antennas," *Antennas and Propagation Society International Symposium, 2007 IEEE*. pp. 1745–1748, 2007.
- [60] A. Syed, K. Demarest, and D. D. Deavours, "Effects of Antenna Material on the Performance of UHF RFID Tags," *2007 IEEE Int. Conf. RFID*, pp. 57–62, 2007.
- [61] A. Bonea, A. Brodeala, M. Vlădescu, and P. Svasta, "Electrical conductivity of inkjet printed silver tracks," *Proc. Int. Spring Semin. Electron. Technol.*, pp. 1–4, 2012.
- [62] J. Siden, M. K. Fein, A. Koptuyug, and H. E. Nilsson, "Printed antennas with variable conductive ink layer thickness," *Microwaves, Antennas & Propagation, IET*, vol. 1, no. 2. pp. 401–407, 2007.
- [63] M. M. Tentzeris, A. Traille, L. Yang, V. Lakafossis, R. Vyas, A. Rida, A. Haque, and D. Staiculescu, "RFID-enabled biosensing wireless modules," *2009 IEEE Radio Wirel. Symp.*, pp. 131–134, 2009.
- [64] H. Lee, S. Kim, D. De Donno, and M. M. Tentzeris, "A novel Universal inkjet-printed EBG-backed flexible RFID for rugged on-body and metal mounted applications," *IEEE MTT-S Int. Microw. Symp. Dig.*, pp. 1–3, 2012.
- [65] G. Orecchini, L. Yang, M. M. Tentzeris, and L. Roselli, "Wearable battery-free active paper printed RFID tag with human-energy scavenger," *Microwave Symposium Digest (MTT), 2011 IEEE MTT-S International*. pp. 1–4, 2011.
- [66] G. Orecchini, M. M. Tentzeris, L. Yang, and L. Roselli, "Smart shoe: An autonomous inkjet-printed RFID system scavenging walking energy," *IEEE Antennas Propag. Soc. AP-S Int. Symp.*, pp. 1417–1420, 2011.

CHAPTER 3

TRANSFER TATTOO TAG SIMULATION, FABRICATION AND MEASUREMENTS

This chapter presents the simulation and fabrication of the transfer tattoo tag. The simulation procedure and the prototyping of the tags with conventional wet etching of a copper clad Mylar sheet is explained. The chapter also introduces the inkjet printing of the epidermal transfer tattoo tags as well as their limitations. Also discussed is the various equipment used to carry out the measurements in this work in terms of their modes of operation, calibration, measurement procedure and steps taken to ensure accurate measurement results.

3.1 Introduction

Various approaches for studying the performance of RFID tags have been taken by different researchers. The most common of these is the use of the tag read range which represents the biggest distance from which the reader can activate or receive signals from the tag. Other significant RFID performance parameters include the backscattered power received by the reader from the tag [1], transmitted power which is an indicator of how much power from the reader is required to activate the ASIC (application specific integrated circuit) [2] and [3]. Additionally, the realized gain of the tag which takes into account the mismatch between the tag antenna and the ASIC can also be used as a measure for the performance of the RFID tag [4] and [5].

Care was taken prior to the measurements in order to ensure the reliability of the obtained results. These include a good understanding of how the equipment works, proper calibration and use of the equipment.

The purpose of this chapter is to present the steps taken to ensure the reliability of the results presented and to layout factors that affect the presented results. Additionally, the inkjet printing process, the printer hardware as well as the calibration and use of equipment will be discussed. The layout of this chapter is as follows: Section 3.1 will discuss the simulator and the simulation procedure as well as introducing steps taken to ensure simulation accuracy. It also discusses the human phantom used for the simulation. In Section 3.3, the tag fabrication is presented which includes the chip selection, copper prototyping and inkjet printing. Section 3.4 introduces the equipment used in this work, its operation, calibration and steps taken to ensure accurate results while Section 3.5 concludes the chapter.

3.2 Tag Simulation

All tags presented in this work were simulated with the CST Microwave Studio Simulator [6]. The finite difference time domain method (FDTD) in CST was used. The FDTD is a grid-based differential time-domain numerical modelling method which uses discretized Maxwell's equations which have been modified to central-

difference equations. The electric field is solved at a given instance followed by the magnetic field in another instance. This process is repeated until predefined convergence criteria are met.

On completion of the 3D geometric modelling process an automatic meshing procedure is applied prior to the start of the simulation engine. The 2015 version of the CST Microwave Studio has various solvers. However, for UHF RFID tags, the most suitable solver is the Transient solver. This is because with its ability to obtain the entire broadband frequency behaviour of a simulated design from a single calculation run, it is the most flexible tool for high frequency applications. The frequency domain solver is more suitable for situations where there are a few frequencies of interest i.e. narrowband, not high frequency [7].

Since the transfer tattoo tag is to be used directly on the skin, it is very important to create a model that will closely imitate the body. In order to achieve this, a multi-layered phantom consisting of the skin, fat, muscle and bone was created in the form shown in Fig 3.1. The initial electrical properties obtained for the phantom were obtained from [8]. The phantom was made to have dimensions close to the circumference of the arm, though in order to reduce simulation time, the length of the phantom was not scaled to the length of the arm since the model already had a large number of mesh cells occasioned by the high dielectric constant of the tissue and the thin tattoo substrate layers. Simulated tests indicated that this did not affect the tag simulation results. This was achieved by comparing simulation results of the tattoo tag on a phantom with the dimension of the full length of the arm to the results obtained from scaled down phantoms. These results showed very minimal disparity with about 0.5% change between the full length phantom and the scaled down phantom.

In order to ensure accurate simulation results, for reduced total mesh size, localized meshing was used throughout this work. This helped to ensure proper meshing in areas of the tag with high energy concentration as well as in areas with fine details such as on the feedline. An insufficient meshing regime would mean that small details cannot be resolved. Conversely, very small meshing would lead to extended simulation times with a possibility of errors.

Perfect matched layers were used to bound the radiation space.

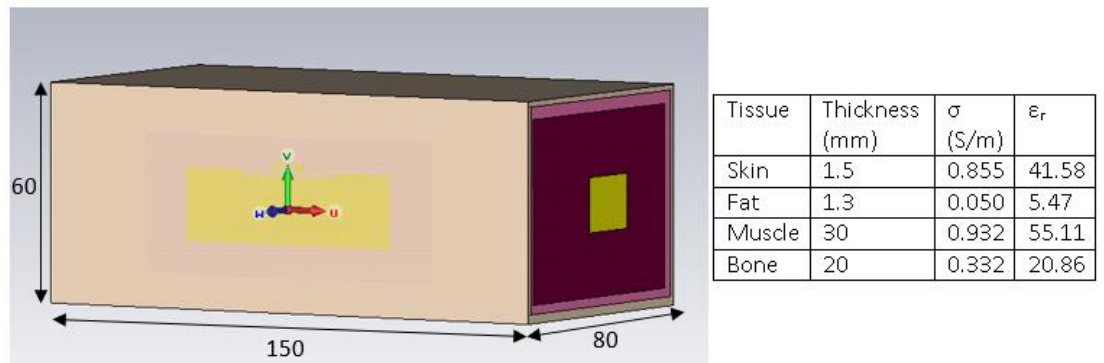


Fig. 3.1 Simulated Human Phantom (dimensions in mm)

To excite the structure, a discrete port with a lumped element was placed across the terminals of the antenna. The port's resistance was set to be the real part of the ASIC's impedance while the chip capacitance was assigned to the lumped component's capacitance.

The prototype transfer tattoo tag [9] developed at the University of Kent was chosen as the tag to be used as a basis for the studies conducted in this work.

The schematic for the simulated tag is shown in Fig 3.2.

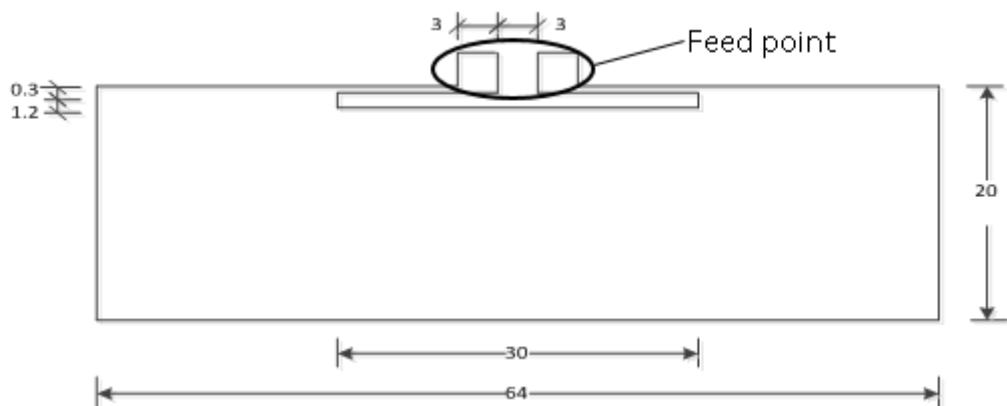


Fig. 3.2 Schematic for Transfer Tattoo Tag (Dimensions in mm)

Being a slot antenna, the electromagnetic radiation in the antenna is due to magnetic currents as a result of the strong electric fields across the slot. Fringing of the field to the human body is minimized as the field lies in the slot. These properties account for the good performance the slot antenna has on-body. Also, the conducting patch around the slot means that the current is not confined to the edges of the slot but rather spread out across the metal sheet, Fig 3.3, improving the radiation efficiency [10]. This makes

more energy available to activate the RFID IC and increases the backscattered signal which translates to improved performance in harsh electromagnetic environments.

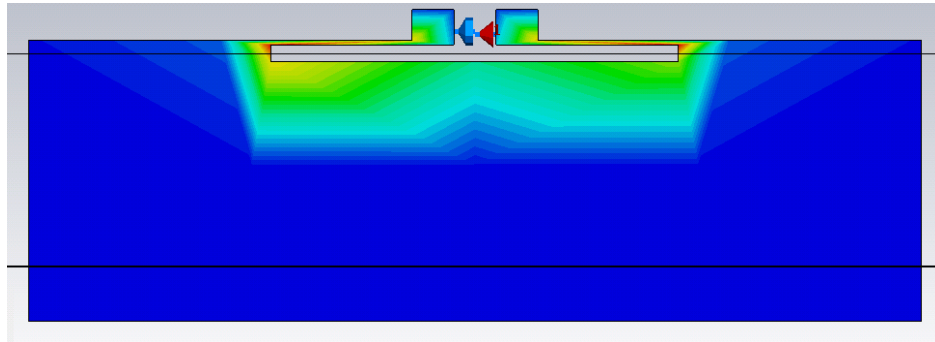


Fig. 3.3 Simulated Surface Current on Transfer Tattoo Tag

The antenna was simulated to have a conjugate match with the NXP G2X chip at the EU UHF resonance frequency of the 867 MHz, Fig 3.4.

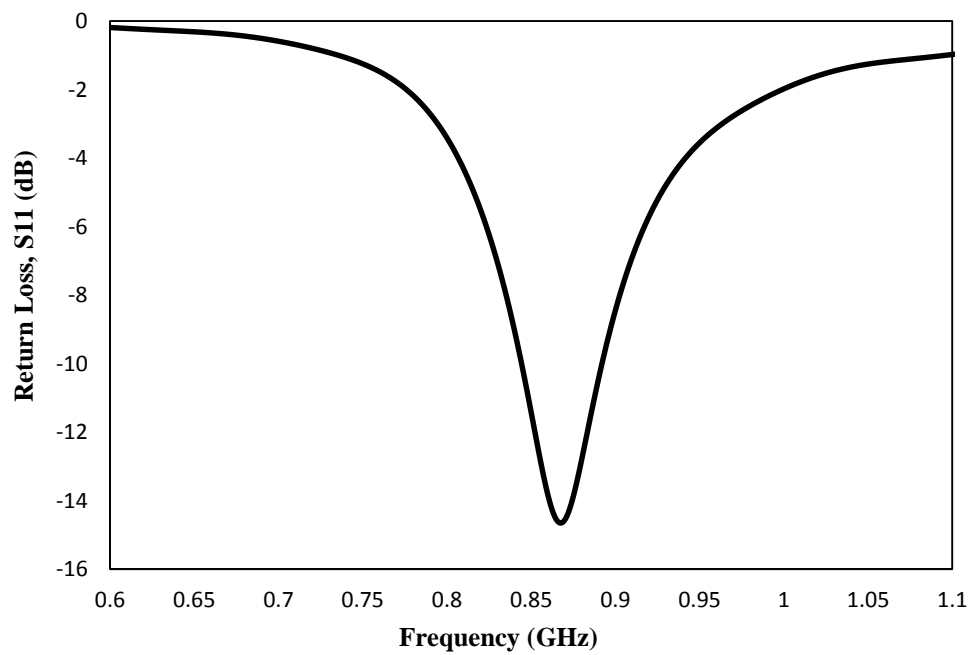


Fig. 3.4 Simulated Return Loss for Transfer Tattoo Tag on Human Phantom

The 3D plot for the gain of the transfer tattoo tag on the human phantom is shown in Fig 3.5. The gain of the tag at the simulated frequency (867 MHz) is -9.67 dB. The tag has low efficiency (-13.96 dB) which indicates the negative effect of body on the tag.

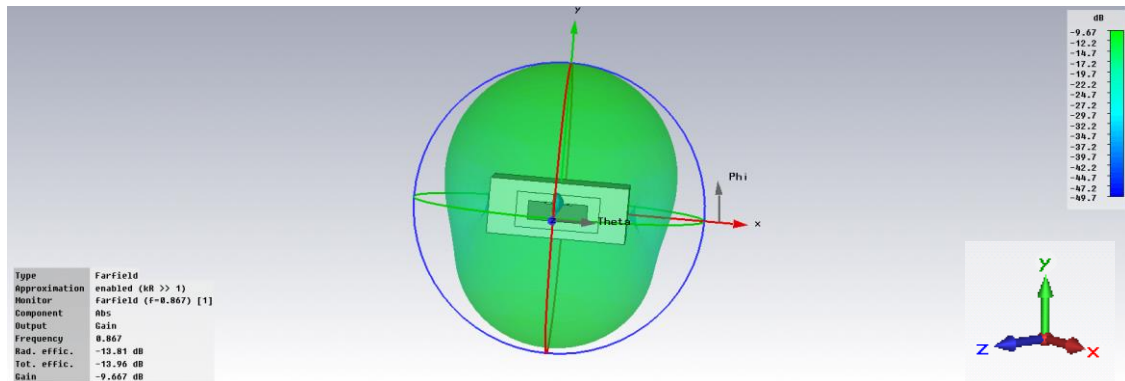


Fig. 3.5 3D Plot of Farfield Gain for Transfer Tattoo Tag on Phantom

Figures 3.6 and 3.7 show the elevation and azimuth polar plots of the tag directivity. The transfer tattoo tag when placed on the human phantom has a directivity of 4 dBi. In the elevation plane, the tag has a 3 dB angular width of 118° while this is 95° in the azimuth plane.

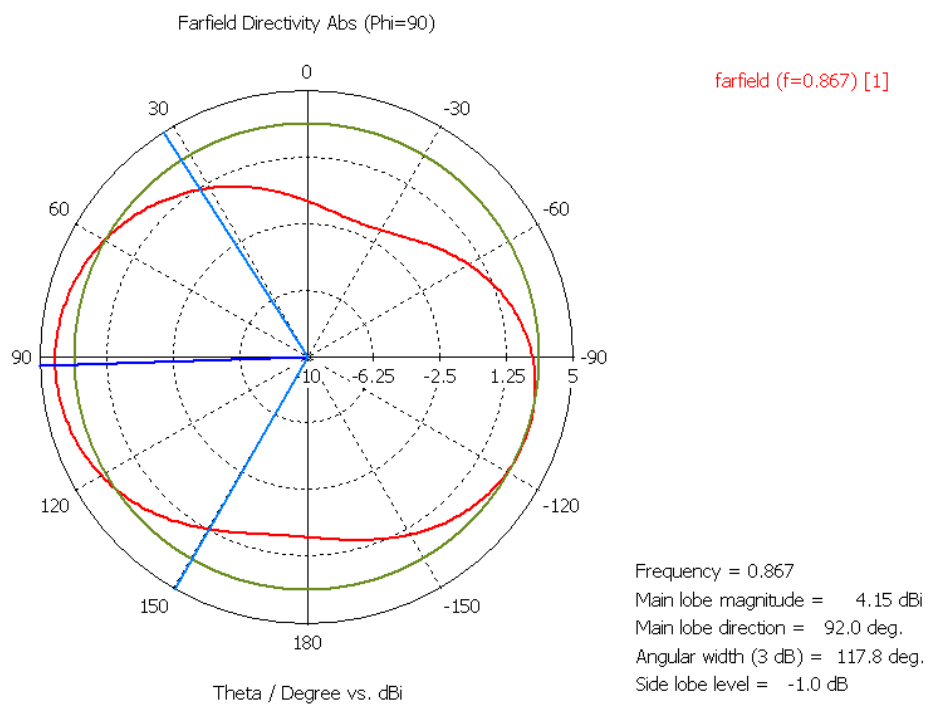


Fig. 3.6 Simulated Transfer Tattoo Tag E_θ component elevation (y-z) plane

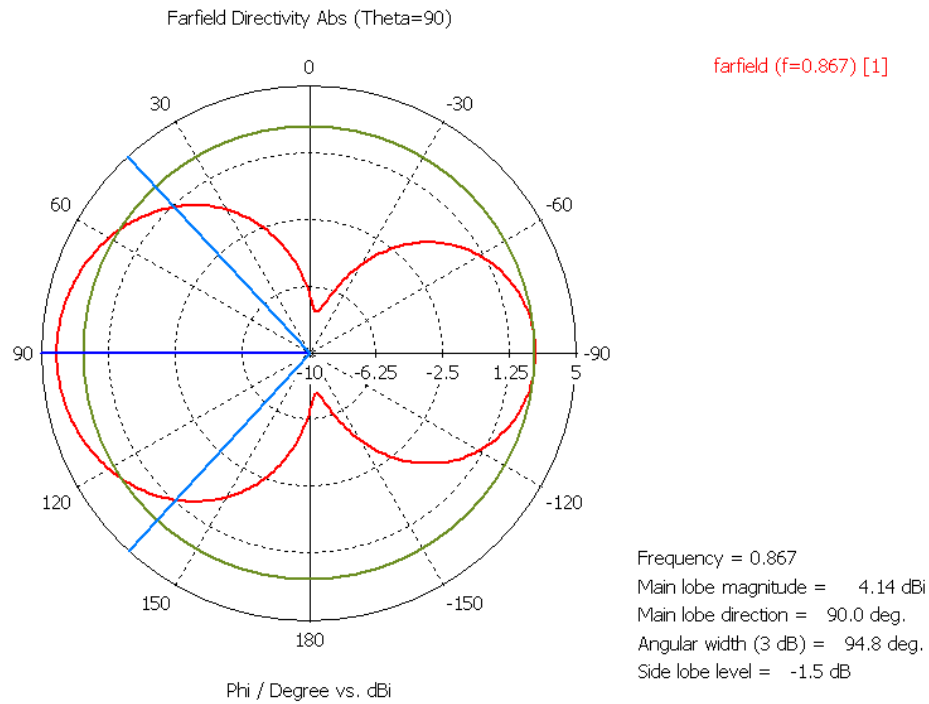


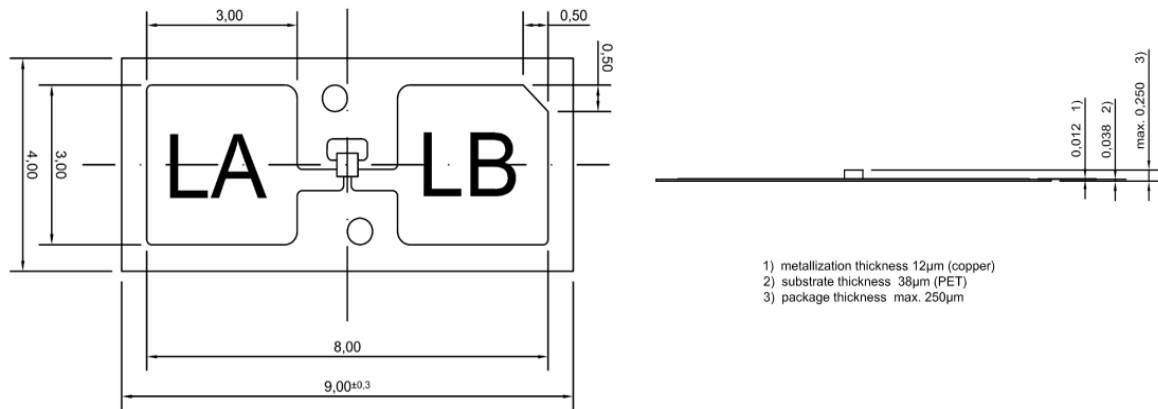
Fig. 3.7 Simulated Transfer Tattoo Tag E_{ϕ} component azimuth (x-z) plane

3.3 Tag Fabrication

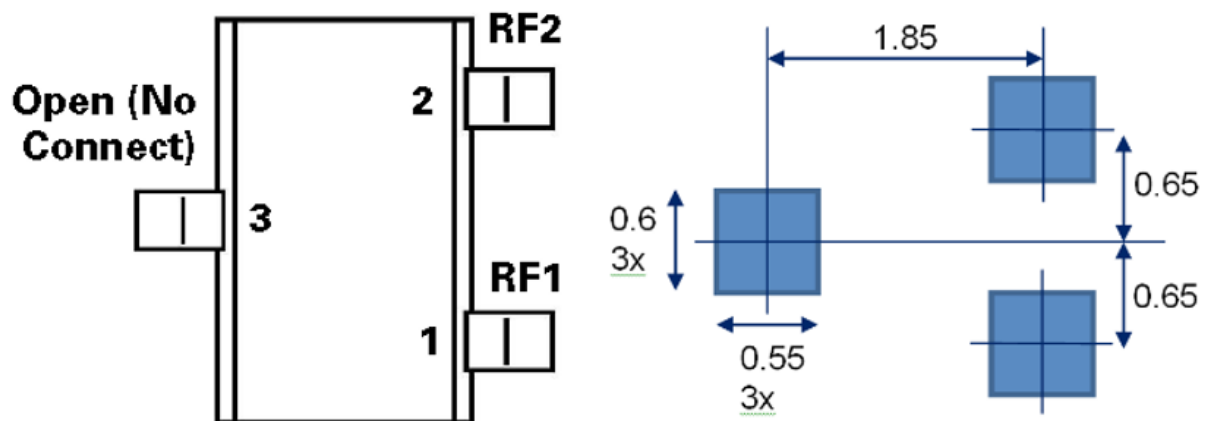
3.3.1 Selection of RFID Chip

Two chips were used for this project. The first which was used for the epidermal RFID tags is the NXP G2X chip. This is an EPC global Class 1 Generation 2 UHF passive RFID chip. It is suitable for use in conditions where ordinary tag operation over several metres and high anti-collision rates are required [11]. Additionally, with a thickness of just 250 μm , this chip suits the low profile sort for the epidermal RFID tag. Also to be considered is the mounting of the chip on the tags. As the deposited ink and transfer tattoo substrate would not be able to withstand the high temperature of soldering, using a chip with straps would enable the use of other means of attachment such as conductive glue and adhesive tape. The manufacturer stated impedance is $14.8-j128\Omega$ with an input capacitance of 1.35pF. The schematic of the chip is shown in Fig 3.8(a). The second ASIC which was used for the sticking plaster tag described in Chapter 6, is a Higgs-4 chip from Alien Technologies [12]. It is also an EPC global Class 1 Generation 2 UHF passive RFID chip with a thickness of about 1 mm. It can either be

attached to an antenna with a conductive glue or by soldering. The schematic of the chip is shown in Fig 3.8 (b).



(a)



(b)

Fig. 3.8 Schematic of showing tag dimensions of (a) NXP G2X chip [11] and (b) Higgs-4 chip [12]. All dimensions in mm

3.3.2 Copper Prototype

Initial fabrication of the tags was done using conventional wet etching of a copper clad Mylar (polyethylene terephthalate (PET)) sheet. This provided a platform to test the performance of the tag in accordance with indications by simulation. The copper clad Mylar sheet had a thickness of about $70\mu\text{m}$. The choice of this thickness is because of the flexibility it provides and also its close resemblance to the transfer tattoo paper

which was the primary substrate used for this work. The photoresist developer used for the etched samples was Potassium Carbonate (K_2CO_3) while the acid used was Iron (III) Chloride (Fe_3Cl). Short intervals were used during exposure of the sample to the acid in order to avoid over etching which could easily affect the thin feedlines of the tag. The attachment of the RFID chip to the antenna was done with the aid of an adhesive tape. Proper contact between the straps of the chip and the antenna ports was ensured and air gaps leading to increased capacitance between the two surfaces were also avoided. This was done by making several depressions on the point of contact between the ASIC strap and the antenna ports. The tag measurement process will be described in Section 3.4. The measured copper prototype tag Read Range is shown in Fig 3.9. The tag was mounted on an arm and the maximum read range can be seen to coincide with the EU UHF RFID frequency of 867MHz.

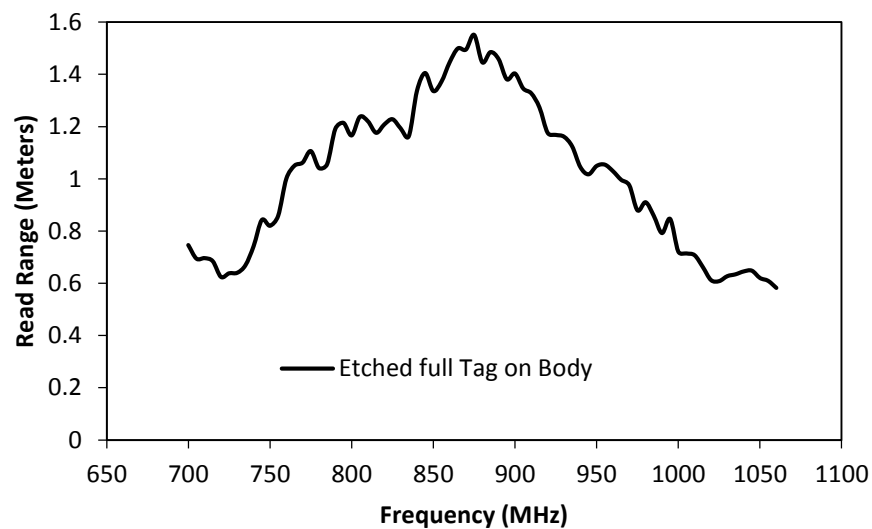


Fig. 3.9 Read Range Measurement of Etched Copper Tag on Arm

3.3.3 Inkjet Printing of Tags

For the inkjet printed fabrication of the transfer tattoo tags, the Dimatix DMP-2831 Materials Printing System [13], Fig 3.10, was used throughout this work. All fabrication (printing and sintering) was done by the Organic Materials Innovation Center (OMIC) located in the School of Chemistry at the University of Manchester who were collaborators for this project.

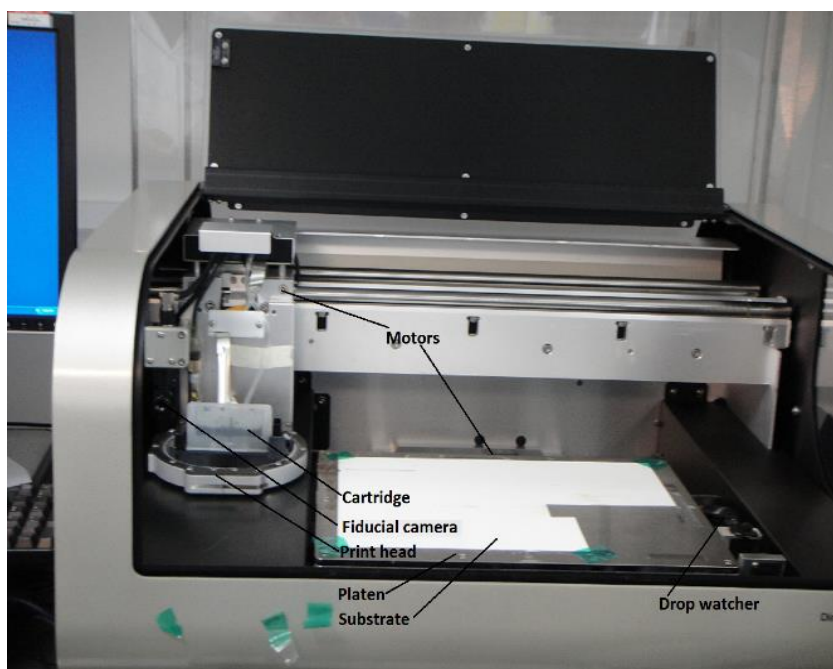


Fig. 3.10 Dimatix DMP-2831 Materials Printing System

This printer allows the deposition of fluidic materials on a 210mm x 315mm or A4 substrate and handles substrates up to 25 mm thick with an adjustable height. The printer is equipped with a disposable piezo inkjet cartridge, Fig 3.11, with 16 linearly placed nozzles separated by 254 μm with a typical drop size of 1 and 10pl. Each cartridge has a usable ink capacity of up to 1.5ml and is user-fillable. The cartridge also has a built-in heater which is capable of heating a fluid (printing solution) to a maximum temperature of 70° to enable controlled jetting of viscous fluids. To hold the substrates in place, the printer is fitted with a vacuum platen whose temperature can be adjusted up to 60°C. With a pattern editor program available, the DMP-2831 offers a variety of patterns. In addition to this, a waveform editor and a drop-watch camera system allows manipulation of the electronic pulses to the piezo jetting device for optimization of the drop characteristics as it is ejected from the nozzle. This system

enables easy printing of structures and samples for process verification and prototype creation



Fig. 3.11 Dimatix Printer Cartridge

The conductive ink used for this work is the 736465 ALDRICH from Sigma-Aldrich (Silverjet DGP-40LT-15C) [14]. This is a silver dispersion nanoparticle ink. It has a concentration of 30-35 wt. % in triethylene glycol monomethyl ether with a specific resistivity of $11\mu\Omega\text{-cm}$ and a surface tension of 35-40dyn/cm. The silver particles have a size of about 50 nm or less. The ideal curing condition is between $120^{\circ}\text{C} - 150^{\circ}\text{C}$ for 30 – 60 mins [15]. This ink has been formulated for printing on plastic films which makes it ideal for the transfer tattoo paper which has a thin layer of polymer.

The inkjet transfer tattoo paper which was used as the substrate for this work was supplied by Crafty Computer Paper [16]. The polymer coated transfer tattoo paper comprises a $26\mu\text{m}$ thick ink-receiving layer which is non-porous. Its primary constitution is polyvinyl alcohol (PVA) which sets a 135°C limit sintering temperature on this paper. The schematic and scanning electron microscopy (SEM) images of the cross-section of the transfer tattoo paper is shown with a deposit of a single layer of the conductive ink in Fig 3.12 [15].

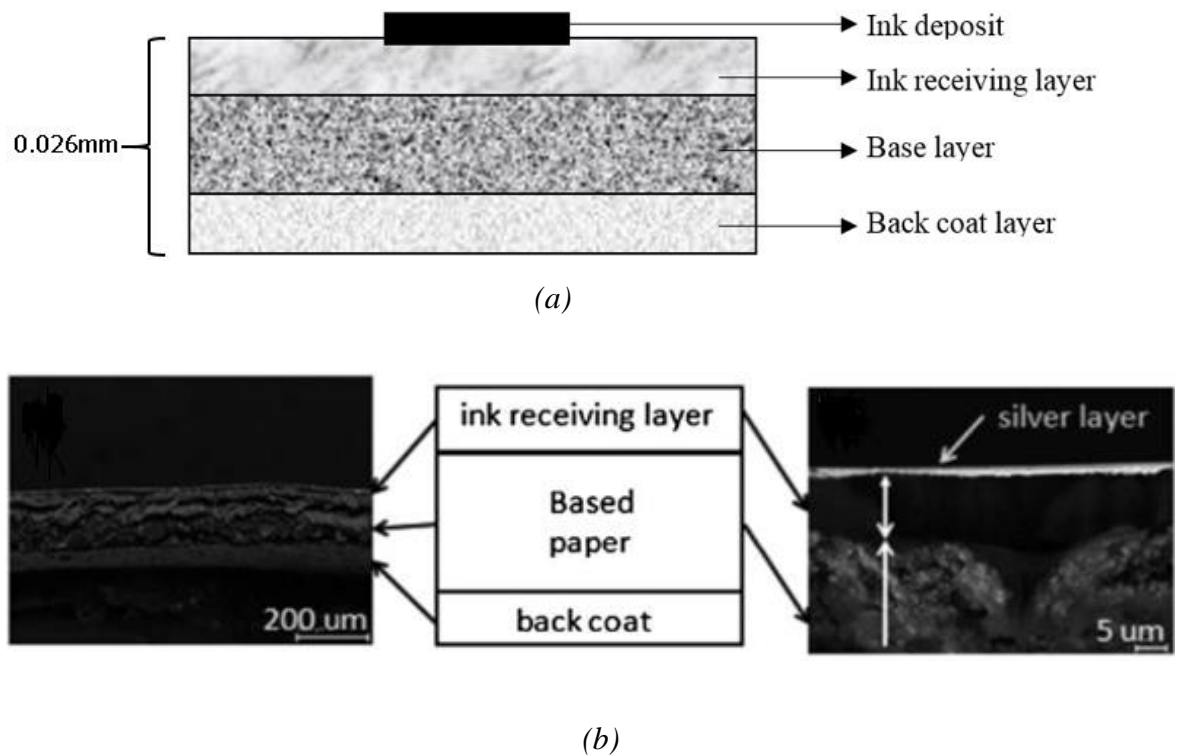


Fig. 3.12 Transfer Tattoo Paper (a) schematic of transfer tattoo paper (b) cross-sectional SEM imaging of transfer tattoo paper [15]

Before printing, the tattoo paper surface was sprayed with a jet of air to remove impurities. Additionally, the paper was given an ozone (O_3) treatment in order to adjust its surface tension. This was done in order to enhance the interaction between the paper and the ink in order to improve print quality, reduce printing defects and reduce the coffee stain effect. This will be discussed in Chapter 5.

As will be seen in Chapter 4, the printing of the samples can be done with different drop spacing. This is usually done in order to reduce the volume of ink used. The drop spacing is set before the start of the printing. The platen temperature is also set to be between 40°C and 60°C . It is important to ensure that the platen is at a suitable temperature since this helps to ensure printing of good quality samples. However, it is noteworthy that when the platen temperature is not properly set, it leads to the faster evaporation of the ink solvent at the substrate – nozzle interface resulting in the clogging of the cartridge nozzles.

For a single layer print, only a single printing routine is required. However, in the case of multiple layers, each deposited layer is allowed to dry before the next layer is

deposited on top of it. This will help in better definition of the details of the printed samples as well as with the even distribution of the ink.

With the ink deposited on the transfer paper, there is need to expose the sample to an elevated temperature. This has two roles:

- i.) To facilitate the evaporation of the solvent (carrier) in which the conductive silver nano-particles are suspended (preventing the agglomeration of the particles) and
- ii.) To enable the sintering of the silver nano-particles which is the formation of ‘necks’ between the particles. This is necessary because although the evaporation of the solvent makes the particles to come close together, conductivity is only possible when there is metallic contact between the particles [17].

The sintering process is illustrated in Fig 3.13.

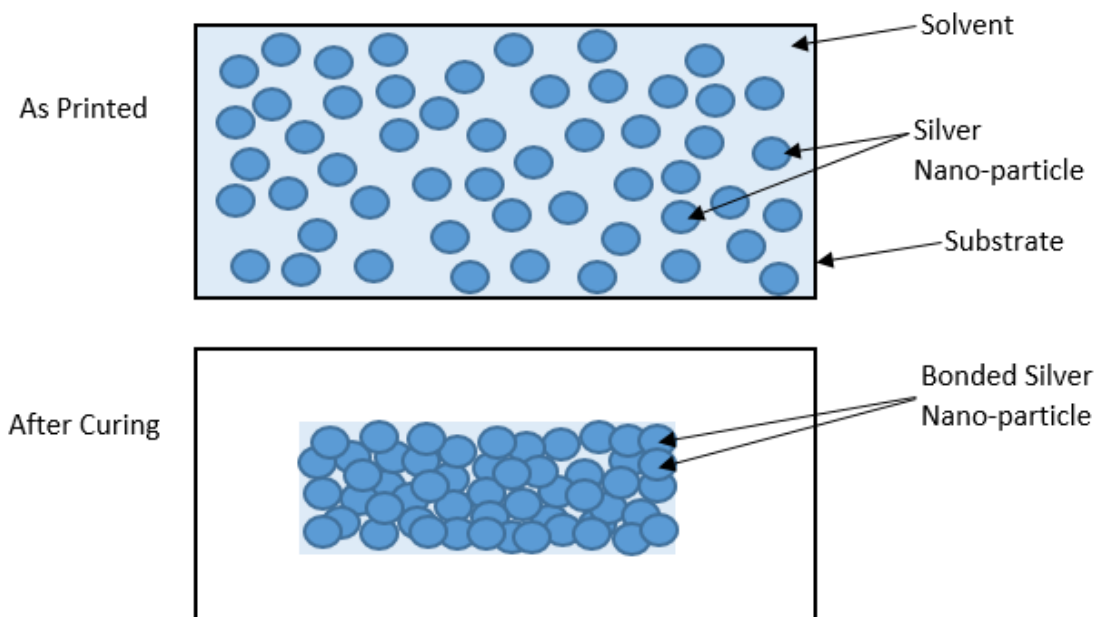


Fig. 3.13 Sintering of Deposited Conductive Ink

The sintering of the ink is done at 135°C for 30 minutes in a convection oven. This temperature, as earlier stated, is the limit placed by the transfer tattoo paper beyond

which it will be severely deformed. Sintering beyond 30 minutes has also been shown to lead to the degradation of the transfer tattoo paper [15].

The mounting procedure of the transfer tattoo tag on the skin will be introduced in Chapter 4.

Although inkjet printing provides a good means for the fabrication of transfer tattoo tags, it also has some limitations and challenges which must be acknowledged. Some of these limitations are summarized as follows:

- Difficulties with printing resolution
- Substrate limitations
- Conductor skin depth losses

The printing resolution of inkjet printing is of concern especially when the performance of the printed sample is heavily dependent on the dimensions of some of its fine resolution parts. Although a printer with high resolution can be used, there is the issue of the spreading of the conductive ink during drying which can lead to up to 25% increase in the width of a printed line [15]. There is the possibility of this increase in line width could lead to slight variations in the resonance frequency of the tag. Although this is a minor issue, the disparities in the inkjet printing process and sintering conditions may lead to slight differences in the performance of two seemingly identical tags. This is not of major concern since it does not present a major inconsistency in tag performance between the samples. It is also good practice to create wideband tags which will still operate even when there is a reduction in the centre frequency due to dielectric loading. Tags should also be designed with an appropriate resolution to suit the printing capabilities and tolerances.

The use of inkjet printing on some substrates may also not be feasible due to the physical properties of the substrate. An example of this the temperature tolerance of a substrate. Some substrates may not be able to withstand the high temperature at which the curing of the printed ink is done. Another factor is the porosity of the substrate. A porous substrate would entail the deposited conductive ink being absorbed into the substrate. In some cases, this can be overcome by saturating the substrate with the conductive ink [18]. This is a very wasteful approach for expensive ink.

Skin depth is defined as the depth below the surface of a conductor at which the amplitude of an incident electric field has decreased by a factor $1/e$ [19]. It gives an indication of how deeply into a conductor a high frequency electromagnetic field will penetrate and it has an inverse proportional relationship with frequency. It has been reported in [15] that the skin depth for a printed sample at the UHF RFID band was $3.7 \mu\text{m}$. This thickness is more than that of a single layer of conductive ink ($\approx 1 \mu\text{m}$), and about the same as 2 layers, while being about 67% of a 3 layer print, Fig 3.14. Bearing this in mind, it is important to have at least two layers of conductive ink in the printed samples in order to satisfy skin depth requirements otherwise an increase in the antenna structure losses due to very small thickness will decrease the antenna radiation efficiency [20].

Despite the factors noted above, none severely affected the performance of the tags and satisfactory read range was obtained for tags that had at least two layers of conductive ink deposited during fabrication.

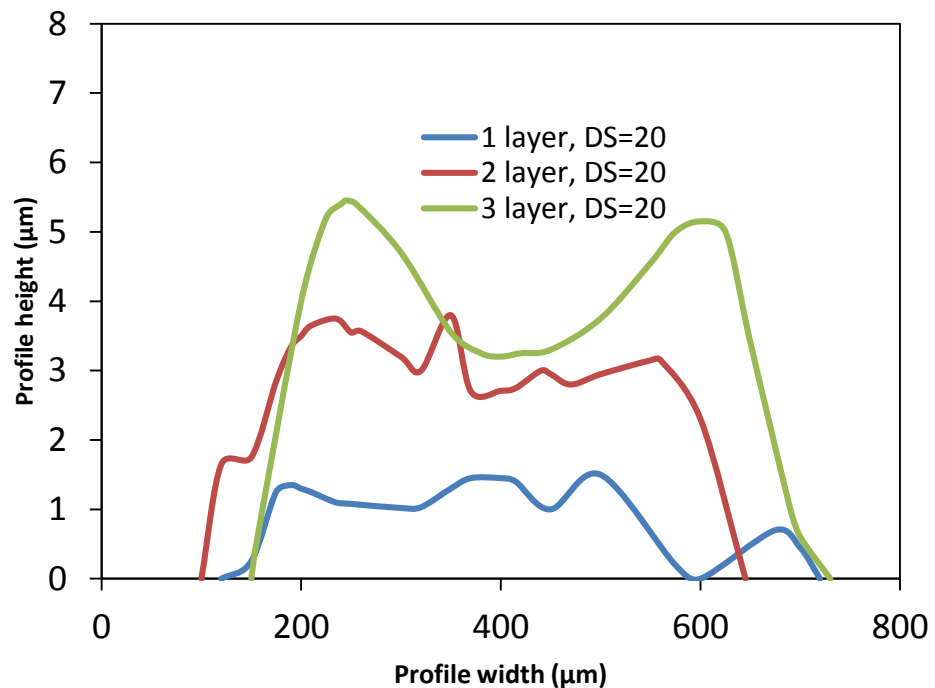


Fig. 3.14 Profile Measurement of Inkjet-Printed Tags

3.4 Tag Measurement

The tag performance measurements for this project was carried out using the Voyantic Tagformance lite UHF RFID measurement system [21]. The measurement unit is actually a network analyser which has been optimized for RFID measurements. It can be used for evaluating the performance and functionality of EPC class 1 Gen2 RFID systems. The equipment can also be used to measure tag sensitivity, test and verify tag protocol, study environmental interference, study forward and return link balance and system level read range and analyse tag population behaviour. The device is connected via USB to a PC that has the measurement software installed in it. The function of this software is the generation of the waveform which is sent to the tag for interrogation as well as the actual measurements. The reader has an operating frequency of 700MHz – 1200MHz and is fitted with a linearly polarized antenna. The carrier specifications of the Voyantic system are shown in Table 3.1

TABLE 3.1 VOYANTIC TAGFORMANCE LITE SPECIFICATIONS

Parameter	TYPICAL VALUE	UNIT
Frequency Range (Standard)	800 to 1000	MHz
Frequency Range (Wideband)	700 to 1200	MHz
Frequency Resolution	100	kHz
Frequency Accuracy	+/- 10	ppm
Output Power	0 to +27	dBm
Output Power Resolution	+/- 0.1	dB
Output Power abs. Accuracy	+/- 1	dB
Output Power Uniformity	+/- 0.5	dB
Output Impedance	50	Ω
Sensitivity	-75	dBm

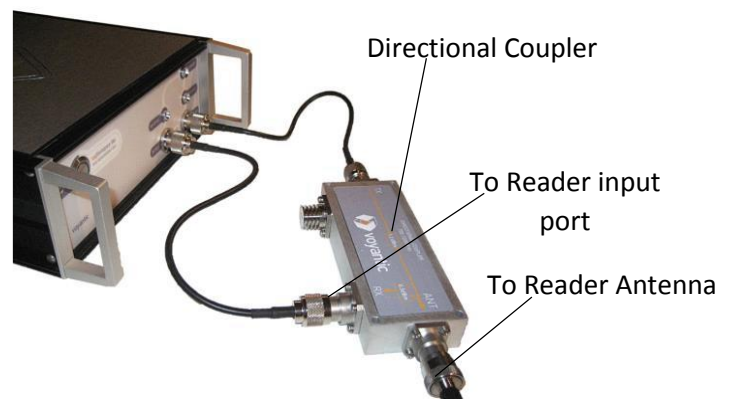
The calibration of the system before measurements was done with a reference UHF RFID tag at a distance of 35cm measured with a tape. Manufacturer instructions recommend a distance of 35 – 50 cm for this calibration. While a wider distance would reduce the signal-to-noise ratio and increase the effects of radio reflections, a distance

of less than 20 cm would lead to measurements being in the reader antenna's near field which would cause inaccuracies. After calibration, it is necessary to measure the tag at exactly the same point as the reference tag as small variations in tag location would affect the measurement. To minimize movements during measurements, the arm was supported by a plastic pole. A minimum clear space distance of 2m was given around the measurement area in order to reduce reflections. For this work, the equipment was used to measure the backscattered power (the received RF signal power of the tag backscatter measured at the device IN port), read range (the maximum distance the reader can receive backscattered power from the tag) and the transmitted power (the power sent to the tag by the reader).

The Voyantic Tagformance equipment is shown in Fig 3.15 while Fig 3.16 shows a tag being measured.



(a)



(b)



(c)

Fig. 3.15 (a) Tagformance lite unit (b) directional coupler (c) wideband antenna

A directional coupler is used inbetween the Tagformance lite unit and the reader antenna to isolate the transmitted signal from the received signal. For this coupler, there is a 1.2dB insertion loss from reader transmitter to reader antenna while this is 6.5db from reader antenna to reader receiver.



Fig. 3.16 Transfer Tattoo Tag performance measurement setup

The operation of the Tagformance lite unit is as follows: 1) the system measured the backscattered power from the tag under test. 2) The transmitted power is used to determine the threshold power of the chip as a function of frequency. 3) The read range can then be extrapolated by the equipment using Friis equation since the cable and other losses have been subtracted during calibration.

The influence of the electrical properties of the skin and different body forms on the functioning of the epidermal RFID tattoo tags was also considered during this work. This aided in the understanding of the variations in read range of the tags observed during measurement on different individuals. In order to achieve this, the conductivity and permittivity of the area on the forearm of 10 individuals were measured. The conductivity and permittivity measurements were carried out using the Dielectric Assessment Kit (DAK) by Schmid & Partner Engineering AG [22]. This is a high precision dielectric parameter (permittivity, loss tangent and conductivity) measurement system. It can be used in the electronics, food, medical and chemical industries for the measurement of solids, semi-solids and liquids for frequencies from

200MHz – 20GHz. The dielectric materials under tests are calculated from the reflection coefficient at the probe-material interface. Owing to this, measurement accuracy is sensitive to change in the phase or amplitude of the incident and reflected signals along the cable and probe. It is necessary to avoid contacts that may change the cable or probe positions during measurements. The system used the open-close-load system of calibration where open is the air, close (short) is a metallic strip and load is a material with known dielectric constant. For this work, water was used for the load calibration. The calibration normalizes the phase changes and magnitude of the probe and cable so that the reflection coefficient normalized to the reference plane at the flange of the probe is measured by the VNA. The presence of the flange at the end of the probe ensures that the ground plane is large enough to be considered an infinite ground to the electromagnetic fields that radiate from the probe end. The measured reflection coefficient is used to derive the permittivity of the material being tested by the DAK software with the method presented in [23].

The applicable range of frequencies and dielectric properties which can be accurately measured is determined by the size of the probe which should be such that the electromagnetic fields from the probe end are coupled to the sample being measured without appreciable radiation into the sample. If the probe is very small compared to the wavelength in the sample, it will not couple fields sufficiently. This will make it appear as an open circuit irrespective of the sample being measured. On the other hand, a very large probe would lead to radiation into the sample which would lead to a reduction in the sensitivity of the measurement.

The Dielectric Assessment Kit and measurement set up are shown in Fig. 3.17.



Fig. 3.17 Measurement of Skin Dielectric Parameters with the DAK

The diversity study of the skin mounted RFID tags discussed in Chapter 6 was conducted with a VICON motion capture system [24]. The systems consists of 8 synchronized infrared cameras which enables the accurate location of the tags and the reader by tracking the reflective markers placed on them. Based on these locations, the x, y, z coordinates of the markers are generated by the motion capture software. The coordinates can then be used to calculate the angles between the RFID reader and the tags using trigonometry.

3.5 Summary

This chapter has discussed the transfer tattoo tag presented in this work. The CST microwave studio simulator used for modelling the tag has been presented. This includes the selection of the appropriate solver for UHF RFID tags. The process the simulator uses to solve the models as well as settings chosen to ensure accurate simulation results were also presented. The multi-layered phantom used to model the human body was also introduced in this chapter.

Also introduced in this chapter was the fabrication of the transfer tattoo tags. The initial prototyping of the sample with the wet etching of a copper clad Mylar sheet was discussed. The inkjet printing of the transfer tattoo tags was also introduced in this chapter. This includes the printer that was used for the fabrication of the tags in this work, the printing process, the transfer tattoo paper used and details of the conductive ink used. The ideal sintering temperature of 135° C and sintering time of 30 minutes was also identified. This is due to the thermal limitations of the substrate. Some limitations of inkjet printing was also discussed in relation to transfer tattoo tags such as limited substrate selection and issues with printing resolution.

The equipment used throughout this work were also presented in this chapter. This includes the Voyantic Tagformance kit, the DAK and the Vicon motion capture system. The look into the equipment covered their mode of operation, calibration schemes and steps taken to ensure accurate measurements results.

References

- [1] P. V. Nikitin and K. V. S. Rao, "Theory and measurement of backscattering from RFID tags," *IEEE Antennas Propag. Mag.*, vol. 48, no. 6, pp. 212–218, 2006.
- [2] J. Virtanen and T. Björninen, "The effect of conductor thickness in passive inkjet printed RFID tags," *IEEE Antennas ...*, no. 1, pp. 1–4, 2010.
- [3] E. Perret, S. Tedjini, and R. S. Nair, "Design of antennas for UHF RFID tags," *Proc. IEEE*, vol. 100, no. 7, pp. 2330–2340, 2012.
- [4] K. Koski, T. Björninen, L. Sydänheimo, L. Ukkonen, and Y. Rahmat-samii, "A New Approach and Analysis of Modeling the Human Body in RFID-Enabled Body-Centric Wireless Systems," *Int. J. Antennas Propag.*, vol. 2014, 2014.
- [5] T. Kellomäki and L. Ukkonen, "Design approaches for bodyworn RFID Tags," *2010 3rd Int. Symp. Appl. Sci. Biomed. Commun. Technol. ISABEL 2010*, 2010.
- [6] CST, "CST MICROWAVE STUDIO." [Online]. Available: <https://www.cst.com/Products/CSTMWS>. [Accessed: 14-Oct-2014].
- [7] "CST MICROWAVE STUDIO® - High frequency 3D electromagnetic field simulation software - Time Domain, Transient Solver." [Online]. Available: <https://www.cst.com/Products/CSTMws/TransientSolver>. [Accessed: 18-Nov-2015].
- [8] "OET -- Radio Frequency Safety." [Online]. Available: <http://transition.fcc.gov/oet/rfsafety/dielectric.html>. [Accessed: 05-Oct-2015].
- [9] M. A. Ziai, J. C. Batchelor, and S. Member, "Temporary On-Skin Passive UHF RFID Transfer Tag," *IEEE Trans. Antennas Propag.*, vol. 59, no. 10, pp. 3565–3571, 2011.
- [10] R. J. M. John D. Kraus, *Antennas For All Applications*, 3rd ed. McGraw-Hill Publishing, 2002.
- [11] NXP, "SL3ICS1002/1202 Product Data Sheet," 2011. [Online]. Available: http://www.nxp.com/documents/data_sheet/SL3ICS1002_1202_139036.pdf. [Accessed: 19-Jan-2015].
- [12] "Higgs Draft IC Specification - Alien-Technology-Higgs-4-IC-Datasheet.pdf." [Online]. Available: <http://www.aliantechnology.com/wp-content/uploads/Alien-Technology-Higgs-4-IC-Datasheet.pdf>. [Accessed: 06-

Oct-2015].

- [13] Dimatix-Fujifilm Inc., “Dimatix Materials Printer DMP-2831 | Deposition Products | Industrial Inkjet Printheads | Fujifilm USA.” [Online]. Available: http://www.fujifilmusa.com/products/industrial_inkjet_printheads/deposition-products/dmp-2800/#overview. [Accessed: 28-Sep-2015].
- [14] Sigma-Aldrich, “Silver, dispersion nanoparticle, 30-35 wt. % in triethylene glycol monomethyl ether, spec. resistivity 11 $\mu\Omega$ -cm, for printing on plastic films | Sigma-Aldrich.” [Online]. Available: <http://www.sigmaaldrich.com/catalog/product/aldrich/736465?lang=en®ion=GB>. [Accessed: 28-Sep-2015].
- [15] V. Sanchez-Romaguera, M. A. Ziai, D. Oyeka, S. Barbosa, J. S. R. Wheeler, J. C. Batchelor, E. A. Parker, and S. G. Yeates, “Towards inkjet-printed low cost passive UHF RFID skin mounted tattoo paper tags based on silver nanoparticle inks,” *J. Mater. Chem. C*, vol. 1, no. 39, pp. 6395–6402, 2013.
- [16] Crafty, “Make your own tattoos and body art using your Inkjet printer.” [Online]. Available: http://www.craftycomputerpaper.co.uk/-Laser-Tattoo-Paper_CPL214I.htm. [Accessed: 29-Sep-2015].
- [17] J. Perelaer and U. Schubert, “Inkjet printing and alternative sintering of narrow conductive tracks on flexible substrates for plastic electronic applications,” in *Radio Frequency Identification Fundamentals and Applications Design methods and Solutions*, no. February, 2010, pp. 265–286.
- [18] J. Virtanen, “Inkjet-Printed UHF RFID Tags on Renewable Materials,” *Adv. Internet Things*, vol. 02, no. 04, pp. 79–85, 2012.
- [19] C. A. Balanis, *Advanced Engineering Electromagnetics*. New York: Wiley, 1989.
- [20] S. Merilampi and T. Bjorninen, “The effect of conductive ink layer thickness on the functioning of printed UHF RFID antennas,” *Proc. ...*, vol. 98, no. 9, pp. 1610–1619, 2010.
- [21] “Tagformance lite | Voyantic.” [Online]. Available: <https://voyantic.com/tagformance>. [Accessed: 30-Sep-2015].
- [22] “RF conductivity measurement | dielectric probe | dielectric measurement | dielectric spectroscopy | permittivity probe | loss tangent | dielectric properties | dielectric probe | complex permittivity probe | permittivity measurement | dielectric par » SPE.” [Online]. Available: <http://www.speag.com/products/dak/dielectric-measurements/>. [Accessed: 02-

Oct-2015].

- [23] W. J. Ellison and J.-M. Moreau, “Open-Ended Coaxial Probe: Model Limitations,” *Instrumentation and Measurement, IEEE Transactions on*, vol. 57, no. 9. pp. 1984–1991, 2008.
- [24] “Homepage | VICON.” [Online]. Available: <http://www.vicon.com/>. [Accessed: 05-Oct-2015].

CHAPTER 4

INKJET PRINTED EPIDERMAL RFID TAGS

This chapter considers the printing of epidermal transfer tattoo tags with a focus on the printing parameters and considerations including the effect of the number of deposited conductive ink layers on the performance. Tag performance on different individuals and placement on different parts of the body is also examined. Techniques for ink usage reduction are also presented in this chapter.

4.1 Introduction

The utilization of RFID technology for the location tracking of people and their activities is widely reported in the literature. This includes tracking in secure locations, monitoring and access control to restricted areas. RFID technology has also been used for making secure payments for transactions [1], [2] and tickets for transportation systems [3]. In these stated scenarios, the tags are rarely used directly on body instead being embedded in other items (e.g. in ID cards and wrist bands for tracking and access restriction, and in bank cards and mobile phones for payments). The attraction of RFID tags for direct use on body arises because of the convenience and potential interface with other on-body devices. However, body mounted tags are preferably non-invasive and it is particularly attractive for tags to be temporary rather than RFID chips that are implanted under the skin. Unlike wristbands, body mounting also offers an additional layer of security because tags cannot easily be transferred from one person to another.

Further to the uses mentioned above, there is potential for growth in the application of cheap and readily available tags. In order to achieve this low cost objective, there has been research into various means of fabrication [4], [5] and [6]. Other means of lowering the cost of tags, for instance by appropriate substrate selection have also been examined [7], [8], [9] and [10]. One such means for fabrication of RFID tags is inkjet printing technology which has been gaining popularity in recent years. This is because of unique features that enable low cost fabrication including the possibility of multilayer deposition of identical or different fluids with unique spatial resolution, the ability to make digitally defined patterns without masks as required by many other printing methods, and thus making it a rapid prototyping technology. Also inkjet printing offers compatibility with ecological and porous substrates like paper which could not be used with corrosive etching chemicals.

Presently, the possibility of using inkjet fabricated RFID tags directly on body has not been exploited in depth as most tags are separated from the body by a dielectric material or an air gap [11], [12] and [13].

The purpose of this chapter is to present an epidermal RFID tag printed on a transfer tattoo paper with a very low profile of a few microns. The use of inkjet printing affords flexibility of the tag hence causing minimal discomfort when attached to the body.

The tag can also be attached to most parts of the body while maintaining appreciable read range. The work presented in this chapter shows the use of inkjet printing as a digital fabrication tool for the cost effective manufacture of RFID tags on low-cost flexible porous substrates [14], and the effect on tag performance of trimming off areas of low current density on the tags in order to reduce the volume of ink used in tag fabrication is presented [15]. Also ink volume reduction is achieved by the use of gridded designs [16].

The layout of this chapter is as follows: Section 4.2 presents general tag printing conditions and considerations. In Section 4.3 the effect of the layer thickness of the deposited conductive ink is discussed with some simulated and measurement studies presented. Section 4.4 examines the performance of the tag when used on different people with the focus on the variations in the measured dielectric properties on the different individuals. In Section 4.5, the effect of the location of the tag on the body in terms of tag read range is examined. Section 4.6 looks at the various techniques that can be used to minimize the amount of ink used in tag fabrication as well as comparison of how they perform in relation to each other. The chapter is concluded in Section 4.7.

4.2 Inkjet Printing of Tattoo RFID Tags

The setup for the inkjet printing of the tags is as stated in Chapter 3, where in order for an optimal print, a 20 μm drop spacing was used for fabrication. This was chosen as results indicated this drop spacing achieves a balance between good performance and volume of ink. This is important because smaller drop spacing, hence increase in conductive ink volume, does not always lead to an appreciable improvement in tag performance but does lead to increased fabrication costs [17]. This is in contrast to one of the main objectives of this work which is low cost of production. The drop spacing is the centre-to-centre distance of two consecutive ink drops (Fig. 4.1). Fig. 4.2 shows the effect of sintering time on the obtainable resistivity of the tattoo tags for 15 μm and 20 μm drop spacing for single and double layer of deposited conductive ink. Resistivity measurements were done with a 4-point probe on 1cm x 1cm squares and

0.8mm x 0.5mm lines. Measurements were obtained by collaborators at the Organic Materials Innovation Center (OMIC), University of Manchester and reported in [18].

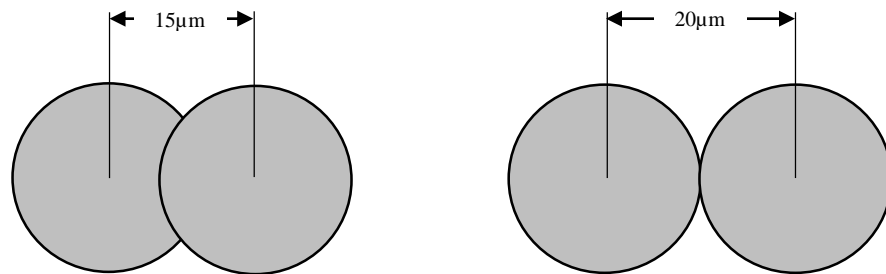


Fig. 4.1 Drop Spacing of 15µm and 20µm

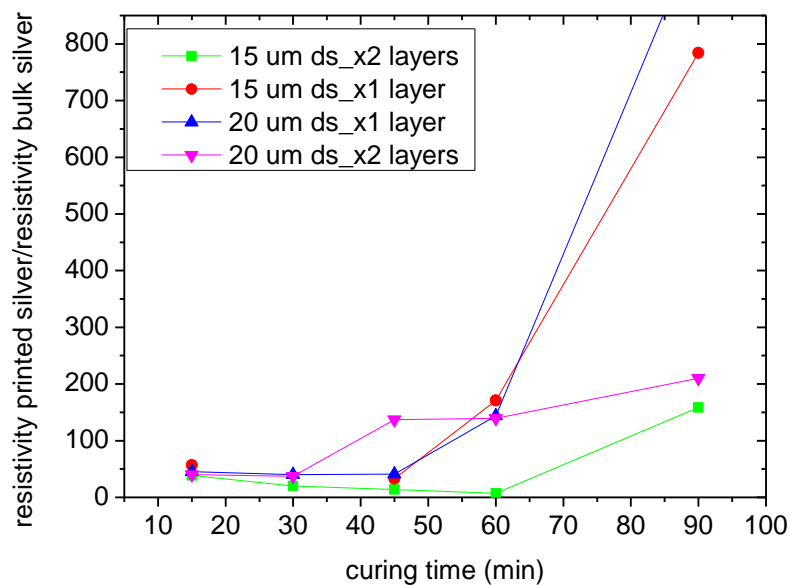


Fig. 4.2 Electrical Performance of Samples with Different Drop Spacing and Thickness [18]

An appropriate sintering temperature and time ensures evaporation of the ink solvent, good sintering of the silver nanoparticles (formation of bonds between the nanoparticles) and hence good conductivity and flexibility of the transfer tattoo tag. Observation shows that the optimum sintering time is 30 minutes due to the temperature tolerance limitations of the transfer tattoo paper. Fig. 4.2 is a plot of increasing resistivity values with respect to bulk silver for tag samples after sintering for 30 minutes. After this time, only the double layer tag with 15µm drop spacing experiences further reduction in resistivity or port to port resistance. After 45 minutes of sintering, the single layer tags showed a rapid increase in resistivity. The increase

in resistivity is more gradual for the double layer tags after this time. From Fig. 4.2, the conductivities of the samples were obtained as presented in Table 4.1.

TABLE 4.1 CONDUCTIVITY OF PRINTED TAGS BY DROP SPACING (DP) AND THICKNESS [18]

Sintering Time	Conductivity (S/m)			
	15 μ m dp 1 Layer	15 dp μ m 2 Layers	20 dp μ m 1 Layer	20 dp μ m 2 Layers
15 mins	1.10E+06	1.57E+06	1.37E+06	1.57E+06
30 mins	1.57E+06	2.73E+06	1.66E+06	1.70E+06
45 mins	2.33E+06	3.14E+06	1.57E+06	1.57E+06
60 mins	3.70E+05	8.98E+06	4.34E+05	4.49E+05

Apart from sintering time, the temperature should also be considered. It is important to understand how high a temperature the substrate can withstand and for how long to avoid damage to the substrate as indicated in Fig. 4.3. The robustness of a printed tag could also be compromised because even though the sample obtained could be conductive, it would be brittle with poor flexibility. This will make it unsuitable for use on body where tag flexibility is essential.

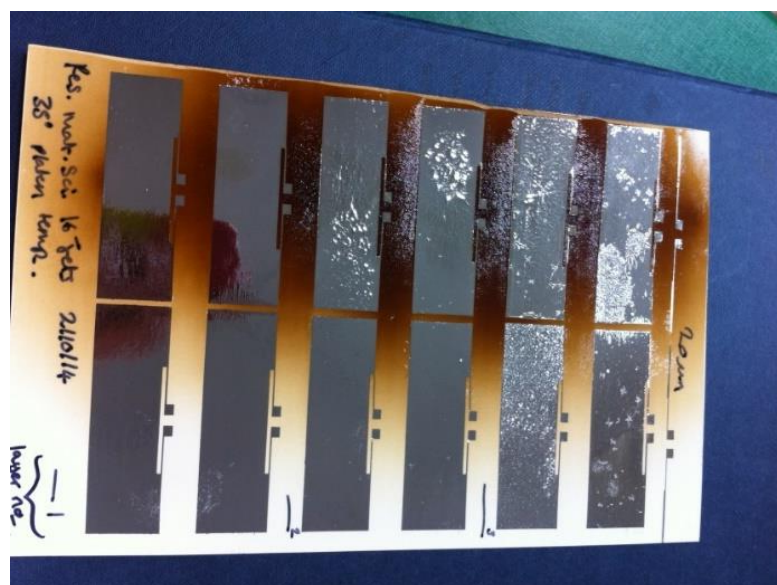


Fig. 4.3 Effect of Excess Sintering Time and Temperature on Transfer Tattoo Paper

The required sintering time and temperature is also dependent on the silver nanoparticle ink used as various inks have different evaporation rates. Inks also interact differently with different substrates hence the need to match ink properties to the properties of the substrate. Fig. 4.4 [19] shows the interaction between an ink and two different substrates (Transfer Tattoo paper [20] and PEL Nano-P60 paper (PEL paper) [21]) where identical sintering temperature was used (150°C). In the case of the tattoo paper, SEM images show that no sintering took place even after 60 minutes of heating. On the other hand, sintering of the nanoparticles of the silver ink is observed on the PEL paper after 15 minutes.

The viscosity of the ink also plays a factor in the quality of the print. A low viscosity results in severe wetting of the substrate which leads to poorly defined patterns, Fig. 4.5.

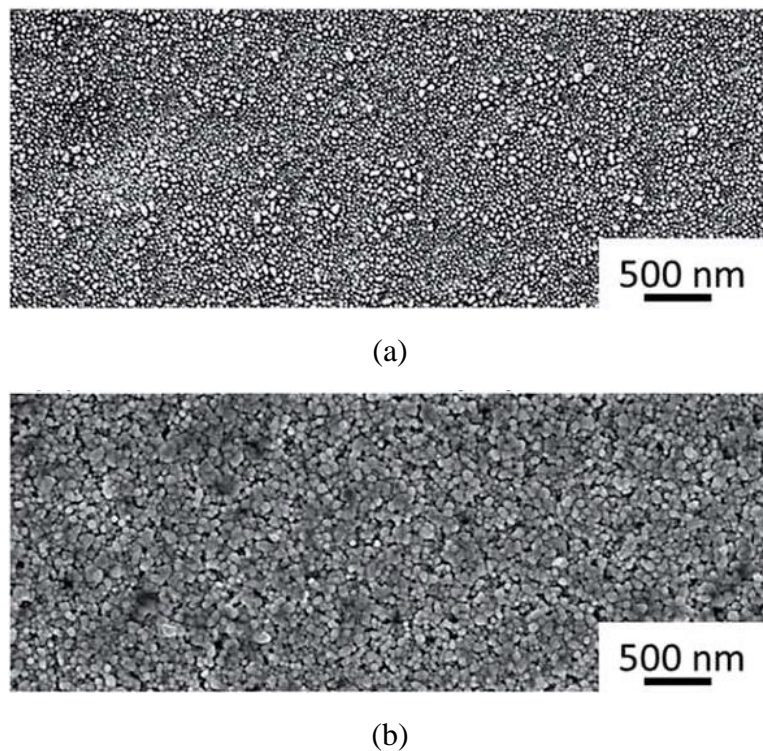


Fig. 4.4 Ink Sintered on (a) Tattoo paper (b) PEL paper [19]

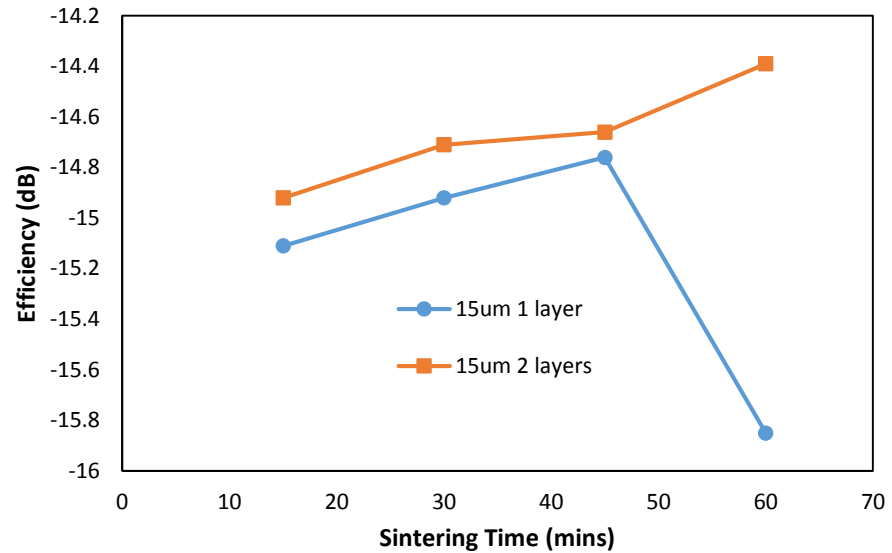


Fig. 4.5 Poorly Defined Pattern due to a Low Viscosity Ink

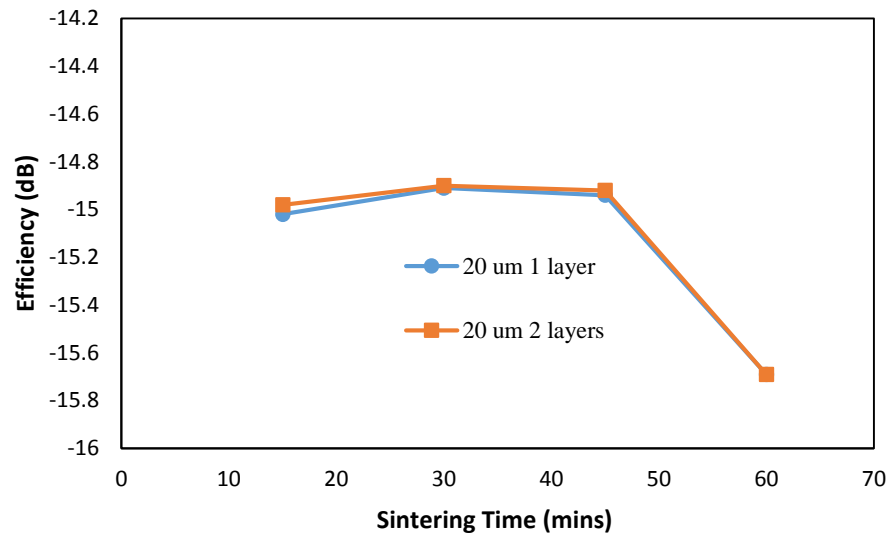
4.3 Effect of Number of Conductive Ink Layers (Total Thickness) on Tag Performance

4.3.1 Simulated Effects

From the conductivity values presented in Table 4.1, the transfer tattoo tag performance can be assessed by simulation. With this, the efficiency, return loss and frequency behaviour of the tags can be modelled in CST using the arm phantom described in Chapter 3. Fig. 4.6 shows the efficiencies of the tag when the drop spacing and thickness are varied. These efficiencies can be compared to the -14.1dB efficiency obtained by a tag made of bulk silver ($\sigma = 6.2 \times 10^7$).



(a)



(b)

Fig. 4.6 Effect of Ink Layer Thickness on Tag Efficiency (a) 15µm dps; thickness \approx 3µm (1 layer), 4µm (2 layers) (b) 20 µm dps; thickness \approx 1µm (1 layer), 3µm (2 layers)

Fig. 4.6 shows that the best radiation efficiency is obtained from the 2 layer tag with 15µm drop spacing. This tag showed improving efficiency with increasing sintering time with a peak efficiency of -14.4dB after 60 minutes. The single conductive layer ink showed the same trend up to 45 minutes with a reduction in efficiency to -15.9dB when the sample had been sintered for an hour. The change in efficiency over sintering time is less noticeable in the 20 µm drop spacing tags with an almost uniform efficiency value for the first 45 minutes (between -15.02dB and -14.94dB for the single

layer tag and -14.98dB and -14.92dB for the 2 layer tag). This is followed by a drop to -15.7dB after one hour. Comparison of the efficiencies after 30 minutes indicates that the $15\ \mu\text{m}$ drop spacing 2 layer tag has the best efficiency. This is followed by the $20\ \mu\text{m}$ drop spacing tags with 2 layers of conductive ink with an efficiency of -14.9dB . In order to improve the efficiency, an additional layer of ink can be added using the same drop spacing.

Fig. 4.7 shows the effect of sintering time on the resonance frequency of one and two conductive ink layer transfer tattoo tags printed with $15\ \mu\text{m}$ and $20\ \mu\text{m}$ drop spacing.

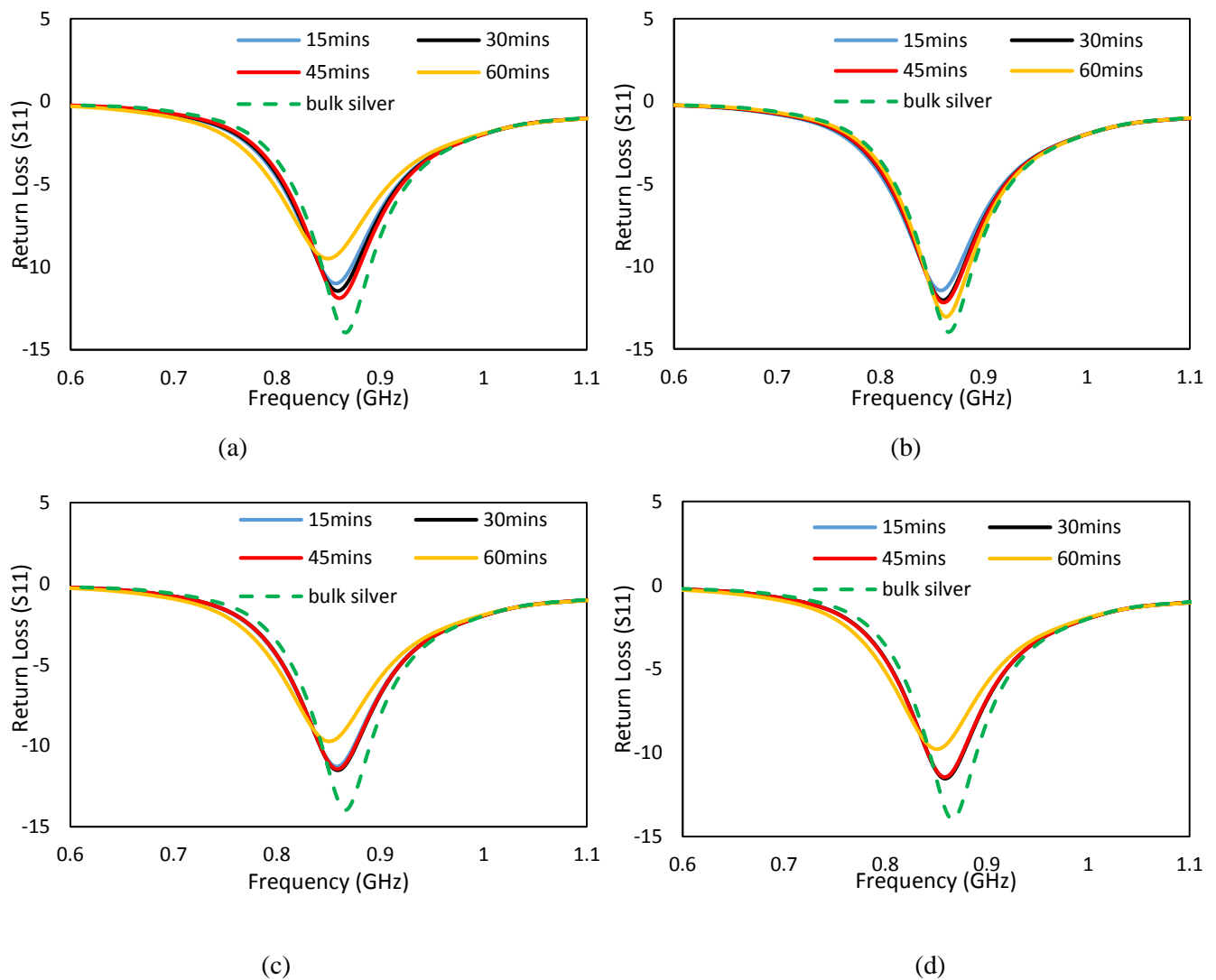


Fig. 4.7 Effect of Ink Layer Thickness on Resonance Frequency (a) $15\ \mu\text{m}$ dps 1 Layer (b) $15\ \mu\text{m}$ dps 2 Layers (c) $20\ \mu\text{m}$ dps 1 Layer (d) $20\ \mu\text{m}$ dps 2 Layers

Pure bulk silver is used as a reference for the simulated resonance frequency for the tags. In all cases, the tags show a deviation from the 867MHz design frequency. The shift in resonance reduces with increasing sintering time as the conductivity of the tag improves. This is best illustrated in the 15 μm dp 2 layers tag (Fig. 4.7 (b)). Due to the reduction in conductivity after sintering for an hour, the simulated resonance frequency of these tags reduced after an hour. The biggest deviation in frequency is seen in the 15 μm 1 layer tag (Fig. 4.7 (a)) with a simulated value of 849MHz, an 18MHz reduction. For both 20 μm tags (Figs. 4.7 (c) and (d)), the effect of prolonged sintering time is less evident with an almost identical resonance frequency for the first 45 minutes. This is followed by a 16MHz reduction after one hour. The Return loss values are shown in Table 4.2.

TABLE 4. 2 SIMULATED RETURN LOSS OF PRINTED TAGS BY DROP SPACING AND THICKNESS

Sintering Time	Return Loss, S_{11} (dB)			
	15 μm dp 1 Layer	15 μm dp 2 Layers	20 μm dp 1 Layer	20 μm dp 2 Layers
15 mins	-11.00	-11.44	-11.28	-11.44
30 mins	-11.44	-12.00	-11.50	-11.53
45 mins	-11.88	-12.18	-11.44	-11.44
60 mins	-9.49	-13.00	-9.73	-9.78

4.3.2 Measured Effects

In order to have a more in-depth study of the 20 μm drop spacing tag performance, three samples were fabricated with respectively 1, 2 and 3 layers. The thickness of a single layer 20 μm drop spacing tag is less than half of the skin depth at the UHF RFID frequency which is about 3.7 μm [18]. This is roughly equal to the thickness of two

layers 20 μm dp of conductive ink and about 75% of the thickness of a tag with 3 layers. Therefore having a tag printed with 20 μm drop spacing with at least two layers of conductive ink would ensure that the skin depth requirements (at least 3.7 μm thickness) are met and conductor losses are reduced.

i. DC Resistance Measurement

The electrical performance of the tags was assessed by taking DC resistance measurements at the tag ports with a multimeter, Fig. 4.8. This was done in order to enable a quick and convenient assessment of the quality of the printed samples. A low DC resistance value indicates a good quality print with good conductivity.

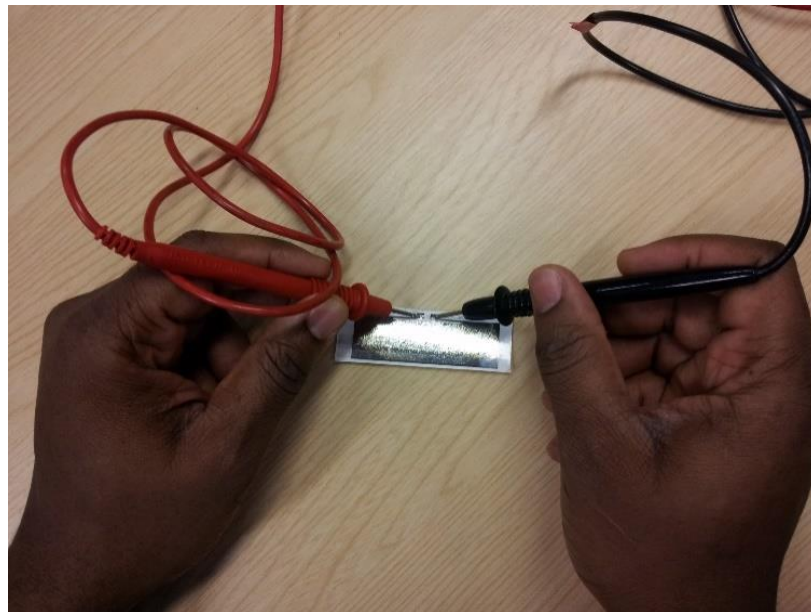


Fig. 4.8 Effect of Ink Layer Thickness on Resonance Frequency

The relationship between the measured DC resistance and number of tag ink layers is shown in Fig. 4.9.

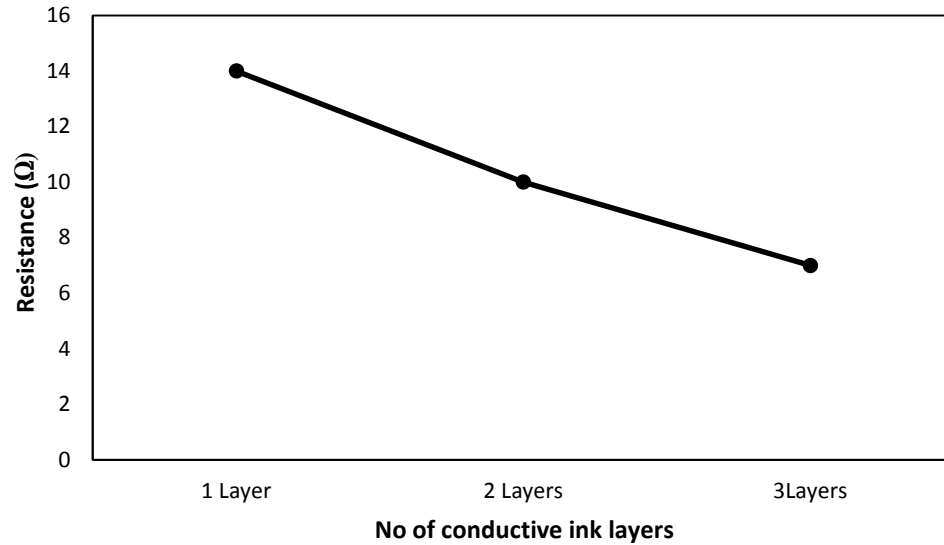
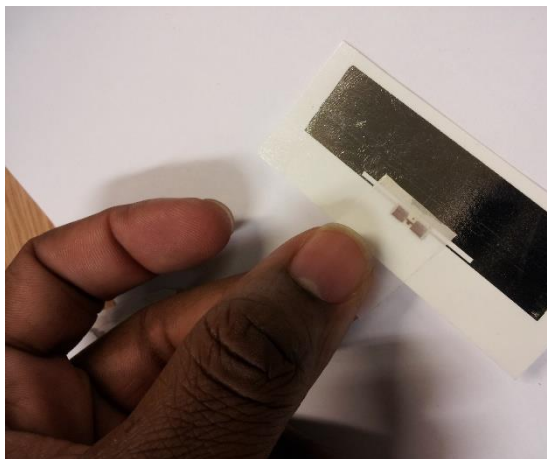


Fig. 4.9 Measured DC Resistance of Inkjet Printed Tag of Transfer Tattoo Paper
Dot Spacing = 20 μm

There is a steady decrease in the tag port DC resistance with increasing ink layers where one layer tag had an average resistance of 14 Ω . This reduced to 10 Ω when an additional layer was added. A further 30% reduction in measured DC resistance was observed when a third conductive ink layer was added to the design.

ii. *Read Range*

The attachment of the ASIC to the printed transfer tattoo tag was achieved with adhesive tape and further enhanced by using point pressure. A thin adhesive layer of about 5 μm was placed on top of the printed tag and then attached to the skin. The backing paper of the transfer tattoo paper was wetted with ordinary water in order to facilitate separation of the thin polymer layer from the paper. This is left to sit for a few seconds after which the backing paper is carefully peeled off leaving only the printed antenna sandwiched between the adhesive and the ink receiving PVA layers. This procedure is illustrated in Fig. 4.10.



(a)



(b)



(c)



(d)



(e)



(f)

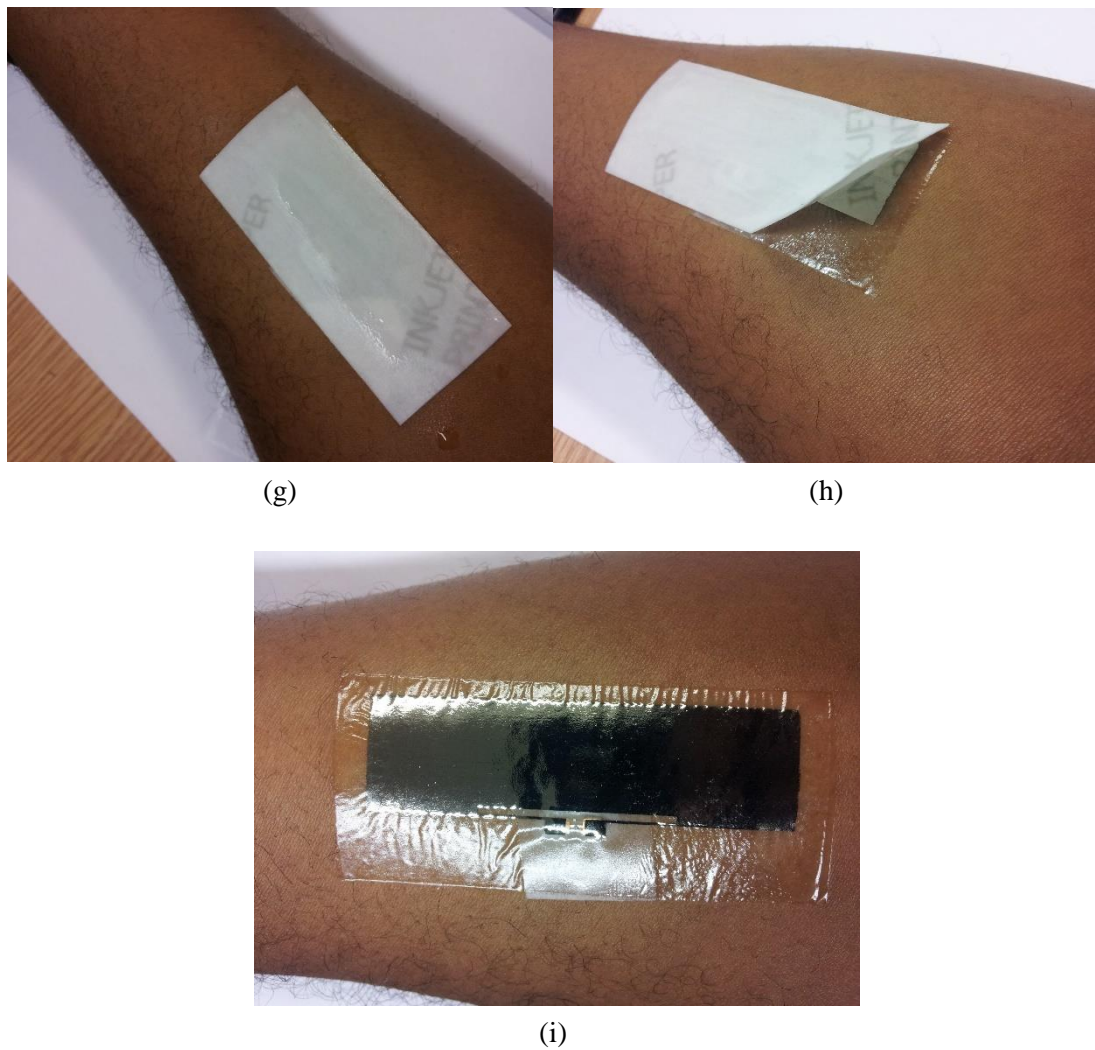


Fig. 4.10 Application of Transfer Tattoo Tag (a) attachment of ASIC to printed tag (b) $5\mu\text{m}$ thick adhesive on transparent film (c) adhesive applied to printed tag (d) removal of adhesive from printed tag (e) printed tag with adhesive layer (f) printed tag mounted on arm (g) back of transfer tattoo paper wetted (h) backing paper peeled off (i) printed tag transferred on arm.

The read range measurement procedure is as described in Chapter 3. Fig. 4.11 presents the measured read range for the 1 – 3 and 5 layer transfer tattoo tags. The presented results are an average of three consecutive measurements.

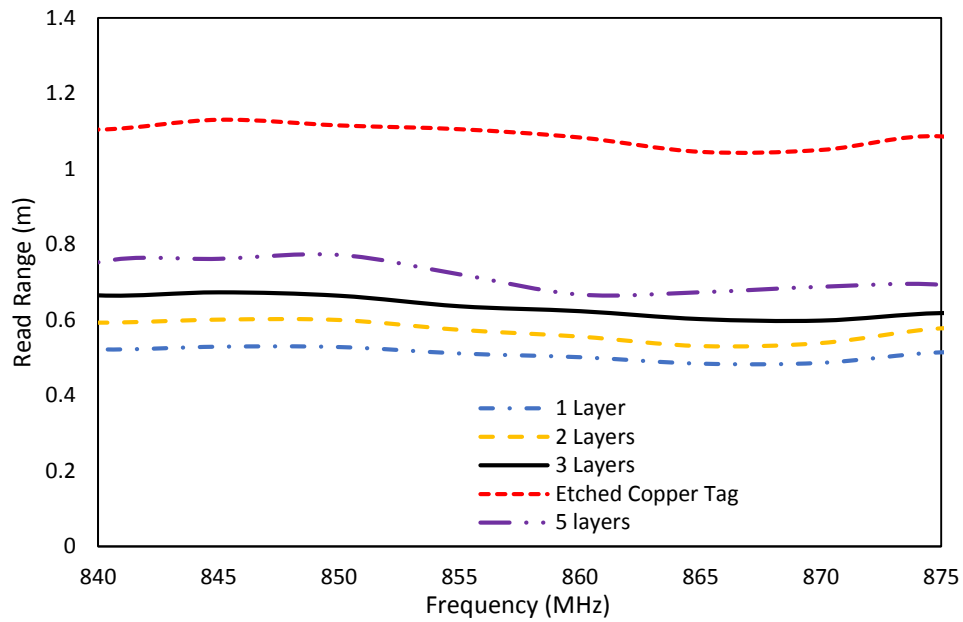


Fig. 4.11 Measured Read Range of Transfer Tattoo Tags

From Fig. 4.11, the read range obtained from the single layer tag at 867 MHz was just 48cm. On the addition of an additional ink layer, there was an increase in read range by 10% to 53cm. For the three layers of conductive ink, a measured read range of 60cm was measured. This is an increase of 12cm when compared to the initial single layer tag. Increasing the number of layers to 5 sees the read range increase by 7 cm to 67cm. However, considering the volume of ink used to achieve this, it is not deemed to be economically viable given the only 12% increase in read range from that achieved with 3 layers. However, it can be concluded that the read range of the transfer tattoo tag increases with reducing DC resistance and increasing conductivity.

Apart from the increased read range, three layer tags have the additional advantage of good robustness and hence can be used in harsh environments as will be demonstrated in Chapter 5.

iii. *Transmitted Power*

The effect of the layer thickness on the transmitted power from the RFID reader was also measured. This is the required power the RFID reader sends to the RFID tag in order to receive a backscattered signal as a function of tag thickness. The measured results averaged over 3 measurements are presented in Fig. 4.12.

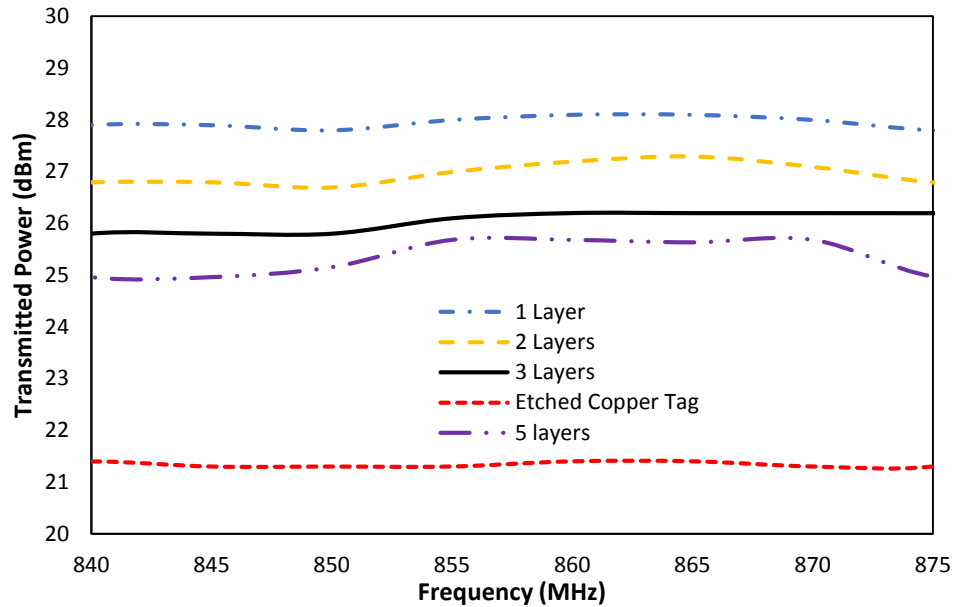


Fig. 4.12 Measured Transmitted Power of Transfer Tattoo Tags

From Fig. 4.12, apart from the 5 layer tag, the least transmission power from the reader at 867 MHz was for the 3 layer tag. The measured transmitted power for this tag was 26 dBm. Decreasing the thickness of the conductive ink results in an increase in transmitted power with a 1 dBm increase measured for the 2 layer tag and a further 1 dBm increase also measured for the 1 layer tag (27 dBm and 28 dBm respectively). Maintaining a low transmitted power is desirable in scenarios where there are power constraints such as in handheld RFID readers which rely on batteries.

In the reverse link, the highest measured backscattered power received by the reader at 867 MHz was from the 3 layer tag with a value of -57.4 dBm. There is also a proportional relationship between the transfer tattoo tag thickness and the received backscattered power with the received backscattered power measured as -59.7 dBm and -60.3 dBm for the 2 and 1 layer tags respectively.

4.4 Tag Performance on Different Individuals Due to Variations in Body Electrical Properties

Bearing in mind that attributes such as the electrical properties of the human body vary on an individual basis [22], it is inevitable that the transfer tattoo tag which is so close to the body will have performance dependent on specific person on which it is mounted. The electrical properties of the body are affected by factors such as the skin thickness which is influenced by environment [23] and ethnicity [24]. Also the density of the underlying fat tissues, muscles and bone in the area being considered can affect the electrical properties of the body [25].

The aim of this experiment was to establish the degree of influence these variations have on the performance of the transfer tattoo tag. For the purpose of this experiment, the relative permittivity and conductivity of the arm region where the transfer tattoo tag was mostly placed was considered. A probe based dielectric system by Schmid & Partner Engineering AG [27] was used. The operation of the equipment is as discussed in Chapter 3. It should be noted that the reflection coefficient measured by the probe is composed of multiple reflections from the tissues underneath the skin and hence the presented results are not solely that of the skin. This is because of the penetration of the electric field of the probe into the underlying deeper tissues [26].

Ten individuals participated in this experiment. These individuals were chosen to represent diverse body types. Physical observation showed that the individuals had different levels of fat and muscle density in their arms and this meant that the circumferences of their arms were different. The tag placement and position of the probe was on the same location on the arm in all of the individuals and it was ensured that the end of the probe was as flat as possible on the skin in order to eliminate the possibility of air gaps. The Measured results are presented in Table 4.3. While the measured relative permittivity and conductivity plots are shown in Figures 4.13 and 4.14 respectively.

TABLE 4.3 MEASURED DIELECTRIC VALUES

User	Arm Circumference (cm)	Relative Permittivity (ϵ_r)	Conductivity (S/m)	Body Type
User 1	32	35.75965	0.50635	Very low fat
User 2	26.5	34.2291	0.4949	Normal
User 3	25	31.1189	0.4767	Normal
User 4	24.5	30.49095	0.43865	Slightly fatty
User 5	27.5	27.6384	0.3408	Fatty
User 6	26.5	32.79975	0.486	Normal
User 7	31	27.52105	0.38585	Fatty
User 8	24	32.84875	0.48895	Normal
User 9	32.5	31.1712	0.4386	Slightly fatty
User 10	25.5	34.39005	0.51	Very low fat

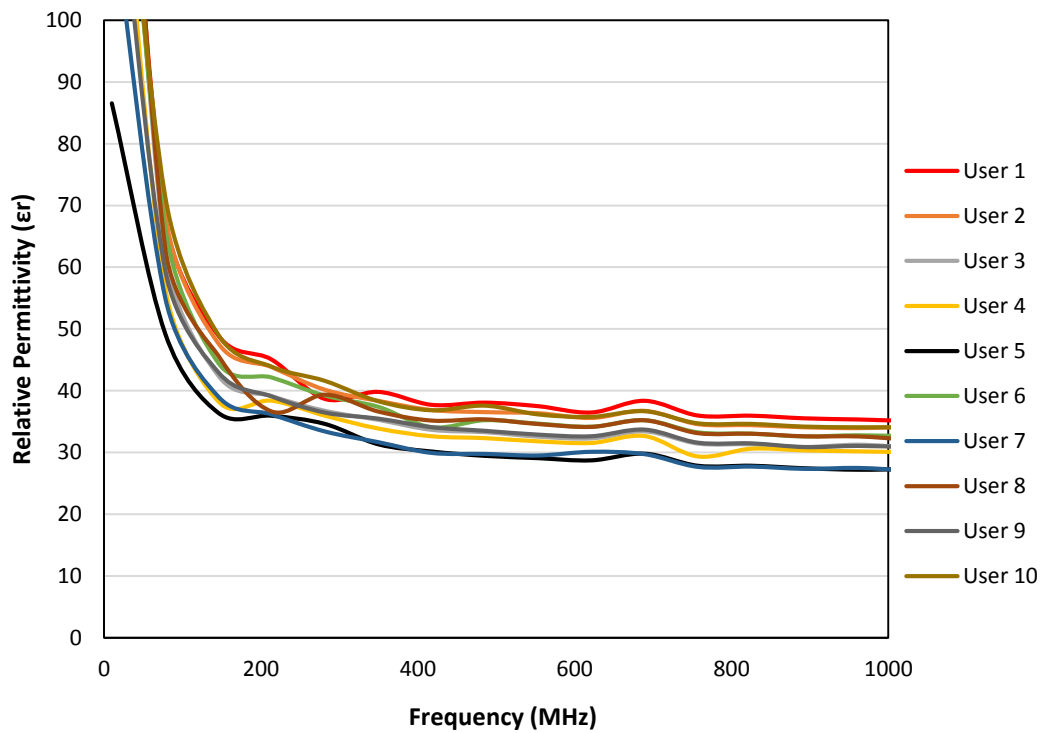


Fig. 4.13 Measured Body Permittivity of 10 Individuals

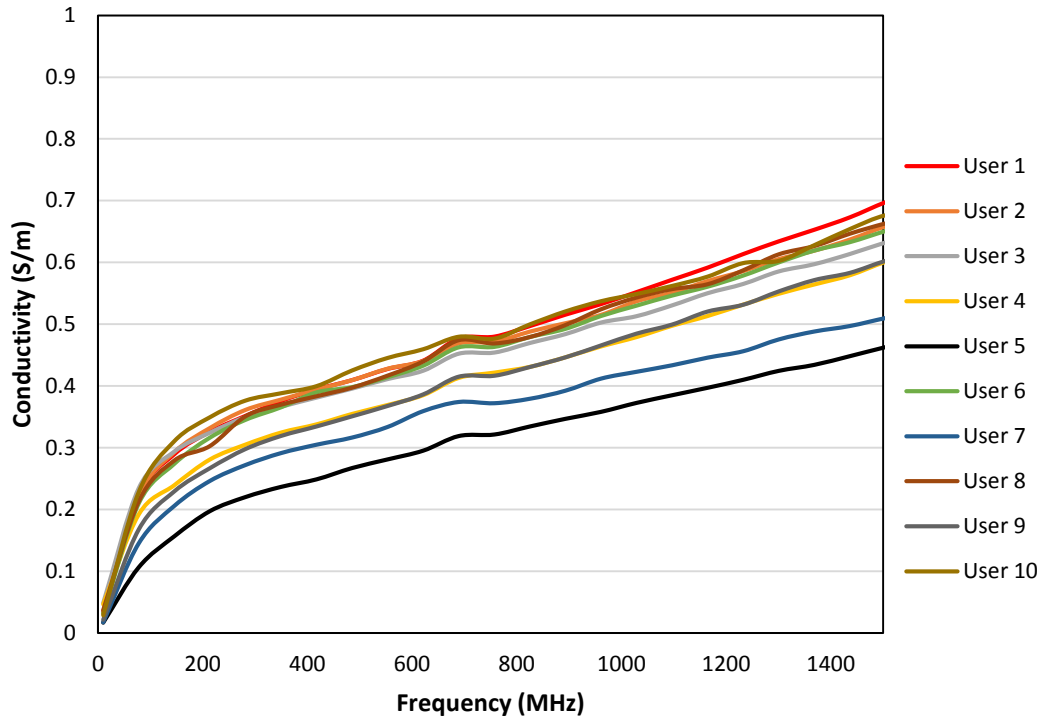


Fig. 4.14 Measured Body Conductivity of 10 Individuals

The measurement results show that the individuals observed to have higher fat content on their arms had lower permittivity and conductivity values than the other participants. In contrast, individuals with higher muscle density (lower fat) in the arms compared to fatty tissues had higher permittivity and conductivity values. The presented arm circumferences in Table 4.3 was to indicate the physical differences in the arms. However, as indicated in Figs. 4.15 and 4.16, there is no direct correlation between the arm circumference and the measured results. This is because the arm circumference (and measured results) is determined by the prevalent tissue in the arm (muscle or fat). An example of this can be seen in User 9 who was observed to have a higher fat content in the arm and with a circumference of 32.5 cm at the measurement point, has a lower dielectric and conductivity value than User 1 with almost same arm circumference (32 cm) but who was observed to be more muscular. On the other hand, User 9 also has lower measured values than User 10 with a smaller arm circumference (25.5 cm) and who was observed to have lower fat content and more muscular arm. The shielding, or lack of, of the dense bone in the arm by the overlying tissue could also be a factor in the measured results.

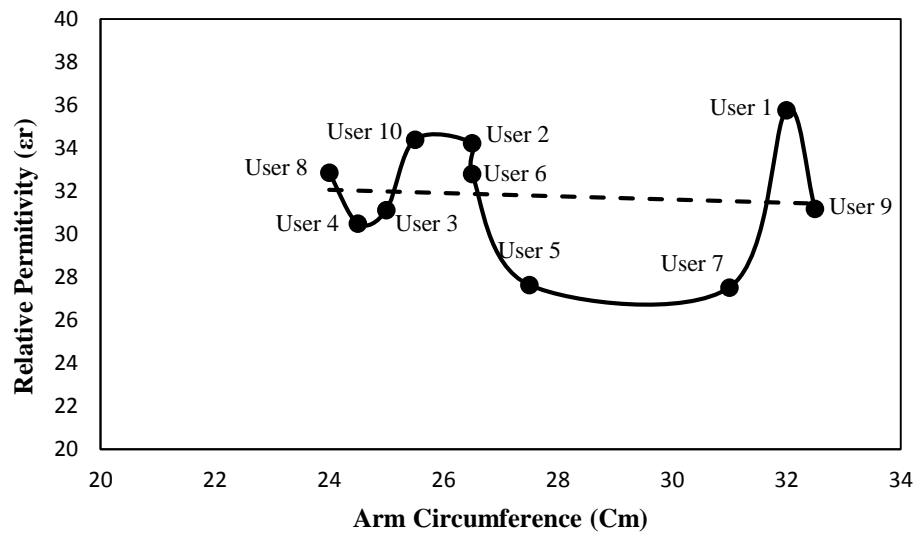


Fig. 4.15 Effect of Arm Circumference on Relative Permittivity

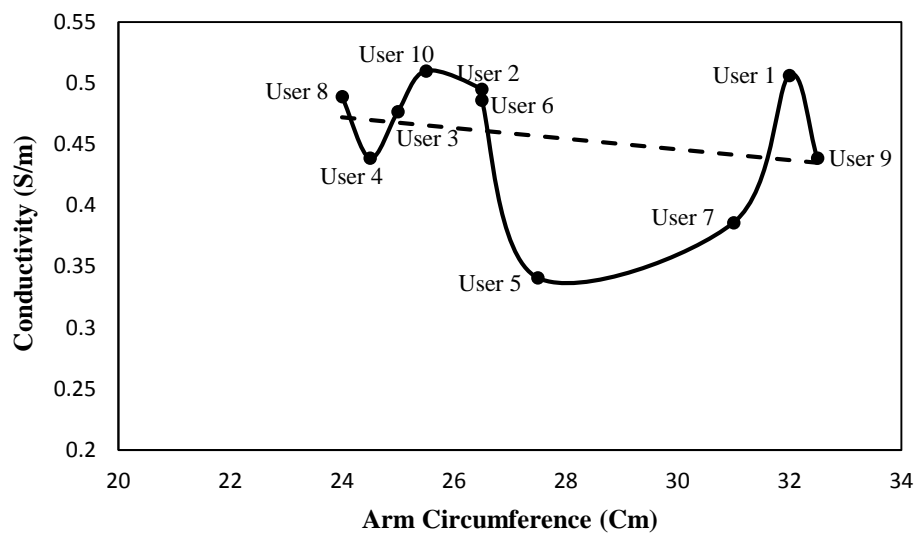


Fig. 4.16 Effect of Arm Circumference on Relative Conductivity

Fig. 4.17 shows the plot of the relationship between conductivity and relative permittivity.

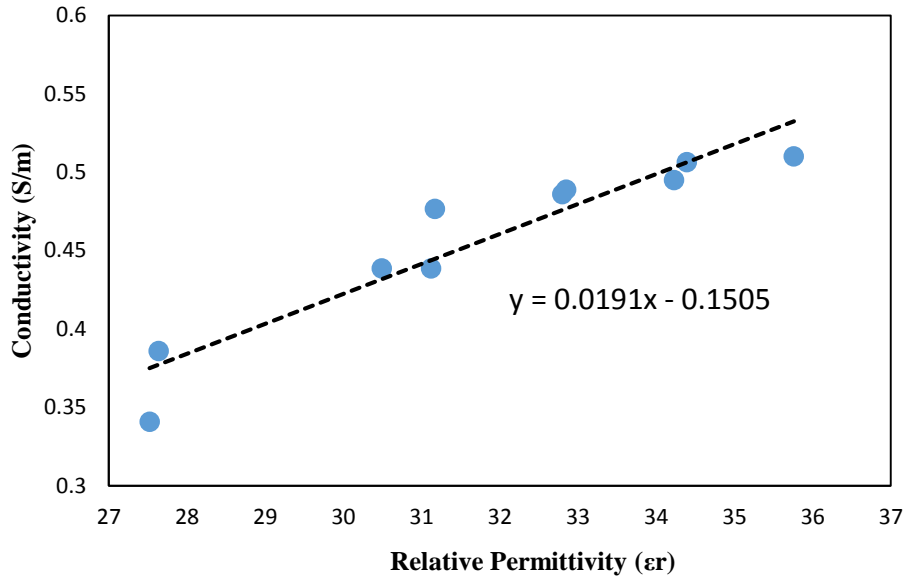


Fig. 4.17 Relationship Between Measured Relative Permittivity and Conductivity

Fig. 4.17 shows a near linear relationship between the measured relative permittivity and conductivity of the individuals at 867MHz. From this plot, an approximate value of permittivity can be found for a given conductivity and vice versa. This is useful for the modelling of a human phantom for use in tag design.

The effects of the dielectric properties of the users' body on the read range of the tag can be seen in Figs. 4.18 and 4.19. Measurements indicate an inverse proportional relationship between the measured read range and the measured parameters (permittivity and conductivity). From the presented graphs for the individuals used for this measurement, 1% increase in the conductivity leads to a 1.5% decrease in the measured read range of the transfer tattoo tag. The rate of reduction in read range decreases to 1.1% for a 1% increase in permittivity. The references for the conductivity and permittivity values are taken from the minimum measured results which are 0.3408 and 27.52105 respectively as shown in Table 4.3. For the read range, transmission power and backscattered power, the references are taken from the corresponding values at the minimum measured dielectric value i.e. conductivity or permittivity.

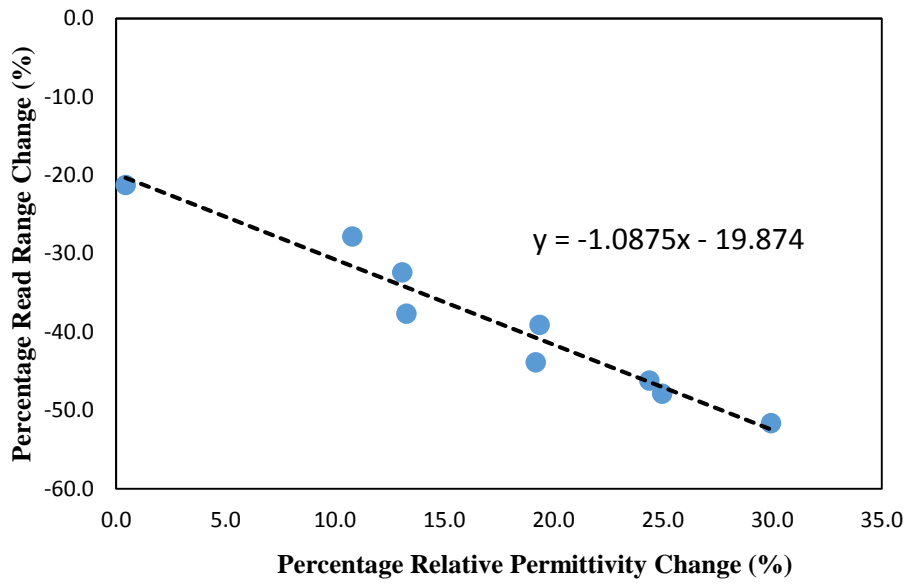


Fig. 4.18 Effect of Relative Permittivity on Read Range

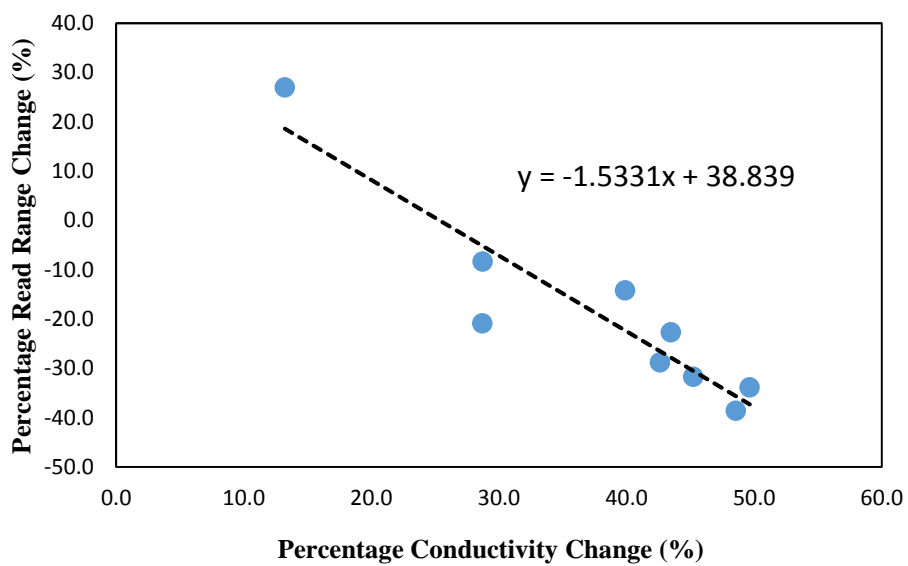


Fig. 4.19 Effect of Conductivity on Read Range

The effect of the relative permittivity and conductivity on the transmitted power from the reader is shown in Figures 4.20 and 4.21.

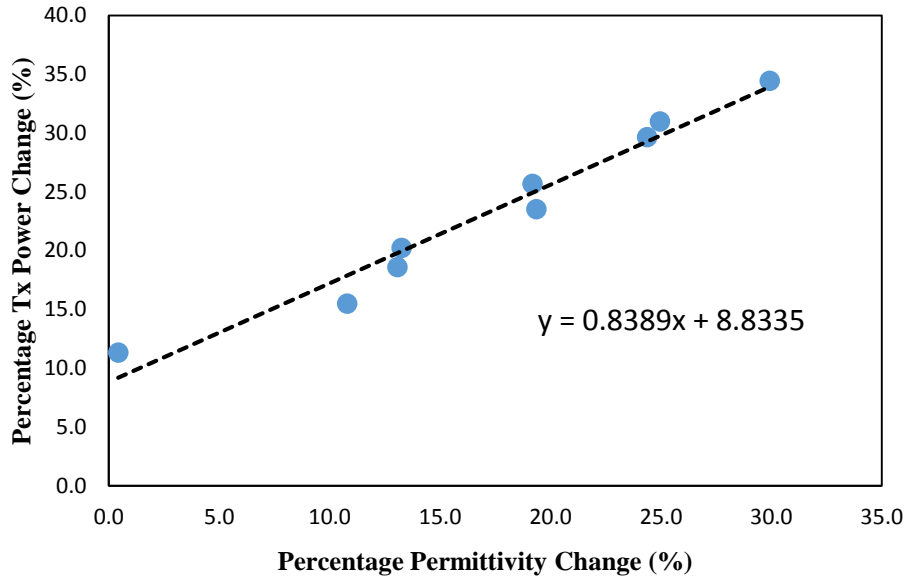


Fig. 4.20 Effect of Conductivity on Transmitted Power

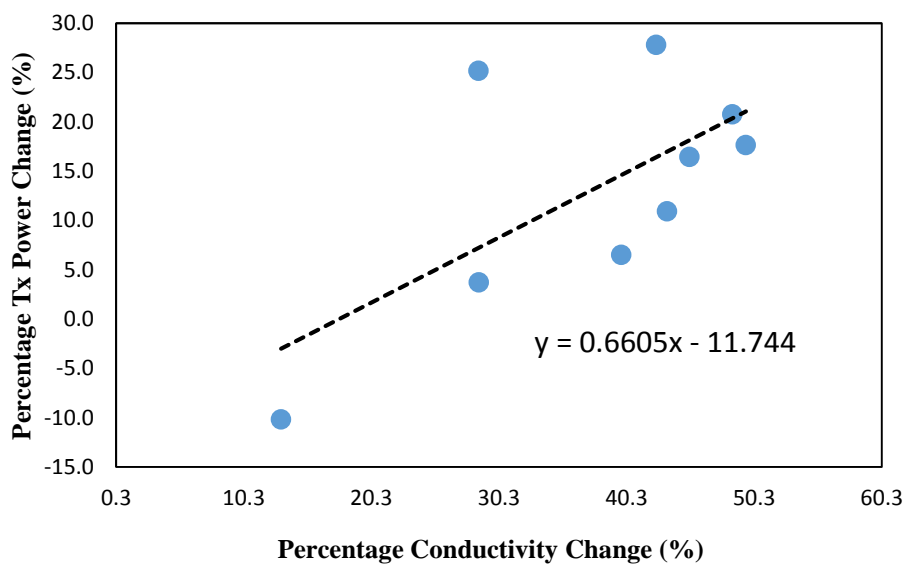


Fig. 4.21 Effect of Permittivity on Transmitted Power

Fig. 4.20 shows that the transmitted power from the reader increases with the permittivity value. A 1% increase in measured permittivity leads to an increase in transmitted power by approximately 0.8%. For increasing conductivity, this increased transmission power by about 0.67%, Fig. 4.21.

A factor in the change of read range observed for the different individuals is the shift in frequency. RFID tags are usually designed at overly high frequencies in free space

so they will become resonant at the desired band when they are loaded by the mounting platform. However to compensate for the variable tissue permittivities, a wide band RFID tag is recommended so that an acceptable read range can be obtained even when there is a shift in the designed resonance frequency.

The simulated effect of the measured dielectric properties of the body on the tag resonance frequency is shown in Figures 4.22 and 4.23.

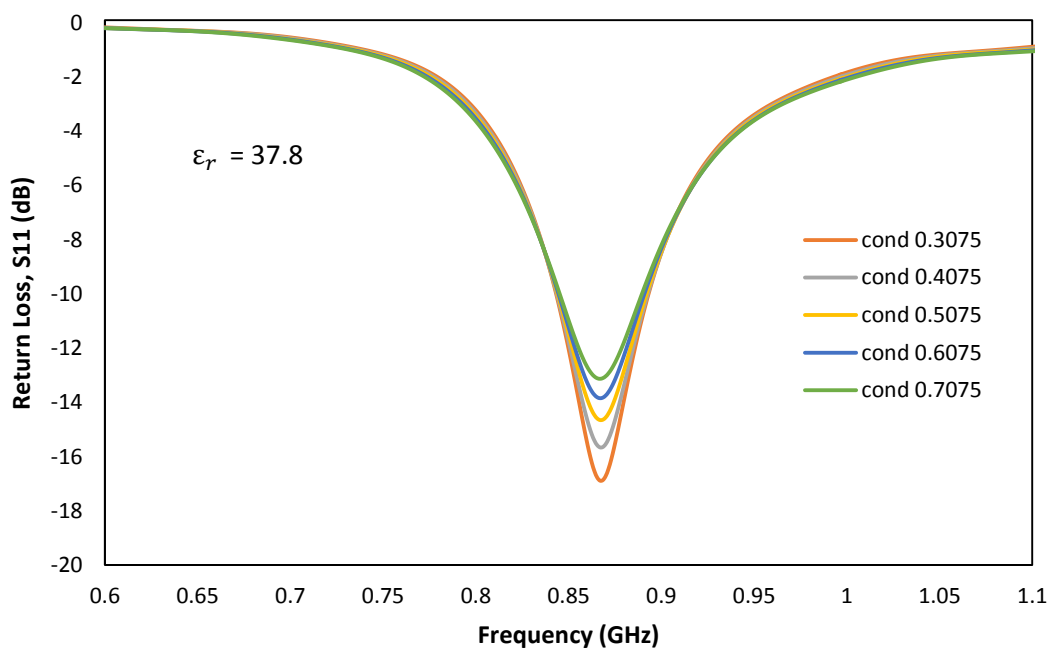


Fig. 4.22 Simulated Effect of Conductivity on Transfer Tattoo Tag

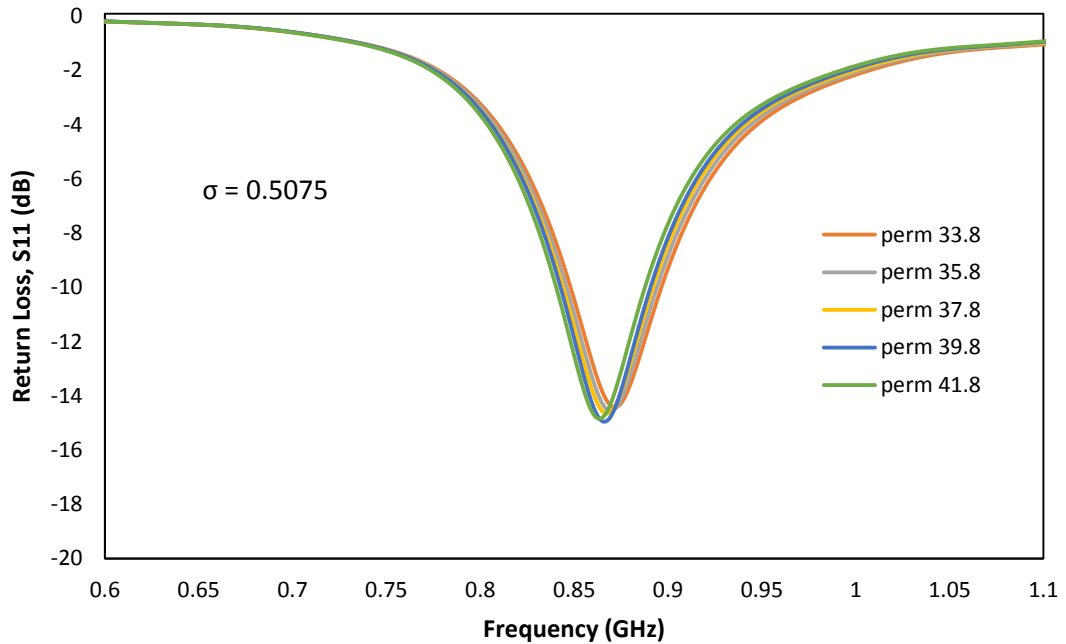


Fig. 4.23 Simulated Effect of Permittivity on Transfer Tattoo Tag

From Figure 4.22, it can be seen that variation in the conductivity of the skin does not lead to change in frequency but rather affects the match of the antenna with the chip. This means that the efficiency of the antenna will be affected more by an increased conductivity. On the other hand, variation in permittivity led to shift in frequency. Fig. 4.23 shows decreasing frequency with increasing permittivity with minimal change in return loss.

4.5 Effect of Tag Location on Measured Read Range

Although most of the measurements for the epidermal transfer tattoo were taken with the tag placed on the arm, its use is not limited to the arms and the performance on other parts of the body was assessed. The same measurement procedure was used for measurements on the chest, forehead and stomach and the measured read ranges are given in Fig. 4.24.

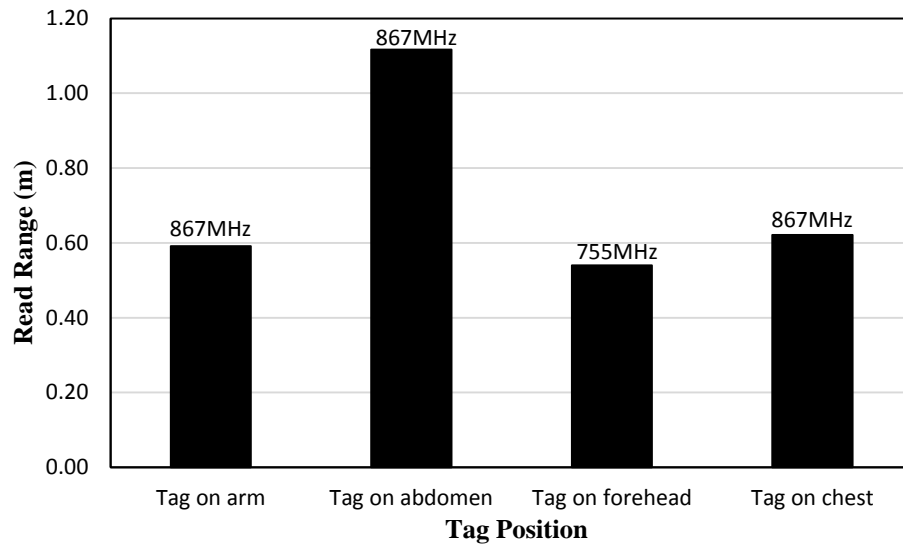


Fig. 4.24 Tag Read Range in Different Parts of the Body

The results show that the best read range is obtained from the tag when it is placed on the abdomen. This is followed by the 0.62 metres read range obtained when the tag was placed on the chest. No read was obtained from the tag in the UHF RFID band when it was placed on the forehead due to a severe frequency shift because of the very dense nature of the head with the presence of skin, skull, brain and cerebrospinal fluid. Since this tag was not modelled for these tissue conditions, it could be retuned to operate at the UHF RFID frequency on the forehead by simulation on an appropriate head phantom [28].

4.6 Ink Usage Minimization Techniques

In order to achieve low fabrication costs, it is desirable to utilize minimal conductive ink volume. Several techniques can be used as follows:

- i. Selective deposition on conductive ink on high current areas of the tag
- ii. Removing low current density areas of the tag and
- iii. Use of gridded designs.

The following sections will examine the effect of these methods on the performance of the inkjet printed epidermal tattoo tags.

4.6.1 Selective Deposition on Conductive Ink on High Current Areas of the Tag

Simulation results indicate that the highest current density region occurs around the feedline. In accordance with this, tags that were fully printed with two layers were overlaid with additional layers over just the feedline and port area. The region of additional conductive ink layer on the tag is shown in black in Fig. 4.25.

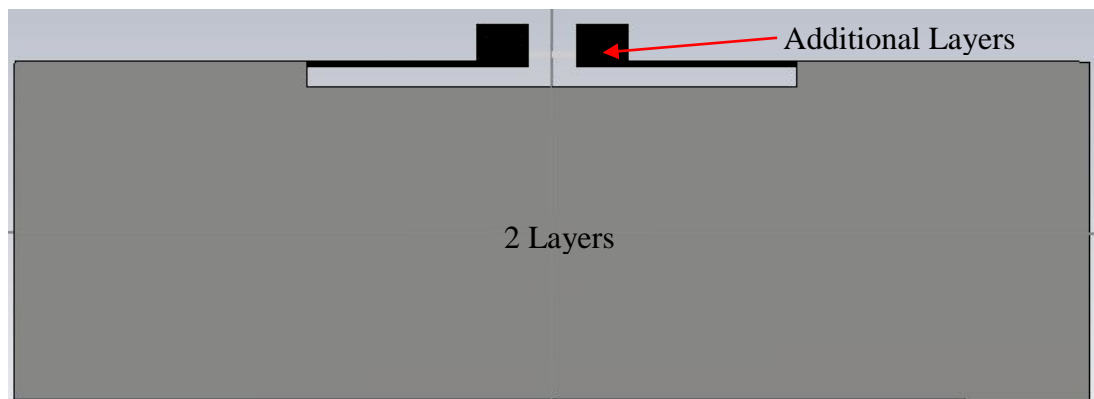


Fig. 4.25 Selective Deposition of Conductive Ink

The percentage change (increase) in read range of these tags compared to the full three layer tags are shown in Fig. 4.26. The result is referenced to a 3 layer tag.

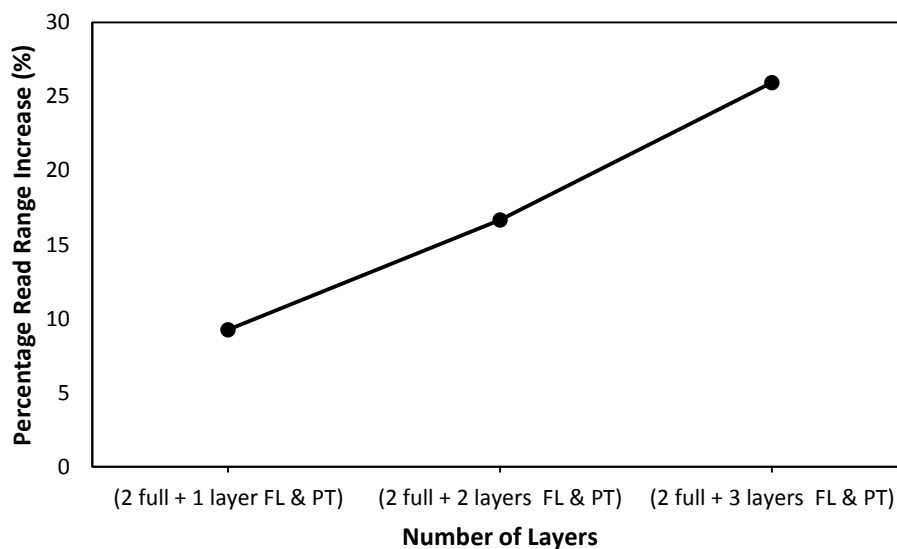


Fig. 4.26 Percentage Read Range of Selectively Deposited Conductive Ink Tags (FL & PT = feedline and ports)

When a single layer of ink is added to the area around the feedline and ports a 9% increase in measured read range is observed. The improvement continues to 26% for 3 layers on the feedline.

Fig. 4.27 shows the relationship between the achieved read range and the used conductive ink with reference to a full 3 layer tag.

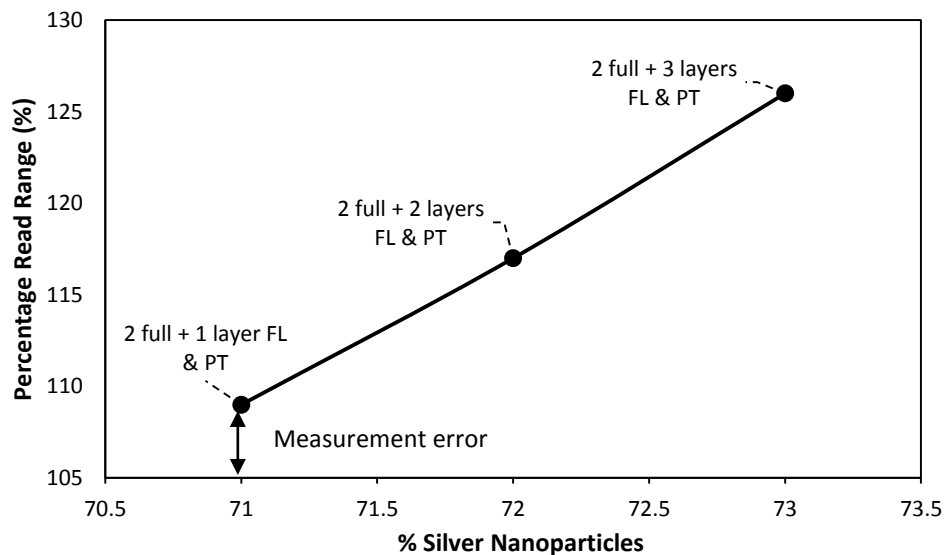


Fig. 4.27 Relationship between Utilized Ink and Achieved Read Range of Selectively Deposited Conductive Ink Tags with Reference to a Full 3 Layer Tag

Fig. 4.27 indicates that each subsequent layer added to the feedline and ports represents a 1% increase in the overall conductive ink quantity used for the tag fabrication.

4.6.2 Trimming of Low Current Density Areas of the Tag

In this technique, instead of printing additional layers in regions with high current density, areas with low current density are removed. This reduces the overall tag surface area while not severely interfering with the flow of current. Two examples of this method was used to demonstrate this. These were designated as Trim 1 and Trim 2, Fig. 4.28. Trim 1 has 48% of its surface area removed while Trim 2 has 65% of its surface area cut.

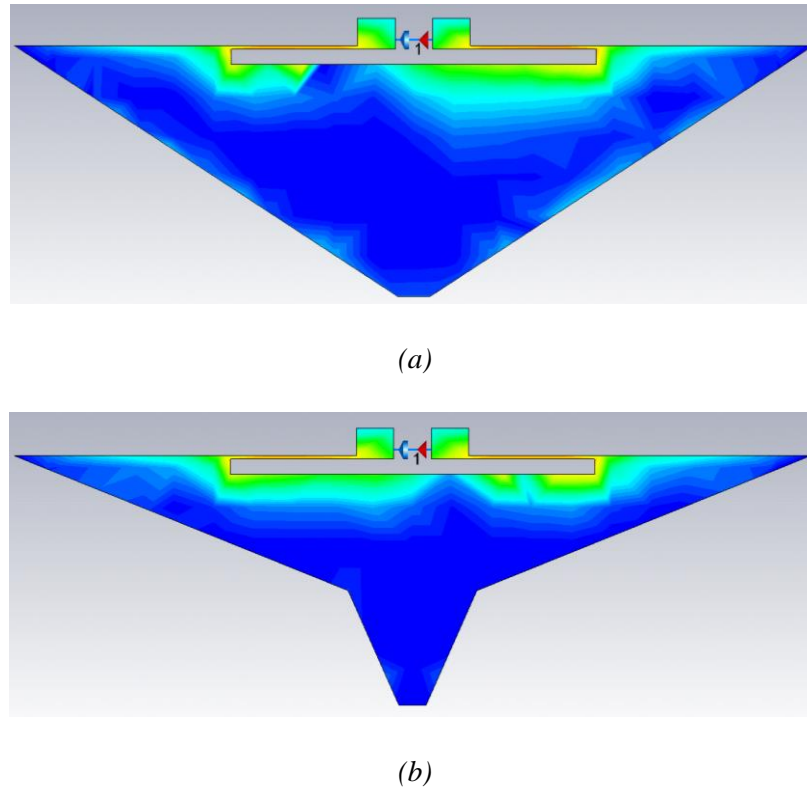


Fig. 4.28 Trimmed Tags (a) Trim 1 – 48% Trimmed (b) Trim 2 – 65% Trimmed

These tags were also printed with a $20\ \mu\text{m}$ drop spacing and three layers of conductive ink. This means that they can be directly compared with the full $20\ \mu\text{m}$ drop spacing tags with three layers of conductive ink.

The simulated efficiencies of the tags are compared in Fig. 4.29.

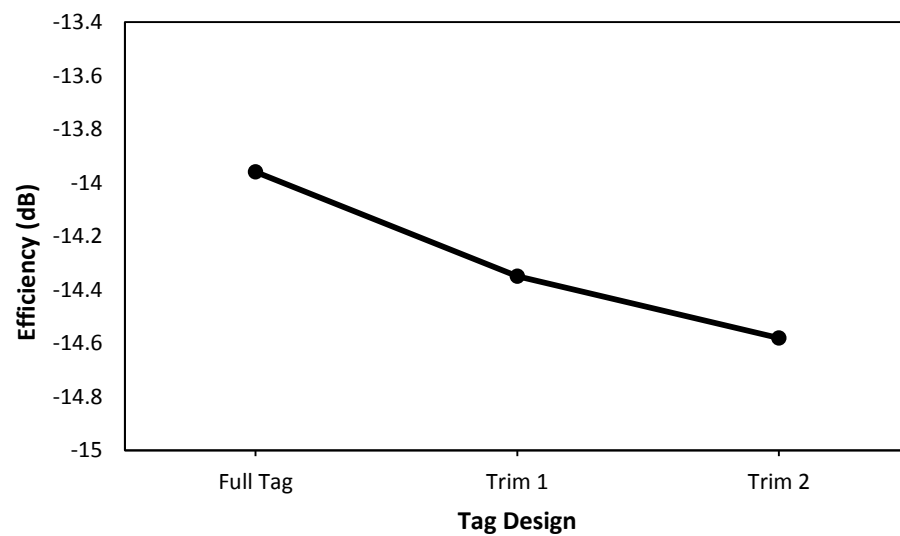


Fig. 4.29 Efficiencies of the Trimmed Transfer Tattoo Tags

From Fig. 4.29, it can be seen that the efficiency of the tag reduces with increasing trimmed area. Trim 1 had a reduction in efficiency by 0.4dB when compared to the full tag. A further reduction was seen when the trimmed off area was increased by 65% resulting in an efficiency of -14.6dB. This is in comparison with the full tag that had a simulated efficiency of -14dB.

The effect of the trimming of the tags on the measured read range is presented in Fig. 4.30.

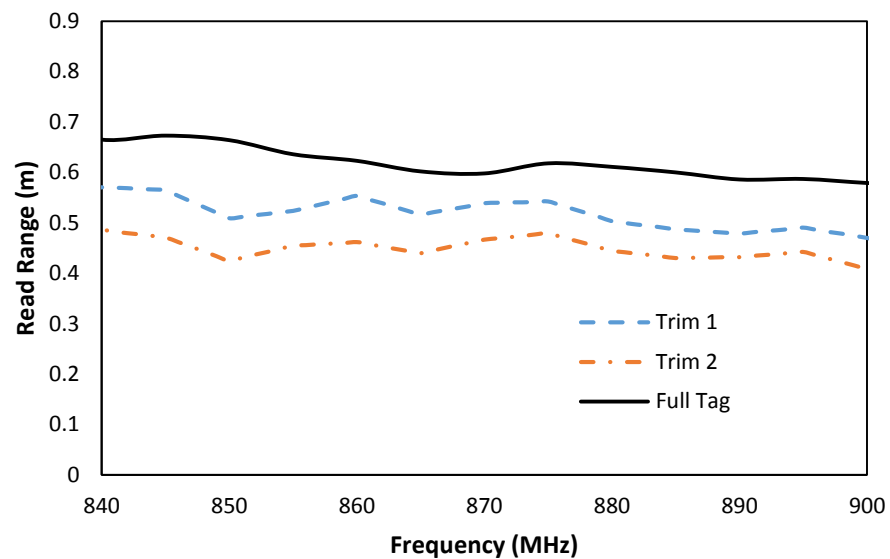


Fig. 4.30 Measured Read Range of Trimmed Tags

The trimming of the tags led to a reduction in measured read range. This can be linked to the reduction in efficiency which was initially observed. As expected, the lowest read range was obtained by the tag with 65% of the surface area cut. Trim 2, had a measured read range of 45cm at 867MHz, a reduction by 16cm (25%) when compared to the full tag. Trim 1 had a better read range of 53cm which translates to a reduction of 11% compared to the full tag.

The effect of trimming the tag on measured transmission power is shown in Fig. 4.31.

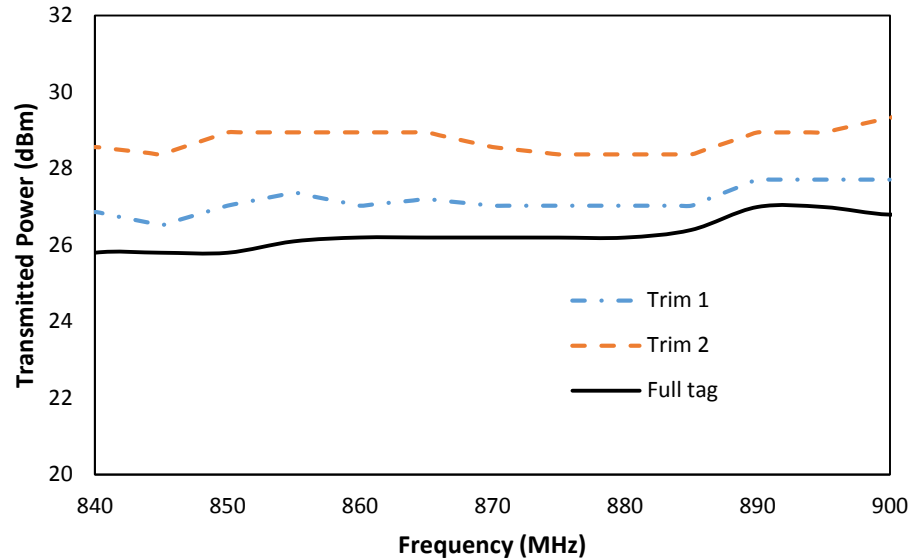


Fig. 4.31 Measured Reader Transmission Power for Trimmed Tags

The results show an increasing measured transmission power for the trimmed design with increasing trimmed off parts. This indicates that as the surface area of the tag was reducing, the reader needed to increase the transmit power level in order to get a response. Trim 1 resulted in an increase in transmitted power at 867 MHz by 1.12 dBm from the initial 26 dBm measured for the full tag. The measured transmitted power for the Trim 2 tag at the stated frequency is 28.8 dBm.

The last parameter examined for the trimmed tag is the backscattered power which is presented in Fig. 4.32.

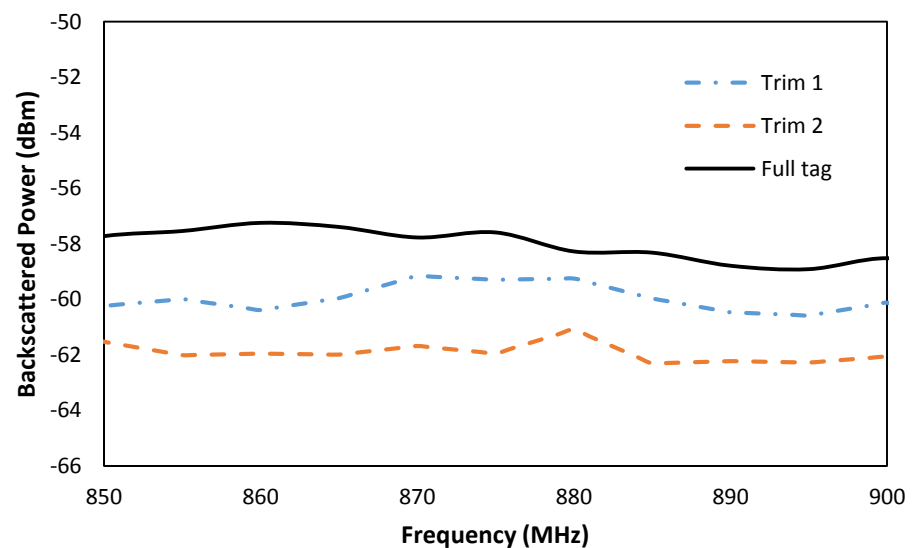


Fig. 4.32 Measured Backscattered Power of Trimmed Tags

Measurement indicated that as the trimmed area is increased, the measured backscattered power from the tags reduced. The least backscattered power was received from Trim 2 with -62 dBm measured. This is a reduction by 5 dBm from the backscattered power of the full tag. Trim 1 tag had a measured back scattered power of 60 dBm.

The quantification of the mass of ink and silver nanoparticle used for each of the tags was also computed. This was obtained from the manufacturer quoted silver content of the ink as 35%. The results of this quantification are presented in Fig. 4.33.

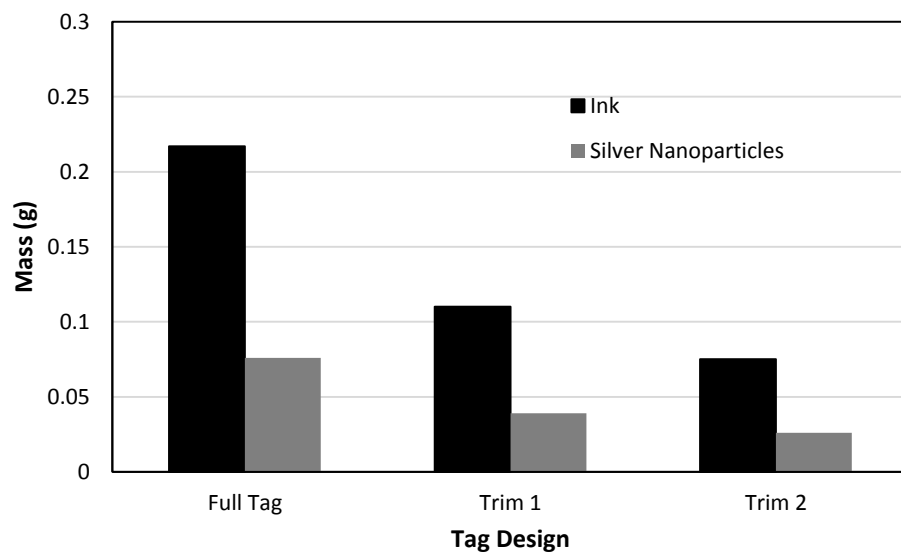


Fig. 4.33 Mass of Silver Nanoparticles and Ink Utilized Per Tag

The total mass of conductive ink used for the fabrication of the full transfer tattoo tag was calculated to be 0.217 g. Of this, the silver nanoparticles consist of 0.076 g. When the tag conductive surface is reduced by 48%, Trim 1, the total mass of silver nanoparticles used for the fabrication of the sample is 0.039 g. This represents a 49% reduction in total silver nanoparticle utilized for the fabrication. For Trim 2, the total mass of silver nanoparticles used was calculated to be 0.026 g which is just 34% of the silver content of the original tag.

4.6.3 Use of Gridded Designs

The use of gridded antennas has been reported in the literature. The purpose of these gridded designs (also known as meshed, see-through or transparent) is for reasons ranging from conformance with the surrounding area [29], reduction of area used by antenna given space constraints [30], and reduction in fabrication material volume which was the case in [31].

For the study of grids as a means to reduce ink volume, two designs will be considered. Grid 1 is a mesh with 0.2mm wide grids and 5mm spacing with 4 horizontal grids in the high surface current area around the slot, while Grid 2 has 1mm wide grids with 5mm spacing and 4 horizontal grids in the area around the slot. The designs are shown in Fig. 4.34.

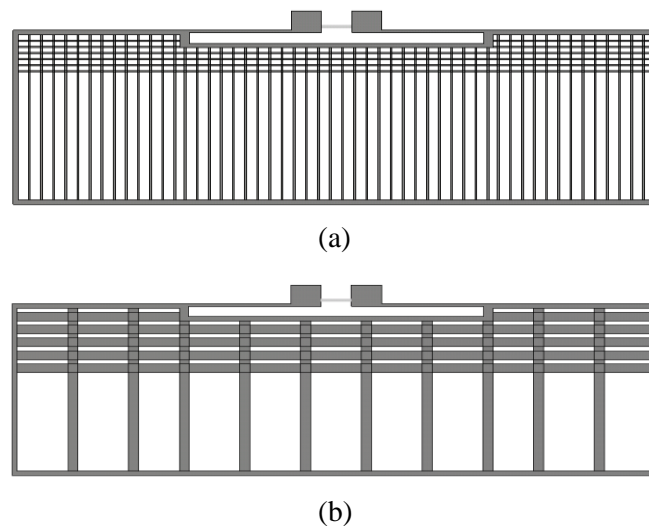


Fig. 4.34 Gridded Designs (a) Grid 1 (b) Grid 2

As before, the performance of the gridded tag is assessed by achieved read range, reader transmitted power and backscattered power received from the tag. Fig. 4.35 shows the measured read range.

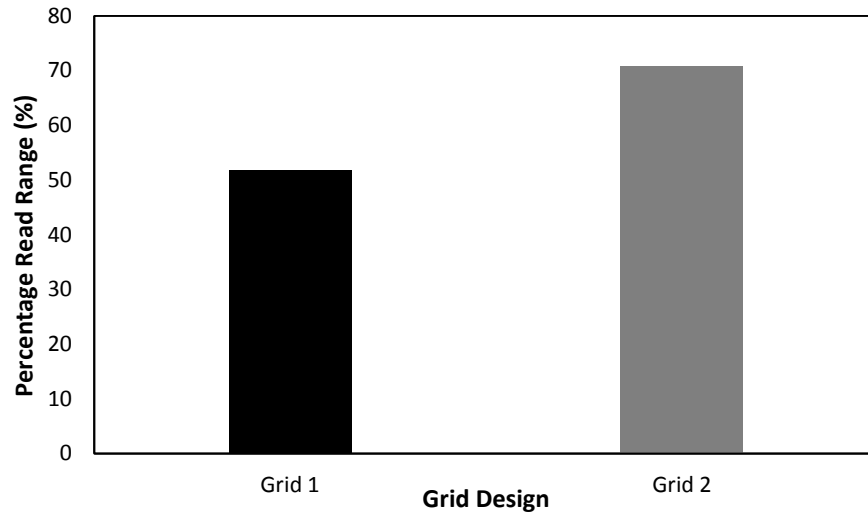


Fig. 4.35 Percentage Read Range of Gridded Tags

From the values presented in Fig 4.35, it can be seen that of Grid 2 with the wider grid widths, achieves a read range of about 71% of the full tag. Grid 1 yielded about 48% reduction in the original measured read range.

The reader transmission power in Fig. 4.36 shows an increased transmitted power for both grids with the highest increase of 26% measured for Grid 1. Grid 2 has a 19% increase in transmitted power.

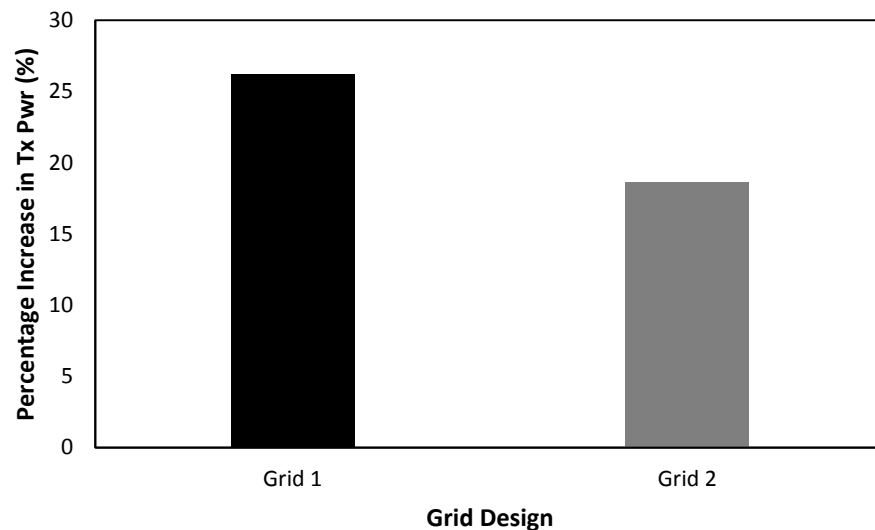


Fig. 4.36 Percentage Increase in Transmitted Power

The effect of the gridded design on the backscattered power is shown in Fig. 4.37.

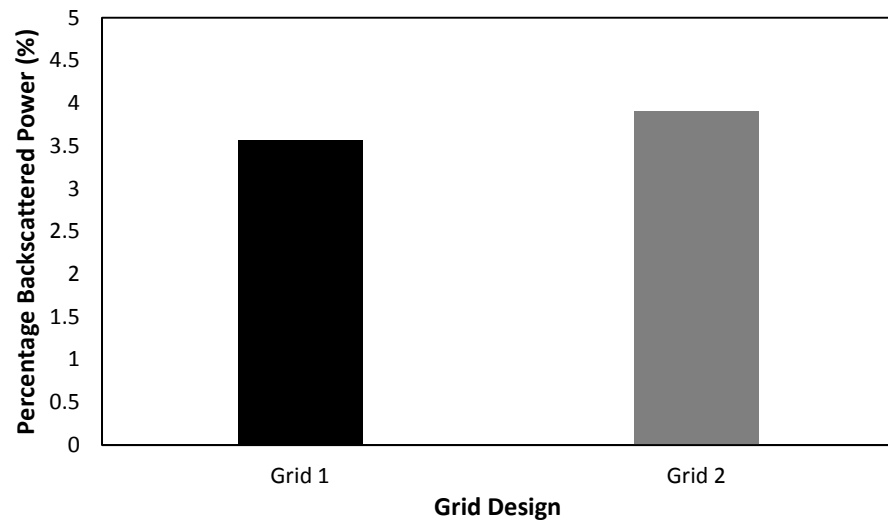


Fig. 4.37 Percentage Backscattered Power

The measured backscattered power from Grid 1 has a 3.5% reduction when compared to the full tag. This value is 4% for Grid 2.

The quantification of the silver nanoparticle used for both Grids is shown in Fig. 4.38.

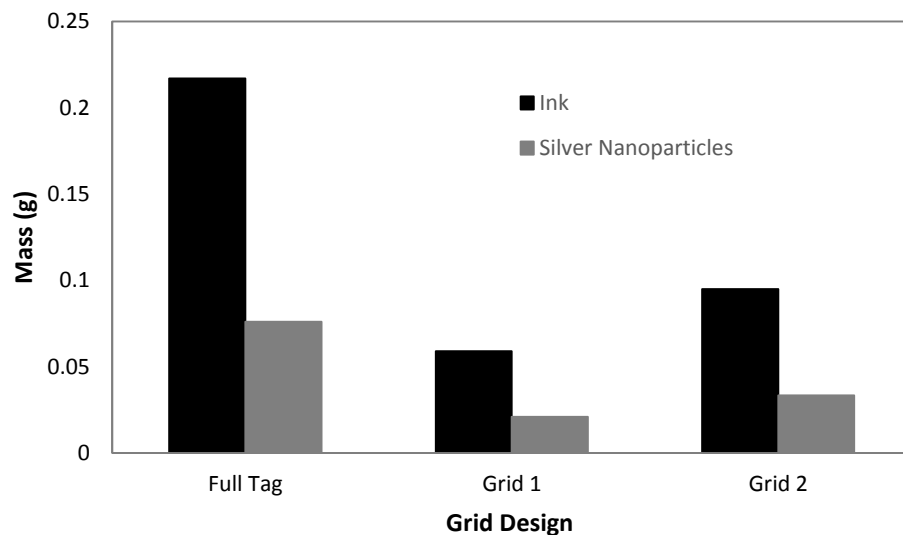


Fig. 4.38 Mass of Silver Nanoparticles and Ink Utilized Per Gridded Tag

From Fig. 4.38, it can be seen that considerably less ink was used for the fabrication of the gridded tags than was used to print the full tag. For Grid 1, only 0.021 g (28% of the mass used for the full tag) of silver nanoparticle was used in printing the tag while 0.03 g (44% of the mass used for the full tag) of silver nanoparticles was used to fabricate Grid 2. These indicate a significant reduction in ink utilization even though it came at a cost of slightly reduced read range.

A summary of the obtainable read range and utilized silver nanoparticles by each tag with reference to the full tag is presented in Table 4.4. The figure of merit was defined as the ratio of the achieved percentage read range with respect to the percentage of conductive ink used for the fabrication of the sample with reference to a full 3 layer tag. Using this approach, a high figure of merit is desirable. $2F + x$ is used to illustrate the tags fabricated by selective ink deposition with x denoting the number of additional layers on the feed line ($1 < x \leq 3$) and $2F$ represents 2 full layers of conductive ink.

TABLE 4.4 COMPARISON OF INK USAGE MINIMIZATION TECHNIQUES

Tag Design	Ink mass (%)	Ag Nanoparticle Mass (%)	Read Range (%)	Fig of Merit
Trim 1	51	51	88	1.72
Trim 2	35	34	75	2.14
Grid 1	27	28	52	1.92
Grid 2	44	44	71	1.61
2F + 1	71	71	109	1.54
2F + 2	72	72	117	1.63
2F + 3	73	73	126	1.73

Results from Table 4.4, show that the tags with selectively deposited ink on the feedline and port provide the best read range. This however comes at a cost of higher conductive ink quantity use. This accounts for the low figure of merit for these tags

with the best being the tag with 3 additional layers on the ports and feedline with FoM of 1.73. The highest read range of 88% was obtained from the Trim 1 tag. However, the trimmed conductive area tag with 65% of its conductive area removed (Trim 2) provided the best conductive ink use and achieved read range balance with the highest figure of merit of 2.14. The least ink utilization was realized with Grid 1 although this also resulted in the most reduced read range measured from any of the tags. Grid 2 was able to achieve 71% of the read range of the original tag with 44% of the conductive ink used for the full 3 layer transfer tattoo tag. The use of the grid designs as a transfer tattoo tag could also be of concern as the thin grids may be a source of tag performance degradation if a break occurs.

From the presented results, a good tag design may be achieved with a combination of Trim 2 and the two full layers with one additional layer on the feedline printing technique.

4.7 Conclusions

This chapter has presented the inkjet printing of epidermal transfer tattoo RFID tags. The printing conditions of these tags in terms of sintering time and temperature as well and the spacing between each drop of ink deposited on the transfer tattoo paper were considered.

The effect of the thickness of the deposited conductive ink (related to the number of ink layers) on the performance of the transfer tattoo was also discussed. The performance was assessed in terms of effect on tag efficiency, resonance frequency and return loss. Additionally, the DC resistance measurements of these tags were carried out as well as read range, reader transmitted power and tag backscattered power measurements. It was shown that tag performance improved with each additional conductive ink layer.

The influence of variations on in body dielectric properties were also presented. Measurement results showed variations in the dielectric properties of the body of 10 individuals. These variations led to variations in measured read range for the individuals. Simulation results confirmed the effect of conductivity and permittivity

of the skin on the tag. Increasing conductivity pointed to a decrease in efficiency, while increasing the permittivity of the body led to a reduction in resonance frequency. Both show how they can play a role in the reduced read range observed during measurements. The measurements indicated that read range of the tag reduced by 1.1% (about 6.5mm) for every 1% increase in the relative permittivity of the body. On the other hand, a 1% increase in body conductivity resulted in a 1.5% reduction (about 9mm) in measured read range. Measurement results when the tag was placed on different parts of the body also showed variations in measured read range.

Methods to reduce the volume of ink used for the fabrication of the tags were also examined in this chapter. These include the selective deposition of ink where simulation showed high current density existed, or trimming off parts of the tag with low current density, and application of meshed designs. These results showed that reasonable read range results can be achieved with a reduction in the amount of ink used. The best read range was achieved when the surface area of the tag was reduced by 48%. Although a 71% read range was obtained from one of the gridded tags, there are concerns about the robustness of this tag because of the thin grid lines. Fig. 4.39 shows a summary of the performance of the ink reduction techniques.

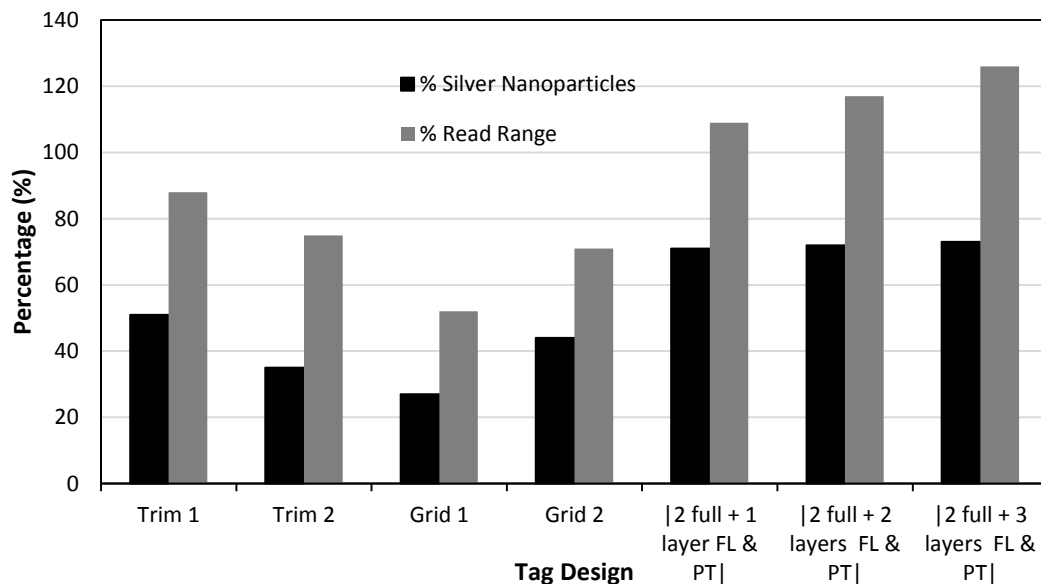


Fig. 4.39 Comparison of Ink Reduction Techniques

References

- [1] “Billion Dollar Mobile Payment Industry Using Secure NFC Technology Projected to Continue Strong Growth | RFID World Canada.” [Online]. Available: <http://www.rfidworld.ca/billion-dollar-mobile-payment-industry-using-secure-nfc-technology-projected-to-continue-strong-growth/2418>. [Accessed: 29-Oct-2015].
- [2] “Near-field communication: mobile payment systems - Engineers Journal.” [Online]. Available: <http://www.engineersjournal.ie/2015/01/27/near-field-communication-mobile-payment-systems-explained-explored/>. [Accessed: 29-Oct-2015].
- [3] “Transport for London builds customer profiles using RFID data analytics.” [Online]. Available: <http://www.computerweekly.com/feature/Transport-for-London-builds-customer-profiles-using-RFID-data-analytics>. [Accessed: 18-Oct-2015].
- [4] A. Blayo and B. Pineaux, “Printing processes and their potential for RFID printing,” in *Proceedings of the 2005 joint conference on Smart objects and ambient intelligence: innovative context-aware services: usages and technologies*, 2005, pp. 27–30.
- [5] B. V. Lakafosis, A. Rida, R. Vyas, L. Yang, S. Nikolaou, and M. M. Tentzeris, “Progress Towards the First Wireless Sensor Networks Consisting of Inkjet-Printed , Sensor Tags,” *Proc. IEEE*, vol. 98, no. 9, pp. 1601–1609, 2010.
- [6] T. Björninen, S. Merilampi, L. Ukkonen, L. Sydänheimo, and P. Ruuskanen, “The Effect of Fabrication Method on Passive UHF RFID Tag Performance,” *Int. J. Antennas Propag.*, vol. 2009, no. 1, pp. 1–8, 2009.
- [7] T. Björninen, J. Virkki, J. Virtanen, L. Sydänheimo, L. Ukkonen, and M. M. Tentzeris, “RFID Tag Antennas on Renewable Materials with Porous Surfaces,” in *7th European Conference on Antennas and Propagation (Eucap 2013)*, 2013, no. Eucap, pp. 1721–1725.
- [8] J. Virtanen, “Inkjet-Printed UHF RFID Tags on Renewable Materials,” *Adv. Internet Things*, vol. 02, no. 04, pp. 79–85, 2012.
- [9] L. Yang, A. Rida, R. Vyas, and M. M. Tentzeris, “RFID Tag and RF Structures on a Paper Substrate Using Inkjet-Printing Technology,” *IEEE Trans. Microw. Theory Tech.*, vol. 55, no. 12, pp. 2894–2901, Dec. 2007.
- [10] D. Bechevet, T.-P. Vuong, and S. Tedjini, “Design and measurements of antennas for RFID, made by conductive ink on plastics,” *Antennas and Propagation Society International Symposium, 2005 IEEE*, vol. 2B, pp. 345–348 vol. 2B, 2005.
- [11] S. Amendola, S. Milici, and G. Marrocco, “Performance of Epidermal RFID Dual-loop Tag and On-Skin Retuning,” *IEEE Trans. Antennas Propag.*, vol. 63, no. 8, pp. 3672–3680, Aug. 2015.
- [12] M. Svanda and M. Polivka, “Extremely low profile UHF RFID TAG antennas for identification of people,” *Antennas Propag. (EuCAP), 2010 Proc. Fourth Eur. Conf.*, pp. 2–5, 2010.

- [13] M. Takahashi, T. Nakajima, K. Saito, and K. Ito, "Characteristics of wristband type RFID antenna," *Antennas and Propagation (EuCAP), 2010 Proceedings of the Fourth European Conference on*. pp. 1–4, 2010.
- [14] D. . Oyeka, M. a. Ziai, J. C. Batchelor, E. a. Parker, V. Sanchez-Romaguera, and S. G. Yeates, "Developing inkjet printing to enable low cost UHF RFID transfer tattoo tags," *2013 IEEE Antennas Propag. Soc. Int. Symp.*, pp. 1726–1727, Jul. 2013.
- [15] D. O. Oyeka, J. C. Batchelor, V. Sanchez-Romaguera, S. . Yeates, and R. . Saunders, "Effect of Conductive Area Trimming on the Read Range of Inkjet Printed Epidermal RFID Tags," in *The 9th European Conference on Antennas and Propagation (EuCAP 2015)*, 2015.
- [16] D. Oyeka and J. Batchelor, "Conductive Ink Usage Optimization Using Grid Designs for Inkjet Printed Epidermal RFID Tags," in *Loughborough Antennas and Propagation Conference*, 2014.
- [17] P. Pongpaibool, "A study of cost-effective conductive ink for inkjet-printed RFID application," *Antennas and Propagation (ISAP), 2012 International Symposium on*. pp. 1248–1251, 2012.
- [18] V. Sanchez-Romaguera, M. A. Ziai, D. Oyeka, S. Barbosa, J. S. R. Wheeler, J. C. Batchelor, E. A. Parker, and S. G. Yeates, "Towards inkjet-printed low cost passive UHF RFID skin mounted tattoo paper tags based on silver nanoparticle inks," *J. Mater. Chem. C*, vol. 1, no. 39, pp. 6395–6402, 2013.
- [19] V. Sanchez-Romaguera, S. Wunscher, B. M. Turki, R. Abbel, S. Barbosa, D. J. Tate, D. Oyeka, J. C. Batchelor, E. A. Parker, U. S. Schubert, and S. G. Yeates, "Inkjet printed paper based frequency selective surfaces and skin mounted RFID tags: the interrelation between silver nanoparticle ink, paper substrate and low temperature sintering technique," *J. Mater. Chem. C*, p. -, 2015.
- [20] "Make your own tattoos and body art using your Inkjet printer." [Online]. Available: http://www.craftycomputerpaper.co.uk/-Inkjet-Tattoo-Paper_CPJ316I.htm. [Accessed: 13-Dec-2015].
- [21] "PEL Nano-P60 paper." [Online]. Available: http://www.printedelectronics.co.uk/Information_Sheet%20for_PEL_Nano_P60.pdf. [Accessed: 01-Dec-2015].
- [22] T. Sunaga, H. Ikehira, S. Furukawa, H. Shinkai, H. Kobavashi, Y. Matsumoto, E. Yoshitome, T. Obata, S. Tanada, H. Murata, and Y. Sasaki, "Measurement of the electrical properties of human skin and the variation among subjects with certain skin conditions.," *Phys. Med. Biol.*, vol. 47, no. 1, pp. N11–N15, 2002.
- [23] R. G. Freeman, E. G. Cockerell, J. Armstrong, and J. M. Knox, "Sunlight as a Factor Influencing the Thickness of Epidermis," *J. Investiative Dermatology*, vol. 39, no. 4, pp. 295–298, Oct. 1962.
- [24] M. Bazin, R. Soderstrom, and T. R. Means, "Ethnic Differences in skin-fold thickness," *Am. J. Clin. Nutr.*, no. July, pp. 864–868, 1971.
- [25] D. Miklavčič, N. Pavšelj, and F. X. Hart, "Electric Properties of Tissues," in *Wiley Encyclopedia of Biomedical Engineering*, John Wiley & Sons, Inc., 2006.

- [26] C. J. Panagamuwa, I. Howells, and W. G. Whittow, "Conductivity and permittivity measurements of children and adult's hands covering mobile communications frequency bands," in *Progress In Electromagnetics Research Symposium (PIERS)*, 2013, pp. 810–814.
- [27] "RF conductivity measurement | dielectric probe | dielectric measurement | dielectric spectroscopy | permittivity probe | loss tangent | dielectric properties | dielectric probe | complex permittivity probe | permittivity measurement | dielectric par » SPE." [Online]. Available: <http://www.speag.com/products/dak/dielectric-measurements/>. [Accessed: 02-Oct-2015].
- [28] R. J. Sadleir and A. Argibay, "Modeling Skull Electrical Properties," *Ann. Biomed. Eng.*, vol. 35, no. 10, pp. 1699–1712, 2007.
- [29] G. Clasen and R. J. Langley, "Meshed patch antenna integrated into car windscreen," *Electron. Lett.*, vol. 36, no. 9, p. 781, 2000.
- [30] T. W. Turpin and R. Baktur, "Meshed Patch Antennas Integrated on Solar Cells," *IEEE Antennas Wirel. Propag. Lett.*, vol. 8, pp. 693–696, 2009.
- [31] J. Siden, T. Olsson, A. Koptioug, and H.-E. Nilsson, "Reduced Amount of Conductive Ink with Gridded Printed Antennas," in *Polytronic 2005 - 5th International Conference on Polymers and Adhesives in Microelectronics and Photonics*, 2005, pp. 86–89.

CHAPTER 5

TRANSFER TATTOO TAG PRINTING DEFECTS AND TAG ROBUSTNESS STUDY

In this chapter the effects of defects arising from inkjet printing as well as printing tolerances on inkjet printed epidermal RFID tags are examined. The sources of these defects in the printed tags are also discussed. The effects of typical geometric defects are studied by simulation and measurement using an etched copper sample. A robustness test of the tattoo tag is also examined by testing tag read range over a period of time intervals and under different conditions. The effect of sweat on the tag is also tested and a more controlled study is carried out using saline solution which has a consistency close to sweat to determine the role mechanical friction plays on the degradation of tag performance during use.

5.1 Introduction

The formation of deformities in Inkjet printed samples is widely reported in literature [1] – [12]. The authors in [4] and [5] examined the influence of the substrate surface energy and the ink surface tension on the resolution of printed conductive features on flexible substrates. These need to be tuned in order to obtain good quality prints. Also, the dot spacing and in-flight droplet diameter also affect the quality of the print. Soltman and Subramanian in [7] demonstrated the effect of different drop spacing and temperature on the structure of printed conductive tracks. They also examined the influence of substrate temperature on the formation of the coffee ring effect (Fig. 5.1[3]) by deposited conductive ink drops. The dynamics of drying drops of fluid was investigated by Deegan et al in [9] in which they proposed the evaporation-rate distribution theory. This study gives more insight into the formation of the coffee ring due to the action of evaporation of fluids.

Studies have also been conducted specifically on inkjet printed conductive traces on various substrates [13] – [17]. These studies have looked into the factors that affect the resolution and quality of printed conductive traces on these substrates. Some of these factors as noted in [13] include the wettability of the substrate, the hydrodynamics of the jetted micro-droplets and the volatility of the constituents of the ink. Fig. 5.2 shows the influence of the substrate surface energy on the resolution of printed conductive tracks as well as the interaction between the substrate and a drop of water as illustrated in that work. Further issues with printed tracks as identified in [1] include: (i) Fluid mechanical instability which leads to the ink moving during or after printing. The result of this motion is a significant loss in shape which can significantly affect the functions of printed elements. (ii) Adhesion and mechanical stability which is a concern when the printed track does not attach to the substrate on which it is printed. The effect of various drop spacings on a printed tag is shown in Fig. 5.3 [7].

These variations in print quality and resolution are of concern because of the presence of a thin feedline in the epidermal transfer tattoo tags. It was noted in [18] that the width of a printed line can increase by as much as 25% after printing due to the spreading of the ink drops. As the matching of the antenna impedance to the impedance of the ASIC is done around this sensitive region, poor printing quality in

this region will have an effect on the tag operation in the form of poor matching and frequency shift. The effects of these defects on the performance of the printed antenna and RFID tags are not widely reported. This will be part of the focus of this chapter. The work presented in this chapter was initially reported in [19].

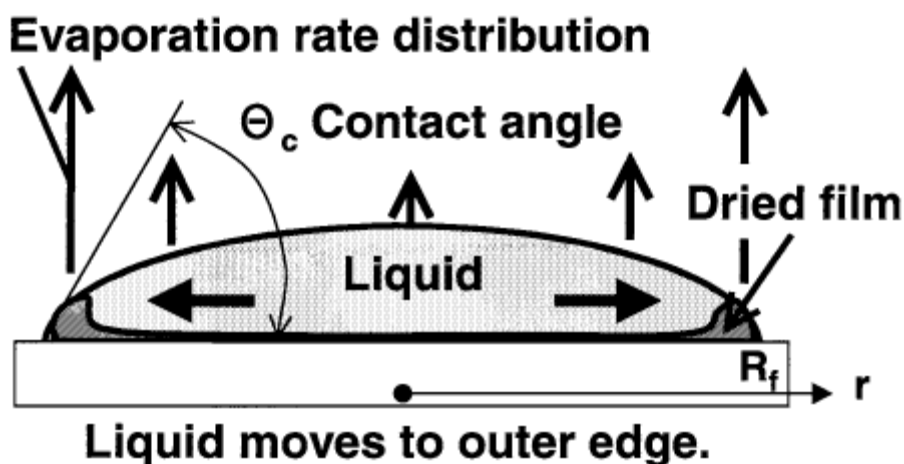


Fig. 5.1 Illustration of coffee stain [3]

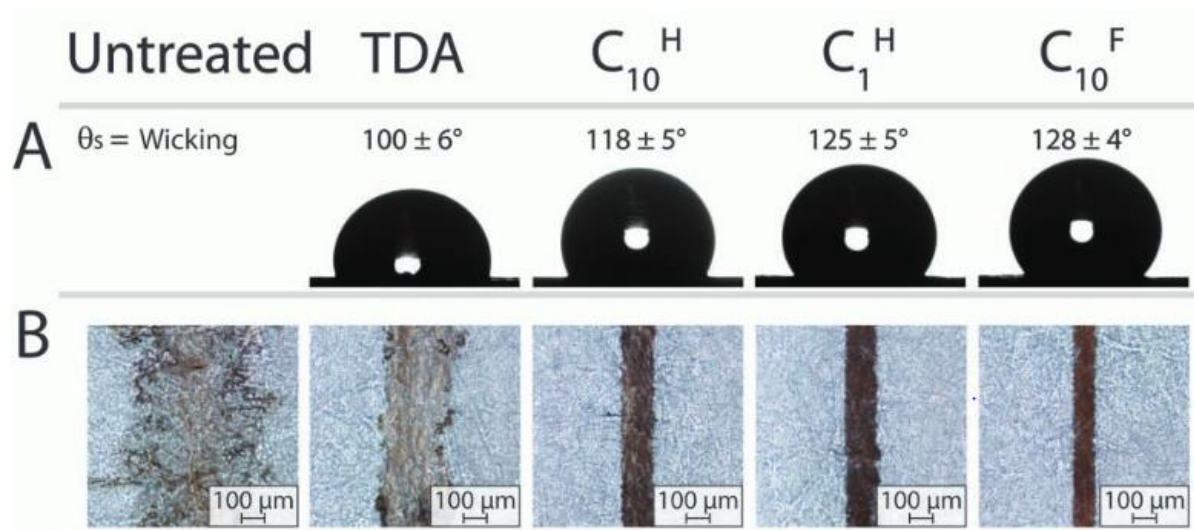


Fig. 5.2 Influence of surface energy on ink interaction (A) Images of 10- μL drops of water on a series of Canson tracing papers, modified with different organosilanes, and their corresponding static contact angles (θ_s) (with standard deviation for $n = 7$ measurements). (TDA = Tris Dimethylamino Silane) (B) Optical micrographs of silver wires printed on the modified or unmodified Canson tracing paper substrates using the reactive silver ink with a target resolution of 80 μm [13].

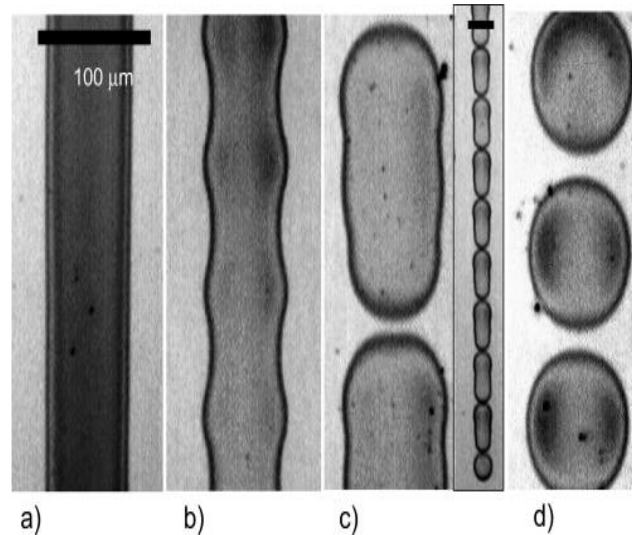


Fig. 5.3 Effect of drop spacing on printed track quality (a) uniform line, drop spacing is $50 \mu\text{m}$, (b) scalloped line, drop spacing is $75 \mu\text{m}$, (c) pairs, drop spacing is $88 \mu\text{m}$ (d) isolated drops, drop spacing is $100 \mu\text{m}$ [7].

The structure of this chapter is as follows: Section 5.2 provides a brief overview on the type and sources of tag defects during printing. The simulated and measurement studies of the defects will be presented in Section 5.3. The robustness tests on the tag are presented in Section 5.4 while Section 5.5 will conclude the chapter.

5.2 Sources of Printing Defects

From the works mentioned in the previous section, the sources of printing defects can be summarized thus:

- i. Blocked printer head nozzle
- ii. Imperfection in the printer's printing algorithm
- iii. Incorrect sintering times and sintering temperature
- iv. Incorrect temperature of the substrate
- v. The temperature of the ink
- vi. Inappropriate viscosity of the ink.
- vii. Unmatched nature of the substrate

The blocking of the printer head nozzle is caused by nanoparticle inks which have high solid fractions. These particles would collect near the nozzle tips and create a plug at the liquid-air interface [1]. It can also be brought about by the evaporation of

the ink solvent in the face of an elevated substrate temperature. Owing to these factors, it is necessary to clean the nozzle tip to prevent bad quality prints brought about by this clogging.

Printing parameters such as the ink drop spacing and ink drop frequency are controlled by the printer's algorithm. This is important because a good algorithm will enable the ink drops to be ejected in the right order to give them time to dry and set down on the substrate before the adjacent droplet is ejected. This would ensure that the drops do not merge together which would result in the bulging of the ink on the receiving surface [11].

Temperature plays a vital role in inkjet printing. This includes sintering temperature, ink temperature and substrate temperature. Incorrect temperature for any of these can lead to poor quality printing. This is shown in Fig. 5.4 [18] in which the effect of substrate temperature on the resolution of the tattoo tag was demonstrated. Two identical transfer tattoo samples were printed under the same conditions with the only variation being the temperature of the substrate during printing. It can be seen from the Fig. 5.4 that with an elevated substrate temperature, the printed structure is finely detailed due to the lack of spreading of the ink. This was facilitated by the faster rate of evaporation of the ink volatiles which increased the ink's viscosity [18]



(a)



(b)

Fig. 5.4 The effect of substrate temperature on print quality (a) substrate at 25°C (b) substrate at 50°C [18]

The viscosity of an ink determines how fast it would spread when it comes in contact with a substrate. An ink with low viscosity will lead to a loss of details in the printed sample. In addition to this, another factor that determines the quality of a printed sample is the nature of the substrate. This includes the substrate's surface profile in terms of how smooth or otherwise it is, how the substrate interacts with fluids i.e. its wettability, and temperature tolerance which will determine the sintering temperature and time the substrate can be subjected to.

5.3 Defects Study

Figures 5.5 – Fig 5.9 show some of the printing defects identified in the inkjet printed RFID tags produced for this research. These defects were categorized as follows:

- Hairline cut on the feedline and ports, Fig. 5.5
- Pinhole defects, Fig. 5.6 and Fig 5.7
- Notched defects due to poor edge definitions, Fig. 5.8
- Variations in feedline width Fig. 5.9

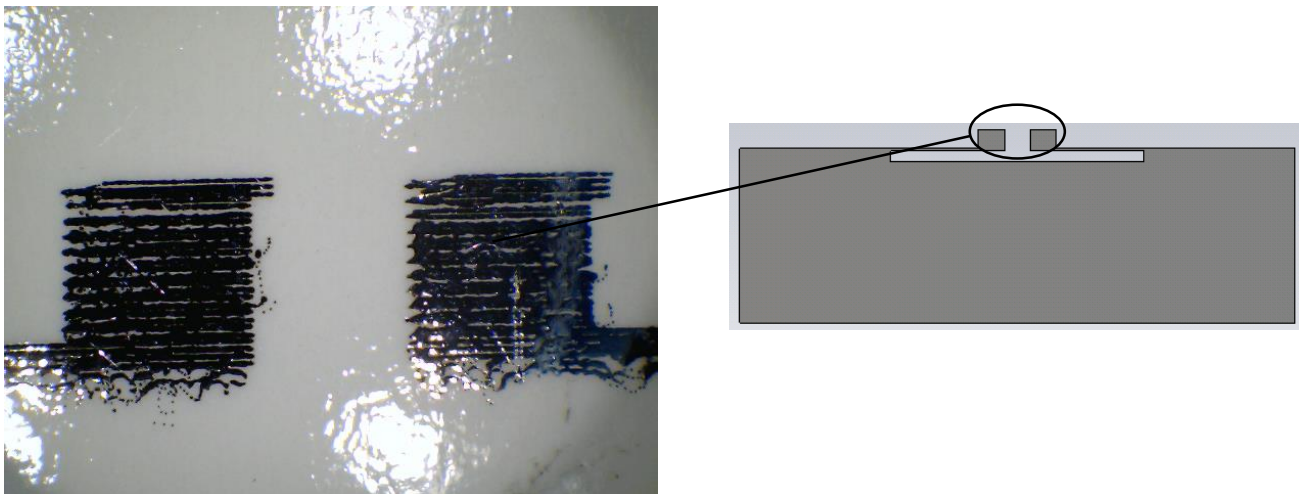


Fig. 5.5 Defects on the RFID tag port due to non-bonding of adjacent print lines



Fig. 5.6 Pinhole defects on the RFID tag port

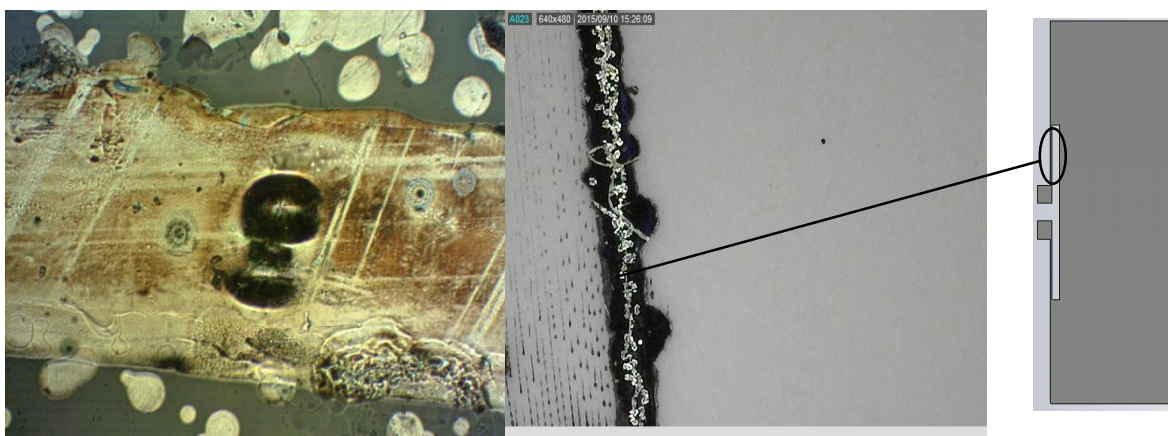


Fig. 5.7 Pinhole on feedline

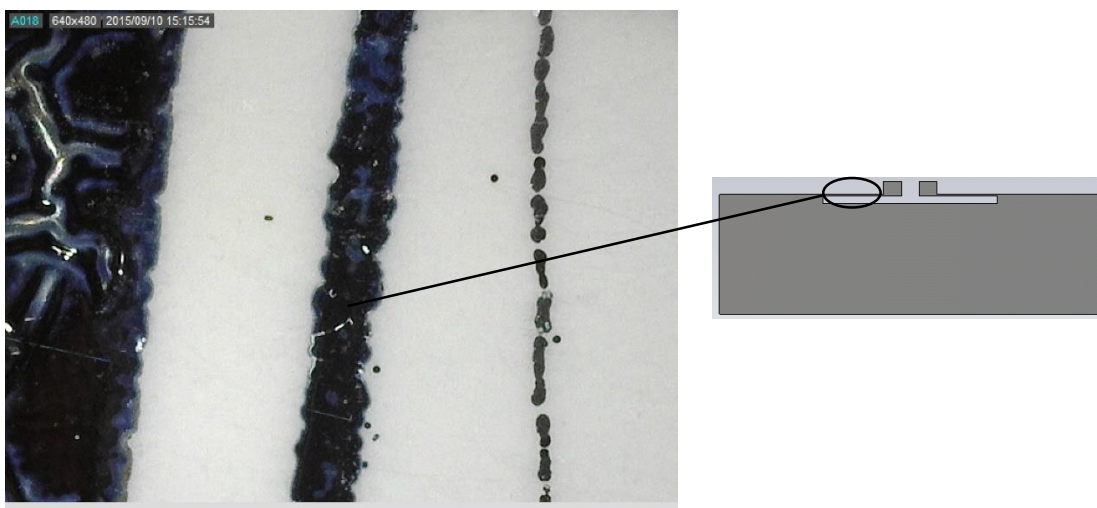


Fig. 5.8 Notched defect on edges

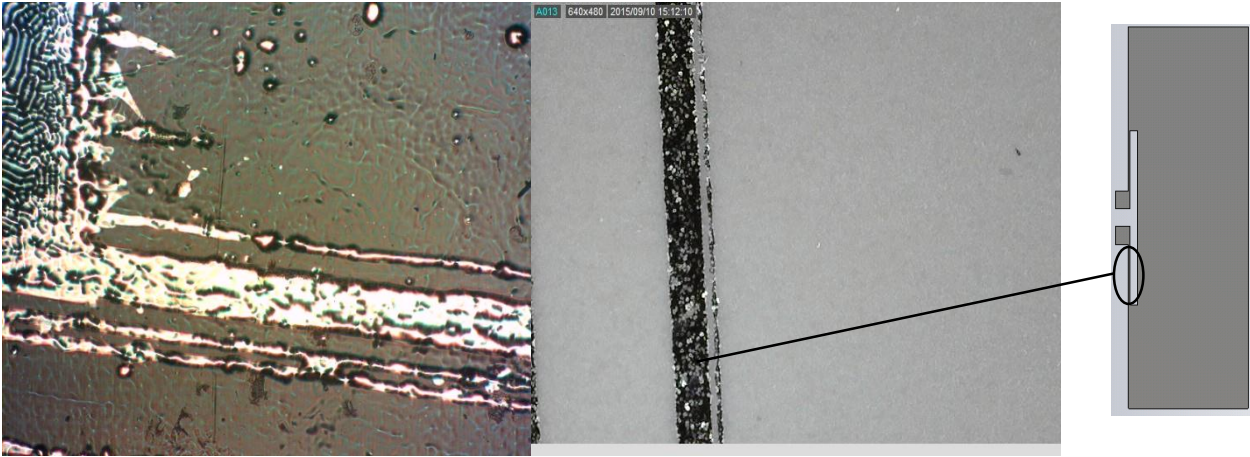


Fig. 5.9 Variation in feedline width

5.3.1 Simulated Defects Study

The defective printed tags were simulated with CST Microwave Studio™. Although the silver conductor was imported from the simulator's conductive materials library, the conductivity was adjusted to represent the conductivity of the printed sample presented in Chapter 4. The simulated defects are as mentioned in Section 5.3. In the case of the pinholes, they were distributed on specific parts of the tag around the slot region where simulation indicated the highest current density to exist. The pinholes were made (i) solely on the tag ports, (ii) solely on the feedlines, (iii) simultaneously on the feedlines and on the ports, (iv) around the entire slot area including the feedline, and (v) around the entire slot area including the feedline and the ports. The diameter of all holes was 0.2mm and their placement was arbitrary in order to mimic the random occurrence of the defects.

For the notched defects, four instances were simulated: (i) with the insertion of a single notch on just one of the feedlines, this notch cuts into the feedline by 50%. (ii) Notched defects on both feedlines. (iii) In order to depict an extreme case, the cut of the notch into both feedlines was extended to 75% of the width of the feedlines. (iv) Finally, multiple notches were made on both feedlines to better resemble what was observed in the printed tags.

A hairline cut defect was also introduced into one of the feedlines. This was done in such a way that it represents a fault that cuts across the feedline of the RFID tag. This kind of defect, as expected, severely affected the functionality of the tag as it directly

affects the tag's connection with the ASIC. As the tag effectively stopped functioning, no further investigation was carried out on the hairline crack.

In all cases, because of the size of the small size of the defects, very fine meshing with dimensions comparable to those of the faults was used during simulation in order to improve simulation accuracy. This was achieved at the cost of increased simulation times.

The simulated defect structures are shown in Figs. 5.10 – 5.13.

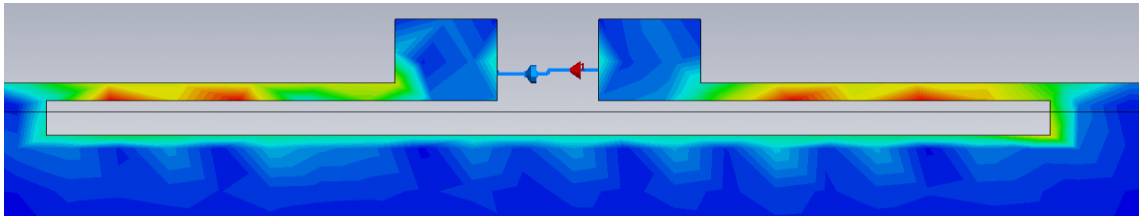
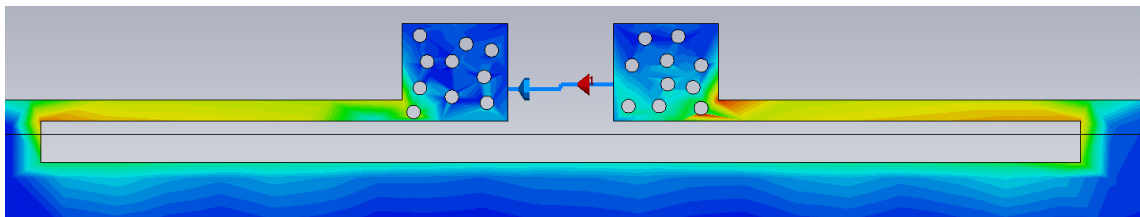
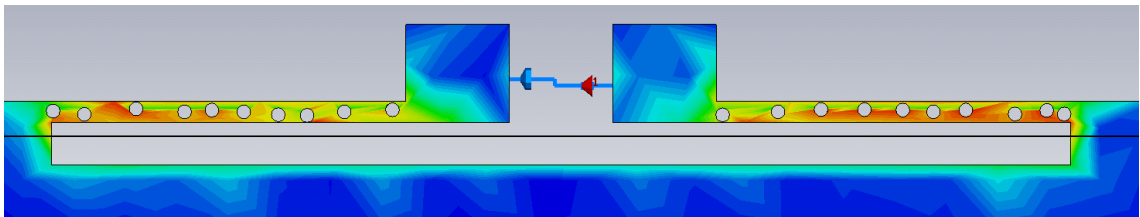


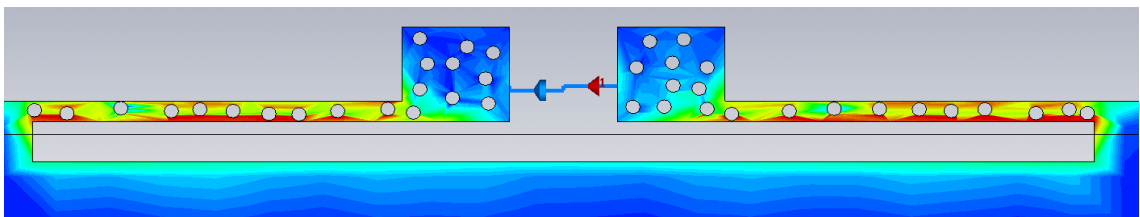
Fig. 5.10 Simulated Tag Feed Area Without defects



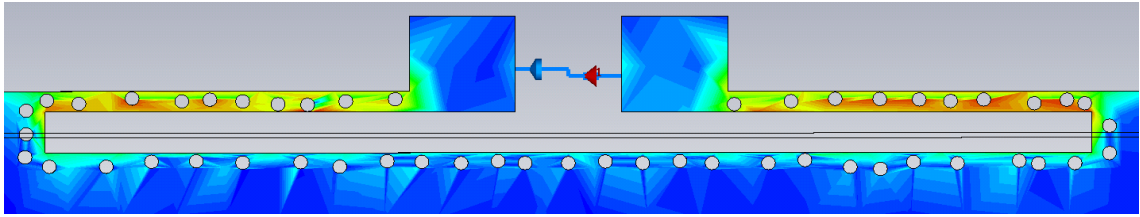
(a)



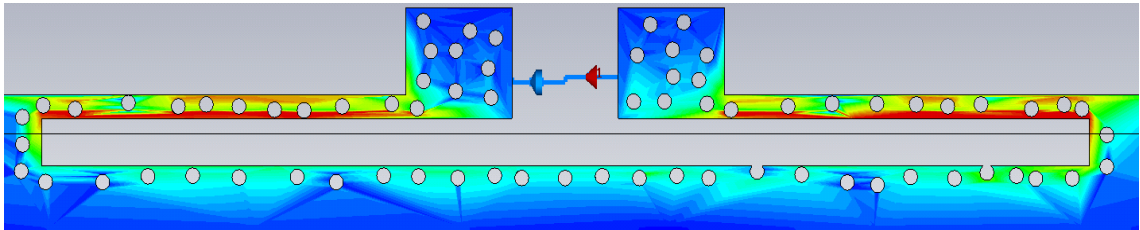
(b)



(c)

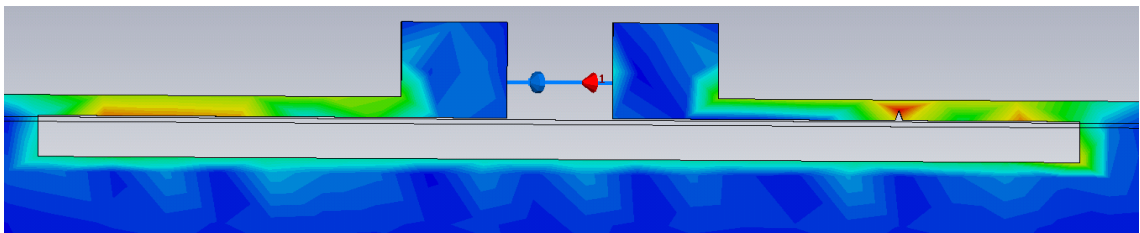


(d)

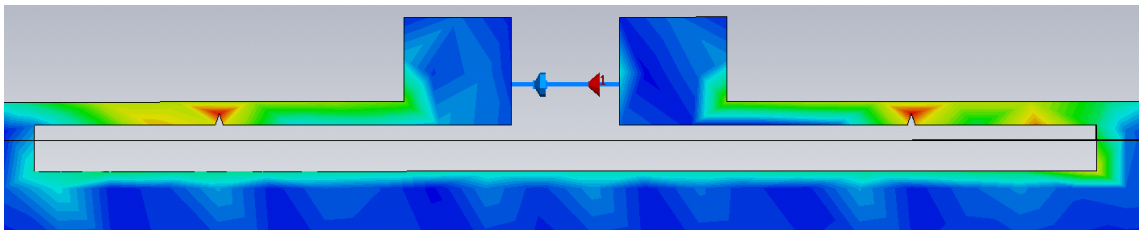


(e)

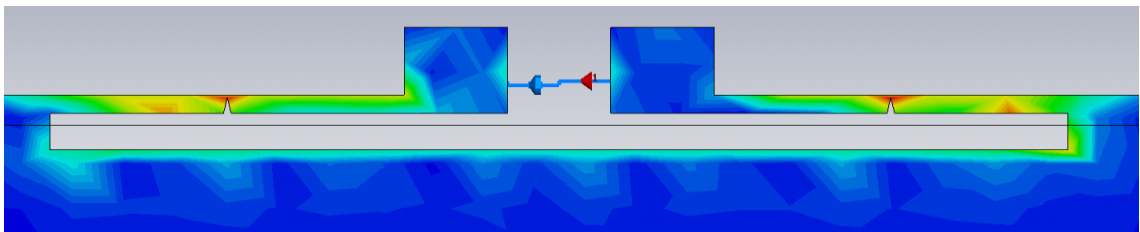
Fig. 5.11 Pinhole defects (a) on ports (b) on feedlines, pinhole FL (c) on ports and feedlines, pinhole FL PT (d) on feedline and around slot, pinhole FL SL (e) on ports, feedlines and around the slot, pinhole PT FL SL.



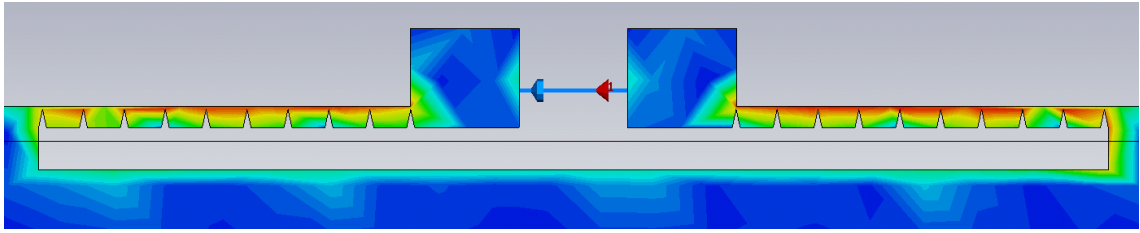
(a)



(b)



(c)



(d)

Fig. 5.12 Notched defects (a) on one feedline, single notch 1 FL (b) 50% into both feedlines width, single notch 2 FL (c) 75% into both feedlines width, deep single notch 2 FL (d) multiple 75% into both feedlines width, deep multi notch 2 FL.

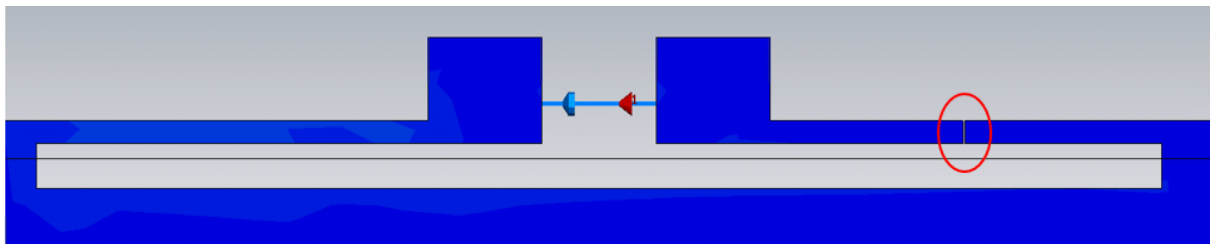


Fig. 5.13 Cut on Feedline

When compared to the tag without defects, it can be seen that in all cases that defects affect the surface current flow in the tag albeit in different manners. This influence on current flow, even though minimal in some instances, indicates that these defects would alter the tag's behaviour. As expected, the tag with a cut feedline shows that there is no current flow on the tag.

The influence of the various defects on the simulated efficiency of the tag is shown in Fig. 5.14.

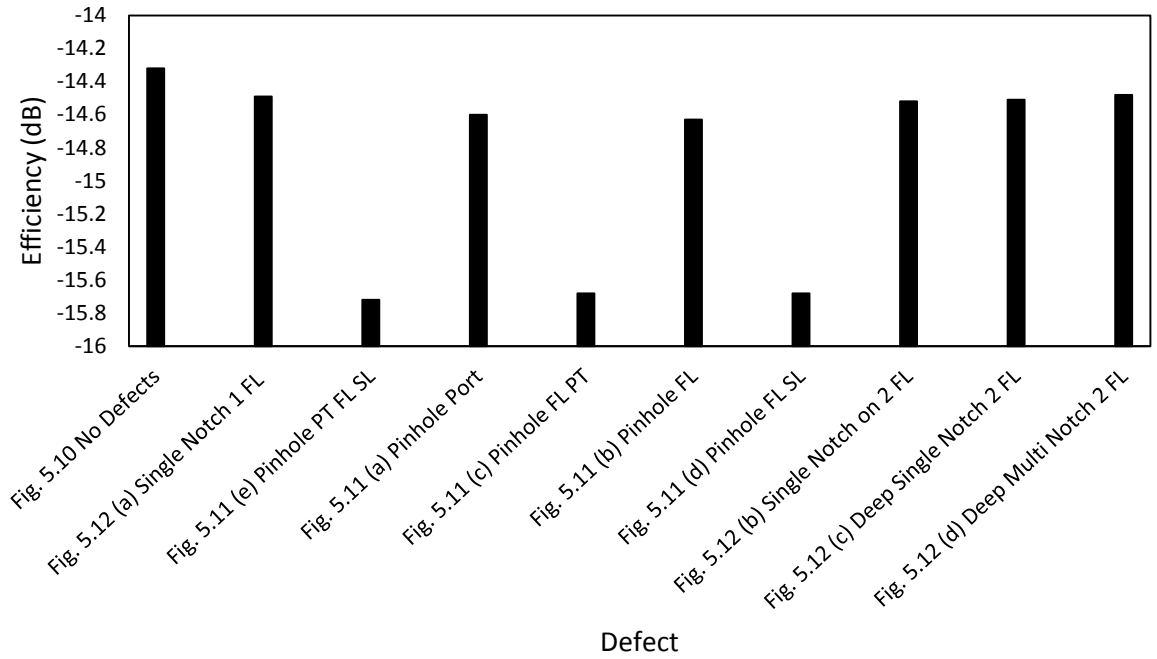


Fig. 5.14 Simulated Tag Efficiency .FL = Feedline, PT = Port, SL = slot

Simulation results show that without defects, the tag has an efficiency of -14.32 dB. It can be deduced from the graph that all the defects have clearly affected the efficiency although this is marginal in some cases especially for the feedline notches. For these notched defects, greatest efficiency reduction, which was for the notched defects in both feedlines (single notch on 2 FL), was only 0.2 dB which is not significant.

The highest effect on the tag efficiency was observed when the pin hole defects were on the region around the slot and including the port (pinhole PT FL SL). In this scenario, there was a reduction in the tag simulated efficiency to -15.7 dB, a 1.4 dB decrease. It was also observed that when the pinholes were either only on the ports or on the feedlines (pinhole port and pinhole FL), the efficiency was not as reduced as observed in the other pinhole defects with simulated efficiency of -14.6 dB. These were closer to the effects of the notched defects.

The simulated gain and return loss (S_{11}) of the tags are shown in Table 5.1.

TABLE 5.1 SIMULATED TAG GAIN AND RETURN LOSS (S₁₁)

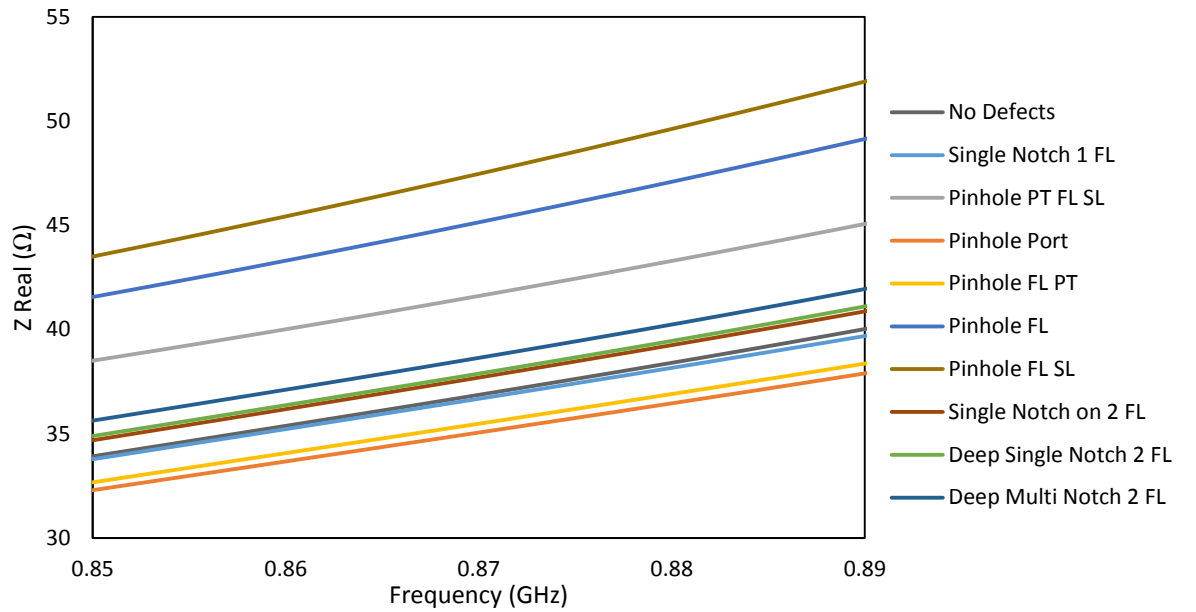
DEFECT	GAIN (dB)	S ₁₁ (dB)
Fig. 5.10 No defects	-9.79	-10.69
Fig. 5.12 (a) Single Notch on 1 FL	-9.87	-9.71
Fig. 5.11 (e) Pinhole PT FL SL	-10.76	-6.94
Fig. 5.11 (a) Pinhole Port	-9.98	-9.69
Fig. 5.11 (c) Pinhole FL PT	-10.61	-6.95
Fig. 5.11 (b) Pinhole FL	-10.02	-9.71
Fig. 5.11 (d) Pinhole FL SL	-10.59	-7.73
Fig. 5.12 (b) Single Notch on 2 FL	-9.91	-9.84
Fig. 5.12 (c) Deep Single Notch 2 FL	-9.96	-10.42
Fig. 5.12 (d) Deep Multi Notch 2 FL	-9.94	-10.25

* FL = Feedline, PT = Port, SL = slot

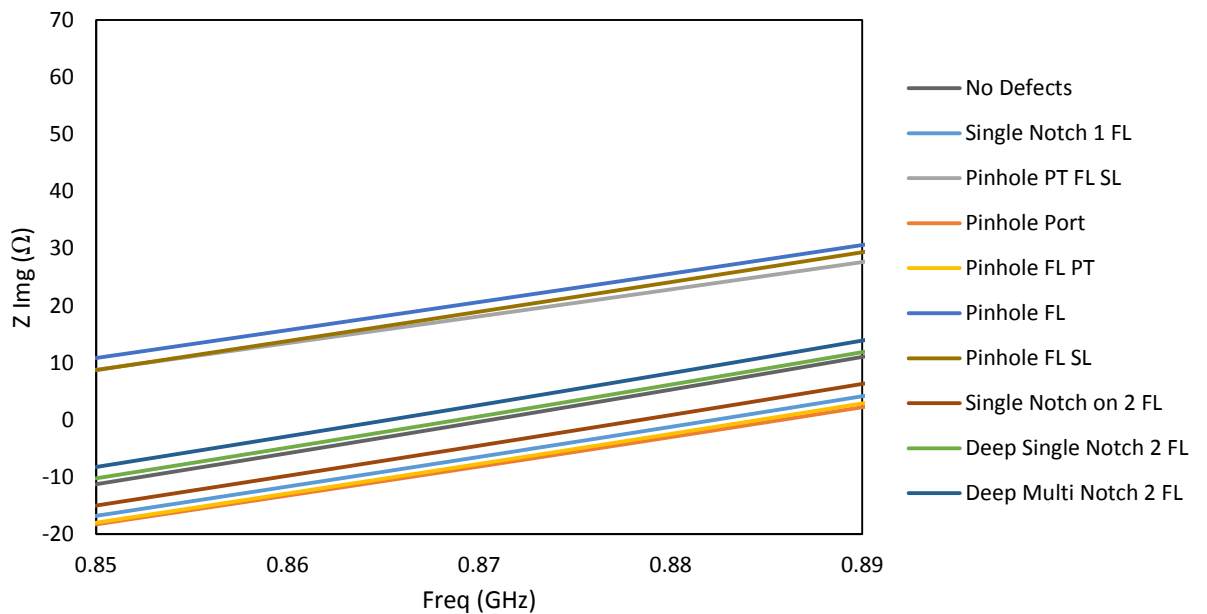
From the data presented in the table, the highest S₁₁ of -6.94 dB was obtained in the case of pinhole defects around the slot including on the port closely followed by an S₁₁ of -6.95 dB which was obtained when the printing defects were located on the feedline and on the port. This suggests that these defects caused the largest impedance mismatch between the tag and the ASIC. This will result in a reduced read range. The best simulated return losses were obtained for the deep single notch on both feedlines and the deep multiple notches on both feedlines with S₁₁ of -10.42 dB and -10.25 dB respectively.

The same trend observed for the return loss values was also seen with the gains. When the pinhole defects were around the slot region as well as on the ports, the simulated gain of the tag dropped by 0.97 dB to -10.76 dB. This is the most reduction in gain caused by any defect on the printed tag. Having a single notch on just one of the feedlines had the least effect on the tag's gain with just a 0.08 dB reduction in tag gain.

The effect of the defects on the tag antenna port impedance is shown in Fig. 5.15.



(a)



(b)

Fig. 5.15 Effect of defect on tag impedance (a) Real Impedance (b) Imaginary Impedance

Fig. 5.15 (a) indicates variation in tag port resistance with the introduction of the defects into the tag. Most of the defects resulted in an increase in resistance with the most increase due to the pinholes on the feedline. Indications from Fig. 5.15 (b) show an increase in tag inductive reactance for most of the defects.

From the tag gain and S_{11} results obtained from the simulation, the ASIC datasheet [20] and a Voyantic Tagformance reading system [21], the read ranges of the tags with these defects were calculated using the equation:

$$R_{max} = \frac{\lambda}{4\pi} \sqrt{\frac{EIRP \cdot G_{Tag} \cdot \tau}{P_{th}}}$$

The percentage change in read range for each defective structure compared to the perfect tag are shown in Table 5.2.

TABLE 5.2 CALCULATED PERCENTAGE CHANGE IN TAG READ RANGE

DEFECT	READ RANGE (% Δ)
Fig. 5.12 (a) Single Notch on 1 FL	-1
Fig. 5.11 (e) Pinhole PT FL SL	-12
Fig. 5.11 (a) Pinhole Port	-2
Fig. 5.11 (c) Pinhole FL PT	-11
Fig. 5.11 (b) Pinhole FL	-3
Fig. 5.11 (d) Pinhole FL SL	-10
Fig. 5.12 (b) Single Notch on 2 FL	-2
Fig. 5.12 (c) Deep Single Notch 2 FL	-2
Fig. 5.12 (d) Deep Multi Notch 2 FL	-2

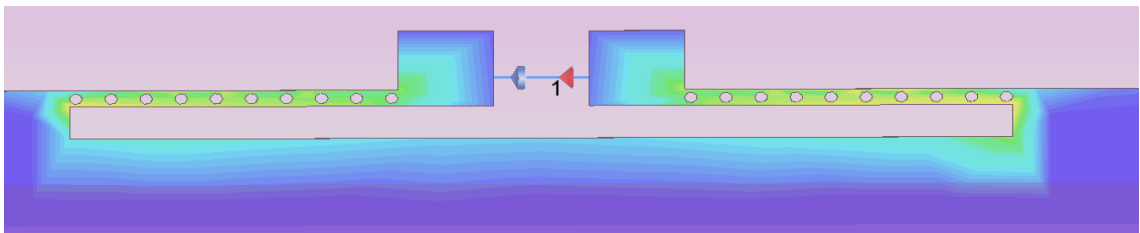
* FL = Feedline, PT = Port, SL = slot

The least reduction in calculated read range was obtained from the tag with a single notch that was 50% into the width of the feedline, Fig. 5.12 (a). This is as expected since this defect caused the least disruption to the feedline current and therefore has a small effect on the antenna-tag matching. Extending this notch to the second feedline as well as increasing the depth, Figures 5.12 (b), (c), (d), did not appear to significantly reduce the read range as only 2% of the read range was lost in all of these instances.

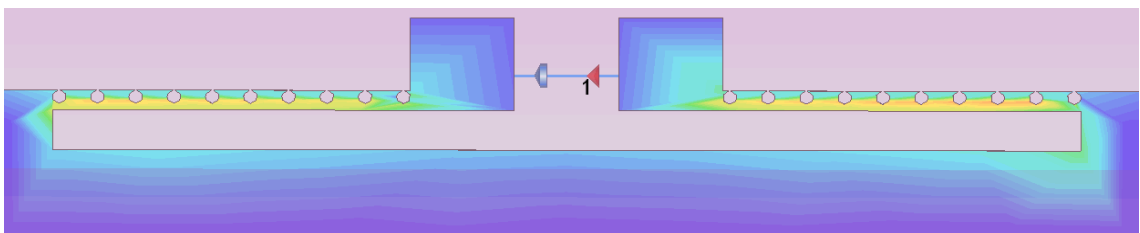
For the pinhole defects, when the pinholes are located only on the feedlines, Fig. 5.11 (b), the reduction in read range was only 2% which is equivalent to that of most of the notched defects (Fig. 5.12(a) – (d)). However, as the number of pinholes was increased, Fig. 5.11(c) – (e), there was a decrease in the tag read range with a maximum reduction of 12% calculated for when the pinholes were on the ports and also around the slot, Fig. 5.11(e).

During the assessment of the pinholes defects on the feedline, it was sought to ascertain if the location of the holes affects the tag performance. For instance, if the pinholes were aligned in a particular non-random way. To this effect, all the holes were aligned and placed in the middle, top and bottom edge of the feedline, Fig. 5.16 (a), (b) and (c) respectively.

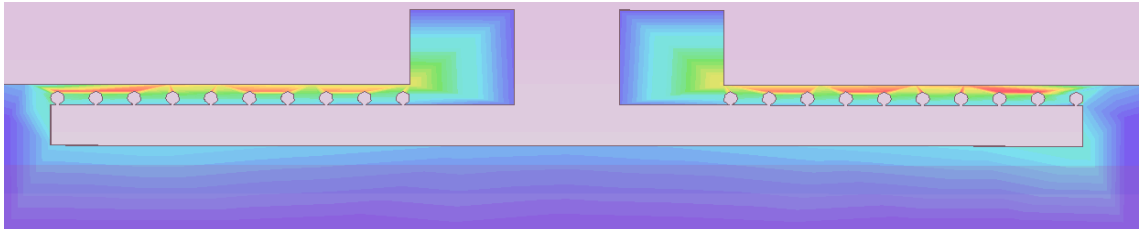
Although it is acknowledged that this linear alignment is unlikely to occur, it had been observed that when holes closer to the edge were removed, improvement on the tag performance were more evident than in other cases.



(a)



(b)



(c)

Fig. 5.16 Pinhole Defects on Feedline (a) Centre (b) Top (c) Bottom

The effect of the position of the pinholes on the feedlines is presented in Table 5.3.

TABLE 5.3 PINHOLE DEFECTS

DEFECT	GAIN (dB)	EFFICIENCY (dB)	S ₁₁ (dB)
Pinhole on FL, Fig. 5.11(a)	-10.02	-14.63	-9.71
Pinhole on FL, Fig. 5.16(a)	-10.59	-15.67	-7.07
Pinhole on FL, Fig. 5.16(b)	-10.79	-16.40	-5.39
Pinhole on FL, Fig. 5.16(c)	-10.75	-16.57	-4.91

It is noticed that when the pinholes are aligned on the top and bottom edge of the feedline, the tag gain and efficiency was more reduced than when the distribution was random or when the alignment of the pinholes was in the middle of the feedline. However, simulations also indicate that pinhole defects close to the edge of the feedline degrade the matching of the antenna to the ASIC more than the randomly distributed pinholes. These effects can be due to the high current flow on the edges of

thin lines (conductors), meaning the realized gain ($\text{Gain} \times \text{input power transfer coefficient}$) would be compromised.

5.3.2 Measured Defects Study

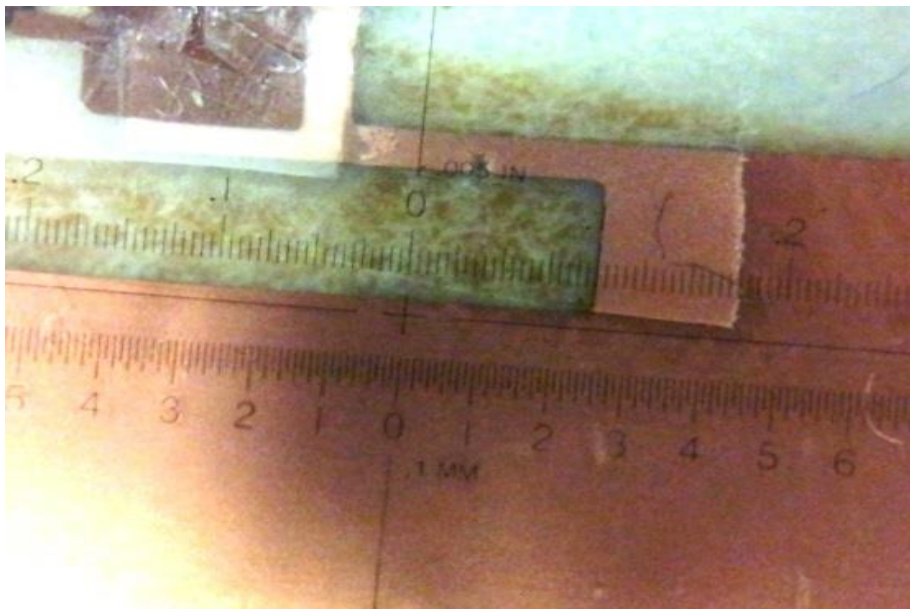
Samples with defects identical to those in Section 5.3.1 were fabricated using a copper clad mylar sheet which had a combined thickness of $< 100\mu\text{m}$. The fabrication was carried out using conventional wet etching. The ASIC was attached to the tag ports using adhesive tape and proper contact between the ASIC strap and the ports was ensured by point pressure. The measurements were carried out using Voyantic Tagformance Lite equipment [21]. The feed area of the fabricated tags are shown in Fig. 5.17.



(a)



(b)



(c)



(d)

Fig. 5.17 Fabricated Defects (a) Pinhole on feedline (b) Pinhole around slot (c) Single notch on feedline (d) multiple notch on feedline.

The defected tag performances were assessed using two parameters:

- Read Range
- Transmitted Power

To strengthen the confidence in the measured results, 10 different samples of each tag defect were fabricated and 10 independent sets of measurements were made. The presented results are an average of these 10 measurements for each fault type.

The graph in Fig. 5.18 illustrates the percentage change in measured read range of the tags

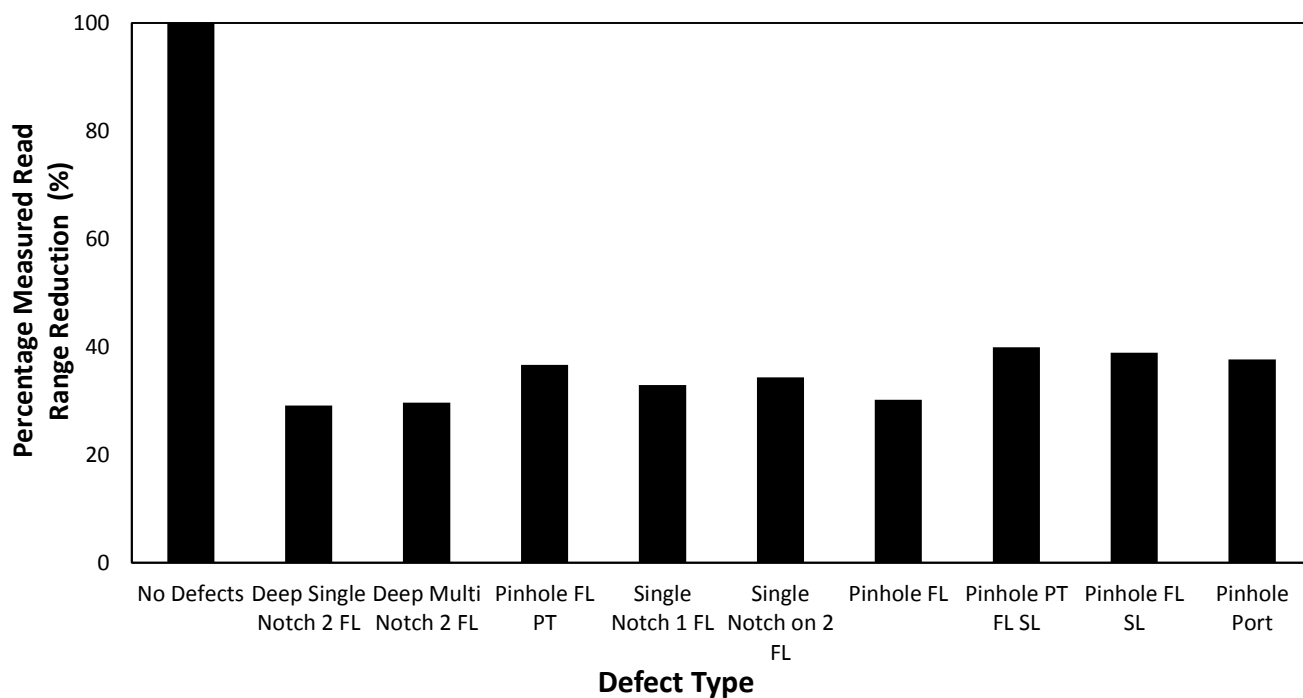


Fig. 5.18 Measured Tag Read Range as Percentage of Perfect Tag. FL = Feedline, PT = Port, SL = slot

Figure 5.18 shows a reduced read range in all tags with defects compared to the tag without defects. The most reduction in read range was seen for the tag that had pinholes around the slot as well as on the port. This has a read range that is 40% of that of the tag without defects. The least reduction in read range was for the deep single notch on both of the feedlines. In this scenario, a 29% reduction from the read range of the undefected tag was measured. This is closely followed by the deep multiple notches on the feedline with a percentage change in read range of 30%. This low influence on measured read range by the notch defects is in agreement with the simulated results seen in Section 5.3.1. In general, the measured results point to the fact that pinhole defects influence the read range of the epidermal RFID tag more than the notched defects.

A comparison made between the measured and calculated read ranges of the defected tags have shown a similar trend on the effect the various defects have on the tag read range. This comparison is shown in Fig. 5.19. It can be seen that although the

simulated defects match well to measurement in trend, in practice physical defects are much more deleterious to performance than expected.

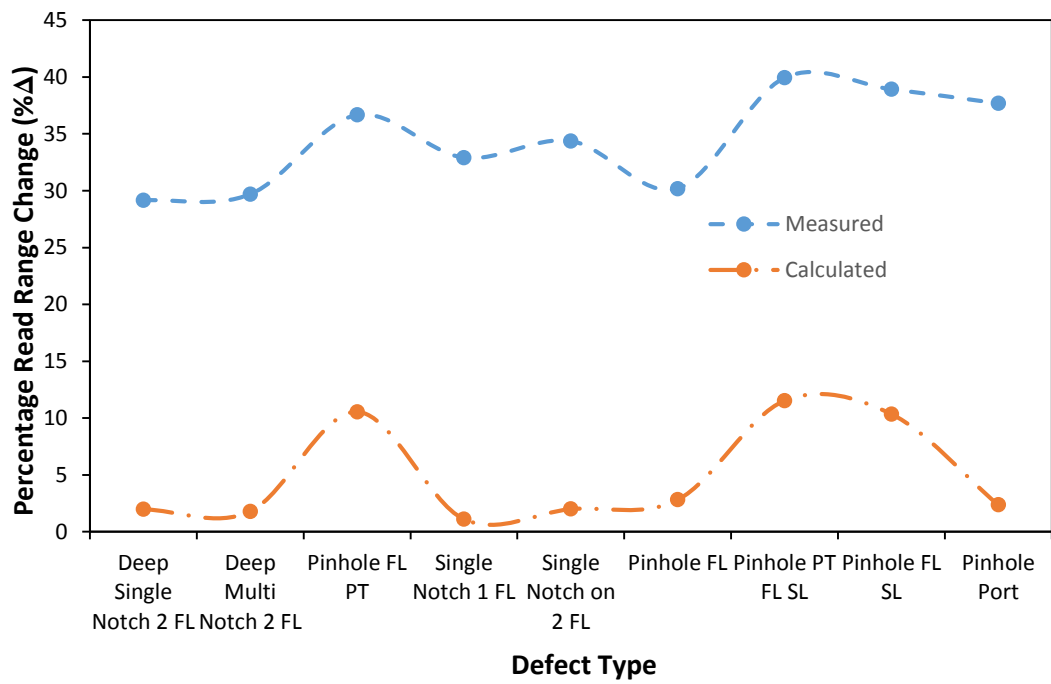


Fig. 5.19 Percentage Read Range Comparison

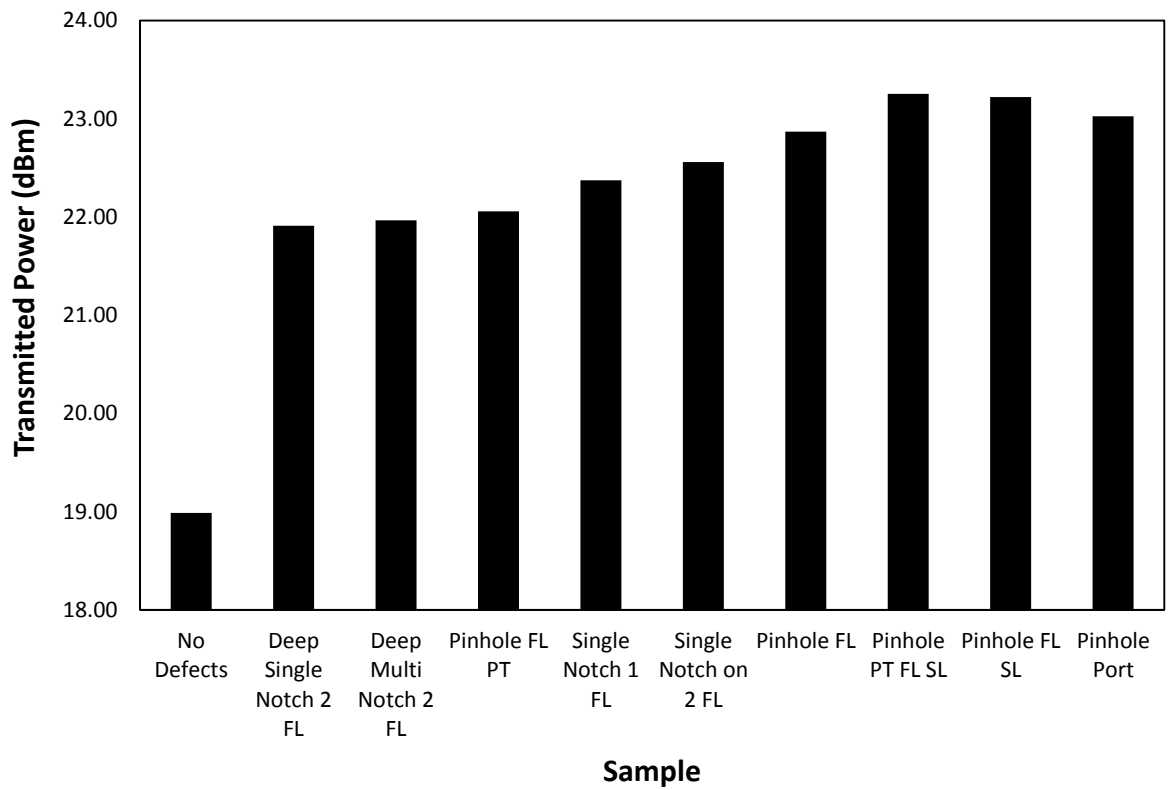


Fig. 5.20 Measured Transmitted Power

The transmitted power from the reader to the tag was also measured. This indicates the level of power required to activate the RFID tag by the reader. From Fig. 5.20, the tag without defects had the lowest transmitted power of 18.99dBm. An increase in measured transmitted power was observed when the defected tags were measured. The highest transmitted power was measured with the tag that had pinhole defects on the area around the tag slot and on the ports. The measured transmitted power obtained for this tag was 23.25 dBm. The high transmitted power for this tag also corresponds with the least read range which was obtained from it. The defected tag with the least transmitted power was the tag with the multiple notched defects on the feedlines with 21.91 dBm measured.

Transmission power is a source of concern in handheld readers where a higher transmitted power would imply a faster draining of the battery by the reader's operation.

The results presented above show that the defects do affect the performance of the tag by varying degrees. Both simulation and measured results indicate that while the defects in the form of notches do not have a significant effect on tag performance, pinhole defects also affect the performance of the tag especially when they are on the feedline area and around the slot. In general however, none of these defect would make the tag lose functionality except in a case where the feedline has been cut by a defect.

5.4 Tag Robustness Test

5.4.1 Transfer Tattoo Performance When Mounted On Skin.

In order to test the robustness of the printed transfer tattoo tags, a sample of the tag was mounted on the arm and measurements were taken at 30 minutes interval for a total of 8 hours. This was to imitate an average working day. This sample was a 3-layer sample which would give the best read range performance. The fabrication is as described in Chapter 3. Proper contact was ensured between the tag and the chip strap by making several depressions on their point of contact in order to eliminate the

possibility of reduced read range over time due to loosening of the attachment.. Fig. 5.21 shows the tag when initially mounted on the arm.

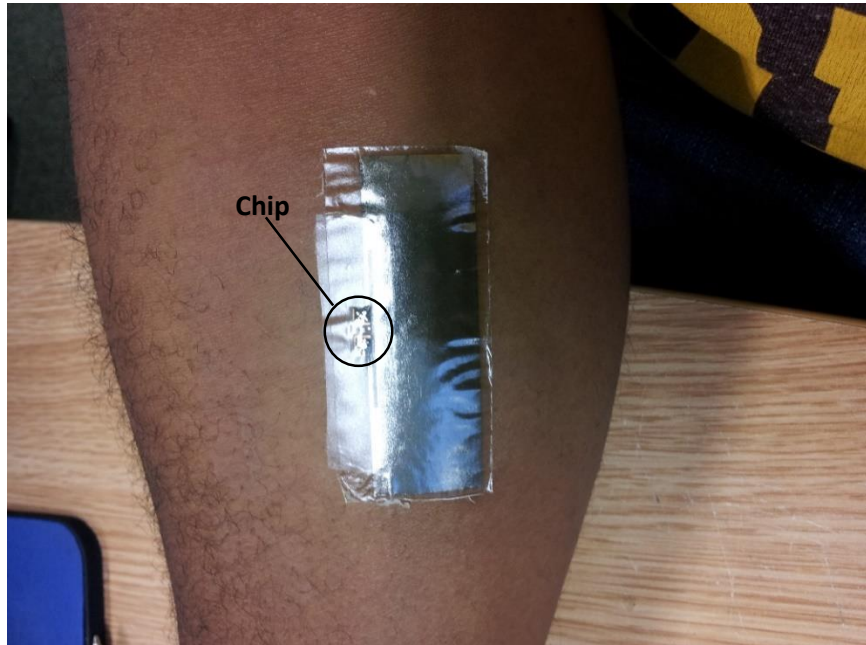


Fig. 5.21 Inkjet Printed Transfer Tattoo Tag initially mounted on arm

After about two hours of regular office use which includes PC keyboard use, writing on a desk and walking around, some creasing was observed on the tag. However, this did not adversely affect the reading of the tag because of the continued functionality over the course of the day. Fig. 5.22 illustrates the creasing on the tag.



Fig. 5.22 Crease on the Inkjet Printed Transfer Tattoo Tag During Use

In Fig. 5.23, the plot of the tag read range over 8 hours is shown

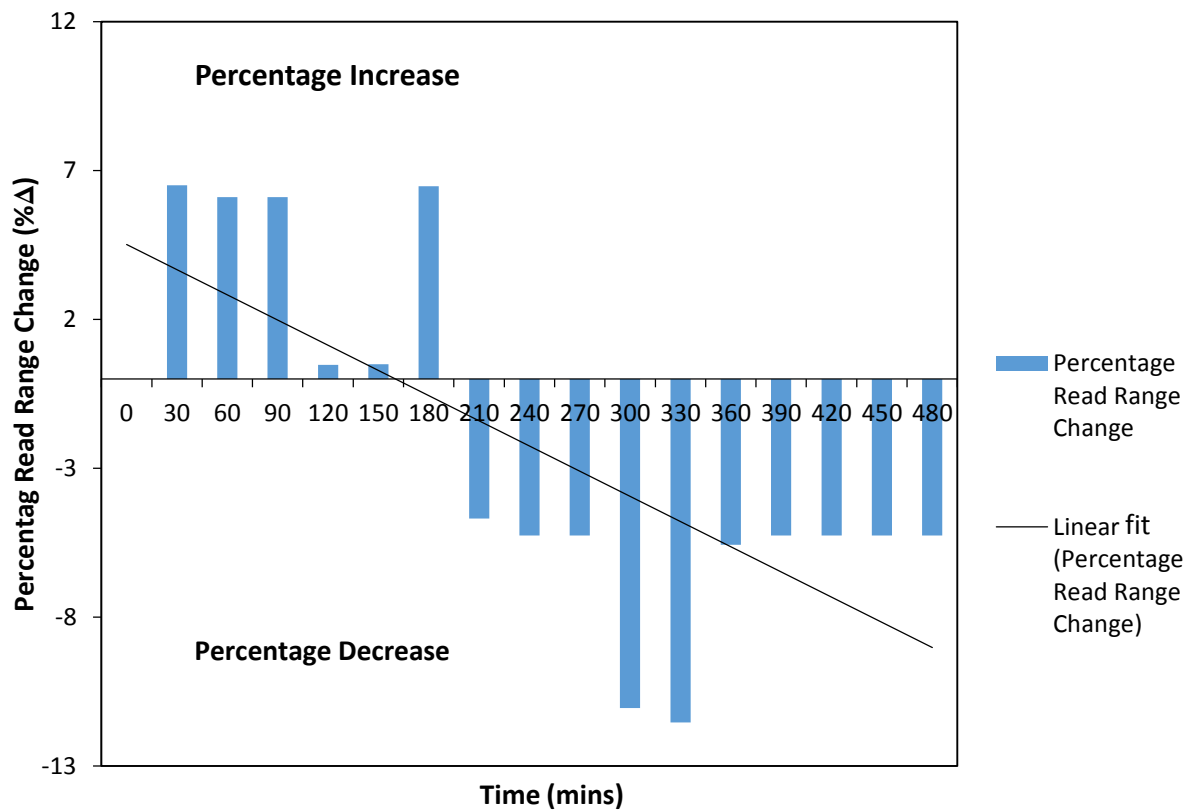


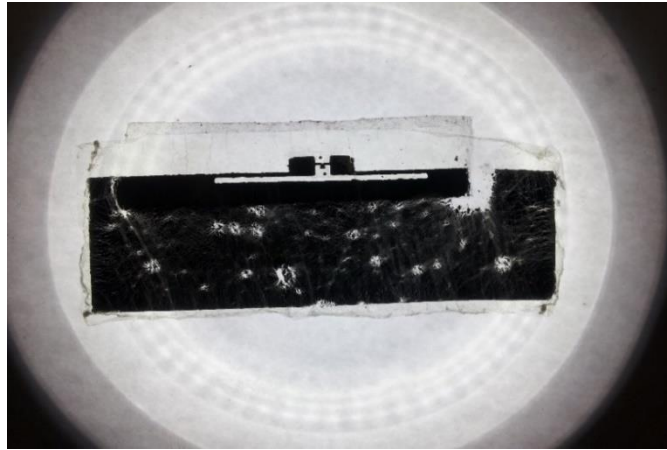
Fig. 5.23 Measured Tag Read Range Over 8 hours

The initial read range obtained from the tag was 0.6m. Although there was an increase in tag read range when the tag was measured after 30 minutes, this does not follow the overall trend of the measurement during the course of the 8 hours. The increase in read range could be attributed to errors during the measurement as slight changes in the distance between the tag and the reader antenna would lead to a seeming increase in read range (tests show that a 1cm change in tag location would result in about 20cm change in measured read range). This also applies to other increases in read range above the previous measured read range seen at any point during the 8 hour measurement. At the end of the experiment, the final read range was measured to be 0.57m – a 5% reduction in read range (3 cm).

In order to test how long the tag can function for, the tag was worn overnight for a further 12 hours. Upon final observation, the tag had suffered a lot of abrasion, no read was obtained from it. Fig. 5.24 shows the tag after the additional 12 hours, (a) on skin and (b) on a light box.



(a)



(b)

Fig. 5.24 Inkjet Printed Transfer Tattoo Tag Robustness Test (a) after 8 + 12 hours (b) after 8 + 12 hours on a light box

The Tag was also worn overnight on the side of the torso to check for its robustness. The reason for this is because unlike the arms which could be very mobile during sleep hence frequently rubbing on various surfaces in different directions, the movement of the torso during sleep is relatively limited. The tag was worn for a sleep duration of about 6 hours 30 minutes. Fig. 5.25 shows the placement of the tag on the body while the measurement result is shown in Fig. 5.26



(a)

(b)

Fig. 5.25 Tag on Torso (a) Before Sleep (b) After Sleep

As with the tag that was placed on the arm, some creasing was also observed on the tag after the sleep. However, this was not enough to cause significant reduction to the tag performance (a reduction in read range of just 1cm is shown in Fig. 5.26).

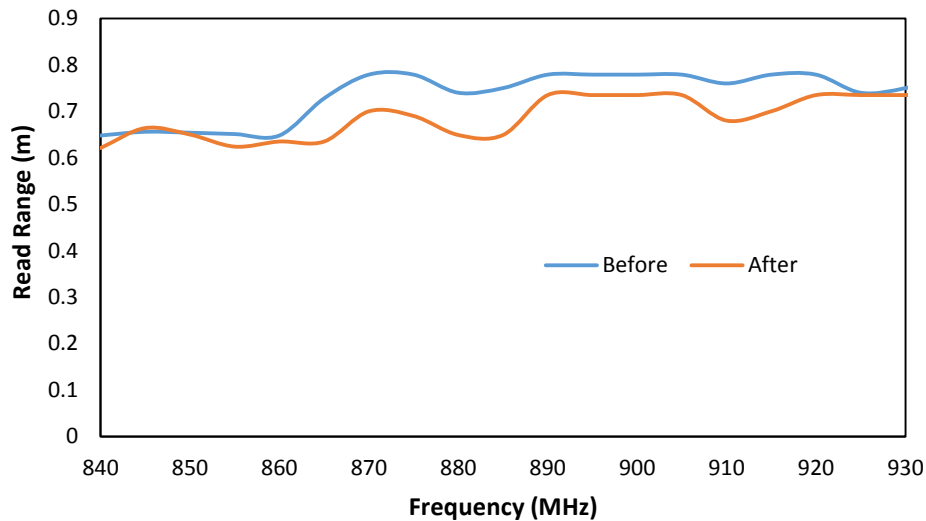


Fig. 5.26 Read Range of Transfer Tattoo Tag Before and After Sleep

5.4.2 Effect of Sweat on Tag Performance

In the previous durability measurement, the wear test was conducted while carrying out normal daily office activities which were not strenuous. Therefore, the long duration (8 hours) of the tag's functionality does not represent an absolute test of robustness bearing in mind its possible use in harsh environments and conditions. In order to assess this, the tag was attached to the torso of a volunteer who undertook 20 minutes of various exercise activities at the gym. The choice of torso as the mounting area is to ensure exposure to sweat as well as body motion during the exercises. Fig. 5.27 shows the attachment of the inkjet printed transfer tattoo tag on torso prior to and immediately after the gym activities.



Fig. 5.27 Tattoo Tag mounted on Torso for Gym Test (a) Before Gym (b) After Gym

Fig. 5.28 shows a comparison of the change in read range for the tag before and immediately after the gym activities.

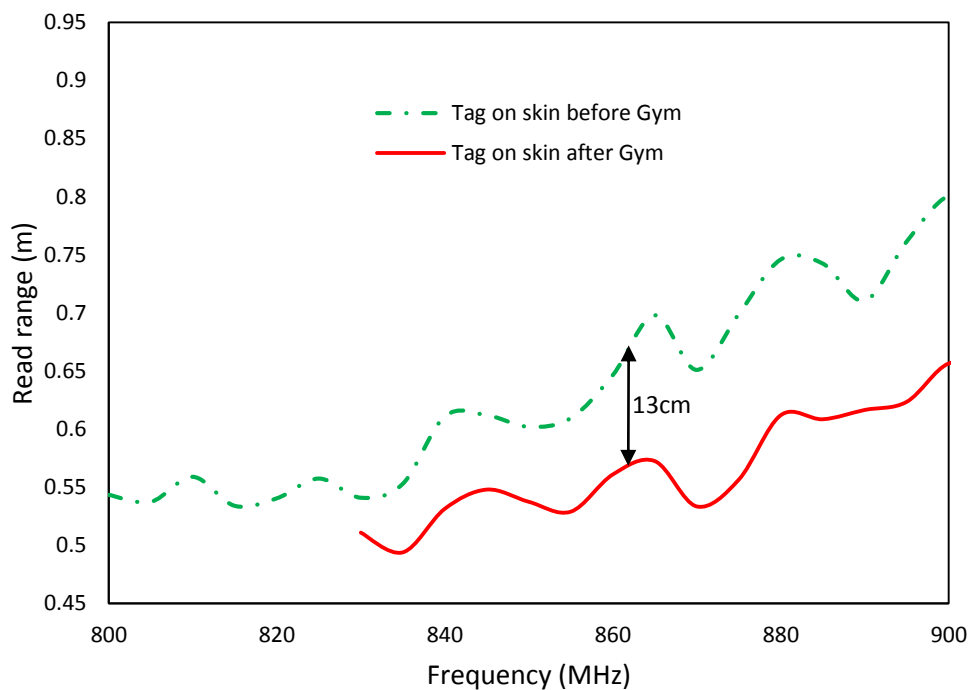


Fig. 5.28 Read Range of Transfer Tattoo Tag Before and Immediately After Gym Activities

Read range measurement after 20 mins of gym activities show a reduced read range when compared to the initial measurements. While the initial read range was about

70cm, the measurement afterwards showed a reduction by about 13cm as seen in Fig. 5.28. This reduction in tag read range was not considered to be adverse since the final read range was about 57cm (approximately 19% reduction).

In order to establish whether or not sweat was a factor in the deterioration of the tag as seen during the previous test, a more controlled experiment was set up in order to eliminate the effect of movements hence friction on the tag. This experiment would also help to determine the effect sweat had on the tag durability as opposed to ordinary water (moisture). For this purpose a saline solution was made to have a close resemblance to sweat. The concentration of salt in this solution was obtained from information from [22] where the reported concentration of sodium in sweat is between 30 – 240mg/100ml.

Two tags were used for this experiment: one exposed to the saline solution and the other exposed to ordinary water. This was done by dampening tissue paper with the salt solution and with water and placing them on the tag samples. In order to ensure that equal amounts of the solution and water were used, each was measured before applying on the tissue paper. This set up is shown in Fig 5.29.



Fig. 5.29 Experiment Setup (a) Top view (b) Bottom view

Prior to the start of this experiment, the tags were mapped as shown in Fig 5.30.

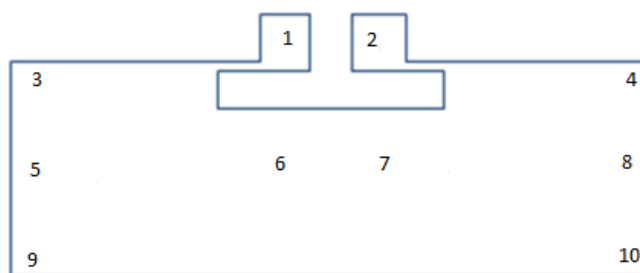


Fig. 5.30 Resistance Measurement Points

Resistance measurements were taken at these points prior to the start of the experiment and then every 5 minutes for 30 minutes using the order: 1-2, 1-3, 2-4, 3-9, 4-10, 3-10, 4-9, 5-6, 6-7 and 7-8. The average of the resistances were taken for every measurement and is summarized in Table 5.4.

TABLE 5.4 TAG RESISTANCE MEASUREMENTS

Time (Mins)	0	5	10	15	20	25	30
Saline Res. (Ω)	1.08	9.91	79.08	31501.68	90302.2	183005.9	1207002
Water Res. (Ω)	1.32	8.93	81.59	41200.46	86000.56	189000.7	1155556

The results from the table are illustrated in Fig. 5.31.

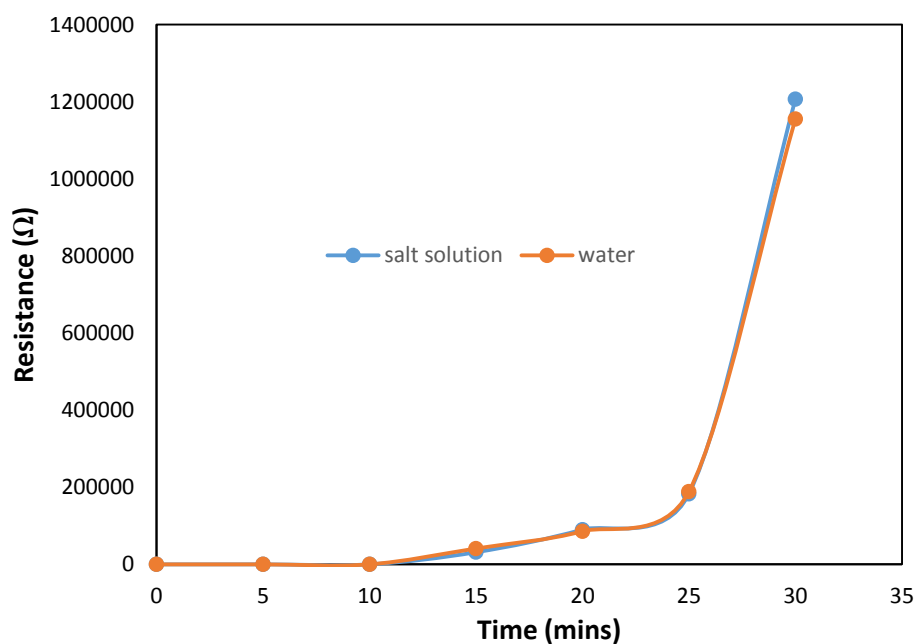


Fig. 5.31 Resistance measurements of sample tags

From the resistance measurements, no significant difference can be seen between the two tags. This would lead to the conclusion that the deterioration of the tag during the gym activities was more as a result of motion and friction than the effect of exposure to sweat. The most reliable indication from these measurements was during the first 15 minutes where both tags were in tact. This is because beyond this point, cracks appeared on both tags which led to an increase in measured resistance. Additionally, there was also folding of the underlying transfer tattoo paper due to exposure to both liquids.

5.4.3 Effect of Showering on Tag Performance

To further test the effect of exposure to liquid, the tag was worn during a shower for about 10-15 minutes. By doing this, the transfer tattoo tag was exposed to water as well as bathing soap. Care was taken not to expose the tag to vigorous rubbing. The image for this experiment is shown in Fig. 5.32 while the measurement results are shown in Fig. 5.33.



Fig. 5.32 Transfer Tattoo Tag During Shower

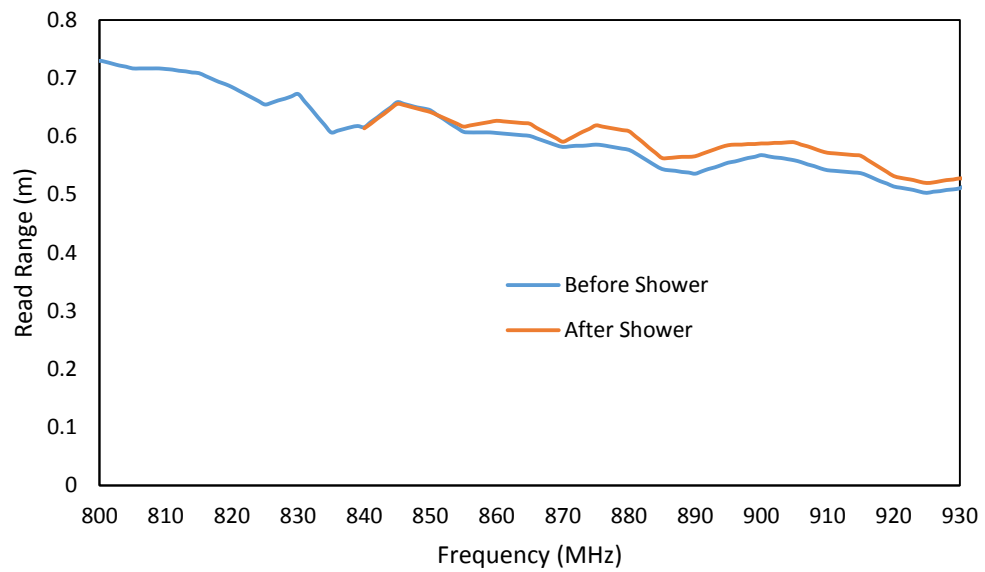


Fig. 5.33 Measured Read Range of Transfer Tattoo Tag Before and After Shower

Fig. 5.33 shows the before and after shower measurements of the transfer tattoo tag read range. The indication is that the tag performance remains relatively unaffected after exposure to water when it was mounted on skin. It can be seen from the graph that there is a slight increase in read range of the tag after shower by about 1.8 cm. This increase in read range is due to the weakening on the adhesion between the skin and the tag hence enabling a slight separation between the two surfaces with a formation of an air gap, Fig 5.34.



Fig. 5.34 Transfer Tattoo Tag After Shower

5.5 Conclusion

In this chapter, the defects that can occur during the inkjet printing of epidermal tattoo tags have been studied. The sources of these defects were presented and include blocked nozzle, temperature conditions during and after the printing process, the ink viscosity and the nature of the substrate.

A simulation based study of various identified defects was presented: pinholes on the ports, feedline and around the slot region; notches on the feedline; and, a hairline cut on the feedline. Simulation results indicated these defects had varying degrees of effect on the tag efficiency, gain and return loss. The greatest effect on the tag efficiency was due to the location of pinhole defects around the slot area and including the ports with a 28% decrease in simulated tag efficiency. The lowest effects came from notches on the feedline where efficiencies only slightly reduced when compared to a tag without any defects. The same trend was also seen in the effects on the gain and return loss of the tag. With a 12% reduction in the tag read range, the read range of the various defects calculated based on simulation results and equipment manufacturer data sheets showed that the read range was most affected when the pinhole defects were around the slot and also on the port.

The simulated defects were also replicated on tags fabricated with etched copper clad mylar sheets. The tag performances were assessed based on read range and transmitted power. The read range performance of the various defected tags had a good agreement with the simulated results with the least read range measured from the tag with pinholes around the slot area and the ports which had a read range of about 40% of a tag without defects. Higher transmitted power for the tags were also measured for the defected tags.

Overall, measurement and simulation results indicated that the defects in the form of notches on the feedline had the least effect on the tag performance while tag performance were more affected by the pinhole defects. Tag functionality was also sustained except in one case where there was a cut on the feedline.

Robustness tests were also conducted on the tag to assess durability during use. The first of these was the use of the tag for a period of 8 hours. Read range measurements showed a gradual decline in tag read range but tag functionality was sustained

throughout the course of the test. The feedline of the tag was however damaged after the tag had been worn for about 20 hours thereby leading to the failure of the tag to read.

Exposure to sweat was also examined in order to determine the effect on tag performance. The tag showed a reduction in read range by about 13cm (19%) after exposure to sweat for about 20 mins. Further experiments showed however that the reduction in tag read range had more to do with wear and tear due to mechanical friction than exposure to sweat as DC resistance tests showed no significant difference between exposing the tag to sweat (saline solution) and to water for a period of 30 mins. Also exposure to water during showering led to no reduction in tag read range.

References

- [1] S.-P. Chen, H.-L. Chiu, P.-H. Wang, and Y.-C. Liao, "Inkjet Printed Conductive Tracks for Printed Electronics," *ECS J. Solid State Sci. Technol.*, vol. 4, no. 4, pp. P3026–P3033, 2015.
- [2] R. D. Deegan, O. Bakajin, T. F. Dupont, G. Huber, S. R. Nagel, and T. A. Witten, "Capillary flow as the cause of ring stains from dried liquid drops," *Nature*, vol. 389, no. 6653, pp. 827–829, Oct. 1997.
- [3] M. Ikegawa and H. Azuma, "Droplet Behaviors on Substrates in Thin-Film Formation Using Ink-Jet Printing," *JSME International Journal Series B*, vol. 47, no. 3, pp. 490–496, 2004.
- [4] B. J. Kang and J. H. Oh, "Geometrical characterization of inkjet-printed conductive lines of nanosilver suspensions on a polymer substrate," *Thin Solid Films*, vol. 518, no. 10, pp. 2890–2896, 2010.
- [5] J. Perelaer and U. Schubert, "Inkjet printing and alternative sintering of narrow conductive tracks on flexible substrates for plastic electronic applications," in *Radio Frequency Identification Fundamentals and Applications Design methods and Solutions*, no. February, 2010, pp. 265–286.
- [6] P. Lenz, W. Fenzl, and R. Lipowsky, "Wetting of ring-shaped surface domains," *Europhysics Letters (EPL)*, vol. 53, no. 5, pp. 618–624, 2007.
- [7] D. Soltman and V. Subramanian, "Inkjet-printed line morphologies and temperature control of the coffee ring effect," *Langmuir*, vol. 24, no. 5, pp. 2224–2231, 2008.
- [8] T. H. J. van Osch, J. Perelaer, A. W. M. de Laat, and U. S. Schubert, "Inkjet Printing of Narrow Conductive Tracks on Untreated Polymeric Substrates," *Adv. Mater.*, vol. 20, no. 2, pp. 343–345, Jan. 2008.
- [9] R. D. Deegan, "Pattern formation in drying drops," *Phys. Rev. E*, vol. 61, no. 1, pp. 475–485, Jan. 2000.
- [10] J. Perelaer, P. J. Smith, M. M. P. Wijnen, E. Van Den Bosch, R. Eckardt, P. H. J. M. Ketelaars, and U. S. Schubert, "Droplet tailoring using evaporative inkjet printing," *Macromol. Chem. Phys.*, vol. 210, no. 5, pp. 387–393, 2009.
- [11] J. Miettinen, V. Pekkanen, K. Kaija, P. Mansikkamäki, J. Mäntysalo, M. Mäntysalo, J. Niittynen, J. Pekkanen, T. Saviuk, and R. Rönkkä, "Inkjet printed System-in-Package design and manufacturing," *Microelectronics J.*, vol. 39, no. 12, pp. 1740–1750, 2008.
- [12] A. M. J. van den Berg, A. W. M. de Laat, P. J. Smith, J. Perelaer, and U. S. Schubert, "Geometric control of inkjet printed features using a gelating polymer," *J. Mater. Chem.*, vol. 17, no. 7, pp. 677–683, 2007.

- [13] J. Lessing, A. C. Glavan, S. B. Walker, C. Keplinger, J. a. Lewis, and G. M. Whitesides, "Inkjet printing of conductive inks with high lateral resolution on omniphobic 'rF paper' for paper-based electronics and MEMS," *Adv. Mater.*, vol. 26, no. 27, pp. 4677–4682, 2014.
- [14] B. J. Perelaer, A. W. M. de Laat, C. E. Hendriks, and U. S. Schubert, "Inkjet-printed silver tracks: low temperature curing and thermal stability investigation," *J. Mater. Chem.*, vol. 18, no. 27, p. 3209, 2008.
- [15] D. a. Roberson, R. B. Wicker, L. E. Murr, K. Church, and E. MacDonald, "Microstructural and process characterization of conductive traces printed from Ag particulate inks," *Materials (Basel)*, vol. 4, no. 6, pp. 963–979, 2011.
- [16] H. Wu, S. W. Chiang, W. Lin, C. Yang, Z. Li, J. Liu, X. Cui, F. Kang, and C. P. Wong, "Towards Practical Application of Paper based Printed Circuits: Capillarity Effectively Enhances Conductivity of the Thermoplastic Electrically Conductive Adhesives," *Sci. Rep.*, vol. 4, p. 6275, 2014.
- [17] A. Bonea, A. Brodeala, M. Vlădescu, and P. Svasta, "Electrical conductivity of inkjet printed silver tracks," *Proc. Int. Spring Semin. Electron. Technol.*, pp. 1–4, 2012.
- [18] V. Sanchez-Romaguera, M. A. Ziai, D. Oyeka, S. Barbosa, J. S. R. Wheeler, J. C. Batchelor, E. A. Parker, and S. G. Yeates, "Towards inkjet-printed low cost passive UHF RFID skin mounted tattoo paper tags based on silver nanoparticle inks," *J. Mater. Chem. C*, vol. 1, no. 39, pp. 6395–6402, 2013.
- [19] D. O. Oyeka, M. A. Ziai, J. C. Batchelor, V. Sanchez-Romaguera, S. G. Yeates, S. Wunscher, and U. S. Schubert, "Inkjet printed epidermal RFID tags," *Antennas and Propagation (EuCAP), 2014 8th European Conference on*. pp. 1403–1406, 2014.
- [20] NXP, "GX2 ASIC Data Sheet," 2011. [Online]. Available: http://www.nxp.com/documents/data_sheet/SL3ICS1002_1202_139036.pdf. [Accessed: 13-Apr-2011].
- [21] Voyantic, "Tagformance | Voyantic," 2014. [Online]. Available: <http://www.voyantic.com/tagformance>. [Accessed: 05-Jun-2014].
- [22] C. F. Consolazio, L. O. Matoush, R. A. Nelson, R. S. Harding, and J. E. Canham, "Excretion of Sodium, Potassium, Magnesium and Iron in Human Sweat and the Relation of Each to Balance and Requirements," *J. Nutr.*, vol. 79, no. 4, pp. 407–415, Apr. 1963.

CHAPTER 6

RFID READ DIVERSITY STUDY OF INKJET PRINTED RFID INTEGRATED MEDICAL STICKING PLASTER TAGS

In this chapter, an Inkjet printed tag which was integrated with medical sticking plaster is presented. This tag was fabricated for use in a medical environment where it could easily be a substitute for the currently used wristbands as well as the potential for including a sensor. A diversity study of the tag was conducted to establish how many tags would be needed to achieve an omni-directional read around a subject. Both horizontal and vertical polarizations were examined for cases involving two tags up to a maximum of four tags. Initial test was carried out with the volunteers turning at a spot. The study was then extended to the volunteers carrying out various other regular motions.

6.1 Introduction

In this chapter, temporarily worn tags will be described for use directly on the body which provides a challenging platform for RFID owing to the electrical parameters of human tissue.

Together with tag chip turn-on power sensitivity the antenna heavily influences the general performance factors of a tag with a given overall size, such as the electromagnetic and mechanical compatibility with tagged objects and the maximum reading range. Also special consideration must be made for the tag design when it is to be placed near metals, liquids and on the human body [1] and in such situations degradation in read range is well documented [2][3][4] and this often leads to severe frequency detuning. UHF RFID tags face similar issues when used near liquids or materials that have high liquid content such as the human body, and surface insensitive designs are used, for instance in [5], and shielding could be employed as described in [6].

For medical applications involving medium to long term skin mounting on patients, a low profile tag is essential, and therefore a thin sticking plaster is a suitable substrate for an RFID tag which could be fabricated on paper using Inkjet printing technology. This has the advantage of flexibility causing minimal irritation to the skin. Such a design will be described in this chapter along with a multiple tag diversity study which seeks to establish tag configurations that result in uninterrupted read access. Such link reliability would be important if the tags were to be performing a sensing function on the skin of a patient

The structure of this chapter is as follows: Section 6.2 describes the tag structure and its matched band as well as presenting a parametric analysis for guidance on input matching. Section 6.3 outlines the fabrication of the prototype inkjet printed sticking plaster tag. Section 6.4 gives measured results for read range on- and off-body together with a study of read diversity when multiple tags are used. Section 6.5 examines tag diversity performance with different body motions based on percentage read times. Section 6.6 concludes the chapter.

6.2 Sticking Plaster RFID Tag Design

6.2.1 Tag Modelling and Simulation

A Higgs-3 EPC Class 1 Gen 2 RFID Tag IC [7] with an impedance of $(31 - j216)\Omega$ was used for the tag and the antenna was designed to present a conjugate impedance at its ports.

The sticking plaster integrated tag was derived from one created for mounting directly on the skin [8] and the modified design is shown in Fig 6.1.

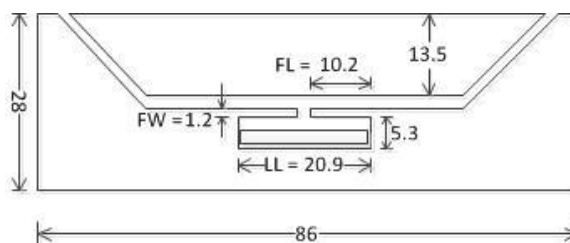


Fig. 6.1 Principal dimensions for the on-body tag with 867 MHz centre match. Tag thickness was 1.5mm.

To ensure that the tag was resilient to any detuning effect of the body, this tag was also simulated on a multilayered block model of human tissue consisting of skin/fat and muscle was implemented using the electrical parameters obtained from [9].

The sticking plaster substrate was highly porous and was represented by a 1.5mm layer of vacuum. The final tag which had the dimensions given in Fig. 6.1 was designed to offer the Higgs-3 chip impedance a conjugate match. Simulation was by CST Microwave Studio to resonate at 867MHz with a reflection coefficient of -24 dB and a fractional bandwidth of 11%. This was sufficient to cover the European (865 – 868MHz), United States (902 – 928MHz) and Korean (905.5 – 914MHz) UHF RFID bands.

The simulated surface current is shown in Fig. 6.2 where maximum intensity is observed to be located around the upper part of the loop on the lines connecting to the

chip. Consequently adjustments made to this area greatly influence the behavior of the tag and this will be confirmed by a parametric analysis in Section 6.3.

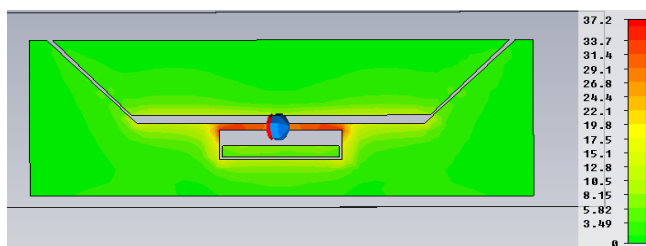


Fig. 6.2 On-body Tag surface current distribution (A/m) at 867MHz

To represent the human who forms the underlying platform for the tag, a torso model shown in Fig. 6.3 was created by 3D scanning of a test subject.

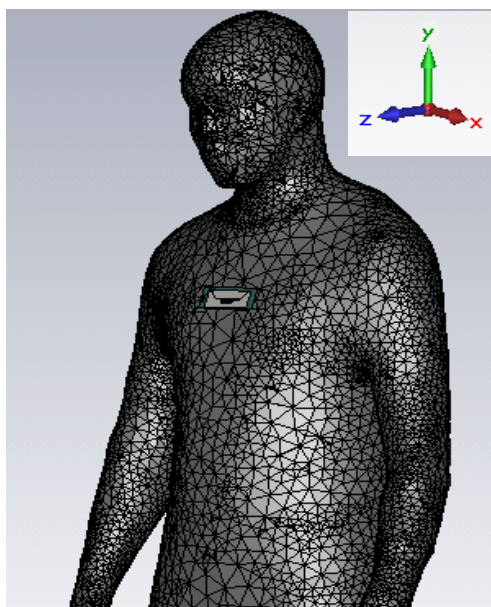


Fig. 6.3 3D Torso Model

The 3D scanning enables a non-hollow full human figure to be obtained with a height of 6ft. However, with the required memory size of this model in mind and in order to reduce simulation time, the lower part of the body was not used for the simulation since the tags were all to be placed on the upper body. As the phantom is homogenous, its material property was set to be that of skin and fat ($\epsilon = 14.5$, $\sigma = 0.25$). A tetrahedral mesh was used for the simulation and the lower limit was set in such a way that the fine details of the structure as well as that of the tag could be properly captured by the simulator. For this simulation, no ground plane was used to account for the floor. The simulated on torso co-polar elevation and azimuthal cuts are shown in Fig. 6.4 and 6.5 respectively. In free space the tag had a dipole-like omni-directional radiation pattern,

but when mounted on-body the pattern is directed forwards. A gain of -12dBi was simulated due to compromised radiation efficiency caused by the low profile of the tag which is separated from the skin by only 1.5mm and has no rear ground plane. This corresponds to a read range of about 2m but one which is adequate for short range reading for equipment surrounding a hospital bed.

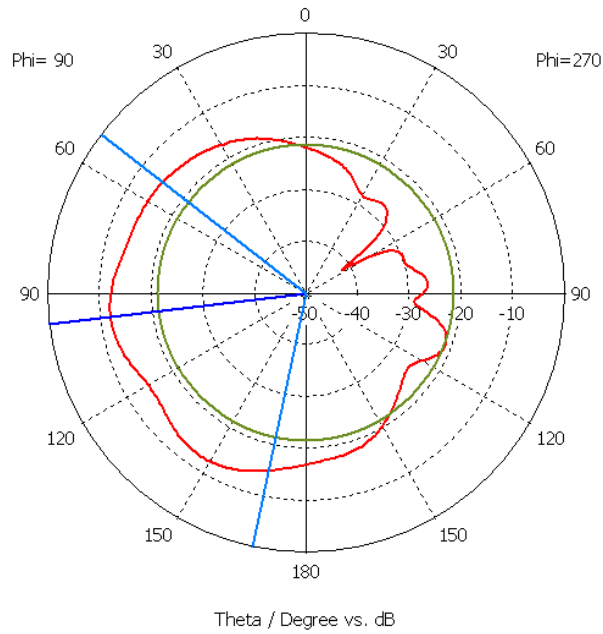


Fig. 6.4 Simulated On-body Tag E_θ component elevation (y-z) plane

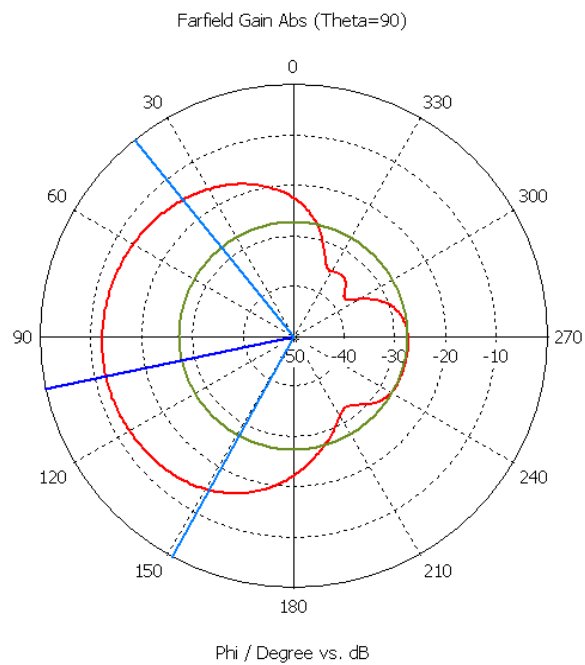


Fig. 6.5 Simulated On-body Tag E_ϕ component azimuthal (x-z) plane

6.2.2 Parametric Analysis of the On-body Sticking Plaster Tag

As the strongest surface currents occur near the port, the dimensions of the feed lines are critical in matching the tag. The length, LL , and width, FW , as defined in Fig.6.1, were therefore the subject of a parametric study. From Fig.6.6 it can be seen that there is a significant, almost linear dependence, between matched frequency and loop length, LL , with a 2mm increase in length corresponding to around 18MHz decrease in matched frequency.

Fig. 6.7 shows that the resistive and inductive parts of the input impedance also vary with loop length, LL , with an almost linear slope. Over the 20 to 35mm range investigated, the real and reactive parts have gradients of 5.2Ohm/mm and 4 Ohm/mm respectively.

The trends in changing feed line width, FW are illustrated in Figs.6.8 and 6.9. Within the range 0.8 to 2mm, an increase in FW causes an almost linear increase in matched frequency of 24MHz, while the real and reactive impedances have linear gradients of about 5.2Ohm/mm and -15.3Ohm/mm respectively.

Therefore, the relative difference between the resistive and reactive tag impedance is mainly controlled by feed width, while the final values are simultaneously set by feed length. The almost linear dependence of impedance on feed dimensions aids the matching process.

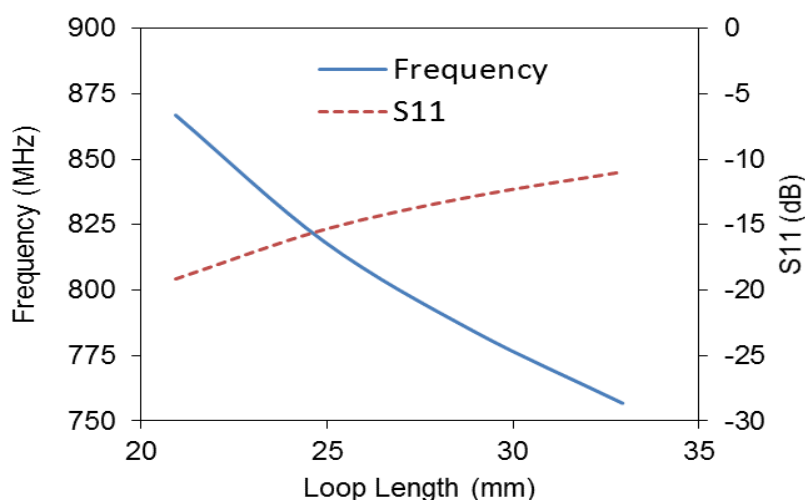


Fig. 6.6 Loop length, LL vs. matched frequency and reflection coefficient

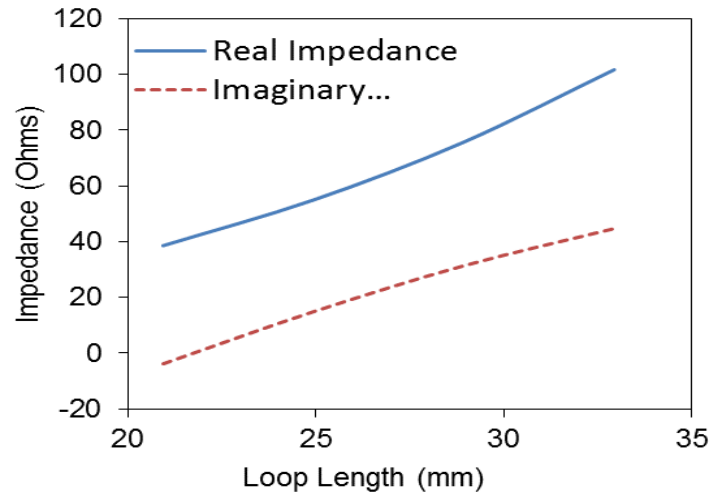


Fig. 6.7 Loop length, LL vs. input impedance at 867MHz

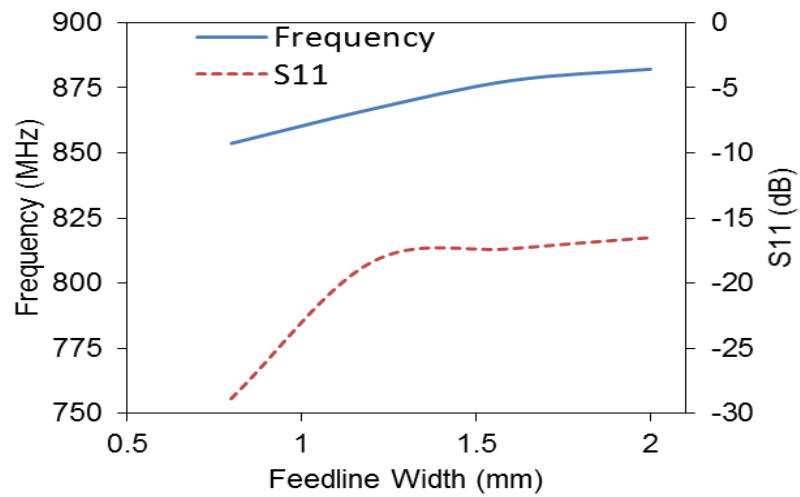


Fig. 6.8 Feed width, FW vs. matched frequency and reflection coefficient

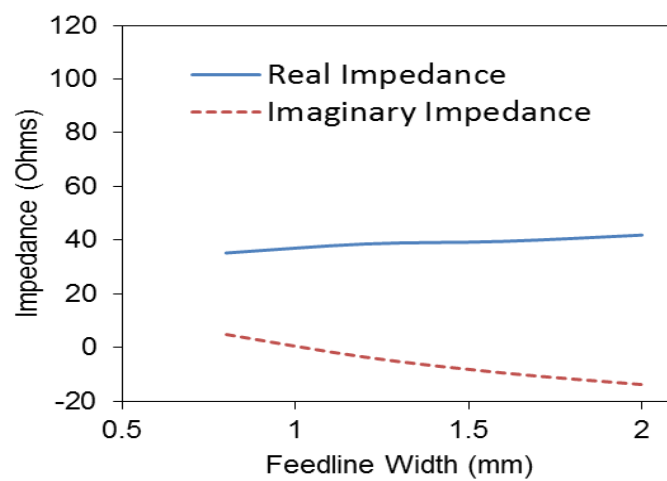


Fig. 6.9 Feed width, FW vs. input impedance at 867MHz

6.3 Fabrication of the On-Body RFID Tag with Inkjet printing

To be mechanically compatible with sticking plaster, the metalized tag patch was fabricated with conductive ink using inkjet printing. This tag Fabrication method was chosen to reduce possible irritation caused by extended use on the skin for sustained periods because of the flexibility it offers.

The tag conducting patch was inkjet printed using the Dimatix inkjet printer [10] and a silver nanoparticle ink by Sigma-Aldrich [11].

In order to achieve good definition of the narrow parts and high conductivity of the tag design, the samples were made of two layers of conductive ink deposition. The second layer was deposited after the initial layer had dried at room temperature. A dot spacing of 20 microns was used for the printing. Finally, a Higgs-3 RFID ASIC was attached to the tag with the aid of a conductive glue and reinforced with an adhesive tape. The sample is shown in Fig. 6.10.



Fig. 6.10 Inkjet printed Tag using conductive ink

6.4 Tag Measurements.

Read range and performance measurements were obtained using a Favite FS-GF801 RFID reader and a Voyantic Tagformance[®] lite RFID measurement kit. The Favite system had a circularly polarized antenna with a gain of 8dBi and 32dBm maximum output power.

6.4.1 Read Range On and Off Body

Using the Voyantic kit, read range measurements were first taken in free space and then on the chest, the arm and the torso. The results presented in Fig. 6.11 show that mounting the plaster on human tissue reduced the read range from about 3.75 to 2m at 867MHz, though when mounted on skin the tag performance was relatively independent of frequency.

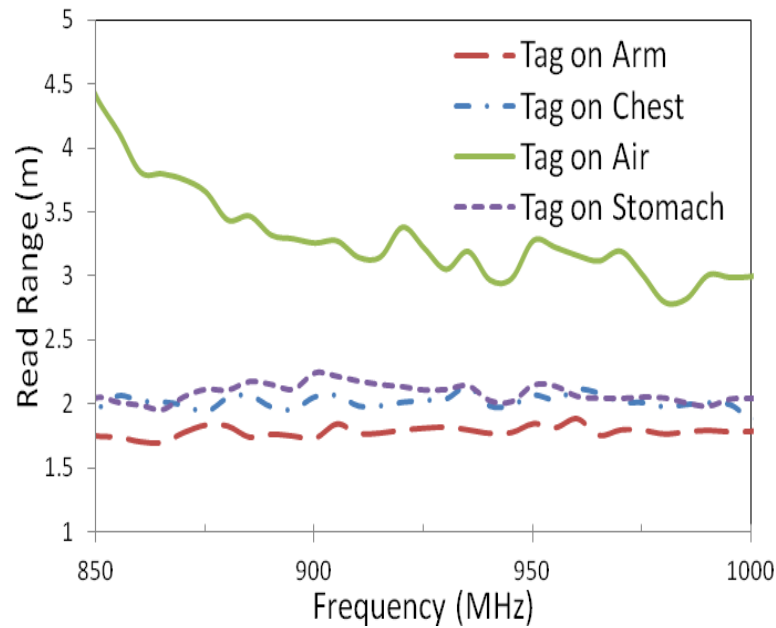


Fig. 6.11 Read range measurements for tag mounted on different parts of the body

Placing the tag on the abdomen or chest gave ranges of 2m, while mounting on the arm gave slightly lower values just below 2m. The dependence of read range on body mounting can be attributed to the different composition of the cavity filled chest region in comparison to the forearm which has denser muscle and bone. At its worst read range performance on body (on the arm), the tag had a range of almost 2m, it was considered adequate for use in person monitoring applications inside buildings, for instance for a patient in a small room or in bed.

Tags used in future medical applications to stream vital data will require diversity to reduce the risk of read outage. Therefore a study was carried out using motion capture equipment to establish the angles where no read occurred and to determine the number

of tags required to offer reliable coverage. This was done for groups of 2, 3 and 4 tags mounted on different body locations with the wearer turning on the spot.

6.4.2 Two Tag Diversity

To appreciate the overall body mounting effect on the plasters, the tags were first measured in free space. Two identical tags were mounted horizontally either side of a 7cm thick expanded polystyrene block ($\epsilon_r = 1.01$) with optical markers on them using the set up shown in Fig. 6.12. The polystyrene block was placed 1m from the reader and rotated on the spot, Fig. 6.13. In free space the tags might be expected to radiate as dipoles, hence the read performance was quite symmetrical with the read sector widths measured to be 173° and 174° for tags 1 and 2 respectively, Fig. 6.14. The tags had a ‘no-read’ sector width of 13° in this polarization and the slight asymmetry in the read sectors is accounted for by fabrication tolerances as well as reflection from the surfaces of the room which measured about 12m x 11m with a height of about 2.3m and was not anechoic. For vertically oriented tags, both read for the entire 360° rotation as would be expected for significantly separated dipoles.

To allow a comparison in performance with respect to the polystyrene block, the two tags were then mounted on the bodies of three volunteers, Fig.6.15. The same human wearers were used for all measurements and the results were averaged over 6 consecutive identical measurements. A Vicon motion capture system [12] consisting of 8 cameras was used to locate the tag and the circularly polarized reader antenna positions and orientations. This was done by tracking the optical markers placed on them [13]. The coordinates of these markers generated by the system were used to compute the relative angles between the tags and the read antenna.

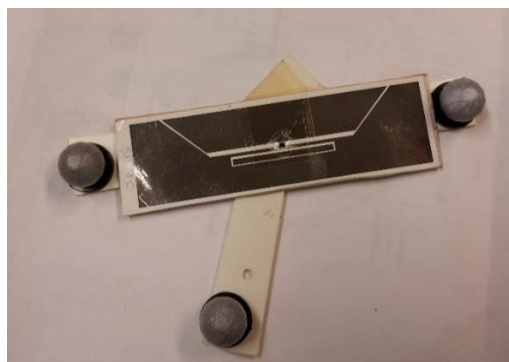


Fig. 6.12 Tag mounting setup showing three optical markers

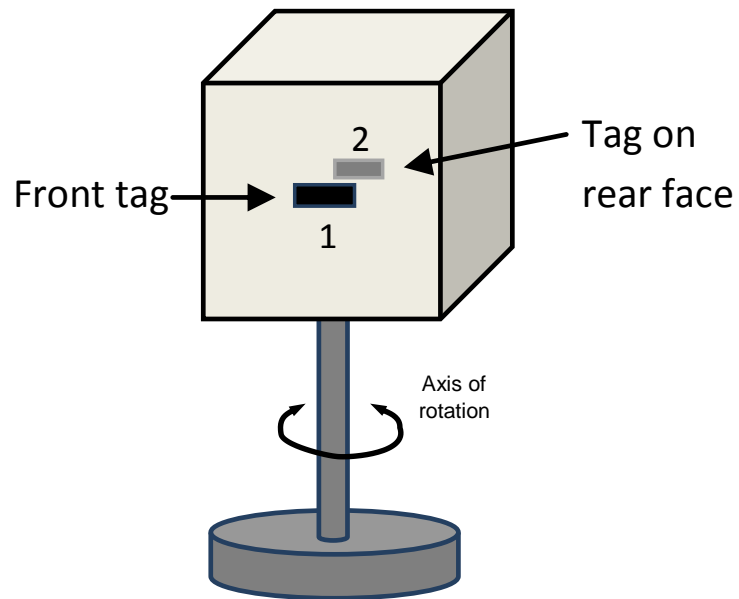


Fig. 6.13 Horizontal tags mounted on opposing sides of a 70mm thick expanded polystyrene block

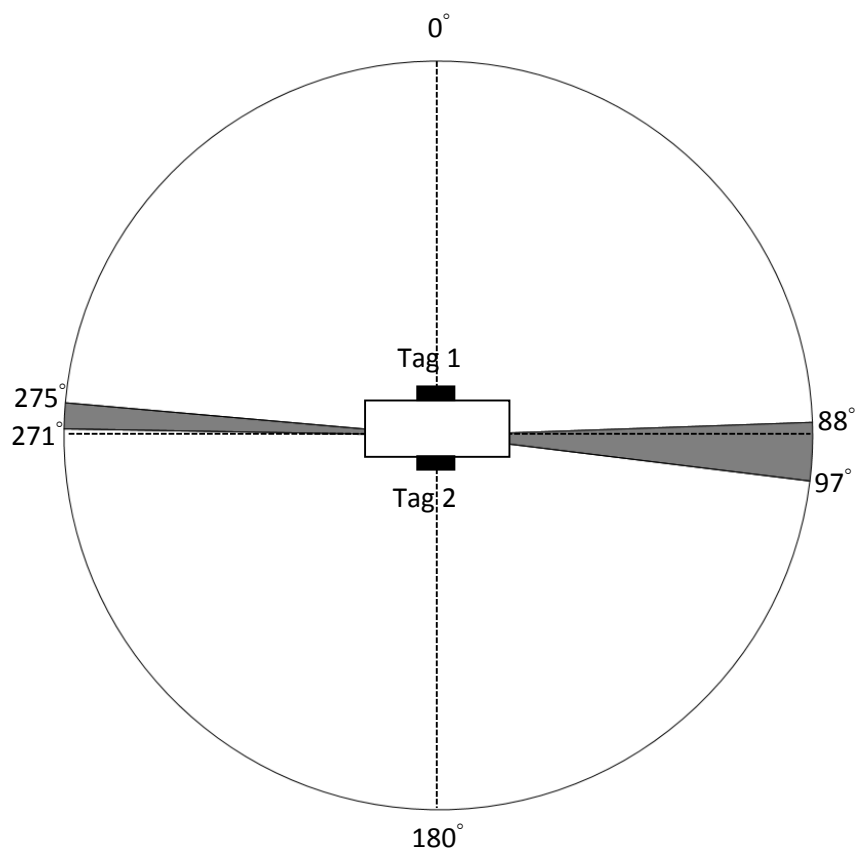


Fig. 6.14 Read sectors of horizontal tags, white and grey sectors correspond to single tag and no tag read angles respectively

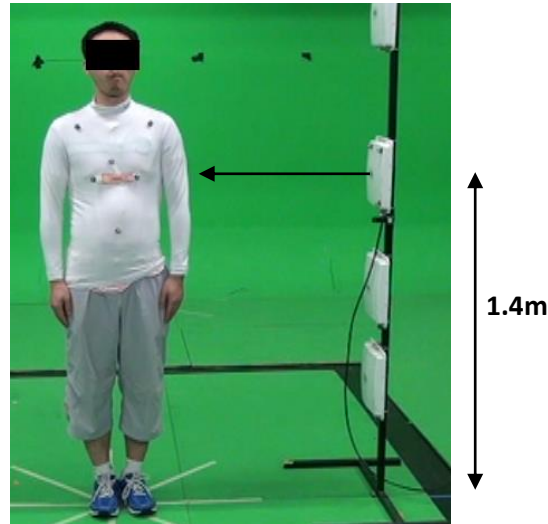
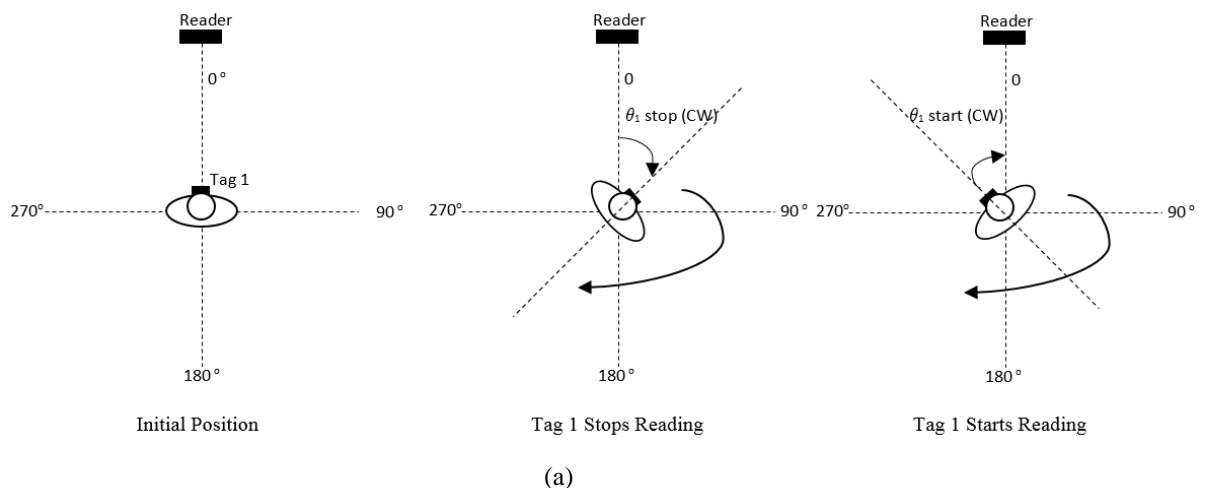


Fig. 6.15 Tag read sector measurement setup

The sector angles were obtained by taking the angles between the tag coordinates and reader coordinates provided by the motion capture system at the points where the tags stop and start reading. In order to determine these two boundaries, a total of 6 measurements were taken – three in the clockwise direction and three in the anti-clockwise direction. This was done in order to cancel out any systematic overshoot errors in the tag read boundaries caused by human response time. In order to properly implement this, the start positions of the clockwise turn were taken to be equivalent to the stop positions in the anti-clockwise turns (since this was in the reverse direction) and the average of these was taken to be one read boundary. The same was done for the stop position of the clockwise turn and the start position of the anticlockwise turn. This formed the second read boundary. The method of forming these boundaries is shown in Fig. 6.16.



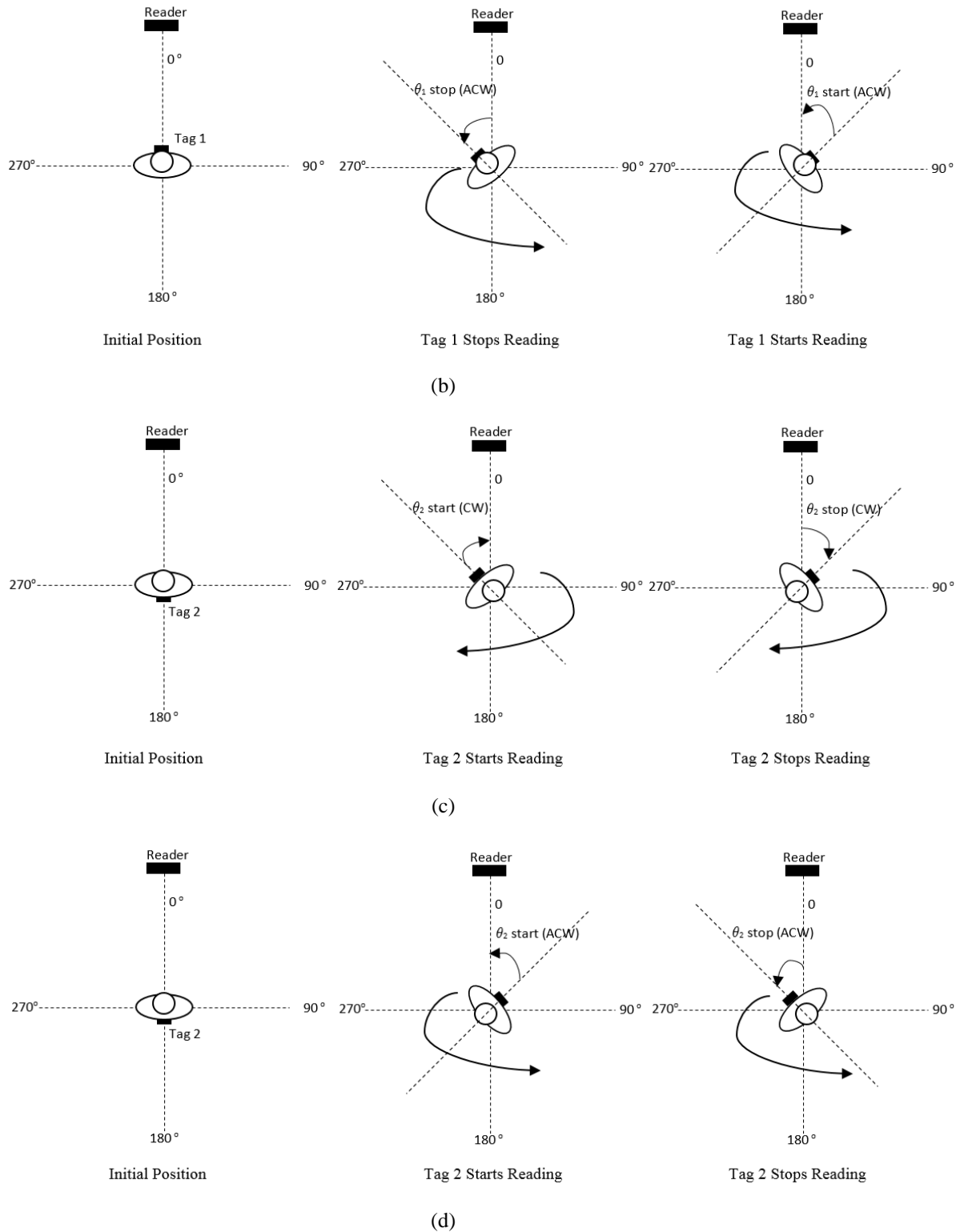


Fig. 6.16 Tag read boundary calculation (a) Tag 1 clockwise start and stop angles measurements (b) Tag 1 anti-clockwise start and stop angles measurements (c) Tag 2 clockwise start and stop angles measurements (d) Tag 2 anti-clockwise start and stop angles measurements.

The boundaries were formed based on the following equations:

For tag 1 read sector boundaries,

$$\theta_{Tag1_{boundary_1}} = \frac{\sum_{n=1}^3 \theta_{1start(CW)_n} + \theta_{1stop(ACW)_n}}{2N} \quad \text{and}$$

$$\theta_{Tag1_{boundary_2}} = \frac{\sum_{n=1}^3 \theta_{1stop(CW)_n} + \theta_{1start(ACW)_n}}{2N}$$

Where n = measurement number and $N = 3$ is maximum number of measurements

$$\text{Tag 1 read sector width} = \theta_{Tag1_{boundary_1}} + \theta_{Tag1_{boundary_2}}$$

Tag 2 read sector boundaries are defined as:

$$\theta_{Tag2_{boundary_1}} = \frac{180 - \sum_{n=1}^3 \theta_{2start(CW)_n} + \theta_{2stop(ACW)_n}}{2N} \quad \text{and}$$

$$\theta_{Tag2_{boundary_2}} = \frac{180 + \sum_{n=1}^3 \theta_{2stop(CW)_n} + \theta_{2start(ACW)_n}}{2N}$$

$$\text{Tag 2 read sector width} = \theta_{Tag2_{boundary_1}} + \theta_{Tag2_{boundary_2}}$$

Where n = measurement number and $N = 3$ is maximum number of measurements

Measurements were taken in the same position of the room used for the polystyrene block measurement and no absorbing material was used so that the channel represented an indoor environment.

The average read boundary angles for the tags over 6 measurements for all three volunteers are shown in Figs. 6.17 – 6.22. These plots show slight differences in the angles which could be attributed to the variations in movement as well as differences in their body forms and posture.

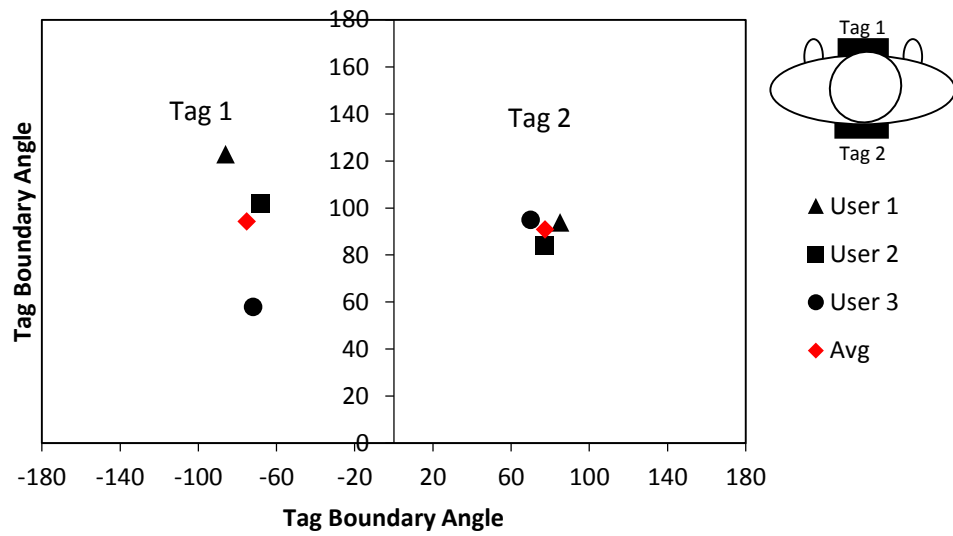


Fig. 6.17 Individual read boundaries for horizontal tags on the chest-back setup

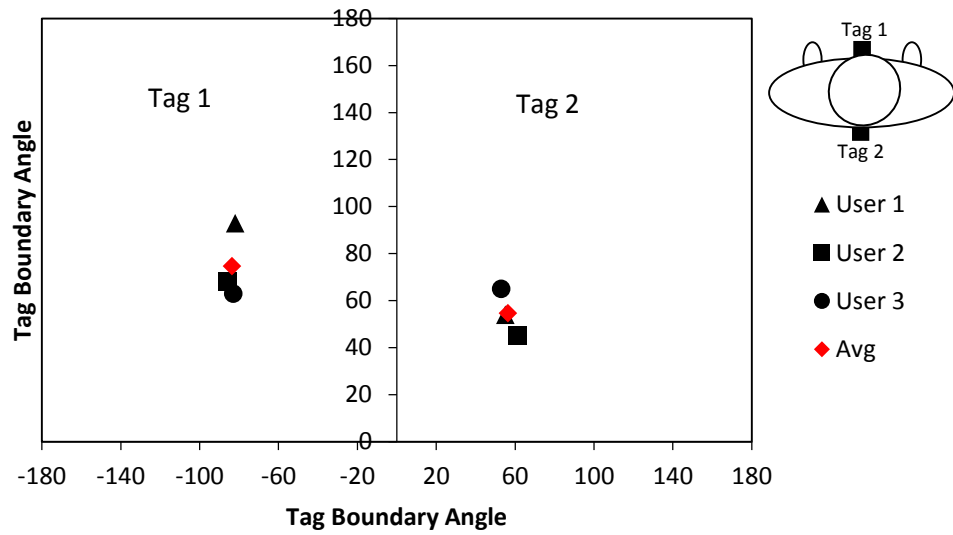


Fig. 6.18 Individual read boundaries for vertical tags on the chest and back setup

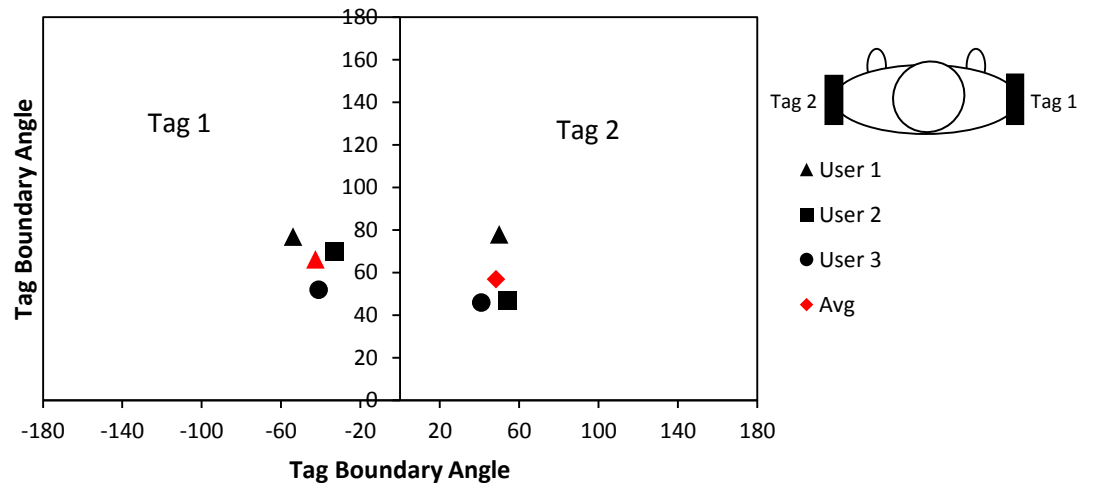


Fig. 6.19 Individual read boundaries for horizontal tags on the arms setup

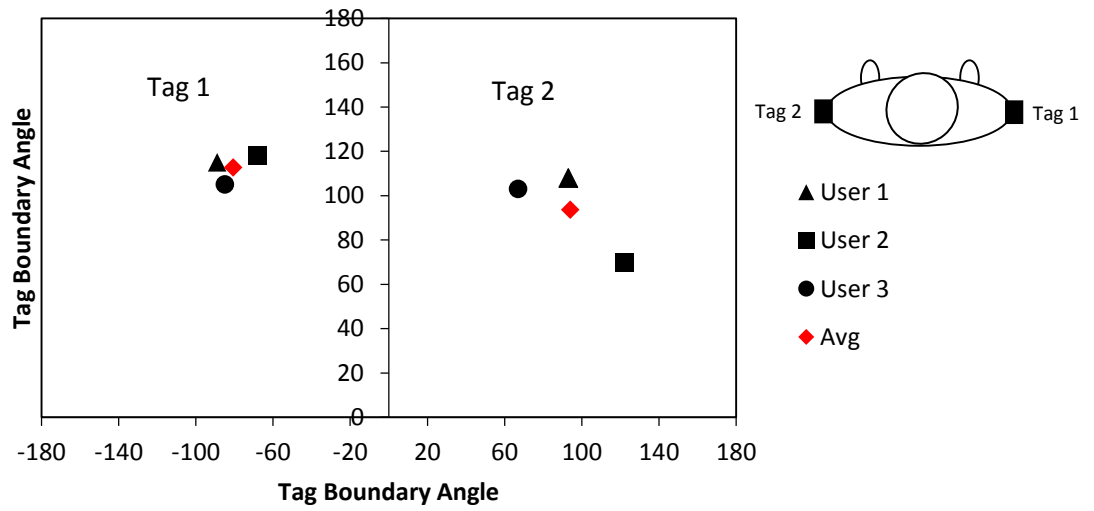


Fig. 6.20 Individual read boundaries for vertical symmetric tags on the arms setup

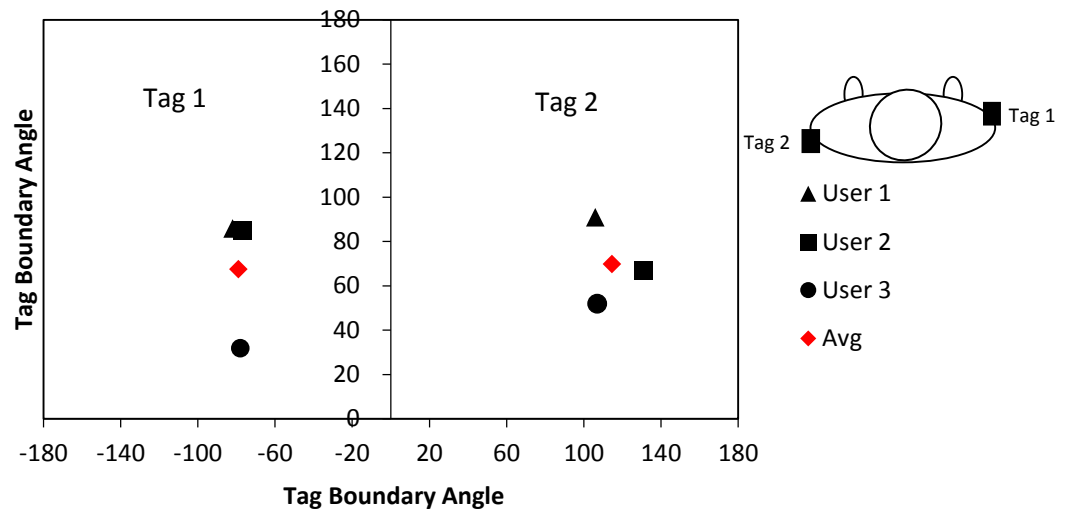


Fig. 6.21 Individual read boundaries for vertical asymmetric tags on the arms setup

A comparison of the average read boundaries for each user for the 2 tag diversity setups are shown in Fig. 6.21. The variations shown the read boundaries are shown by the spread in the plot.

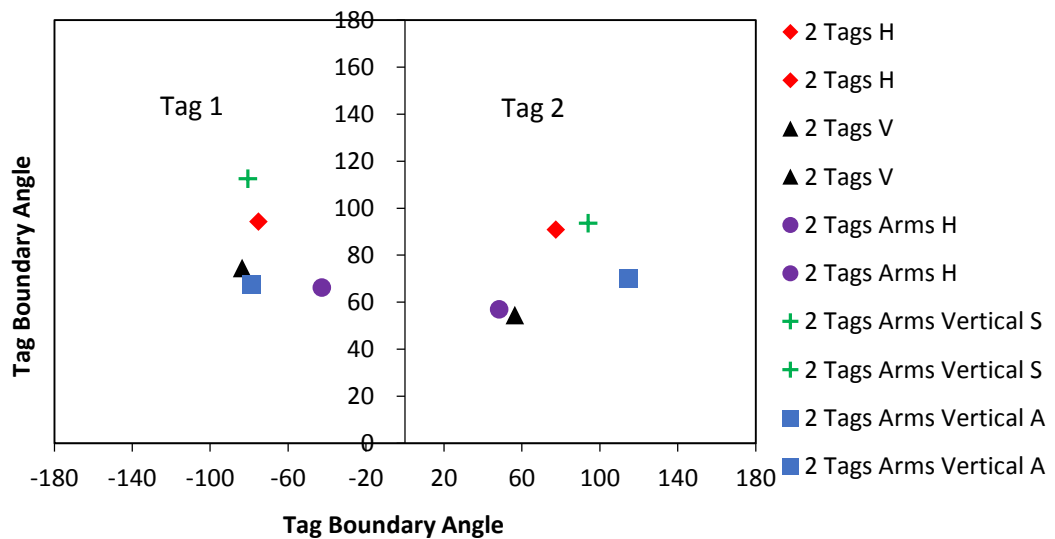


Fig. 6.22 Average read boundaries for 2 tag diversity setups

When the horizontally placed tags on the chest and back are compared with the horizontally placed tags in free space, there is a further 10° reduction in read sector as seen in Fig. 6.23. On the other hand, in the case of the vertically placed tag seen in Fig. 6.24, mounting on the body resulted in a 91° increase in the non-read sectors of the tag compared to the omni-directional result obtained in free space. This is

significantly smaller than the horizontal orientation condition. This change is primarily due to body blockage which could be attributed to the broadness of the torso.

Table 6.1 shows a summary of the standard deviation of the two boundaries for the read sector of the tags in each two tag set up. Each boundary is obtained from a combination of the boundary values from 6 consecutive measurements from the three volunteers.

TABLE 6.1 STANDARD DEVIATION OF TAG READ SECTOR BOUNDARIES

Tag Setup	Tag 1		Tag 2	
	Boundary 1	Boundary 2	Boundary 1	Boundary 2
Chest and Back Horizontal	19°	34°	20°	21°
Chest and Back Vertical	17°	22°	19°	31°
Arms-Vertical Symmetrical	22°	22°	34°	24°
Arms-Vertical Asymmetrical	13°	33°	20°	19°
Arms-Horizontal	18°	21°	15°	18°

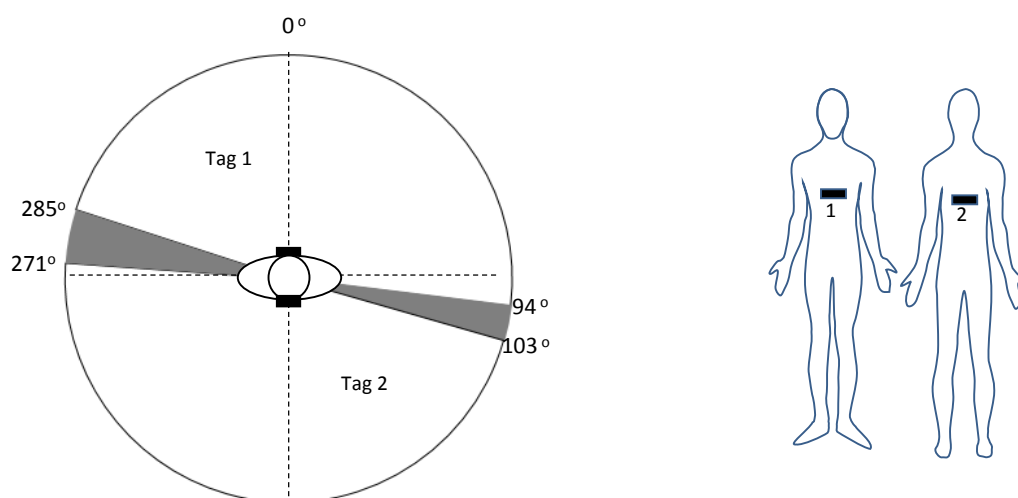


Fig. 6.23 Read sector plot for horizontally oriented tags placed on the chest and back
White and grey are single tag and no tag read sectors respectively

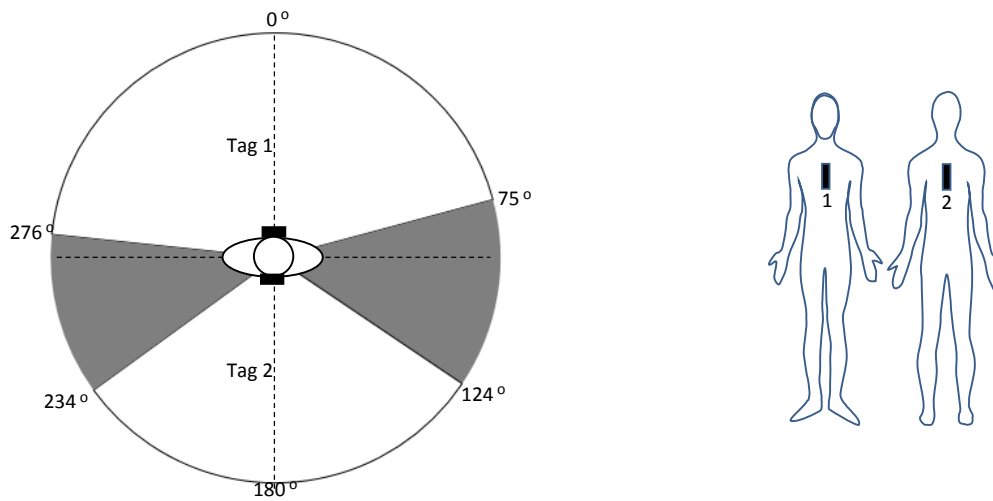
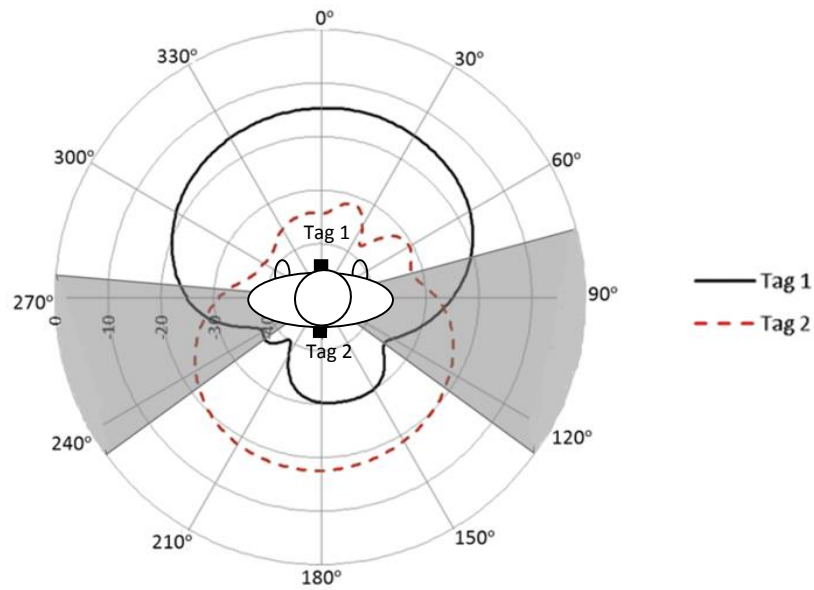
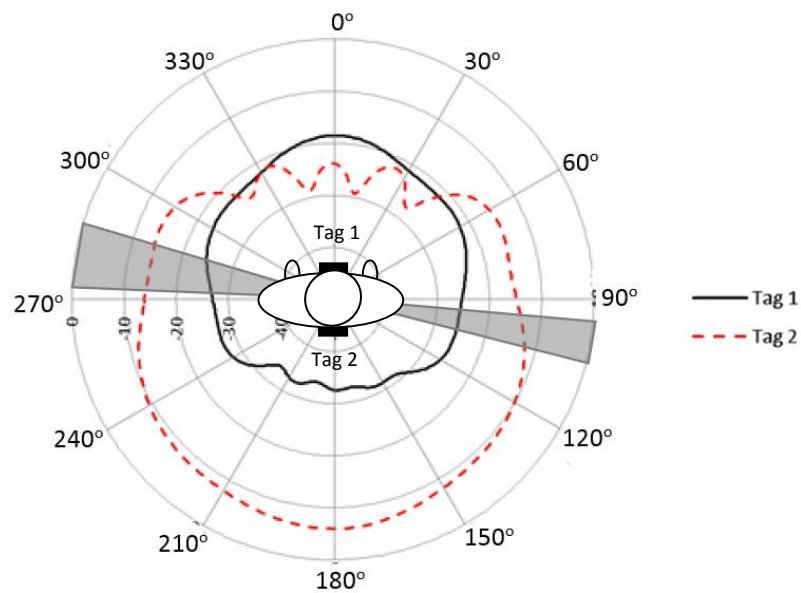


Fig. 6.24 Read sector plot for vertically oriented tags placed on the chest and back
White and grey are single tag and no tag read sectors respectively

Apart from the instance noted previously, in general the vertically oriented tags had wider read sectors in the two tags scenarios. The simulated far-field plots shown in Fig. 6.25 show that Tag 1 with the wider read sector is in agreement with its having the higher efficiency in the vertical orientation. The reduced gain of the vertically oriented Tag 2 (on the back) is because of the increased contact between the tag and the body owing to the fact that the tag was placed parallel to the body. This increased surface of contact translates to increased loading of the tag by the body. This is not the case with Tag 1 on the chest where there is less contact between the body and the Tag given the more flat surface provided by the chest. Although the tags are flexible they were placed on a rigid frame to facilitate placing the optical markers. Therefore tag contact to body surface varied according to body curvature. It can also be seen from the simulated farfield radiation pattern that the non-read sectors of the vertically oriented tags also coincide with the field nulls. The nulls are less evident for the horizontally oriented tags, though the cut off boundaries seem to occur at the -6dB beam width points.



(a)



(b)

Fig. 6.25 Azimuth plots for (a) vertically oriented tags placed on the chest and back (b) horizontally oriented tags placed on the chest and back

Figs. 6.26 – 6.28 show read sectors for tags mounted on the arms for vertical and horizontal orientations. When the tags were placed on the arm, the vertically oriented tags performed better than the horizontally polarized tags. This can be seen from the combined read sector of the symmetrically placed vertical tags being 98% of the total coverage area, Fig. 6.26, compared to the 61% read area for the horizontal tags, Fig. 6.27. Additionally, it is also seen that there was a region where the two tags read simultaneously. This is because of the reduced blockage by the body on the tag unlike

when the tags are placed horizontally. In a bid to increase the read sector of the vertically polarized tags, the tags were placed asymmetrically, Fig 6.28. This however did not yield the intended result as the total read sector reduced to 91% with an increase in the no read region and a decrease in the overlapping region as seen in Fig. 6.28.

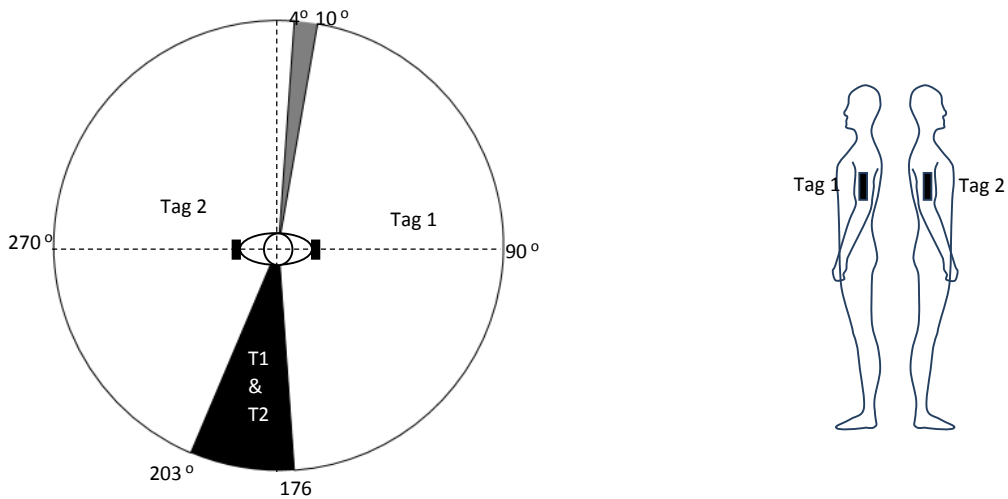


Fig. 6.26 Read sector plot for vertical tags mounted symmetrically on upper arms.
White, grey and black are single tag, no tag and two read sectors respectively

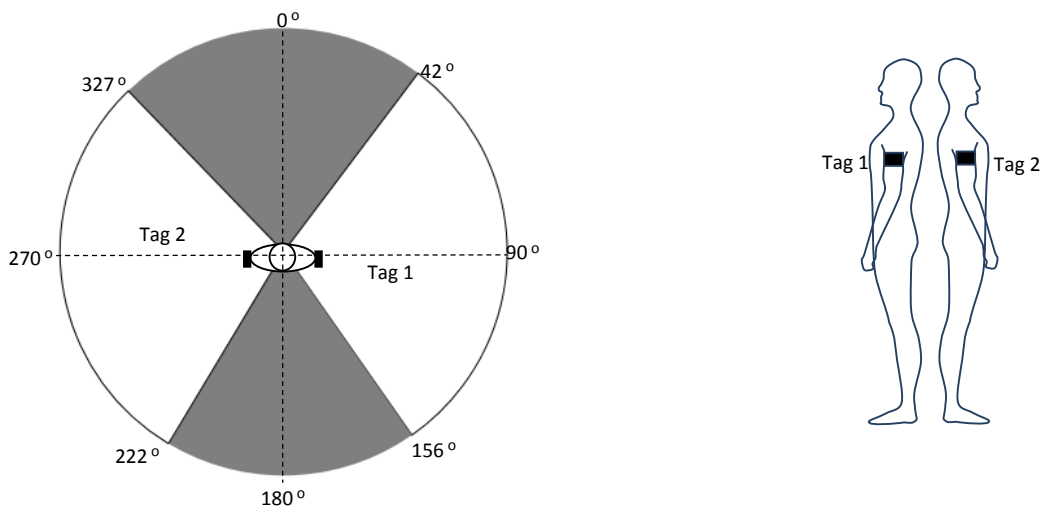


Fig. 6.27 Read sector plot for Horizontal tags mounted symmetrically on upper arms
White and grey single and no tag and sectors respectively

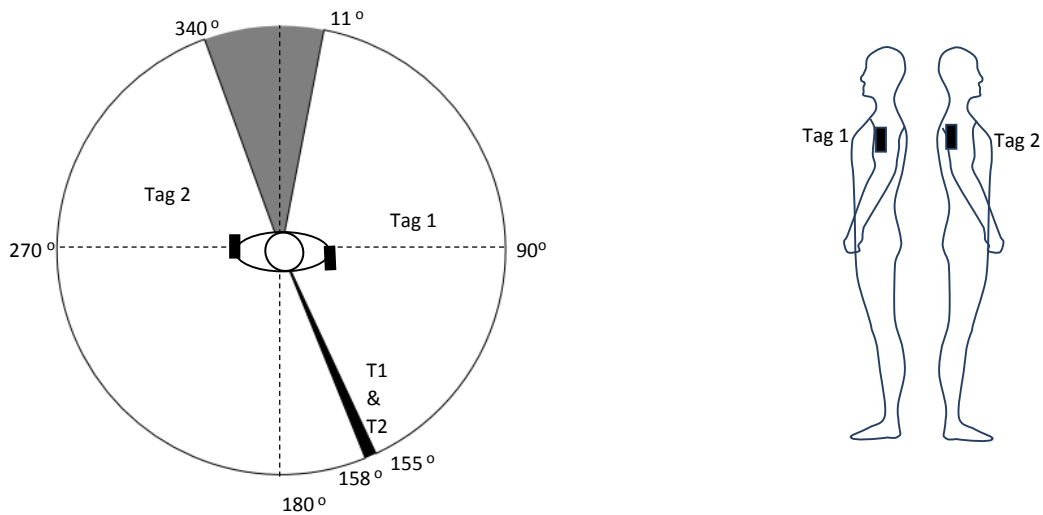


Fig. 6.28 Read sector plot for Vertical tags mounted asymmetrically on upper arms . White, grey and black are single tag, no tag and two read sectors respectively

In [14] it was noted that for a 3mm thick textile based RFID body mounted tag, vertical polarization offered better performance on the chest while horizontal tags were preferred on the arms. This runs counter to the data presented here, but is likely to be caused by the specifics of the different tag geometries.

It can be seen that in all the two tag diversity cases, the body blockage and mounting effects have caused regions where neither tag read (grey sectors). The Read/No Read sector widths in each case are summarized in Table 6.2. From the read sector widths provided, it is clear that the best coverage was achieved when the two tags were placed vertically on the arms with a total non-read width of 6° . When the tags were placed horizontally on the arms, the non-read sector increased to a total of 147° which is the largest non-read sector achieved with any of the two tag setups.

As no combination of 2 tags offered complete round body coverage, therefore studies were carried out for 3 and 4 tag diversity with the objective that for critical health applications a higher degree of diversity would be required. Additionally, in a case where one of the tags fails, this would give rise to a situation where 50% or more coverage is lost. This would result in a much reduced effectiveness of this tag diversity system.

TABLE 6. 2 READ SECTOR WIDTHS FOR 2 TAG DIVERSITY
ON AND OFF BODY

Tag mount & polarization	Sector Width				Total non-read width
	Tag1 read	T1 to T2 no-read/overlap	Tag2 read	T2 to T1 no-read	
Free space (V)	360°	0°	360°	0°	0°
Free space (H), Fig.6.14	173°	9°	174°	4°	13°
Arms (V), Fig.6.26	166°	27°	161°	6°	6°
Arms Asymmetrical (V), Fig.6.28	144°	3°	182°	31°	31°
Arms (H) Fig.6.27	108°	66°	105°	75°	141°
Chest & Back (V), Fig.6.24	159°	49°	110°	42°	91°
Chest & Back (H), Fig.6.23	169°	9°	168°	14°	23°

6.4.3 Three Tag Diversity

The previous section illustrated the limitations of the two tag system which includes limited coverage and susceptibility to large non read sector (up to 180° or 50%) should one of the tags fail. Due to this reason the number of tags was increased to 3. The tags locations were identified empirically to establish the configuration with the largest possible sectors of simultaneous tag reading. The averaged read sectors for each individual is shown in Figs. 6.29 and 6.30. Mounting positions together with measured read sectors are shown in Fig. 6.31 and Fig. 6.32.

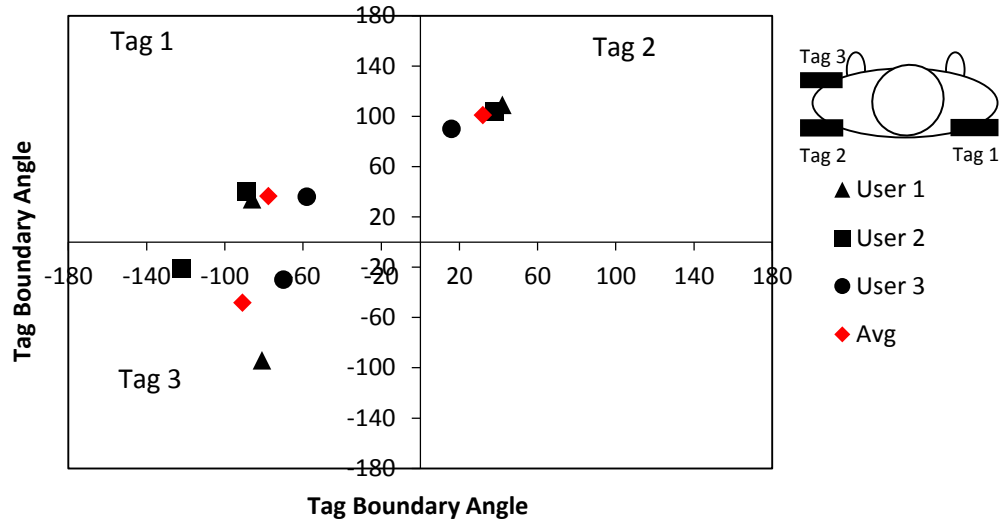


Fig. 6.29 Individual read boundaries for 3 horizontally oriented tags

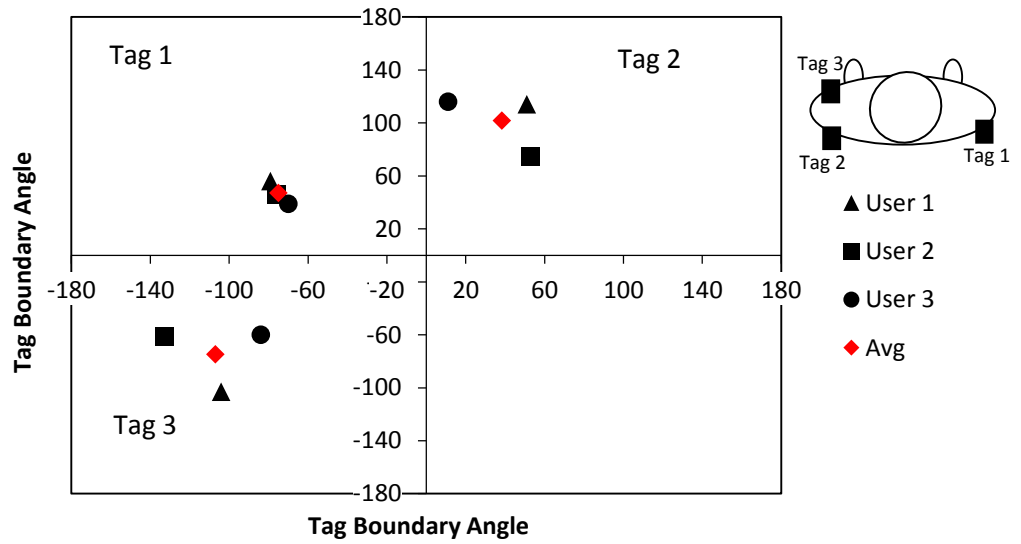


Fig. 6.30 Individual read boundaries for 3 vertically oriented tags

Table 6.3 shows a summary of the standard deviation of the two boundaries for the read sector of the tags in each three tag set up. As before, each boundary is obtained from a combination of the boundary values from 6 consecutive measurements from the three volunteers.

TABLE 6. 3 STANDARD DEVIATION OF TAG READ SECTOR BOUNDARIES

Tag Setup	Tag 1		Tag 2		Tag 3	
	B1	B2	B1	B2	B1	B2
3H	19°	21°	21°	16°	26	32
3V	17°	22	19°	31°	24	23

For horizontal tags, Fig. 6.31, 90% coverage was obtained by the three tags with regions of simultaneous tag read accounting for 19% of this coverage. There is a 36° region of no read during the transition between Tag 3 which was on the chest and Tag 1 which was on the back of the right arm. This represents about 10% of the total read area. The wider overlap region between Tag 1 and Tag 2 is expected since they are both facing backwards.

For 3 vertical tags, Fig. 6.32, the transition gap between Tag 1 and Tag 3 has been completely eliminated giving rise to a region of 2° overlap between the two tags. This is a significant improvement on the 36° gap observed for the horizontally oriented tags. Additionally, the regions of simultaneous tag read increased to a total of 83° which represents 23% of the total read area. This is an increase on the 62° overlap region obtained with the horizontal tags. This increased region of overlap indicates that wider region of coverage will be maintained by the vertically polarized tags should one of the tags cease to be functional or be blocked.

The above results are consistent with what was earlier noted with the vertically polarized tags providing better coverage when mounted on the body than the horizontally polarized tag. However, the overlap of only 2° between Tags 1 and 3 means that the diversity is not robust.

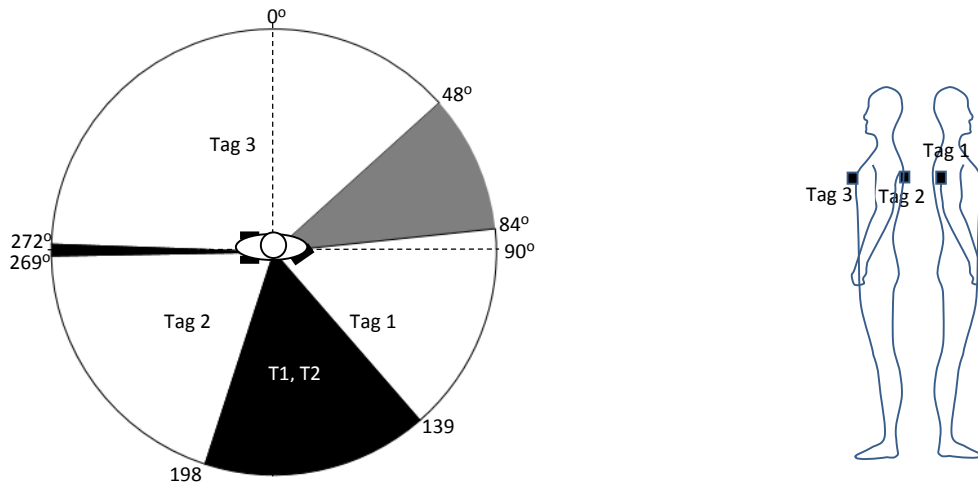


Fig. 6.31 Read sector plot for 3 Horizontal tags. White, black and grey sectors are single tag read, 2 tag read and no-read sectors respectively.

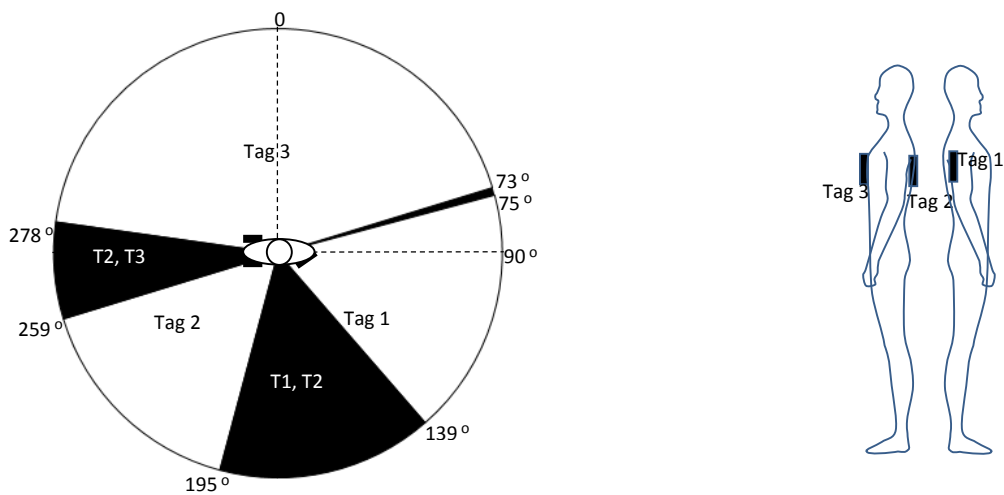


Fig. 6.32 Read sector plot for 3 vertical tags. White and black sectors are single tag read and 2 tag read respectively.

In order to assess how robust the three tag diversity set up can be in a case where there is a failure or blockage of one of the tags, the effect the removal of each tag on the outage region is determined and summarized in Table 6.4. The no read regions for the horizontally placed tags presented in the table includes the no read region between Tag 3 and Tag 1.

TABLE 6. 4 READ SECTOR WIDTHS FOR 3 TAG DIVERSITY

Tag Setup	Failed Tag	No Read (deg)	No Read (%)
3H, Fig 6.31	Tag 1	91°	25%
	Tag 2	107°	30%
	Tag 3	172°	48%
3V, Fig 6.32	Tag 1	64°	18%
	Tag 2	58°	16%
	Tag 3	155°	43%

From the results presented in Table 6.4, the effect of a single failed or blocked tag can be seen to be less detrimental in the case of vertically oriented tags. This is as a result of the wider read sectors the tags have in this orientation which enables the overlapping of read sectors.

6.4.4 Four Tag Diversity

In critical situations where robust diversity is essential, 4 tag systems must be considered. Therefore, a four tag diversity study was carried out with tags on the chest, back and on both upper arms. As presented in the 2 and 3 Tags diversity cases, the averages for all three volunteers are presented in Figs 6.33 and 6.34.

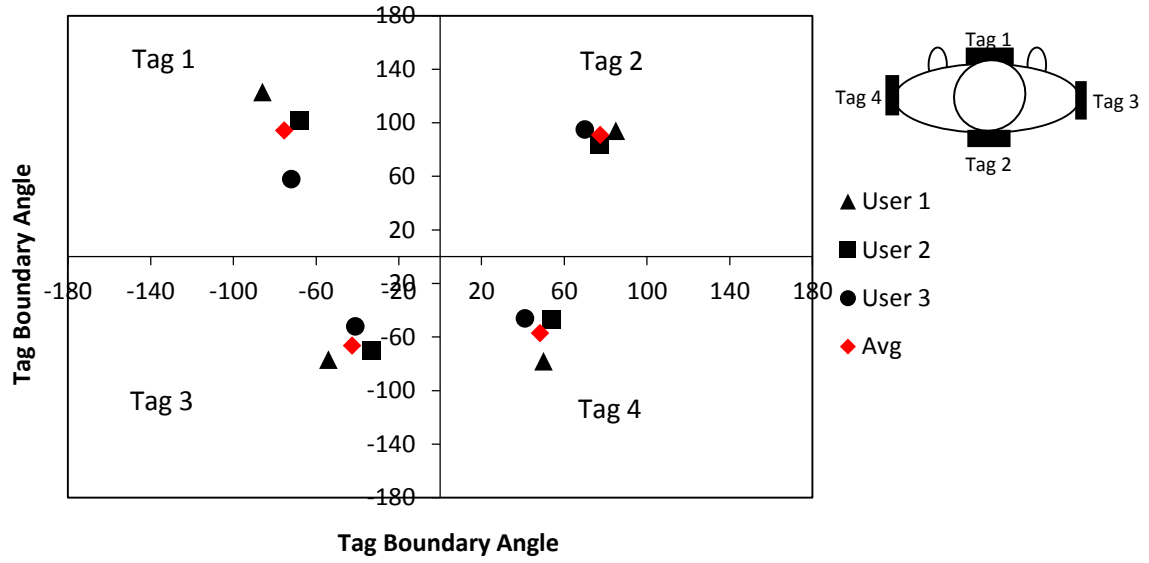


Fig. 6.33 Individual read boundaries for 4 horizontally oriented tags

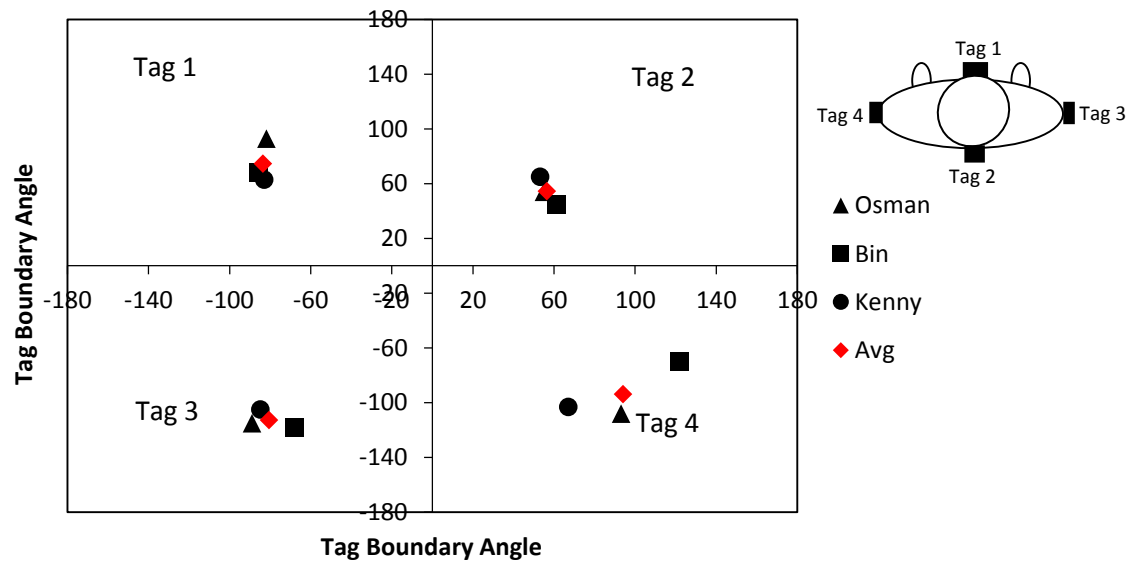


Fig. 6.34 Individual read boundaries for 4 horizontally oriented tags

Table 6.5 shows the standard deviation of the two boundaries for the read sector of the tags in both horizontal and vertical orientations of the four tags. Each boundary is obtained from a combination of the boundary values from 6 consecutive measurements from the three volunteers.

TABLE 6. 5 STANDARD DEVIATION OF TAG READ SECTOR BOUNDARIES

Tag Setup	Tag 1		Tag 2		Tag 3		Tag 4	
	B1	B2	B1	B2	B1	B2	B1	B2
4H	19°	34°	20°	21°	18°	21°	15°	18°
4V	17°	22	19°	31°	22°	22°	34°	24°

For horizontal tags, Fig. 6.35, omni-directional reading occurred and the combined simultaneous multi-tag read sectors was 190° (53%) of the read area. When the tags were placed vertically, Fig. 6.36, the overlapping regions where at least two tags read represented 73% (263°) of the total read area. In addition to the better simultaneous tag read coverage afforded by the use of vertically oriented tags, it can be seen that vertical orientation provides a region of 26° where Tag 2, Tag 3 and Tag 4 read at the same time. This provides very good robustness for 4 vertically oriented tags. The noted observation is again consistent with the previous results where vertically oriented tags provided better on-body performance than horizontally oriented tags.

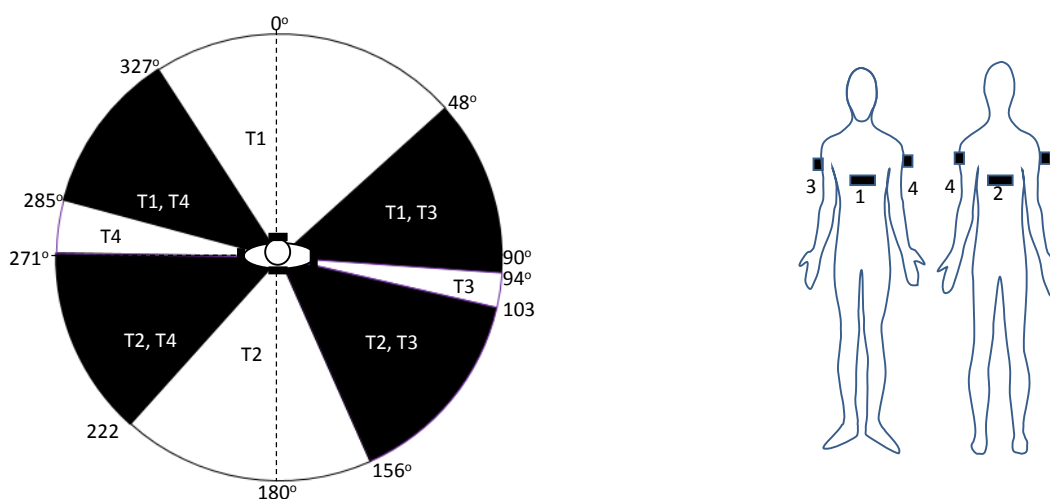


Fig. 6.35 Read sector plot for 4 Horizontal tags. White and black are single tag and 2 tag read sectors respectively

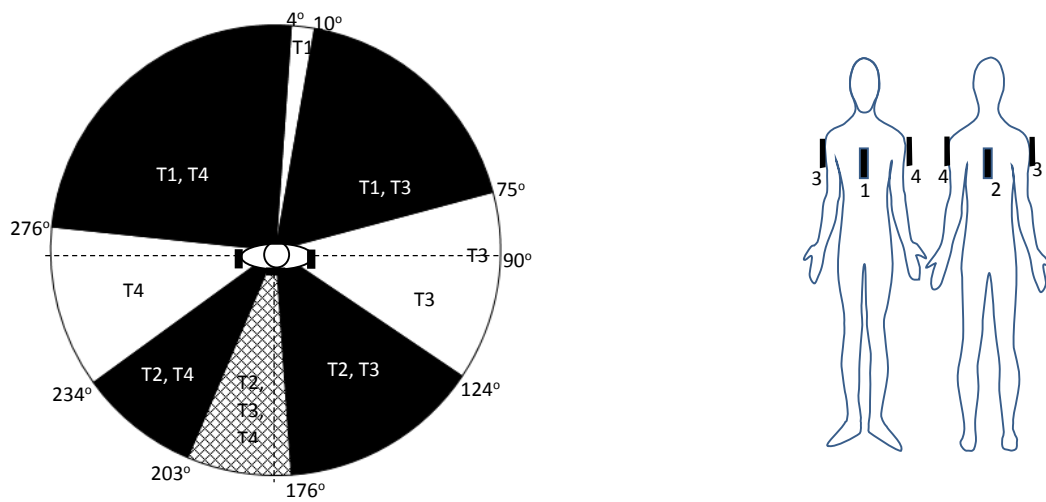


Fig. 6.36 Read sector plot for 4 Vertical tags. White, black and hashed are single tag, 2 tag and 3 tag read sectors respectively

The effect of the failure of any of the tags on the overall coverage of the 4 tag diversity system is summarized in Table 6.6.

TABLE 6.6 READ SECTOR WIDTHS FOR 4 TAG DIVERSITY

Tag Setup	Failed Tag	No Read (deg)	No Read (%)
4H	Tag 1	81°	23%
	Tag 2	66°	18%
	Tag 3	9°	3%
	Tag 4	14°	4%
4V	Tag 1	6°	2%
	Tag 2	0°	0%
	Tag 3	49°	4%
	Tag 4	42°	2%

Table 6.6 shows very low percentage outage for the horizontally placed tags on the arms. This is due to the wide read sector of the horizontally oriented tags placed on the chest and on the back. The same explanation holds for the low outage percentage for Tag 1 and Tag 2 for the vertically oriented tags with Tag 3 and Tag 4 which have wide read sectors making up for the loss of any of the tags. This indicates that a 4 tag system is highly robust.

Table 6.7 gives the results for the 2, 3 and 4 tag diversity studies.

TABLE 6.7 TAG READ SECTOR WIDTHS FOR 2, 3 AND 4 TAG DIVERSITY

Study	Pol	Read Sector Width			
		Tag1	Tag2	Tag3	Tag4
2 tags (Chest-Back)	V	Chest 159°	Back 110°	-	-
	H	169°	168°	-	-
2 tags (Arms)	V	193°	188°		
	H	108°	105°		
3 tags		Rear Right Arm	Rear Left Arm	Left Chest	-
	V	148°	139°	182°	
	H	114°	171°	139°	-
4 tags		Chest	Back	Right arm	Left arm
	V	159°	110°	193°	188°
	H	169°	168°	108°	105°

For better Illustration, the read sectors in Table 6.8 are presented in percentages of the total area in Table 6.8.

TABLE 6.8 PERCENTAGE TAG READ SECTOR WIDTHS FOR 2, 3 AND 4 TAG DIVERSITY

Study	Pol	Read Sector Width			
		Tag1	Tag2	Tag3	Tag4
2 tags (Chest-Back)	V	Chest 44%	Back 31%	-	-
	H	47%	47%	-	-
2 tags (Arms)	V	54%	52%		
	H	30%	29%		
3 tags	V	Rear Right Arm 41%	Rear Left Arm 38%	Left Chest 51%	-
	H	32%	48%	39%	-
4 tags	V	Chest 44%	Back 31%	Right arm 54%	Left arm 53%
	H	47%	47%	30%	29%

From these results for the sticking plaster tag of Fig. 6.1, we conclude that vertically mounted tags have better performance than horizontally mounted tags in terms of combined read sector widths though horizontally placed tags can also offer reliable omni-directional reading for 4 tag diversity. All measurements presented here refer to a single reader, using multiple readers will improve read reliability and range, though this would come at an increased infrastructure cost which may be undesirable [14].

6.5 Tag Diversity Performance with Regular Body Movements

As a patient may be mobile while being monitored, the performance of multiple tags on the body during regular body motions was studied. Two, three and four tags as defined in sections 6.4.2 – 6.4.4 were placed on the body and the volunteers were asked to make picking, bending and twisting motions. The volunteers repeated the motions for a fixed time and the tag read was determined using the read count on the reader which read about 35 times per second. A tag placed on the body while standing still for the same duration was used as a benchmark for gauging the tag read count in percentage. The various motions are shown in Figs. 6.37 – 6.39.

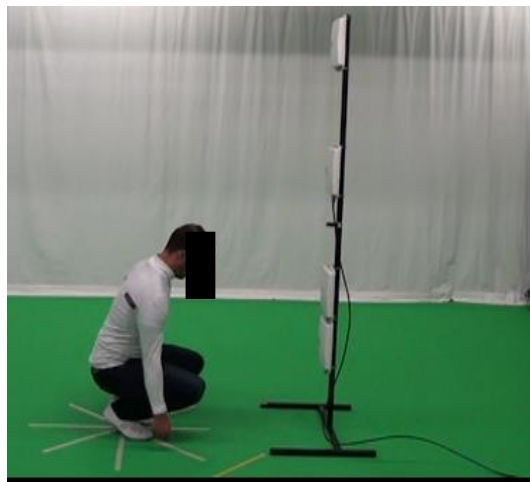


Fig. 6.37 Picking Motion



Fig. 6.38 Bending Motion

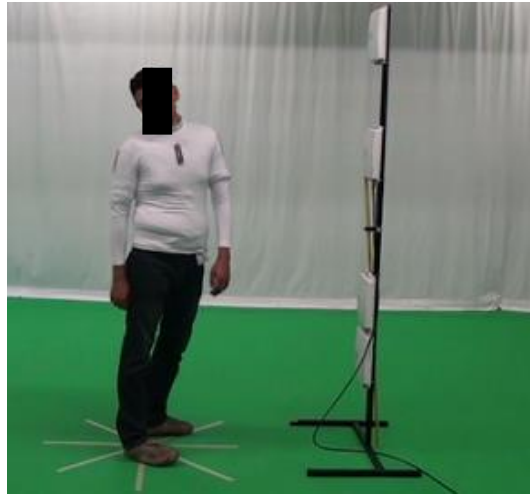


Fig. 6.39 Twisting Motion

The plots of the tag read counts in each diversity and motion are shown in Figs. 6.40 – 6.48. Horizontal and Vertical tag orientations are also compared.

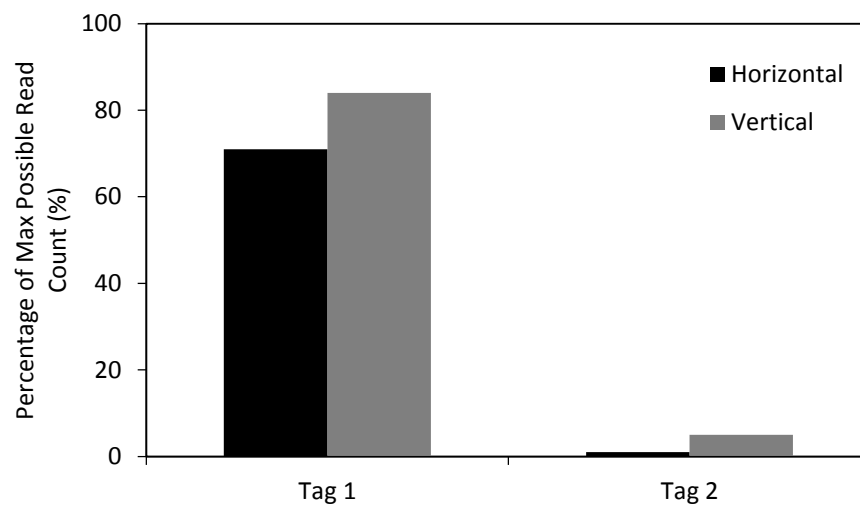


Fig. 6.40 Picking motion with 2 tags on chest and back

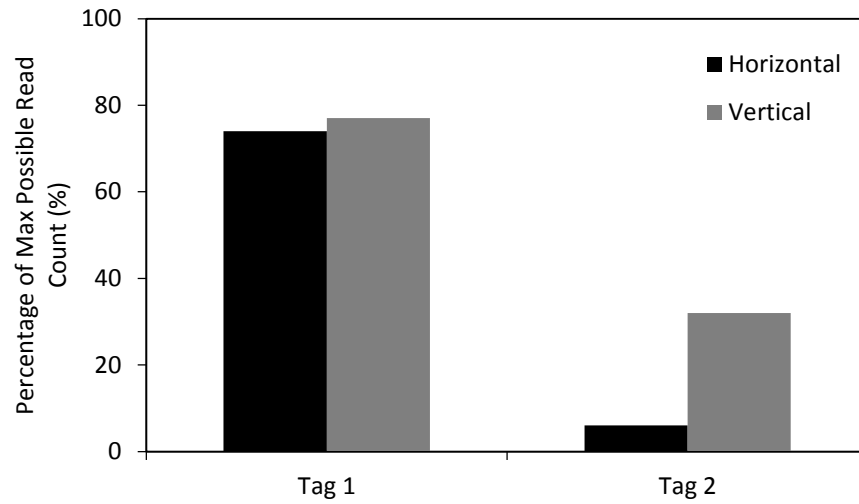


Fig. 6.41 Bending motion with 2 tags on chest and back

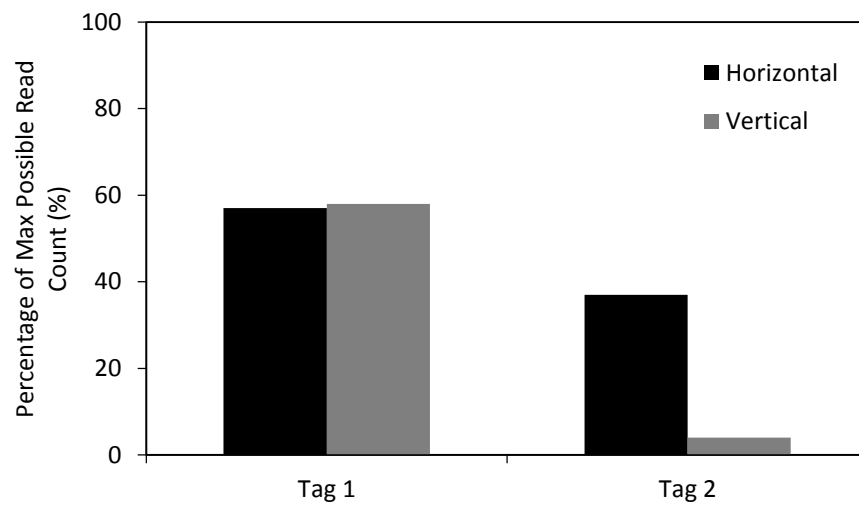


Fig. 6.42 Twisting motion with 2 tags on chest and back

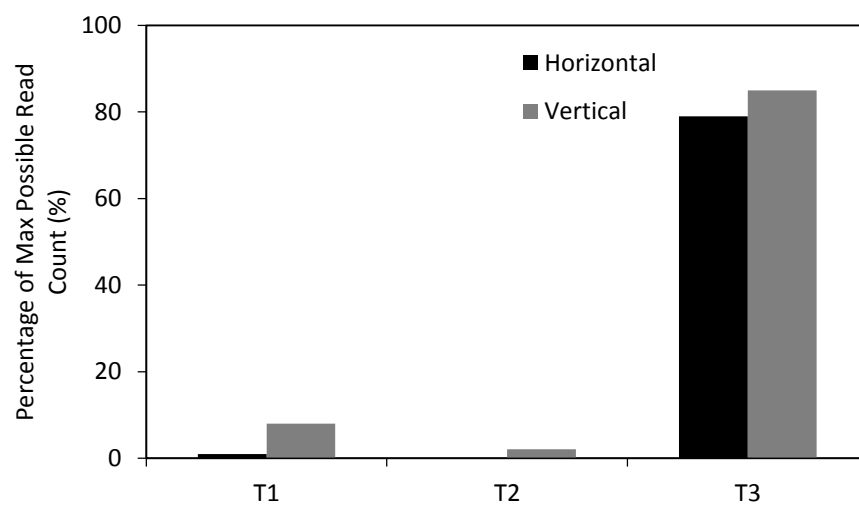


Fig. 6.43 Picking motion with 3 tags on body

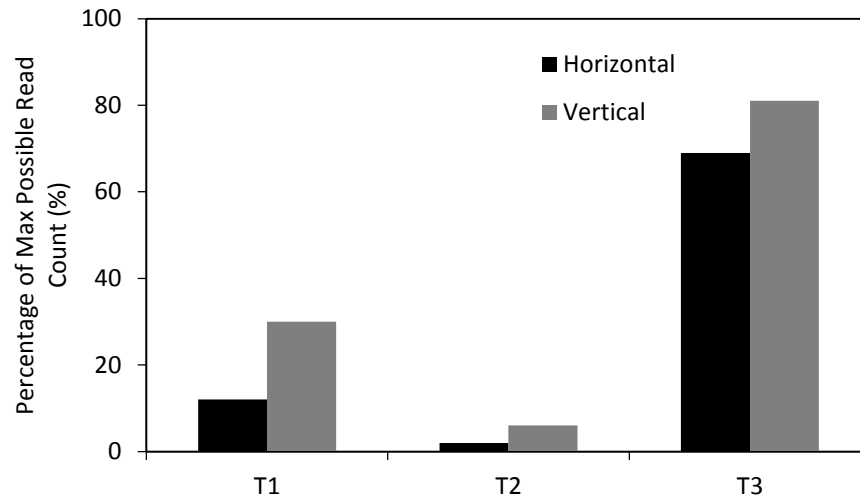


Fig. 6.44 Bending motion with 3 tags on body

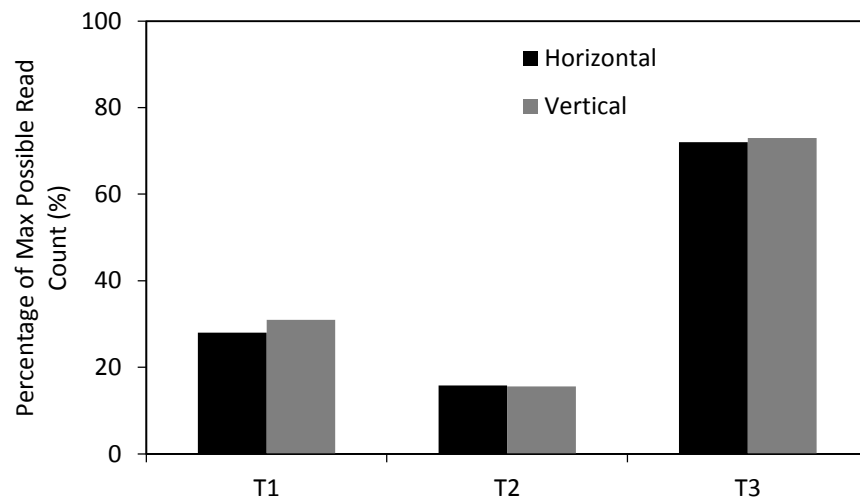


Fig. 6.45 Twisting motion with 3 tags on body

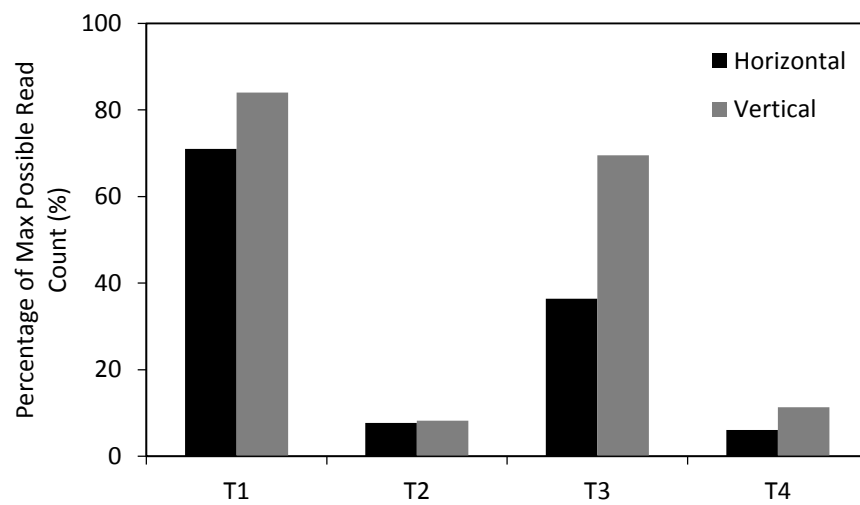


Fig. 6.46 Picking motion with 4 tags on body

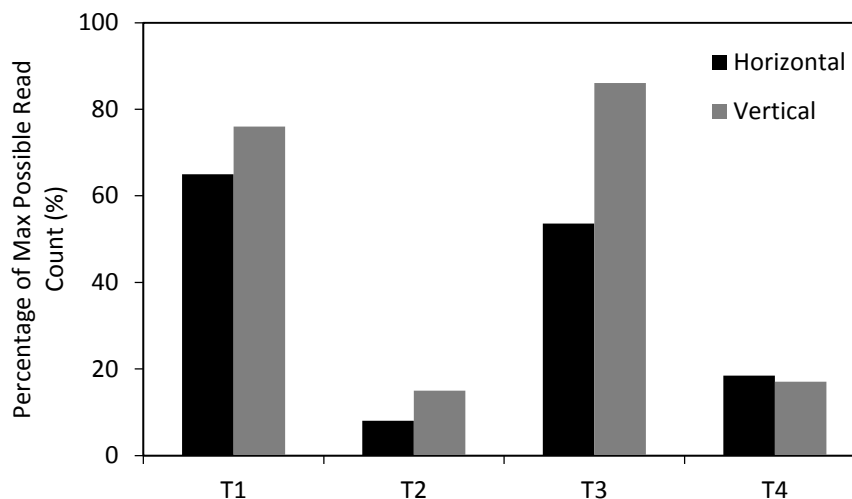


Fig. 6.47 Bending motion with 4 tags on body

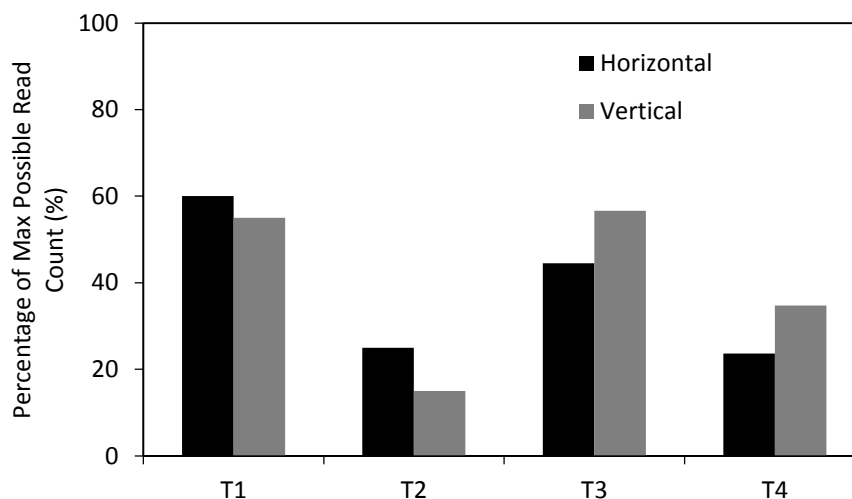


Fig. 6.48 Twisting motion with 4 tags on body

A summary of the tag performance is shown in Table 6.9. It can be seen that as earlier observed, the tags which were placed in a vertical orientation performed better than the tags in the horizontal orientation although the difference is marginal in some cases.

The tags that were placed on the back had low read percentages due to blocking as the user was facing forward. The tags placed on the chest also experienced some blocking during picking and bending because of the position of the head during these motions. The tags on the three volunteers experienced varying degrees of blocking leading to no-read because of the differences in their natural motion patterns as well as body shape.

TABLE 6.9
READ PERCENTAGE FOR 2, 3 AND 4 TAG DIVERSITY

Motion	Pol	Diversity								
		2		3			4			
		T1	T2	T1	T 2	T3	T1	T 2	T3	T4
Bending	H	74	6	12	2	69	65	8	54	18
	V	77	32	30	6	81	76	15	86	17
Picking	H	71	1	1	0	79	71	8	36	6
	V	84	5	8	2	85	84	8	70	11
Twisting	H	57	37	28	16	72	60	25	45	24
	V	58	4	31	15	73	55	15	57	35

Table 6. 9 read percentage for 2, 3 and 4 tag diversity

6.6 Conclusion

An inkjet printed RFID tag integrated with a sticking plaster has been presented. The modeled tag had a return loss of 24dB at 867 MHz with a 10 dB bandwidth of 32 MHz. The simulated surface current distribution indicated high density around the slotted loop in the antenna which accounted for the dominating influence of the loop dimensions in determining the tag input impedance and resonance frequency. This tag had a read range of over 4m on air and at least 1.6m when placed on other parts of the body. The lowest measured range for this tag was for the arm which can be attributed to the presence of dense muscle and bone.

Diversity studies were carried out using motion capture equipment to ascertain which mounting positions would offer reliable read coverage using 4 tags or fewer. The

indications are that horizontally mounted tags on the chest and back can provide better overall coverage than vertically mounted tags which had narrower read sectors on the back due to increased influence of the body on the tag as a result of increased contact. With wider read sectors and narrower non-read sectors, 2 vertical tags mounted symmetrically on the arm offered significantly better performance than the horizontally mounted tags. In a bid to improve the read of the vertical tags, the tags were mounted so that one is displaced slightly forward, and the other displaced to the rear. This did not yield the desired result as it led to a decrease in the overall read sector of the tags.

Three and 4 tag diversity were also investigated for improvement in read sector coverage. The three tags were placed in such a way that at least one tag could read at any given rotation of the wearer. Although this mounting technique ensured that there were multiple regions with an overlap where two tags read concurrently, there was a region where no tag read during the transition from the read sector of Tag 3 to the read sector of Tag 1 for the horizontally oriented tag. The stated gap was eliminated in the vertically oriented tags by a small region of overlap between the two tags. In the case of 4 tag diversity, with tags on the arms and on the chest and back, a situation was obtained where at two tags read simultaneously in all overlap regions. The vertically oriented tags had 73% overlap regions compared to 53% for horizontally polarized tags. 4 vertically oriented tags also had a 26° region where three tags read at the same time. With this set up, reading should remain reliable even for recumbent patients lying on their backs or sides. A summary of the performance of the different tags setup is shown in Table 6.10.

Different body motions were also tested. The tags' read percentages also indicated better overall performance of the vertically oriented tags with these motions although the advantage was minimal in some cases.

TABLE 6.10 TAG DIVERSITY PERFORMANCE ASSESSMENT

TAG SETUP	TOTAL DIVERSITY	DIVERSITY WITH ONE FAILED TAG
2 TAGS CHEST/BACK H	Good	Poor
2 TAGS CHEST/BACK V	Moderate	Poor
2 TAGS ARMS H	Poor	Poor
2 TAGS ARMS V (SYMMETRICAL)	Good	Poor
2 TAGS ARMS V (ASYMMETRICAL)	Good	Poor
3 TAGS H	Good	Poor
3 TAGS V	Excellent	Moderate
4 TAGS H	Excellent	Very Good
4 TAGS V	Excellent	Excellent

References

- [1] G. Marrocco, "RFID Antennas for the UHF Remote Monitoring of Human Subjects," *IEEE Trans. Antennas Propag.*, vol. 55, no. 6, pp. 1862–1870, Jun. 2007.
- [2] K. V. S. Rao, P. V. Nikitin, and S. F. Lam, "Antenna design for UHF RFID tags: A review and a practical application," *Antennas Propagation, IEEE Trans.*, vol. 53, no. 12, pp. 3870–3876, Dec. 2005.
- [3] D. D. Deavours, "Improving the near-metal performance of UHF RFID tags," *RFID 2010 Int. IEEE Conf. RFID*, pp. 187–194, 2010.
- [4] L. Ukkonen, L. Sydänheimo, and M. Kivikoski, "Effects of metallic plate size on the performance of microstrip patch-type tag antennas for passive RFID," *IEEE Antennas Wirel. Propag. Lett.*, vol. 4, no. 1, pp. 410–413, 2005.
- [5] P. V. Nikitin and K. V. S. Rao, "Performance limitations of passive UHF RFID systems," *2006 IEEE Antennas Propag. Soc. Int. Symp.*, pp. 1011–1014, 2006.
- [6] P. Milan, Š. Milan, and P. Hudec, "UHF RFID of people," in *Development and Implementation of RFID Technology*, Vienna: I-Tech Education and Publishing, 2009, pp. 63–88.
- [7] Alien Technology, "Higgs-3 Product Overview." [Online]. Available: http://www.alientechnology.com/docs/products/DS_H3.pdf. [Accessed: 23-Aug-2011].
- [8] M. Ziai and J. Batchelor, "UHF RFID tag antenna design for on-body applications," in *Antennas and Propagation Conference (LAPC), 2010 Loughborough*, 2010, no. November, pp. 185–188.
- [9] M. A. Ziai and J. C. Batchelor, "A prototype passive UHF RFID transfer tattoo tag," in *Proceedings of the 5th European Conference on Antennas and Propagation, EUCAP 2011*, 2011, pp. 3811–3814.
- [10] Dimatix-Fujifilm Inc., "Dimatix Presents DMP-2800 – A Revolutionary Materials Deposition System | Press Center | Fujifilm USA." [Online]. Available: http://www.fujifilmusa.com/press/news/display_news?newsID=880140. [Accessed: 19-Jan-2015].
- [11] Sun Chemicals, "Silver Nanoparticle ink." [Online]. Available: <http://www.sigmaaldrich.com/catalog/product/aldrich/719048?> [Accessed: 19-Dec-2014].
- [12] Vicon, "What is motion capture | VICON." [Online]. Available: <http://www.vicon.com/what-is-motion-capture>. [Accessed: 18-Sep-2015].

- [13] S. Swaisaenyakorn, P. R. Young, and J. C. Batchelor, "Animated human movement and posture capture for body worn antenna simulation," *Antennas and Propagation (EUCAP), Proceedings of the 5th European Conference on*, pp. 3635–3639, 2011.
- [14] S. Manzari, C. Occhiuzzi, and G. Marrocco, "Feasibility of body-centric systems using passive textile RFID tags," *IEEE Antennas Propag. Mag.*, vol. 54, no. 4, pp. 49–62, 2012.

CHAPTER 7

CONCLUSION AND FUTURE WORK

The work presented in this thesis has considered inkjet printing as a fabrication technology for body mounted RFID tags in the form of transfer tattoo tags as well as tags integrated with sticking plaster. Various printing parameters have been discussed as well as their influence on the performance of the printed tags. The robustness of these tags in the face of fabrication limitations as well as exposure to wear and tear during use was explored. Also presented was the performance of multiple printed tags on the body with the aim on providing good diversity in a case where there is limited mobility of the user. The purpose of this chapter is to present conclusion arising from the work contained in this thesis as well as provide suggestions for future possible work.

7.1 Conclusions

The growing use of RFID technology for basic purposes such as inventory tracking and access control has been accompanied, in recent years, with an increase in ingenious use of it such as for sensors on their own or when integrated with a full stand-alone sensor. In the 21st century, the growth of RFID has been fuelled by its potential key role in the concept of Internet of Things (IoT) where it is expected to interface between devices as well as act as a bridge between these devices and humans. This growth in RFID adaptation has also led to better understanding of the technology as well as its problems and limitations when used on different environments such as on the human body. Some of these have been discussed in Chapter 2 of this Thesis.

There is also need to widen the growth of RFID by using fabrication methods that will not only quicken the conventional means of making these RFID tags but also make the fabrication costs lower. These new fabrication methods also seek to manufacture RFID tags with materials and on substrates that would not have been achievable with the traditional copper etching approach which employs corrosive chemicals which a lot of materials cannot withstand. One of these alternative fabrication methods is the inkjet printing of the tags with silver-nanoparticles based conductive ink.

Inkjet printing technology has some advantages such as the drop-on-demand (DOD) feature which ensures that ink is not wasted and it is only released from the ink cartridge when needed instead of having a continuous flow. Another feature of inkjet printing which ensures that the ink is not wasted is the ability to selectively deposit on only the parts of the sample being printed. These are usually the critical areas such as regions of high current density where proper definition has an effect on the performance of the tag. The wide range of substrates on which inkjet printing can be used is also an added advantage to this fabrication technology. Fabrication with inkjet printing can be made on a wide range of substrates such as wood, plastics, metals and even porous materials such as paper. This suits well with the nature of the RFID tag described in this work which is a transfer tattoo tag. A further advantage provided by inkjet printing technology for the purpose of the epidermal transfer tattoo tag is flexibility. One of the requirements of a body mounted tag is the comfort of the user. A body mounted tag should not interfere with the daily activities of the person wearing

it and should be worn with the user not bearing its presence in mind. Although the transfer tattoo tag presented in this work is only a few microns thick ($< 35 \mu\text{m}$), the flexibility of the deposited conductive ink ($\approx 5 \mu\text{m}$) ensured that the transfer integrates seamlessly with the body making it comfortable to use and not cause any irritation to the skin due to friction.

In-depth details of the inkjet printed epidermal transfer tattoo tag were given in Chapter 4. It was seen that a good balance between the amount of ink utilized for the printing of the tags and the achievable read was achieved with tags that were printed with $20 \mu\text{m}$ drop spacing and had 3 layers of deposited conductive ink. This thickness satisfied skin depth requirements and also had a reduced DC resistance. The importance of proper sintering of the printed sample was also noted. Improper sintering would lead to samples that are brittle and would affect the needed flexibility of the tag. For $20 \mu\text{m}$ drop spacing tags, there was an increase in the simulated tag efficiency after up to 30 minutes of sintering followed by efficiency drop. Owing to temperature constraints in the transfer tattoo paper, sintering beyond 30 minutes is not advisable.

A 60 cm read range was achieved from the tag. This is a reduction of about 40cm that obtained with an etched copper tag. The printed tag measured required transmitted power was 26 dBm which compared to the 21 dBm obtained from the etched copper tag. Increasing the number of conductive ink layers to 5 increased the achieved read range but this was not deemed to be economically viable because this improvement was not commensurate with the increase in deposited ink hence fabrication costs.

Owing to expected variations in the dielectric properties of individuals, a performance study of the transfer tattoo tag on 10 individuals was carried out. This was done using a probe based dielectric measurement equipment. The study showed variations in read range of the tag on the individuals which was related to the fat and muscle density of their body. It was also seen that a 1% increase in the relative permittivity of the body led to a 6.5mm reduction in measured read range while the same degree of increase in conductivity resulted in a 9mm reduction. Performance assessment of the tag on various parts of the body was also carried out and resulted in variations in measured read range.

The effect of ink volume reduction techniques in order to reduce fabrication cost on the performance was also examined. Techniques which involved the selective deposition of conductive ink on critical parts of the tag such as the feedline and ports, trimming of low current density parts of the tag as well as used of grid antennas were examined.

The selective deposition of ink saw a tag printed with two full layers while additional layers were added on the feedlines and ports. Additional layers from 1 up to a maximum of 3 were deposited. Each additional layer saw an increase by 1% in the total conductive ink volume used for tag fabrication of the tag when compared to that used for the fabrication of tags with 3 full layers of conductive ink. This also resulted in an increase of up to 26% in read range for the tag with additional three layers on the feedline and ports. A drop in read range by 25% was measured for the tag with 65% of its conductive area trimmed off. On reduction of the trimmed area to 48%, the read range was reduced by 11% to 53cm. 0.11 g of ink was used to fabricate this tag compared to the 0.22 g used for the full 3 layer tag. This proved to be a good utilization of conductive ink given the achieved read range. The grid tag utilized the least quantity of ink although with a reduced read range and robustness concerns.

There are some issues with inkjet printing technology such as the formation of holes in a printed sample due to blocked nozzle and coffee stain effect which can affect the resolution of a thin printed line. This work has examined the impact of these defects, some of which are formed by the limitations of inkjet printing technology, on the performance of the epidermal transfer tattoo tag.

The studied defects were in the form of hairline cut on the feedline, pinhole defects, notched defects and variations in feedline width. The effects on these defects were studied using simulation and measurement. The most detrimental defect to the tag performance was the hairline cut on the feedline which resulted in the total loss of functionality. Apart from the cut on the feedline, the most effect on tag performance was by the pinhole defect which were located in the ports as well as on the area around the slot of the tag which led to a 28% reduction in efficiency and 12% reduction in tag read range. On the other hand, the least effect on tag performance were by the notched defects on the feedline. Experimental results have also confirmed indications by the simulations.

The epidermal transfer tattoo tag was subjected to a robustness test in order to gauge its performance and suitability for everyday use. The tag showed good performance in the course of a normal day office use. There was a gradual decrease in measured read range during this test, however the tag did not stop functioning after 8 hours of testing but failing after about 20 hours due to a cut on the feedline. Additionally, rigorous test on the tag was carried out by wearing the tag for 20 mins of exercise activities in a gym. The tag showed a reduction in read range by 19%. A more controlled experiment using a saline solution however indicated that this reduction in read range was more as a result of wear and tear due to mechanical friction than exposure to sweat. There was no reduction in measured read range of the tag after a shower.

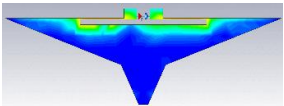
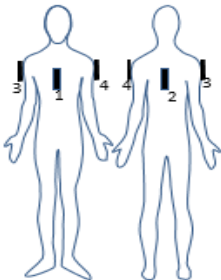
This research work has also evaluated the diversity performance of an inkjet printed tag integrated with a medical sticking plaster. The idea behind this is the suitability of the use of multiple tags in situations where the user may be incapacitated and also when the use of multiple readers may not be feasible due to cost constraints.

Two tag diversity studies indicated a better coverage provision by the tags placed horizontally on the chest and back. Vertically oriented tags placed in the same manner showed a narrower coverage area. When the two tags were mounted symmetrically on the upper arms, the vertically oriented tags provided better coverage when compared to the horizontally oriented tags. Mounting the tags asymmetrically in a bid to improve read area did not yield the desired results as the coverage area reduced.

Three and four diversity tag implementation resulted in significant improvement in the two tag diversity system. With the three tag diversity system, the vertically oriented tags provided better coverage than the horizontally oriented tags which had regions where no tag read. For the four tag diversity system, the vertically oriented tags provided 73% overlap region compared to 53% overlap region the horizontally oriented tags had. This is in addition to a 26° region where three tags read simultaneously. With the four tags vertical orientation set up, reading should remain reliable even for recumbent patients lying on their backs or sides.

Although minimal in some cases, further diversity performance studies with volunteers performing routine movements also indicated the superiority of the vertically oriented tags over the horizontally oriented tags for diversity purposes. A summary of the tag fabrication parameters and performance are shown in Table 7.1.

TABLE 7.1 RECOMMENDED FABRICATION AND PERFORMANCE PARAMETERS FOR COST EFFECTIVE INKJET PRINTED EPIDERMAL TRANSFER TATTOO TAG

Substrate	Transfer tattoo paper (from crafty computer paper)
Substrate thickness	26 μm (ink receiving layer)
Conductive Ink	Sigma-Aldrich (Silverjet DGP-40LT-15C)
Drop spacing	20 μm
Conductive ink layers	3
Sintering Time	30 minutes
Sintering Temperature	135°C
Read Range	\approx 60 cm on arm, 1.1m on abdomen (peak)
Average Body ϵ_r	31.8
Average Body σ	0.46 (S/m)
Effect of body dielectric	1% increase in conductivity (0.46 S/m) = 9 mm reduction in read range 1% increase in permittivity (31.8) = 6.5 mm reduction in read range
Best ink utilization design	Trim 2 (65% cut area) with 35% of total ink mass used to achieve a read range 75% of full 3 layer tag. Trim 2 has the highest FoM $\left(\frac{\% \text{ read range}}{\% \text{ used ink}}\right)$ of 2.14
	
Worst ink utilization design	Two full layers with one additional layer on feedlines and ports with 71% of total ink mass achieves a read range 9% greater than that of a full 3 layer tag. Has the lowest FoM of 1.54
Durability	> 8 hours
Most detrimental defect	Pinholes around slot and ports
Best tag diversity	4 vertically polarized tags offering multiple simultaneous read regions and performance when one tag fails
	

7.2 Further work

This work has described a novel inkjet printed epidermal transfer tattoo RFID tags. While it has presented a study of the inkjet printing of this tag with a focus on the printing techniques, effects of the method of fabrication on the performance of the tag as well as a robustness assessments of this tag, it is acknowledged that this was carried out using a single tag design. Although this has led to a reduction in the variables in the study, there is need to carry out further study on the on-body performance of inkjet printing for tattoo tag fabrication with other tag designs. This would help to further assess the viability of inkjet printing technology as a means for fabrication of epidermal transfer tattoo tags. Other means of ink usage minimization can also be exploited by using alternative tag designs.

The effect of body dielectric parameters variation on the performance of epidermal transfer tattoo RFID tags carried out in this work was done with a sample size of 10. This sample size did not adequately cater to sources of these variations such as gender, race and age. Additional work using a larger sample size is needed in order properly develop a system that can be used to evaluate the performance of epidermal transfer tattoo tag based on these parameters. This would aid in understanding how these parameters affect tag performance leading to a possible performance prediction metrics.

Preliminary work on the implementation of an active epidermal transfer tattoo tag has been carried out and reported in [1]. This initial work has shown very promising results with a remarkable increase in read range when compared to the passive tag. This was achieved by using a flat soft battery [2]. Further work is needed in order to fully integrate the epidermal transfer tattoo tag with a printed battery of the kind reported in [3]. A tag of this nature would lead to a less bulky, longer read range epidermal tattoo tag.

There is also a possibility of extending the motions used for the diversity performance study presented in this thesis. The motions discussed in this work involved the volunteer standing while performing these motions. Further study is required to assess the performance of the various tag diversity systems for motions carried out while sitting and lying down.

References

- [1] D. O. Oyeka, J. C. Batchelor, and B. M. Turki, “Enhanced read range Tattoo RFID tags,” *Antennas and Propagation & USNC/URSI National Radio Science Meeting, 2015 IEEE International Symposium on*. pp. 197–198, 2015.
- [2] “SoftBattery | Enfucell.” [Online]. Available: <http://www.enfucell.com/softbattery>. [Accessed: 07-Dec-2015].
- [3] “Startup Makes a New Kind of Flexible, Printed Battery | MIT Technology Review.” [Online]. Available: <http://www.technologyreview.com/news/528996/flexible-printed-batteries-for-wearable-devices/>. [Accessed: 07-Dec-2015].